VACUUM ULTRAVIOLET DISCHARGE EXCITED LASERS

A.M.RICHMOND

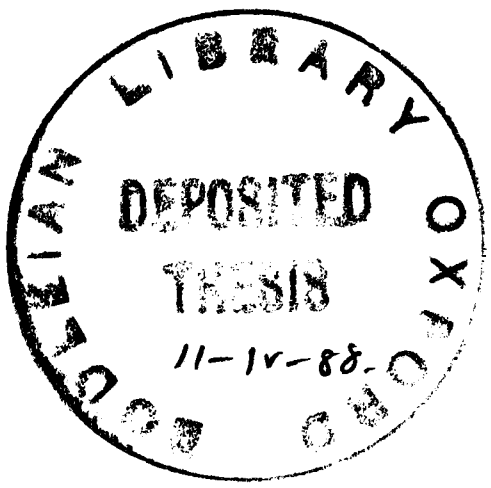
LINCOLN COLLEGE

THESIS SUBMITTED FOR DEGREE OF

DOCTOR OF PHILOSOPHY

IN THE

UNIVERSITY OF OXFORD



HILARY TERM, 1987

VACUUM ULTRAVIOLET DISCHARGE EXCITED LASERS

A.M.Richmond
Lincoln College, University of Oxford

Abstract of thesis submitted for
degree of Doctor of Philosophy
Hilary Term, 1987

The thesis concerns experimental studies of discharge excited lasers operating in the vacuum ultraviolet (VUV) region of the spectrum.

The known molecular fluorine laser operating at 157nm, on a bound-to-bound transition of the F_2 molecule was selected for initial study. As a result of the work reported here the energy per pulse was increased by a factor of five (10mJ to 50mJ) from that of earlier F_2 lasers. Similary the working lifetime of the gas mixture was increased from a few shots to several thousand by the application of cryogenic gas purification techniques. These improvements have resulted in the development of a practical commercial F_2 laser. The performance characteristics of the fluorine laser and their relationship to the physical mechanisms are discussed.

With the objective of achieving laser action in the 110 to 130nm region of the VUV a novel scheme is investigated. The scheme involves the production of a population inversion between the v'=1 level of the $b^1\Pi_u$ state of molecular nitrogen and high lying levels of the $X^1\Sigma_g^+$ ground state. The excitation of the upper laser level involves production of N_2 molecules in the $a^1\Pi_g$ state by means of a pulsed discharge. Transfer of population from this intermediate 'a' state to the upper level is accomplished by absorption of radiation at 308nm from a discharge excited xenon chloride laser. The practicality of this scheme has been investigated to the extent that populations of the order of 10^{13} molecules per cm^3 have been produced in the 'a' state and laser induced fluorescence on the 'b' to 'X' band has been observed. Under the conditions of the present experiments the potential VUV gain is too small ($10^{-4} cm^{-1}$) to reach laser threshold. The problems of increasing the gain to reach threshold for a practical device are discussed.

To my parents and my wife

- for their loving support.

ACKNOWLEDGEMENTS

I would like to acknowledge the assistance of the following during the course of this work.

Dr C E Webb for his helpful advice, the many hours spent in reading and discussing this thesis and for his wholehearted and invaluable guidance and support as my supervisor.

Dr D J Bedwell for his sustained and important contribution to many aspects of this project.

Professor E W J Mitchell for the use of the Clarendon Laboratory and its facilities.

The SERC for its financial support of myself and this work.

Members of the Laser Group, who freely gave of their knowledge and expertise.

And finally, the staff at the Clarendon Laboratory, whose willing cooperation facilitated the work and was much appreciated.

CONTENTS

CHAPTER 1 : INTRODUCTION TO THE VACUUM ULTRAVIOLET SPECTRAL REGION
1.1 Preliminary comments
1.2 Applications of VUV lasers
1.2.1 Photodissociation studies
1.2.2 Photoexcitation studies
1.2.3 Photolithography
1.2.4 Medical applications
1.3 Disscussion of specific problems for the production of VUV radiation
1.3.1 Absorption
1.3.2 Impurities
1.3.3 Optical materials
1.4 Lifetimes of states and production of population inversions
1.4.1 Factors determining atomic and molecular lifetimes
1.4.2 Conditions for a population inversion
1.4.3 Discussion of fast discharge circuits
1.5 Conclusion

CHAPTER 2 : REVIEW OF VACUUM ULTRAVIOLET GAS LASERS
2.1 Introduction
2.2 Bound-free laser transitions
2.2.1 Argon fluoride laser at 193nm
2.2.2 Argon chloride at 175nm
2.2.3 Rare gas excimers
2.3 Bound-bound laser transitons
2.3.1 Molecular hydrogen on the Lyman and Werner bands
2.3.2 Carbon monoxide at 181 to 197nm
2.3.3 Molecular fluorine at 157nm
2.4 Conclusion

CHAPTER 3 : MOLECULAR FLUORINE LASER
3.1 Introduction
3.2 Historical review of the molecular fluorine laser
3.3 Laser transition : spectroscopy of the fluorine molecule
3.4 Kinetic model
3.5 Laser design
3.5.1 Design criteria
3.5.2 Gas envelope
3.5.3 Gas handling
3.5.4 Discharge excitation circuit
3.5.5 Optics
3.5.6 Radiation detection
3.6 Conclusion

CHAPTER 4 : OPERATIONAL PARAMETERS OF FLUORINE LASER
4.1 Introduction
4.2 Initial investigations
4.3 Improved performance
4.4 Energy scaling results and discussion
4.5 Conclusion

CHAPTER 5 : PROPOSED NEW LASER SYSTEM IN NITROGEN
5.1 Introduction
5.2 Outline of the proposed scheme for a VUV laser
5.3 Excitation of nitrogen molecules to the intermediate 'a' state
5.3.1 Discharges and afterglows
5.3.2 Optical methods of excitation
5.4 Absorption of radiation from the "transfer" laser

5.4.1 Absorption linewidths
5.4.2 Overlap of 'a'-'b' absorption band with "transfer" laser radiation
5.4.3 Absorption intensity on rotational lines
5.5 Lower level population
5.5.1 Vibrational excitation of the $X^1\Sigma^+_g$ ground state by electron collisions
5.5.2 Electron energy distribution function
5.5.3 Vibrational distribution
5.6 Timing considerations
5.7 Conclusion

CHAPTER 6 : XENON CHLORIDE TUNED LASER
6.1 Introduction
6.2 Laser design
6.3 Operational characteristics of the XeCl laser
6.3.1 Untuned oscillation
6.3.2 Initial tuned configuration
6.3.3 Optimisation of performance
6.3.4 Gain measurements
6.3.5 Linewidth measurements
6.3.6 Tuning range
6.4 Conclusion

CHAPTER 7 EXPERIMENTAL ARRANGEMENTS FOR PRELIMINARY INVESTIGATIONS OF THE PROPOSED NITROGEN VUV LASER SCHEME
7.1 Introduction
7.2 Experimental apparatus
7.2.1 General
7.2.2 Vacuum and gas handling considerations
7.3 Radiation dectection system
7.3.1 Monochromator
7.3.2 Scintillator and photomultiplier tube
7.4 Signal recording system
7.4.1 Boxcar integrator - general
7.4.2 Timing considerations
7.4.3 Averaging
7.4.4 Time constants and aperture duration
7.4.5 Accuracy
7.4.6 Oscilloscope
7.5 Computer aided experiment
7.5.1 General considerations
7.5.2 Hardware
7.5.3 Software
7.6 Conclusion

CHAPTER 8 : INVESTIGATIONS OF THE PROPOSED NITROGEN VUV LASER SYSTEM
8.1 Introduction
8.2 Initial investigations
8.2.1 Discharge tube
8.2.2 Laser induced fluorescence of hydroxyl radical
8.2.3 Carbon monoxide fluorescence
8.3 Excitation of molecules to the $a^1\Pi_g$ state
8.3.1 Conditions needed for production of N_2 in the 'a' state
8.3.2 Estimate of number density of the $a^1\Pi_g$ molecules
8.4 Emission from $b^1\Pi_u$ state
8.5 Laser induced fluorescence from $b^1\Pi_u$ state of nitrogen
8.5.1 Method of detection of laser induced fluorescence
8.5.2 Relative timing considerations of discharges and detection system
8.5.3 Discharge tube and circuit
8.5.4 Experimental investigations

8.6 Conclusion

CHAPTER 9 : POTENTIAL OF PROPOSED VUV LASER
9.1 Introduction
9.2 Discussion of results
9.2.1 Population of excited molecules due to discharge excitation alone
9.2.2 Population density of excited molecules transferred by XeCl laser
9.2.3 Calculation of gain coefficients for the VUV
9.3 Appraisal of proposed new laser system
9.3.1 Steady state conditions for laser oscillation
9.3.2 Dynamic conditions for laser oscillation
9.3.3 Considerations of laser pulse energy
9.3.4 General considerations
9.4 Proposed improvements to produce laser action
9.4.1 Potential for scaling to larger volumes and gain lengths
9.4.2 Considerations of gas pressure
9.5 Concluding remarks

APPENDIX 1 : HIGH VOLTAGE RAPID DISCHARGE CIRCUITS AND SWITCHES
A1.1 Capacitor transfer circuit
A1.2 LC inverter
A1.3 Blumlein circuit
A1.4 Marx bank
A1.5 Triggered spark gap
A1.6 Solid dielectric switch
A1.7 Rail gaps

APPENDIX 2 :APPLICATIONS OF VUV LASERS
A2.1 Photodissociation
A2.2 Photoexcitation
A2.3 Photolithography
A2.3.1 Mechanisms of image formation
A2.3.2 Laser systems suitable for photolithography
A2.4 Medical applications

APPENDIX 3 : COMPUTER PROGRAMMES
A3.1 Introduction
A3.2 Control programmes
A3.3 Analysis programmes
A3.4 Data generation programmes

REFERENCES

CHAPTER 1 : INTRODUCTION TO THE VACUUM ULTRAVIOLET SPECTRAL REGION

1.1 PRELIMINARY COMMENTS

This chapter provides an introductory discussion of the sources and techniques applicable to the vacuum ultraviolet (VUV) spectral region. Existing types of laser which operate in this region are discussed, together with some of their applications. The necessary condition for obtaining a population inversion is derived. The constraint this places on the excitation pulse of certain types of VUV laser is discussed.

The VUV spectral region lies between the ultraviolet, on its long wavelength boundary, and the extreme ultraviolet and soft X-rays , on the short wavelength side. It is so called because of the absorption of radiation in this wavelength range by the atmosphere (due to the strong Schumann - Runge absorption continuum in Oxygen) which implies that an air free, or vacuum path is needed in which to transmit the radiation. For the purpose of this thesis the VUV region of interest is taken to be 100 to 200nm. The long wavelength boundary arises from the onset of the Schumann-Runge continuum at around 180nm, and the short wavelength boundary from the cutoff wavelength for transmission by crystalline lithium fluoride at 104nm, which has the shortest cutoff wavelength for any material suitable for use as cell windows.

There is interest in extending the range of available lasers to cover the VUV region for two main reasons:

Firstly the short wavelength means that there will be less divergence in the laser beam due to diffraction if it passes through a small aperture. This has advantages in photolithography.

Secondly the high photon energy means that high lying atomic and molecular levels can be obtained by single photon transitions, as opposed to multiphoton absorptions.

Using a laser in this region with its high photon flux opens up a whole

new area of study of highly excited populations. Also, since many of the high lying levels of molecules are repulsive, the interaction with VUV radiation causes the dissociation of molecules or polymers. All these advantages have found applications and are discussed further in the next section.

Lasers operating on VUV transitions are not the only means of producing high intensity VUV radiation. Coherent VUV radiation can be produced using nonlinear optical techniques. Third harmonic generation (Ganeev et al, 1986), frequency mixing (Reintjes, 1980, Hutchinson and Manning, 1985) and Raman sifting of UV laser radiation (Caro et al 1985) are techniques that have been employed. Incoherent radiation is produced from discharges. Helium containing traces of gaseous elements such as carbon, oxygen and nitrogen gives rise to discrete emission lines when discharged. High pressure discharges in rare gases emit "broad band" radiation over a few nanometers.

These sources are not generally as useful for the applications outlined due to their low photon fluxes. A review of laser sources in the VUV region is deferred until chapter 2.

The thesis, then, investigates the only currently available VUV discharge pumped laser capable of multimillijoule operation: the molecular fluorine laser. This is studied from a theoretical, technological and practical view point in chapters 3 and 4. Significant improvements in the output capabilities of the laser are reported.

The rest of the thesis is dedicated to an investigation of a proposed new laser system in molecular nitrogen. The laser has a two-stage scheme of excitation to the upper laser level, involving discharge excitation to a metastable level followed by transfer of population to the upper laser level using the optical interaction with the radiation from a UV laser. The scheme is proposed and the conditions for laser action are discussed in chapter 5. Chapter 6 investigates the "transfer" laser needed for this scheme. The experimental investigations are detailed in chapters 7 and 8, with the results of the procedures undertaken to realise the scheme as a practical laser

presented. Chapter 9 concludes the thesis with a discussion of those results and of future work that could be undertaken on this proposed laser.

The remainder of this chapter outlines some of the applications which presently available VUV lasers have found. This is followed by a section detailing the problems peculiar to the production of laser systems which operate in the VUV spectral region, and possible solutions to these problems.

1.2 APPLICATIONS OF VUV LASERS

It is worthwhile to review some of the applications which the argon fluoride and molecular fluorine lasers, emitting at 193nm and 157nm respectively, have already found. These are the only VUV lasers commercially available at the present time, and the only ones with sufficiently large output energies to make them useful for the applications mentioned below. A more complete review of the literature published on the use of VUV lasers in these applications is given in appendix 2.

Both the molecular fluorine and ArF laser systems belong to a group rather imprecisely called "excimer" lasers. The term "excimer" laser is most correctly applied to a laser in which the lasing species is an excited dimer (excimer), such as Xe_2. An excimer is a homonuclear molecule whose ground state is unstable and dissociates. The upper laser level is a bound state. However during the past decade the term has come to be applied to any species in which the ground state is dissociative, and for which there exists stable excited states. In particular it was applied to that class of lasers called Rare Gas Halides (RGH) lasers, of which ArF, XeCl and KrF are examples. The term has also been applied more generally to lasers in which the lower laser level is no longer dissociative such as molecular hydrogen, nitrogen and fluorine as they operate in a similar manner to the true excimer lasers.

The applications of VUV lasers are given below, together with a summary

of the parameters for the lasers used in previous investigations. A full list of references for all these studies is given in appendix 2.

1.2.1 Photodissociation studies

The photodissociation of molecular oxygen was studied using a fluorine laser giving an output pulse of 10mJ. When this was focussed to a beam waist of 1mm dissociation efficiencies approaching 100% were recorded. The dissociation of OCS with 25mJ pulses from a fluorine laser has also been recorded.

An ArF laser has been used in the photodissociation of alkali-halides. In the particular case of indium iodide, ArF pulse energies of 30-40mJ produced superradiant emission from a transition in In at 451nm.

1.2.2 Photoexcitation studies

Emission from the molecular fluorine laser at 157nm has been used to excite NO, due to a close coincidence with one of the F_2 laser lines. A 1cm long cell containing NO at a pressure of 1Torr was found to absorb 13% of the laser radiation.

1.2.3 Photolithography

An argon fluoride laser has been used to produce features as small as 500nm using conventional lithography techniques. An exposure of 930mJ/cm^2 in a 20ns pulse was used.

The fluorine laser was used in a "self developing" technique, with nitrocellulose as the photoresist, to produce features as small as 200nm. A threshold flux of 25mJ/cm^2 was found to be necessary for this process.

1.2.4 Medical applications

In medical applications involving the removal of organic matter, VUV lasers are able to undertake the task with a minimum of damage to surrounding

tissue.

An ArF laser has been used to produce incisions as narrow as 20μm on the cornea of an eye, with a damage zone of only 0.1-0.3μm.

1.3 DISSCUSSION OF SPECIFIC PROBLEMS FOR THE PRODUCTION OF VUV RADIATION

1.3.1 Absorption

Many materials in gaseous or vapour form absorb quite strongly in the VUV region. As was shown in the previous section, this property can be put to advantage in various applications. However, during the production of the VUV radiation, and its transport to the interaction region, absorption is a distinct disadvantage. If absorbing species are present within the laser cavity they act as a loss mechanism, decreasing the gain of the laser, and thus its output energy. To reach threshold for oscillation the round trip gain must equal the round trip losses, and if these are large it may mean in some cases that it is not possible to pump the gain medium hard enough to achieve laser oscillation. In the case of UV preionised gas lasers these absorbing species have a further detrimental effect in that they also absorb the preionising radiation, thus reducing the homogeniety of the discharge and the pumping power.

There is thus a necessity to avoid the presence of VUV absorbing gases within the laser envelope. This can be achieved by making it sufficiently leak-tight that the build up of the absorbing species does not affect the laser output significantly during a full day's operation. It is also necessary to use the correct grade of gas for the laser mix, as impurities can also admitted from the gas supply.

The path for the laser radiation to the reaction region must also be purged of these absorbers otherwise the available energy for the interaction will be reduced: this can be a large effect due to high absorption coefficients of some molecules.

Absorption coefficients for a number of common gases are shown in figures 1.1 and 1.2. The data for these figures have been taken from a number of references (Edward et al, 1953, Nee and Lee, 1984, Murray and Rhodes, 1976,), and show the extent of the problem of gaseous absorption. The oxygen absorption at wavelengths longer than 175nm is due to the Schumann-Runge bands ($X^3\Sigma^-_g$ v"=0 - $B^3\Sigma^-_u$ v'=0-20). Between 175 and 130nm the absorption is the Schumann-Runge absorption continuum resulting from the photodissociation of ground state oxygen. At shorter wavelengths there are complex absorption bands, many of which have not been fully identified.

Liegel et al (1984) measured a small absorption from helium in the VUV region of about $3x10^{-2}$ cm^{-1} at a pressure of 10 bar. The absorption was from the lowest excited states of atomic helium, He(^{3}S), and molecular helium, $He_2(a^3\Sigma)$ formed by electron beam excitation. Helium is widley used as a buffer gas and this absorption could prove a hindrance to scaling to higher power lasers using higher gas pressures to increase the available inversion density on low gain systems.

1.3.2 Impurities

Impurity species within the laser gas envelope can be detrimental to the performance of the laser. As described above, they can absorb radiation at the laser wavelength. They can also quench the excited states of the upper laser level. The preionisation of the discharge volume can also be blocked by absorption of the UV radiation, though in some cases impurities with low ionisation potentials can actually aid the preionisation. For lasers with gas mixtures containing reactive species, reactions with impurity compounds can cause depletion of that component of the laser mix. Moreover there is also a problem of absorption of preionising radiation by excited and ionic species created transiently during the discharge.

Sources of impurities.

Impurities can appear in the discharge from a number of sources. Firstly they can enter the gas envelope as gases, as descibed in the previous subsection. Alternatively, they can be formed by chemical reactions within the discharge volume, or close by where there is a strong flux of hard UV radiation which can photoinitiate these reactions. The problem is aggravated by the presence of reactive components in the gas mixture, such as halogens or halogen-containing compounds in some VUV lasers, which are necessary constituents of the gas mixture. Reactions can also take place with gaseous impurity components and with materials present within the laser envelope, or those actually forming it. To minimise this cause of impurity build-up, a judicious choice of materials that will come into contact with the gases forming the laser mixture must be made. The materials should have the following properties:

Firstly, they must not readily adsorb molecules into their surface. This could happen when the material is exposed to the air, and the molecules later released in to the discharge volume.

Secondly, the material should not have loosely bound groups as part of its chemical structure as these can dissociate from the surface in the presence of hard UV radiation from the discharge. Often, these radicals will have absorptions in the VUV region.

Thirdly, the materials must be resistant to attack by halogen-containing compounds.

During the course of these studies, and previous work undertaken by the Laser Group at the Clarendon Laboratory, it has been found in practice that only certain materials fulfil these requirements. For metal surfaces, nickel should be used. However to reduce the weight, machining time and cost, a nickel coating on brass is effective and can be used. When insulators are needed, or it is necessary to use plastics for another reason fully fluorinated compounds such as polytetrafluoroethlyne (PTFE) or poly-vinylidene fluoride (PVDF) are 'clean' and stable.

Gower et al (1980) used a glass-bodied tube for their studies of the various impurities in an ArF laser mix. Measurements of the absorption of radiation at 193nm in the laser cell, and IR absorption of the products collected in a cold trap were used to monitor the impurities present. The absorption at 193nm was found to increase from 0.02%/cm to 0.22%/cm after 1000 laser pulses. In the same time the fluorine concentration dropped by 25% - a loss attributed to chemical reactions. The IR absorption studies showed that NO_2, SiF_4, CO_2, ClO_2, F_2CO, FNO, FNO_2 and NF_3 were present. Silicon came from reactions with the glass vessel, chlorine from CCl_4 as an impurity in the fluorine gas, and nitrogen and oxygen from air as gas supply impurity and leakages into the system. They also found that use of the cold trap decreased slightly the absorption at the laser wavelengh within the laser.

Kearsley et al (1983) caried out similar investigations on a PVC-bodied laser tube. An undischarged laser gas mix which had been left standing was found to have a high concentration of CCl_3F, whilst after discharging the proportion of CCl_2 and CF_4 was much higher. The chlorine was assumed to have come from reactions with the PVC. Coating the tube wall with PTFE decreased these impurities. However it was then found that the epoxy coating of the capacitors placed inside the gas envelope were being attacked, forming aromatic fluorocarbons in much larger quantities than had existed previously. This was because the longer gas lifetime gave a greater exposure time and so a larger build up of these impurities. Again, coating in PTFE served to alleviate the situation. Use of a cold trap was found to give dramatic improvements to the laser gas mix lifetime. Lifetimes of up to several days could be obtained with the addition of fluorine on a daily basis to replace that lost by reactions.

In confirmation of the earlier work at Oxford, Govindanunny and Maitland (1983) used a mass spectrometer to investigate the stable impurities in a helium-fluorine laser. They used two different materials (PMMA and PTFE) for the gas envelope. The PMMA system adsorbed much greater quantities of CO_2 and

H_2O. When a fresh laser mix was left to stand in this laser the measured concentrations of the components increased with time due to outgassing from the walls. When the discharge was turned on this led to a much greater increase in the partial pressures of COF_2, CF_4, O_2 and HF, due to reactions of the water and carbon dioxide with the fluorine. The decrease in the concentration of fluorine itself was also found to be greater in the PMMA system, implying a faster rate of reactions with the impurity species. The lifetime of the laser mix was found to be increased by ten times by using a PTFE body rather than the PMMA one. This lifetime was further increased by the inclusion of a simple liquid nitrogen temperature trap into the gas circulation loop. The trap was also found to decrease the rate of build up of the impurities, and in some cases actually reduced their concentrations.

Removal of impurities

In spite of these precautions there will still be some impurities present which will need to be removed. One method is to circulate the gases from the discharge volume through a cryogenic trap. Many of these impurities have very low vapour pressures at the temperature of liquid nitrogen (77K). Thus, using a trap cooled by liquid nitrogen proves a simple and effective way to clean the gas mix. The schematic design of such a trap is shown in figure 1.3. The heat exchanger precools the incoming gases before they pass through the coil in the liquid nitrogen. The technique acts to reduce the "boil-off" rate of the liquid nitrogen, as does surrounding the bucket with a thick layer of insulating foam. The gas is circulated through the trap by means of a compressor. Valves are provided to seal the lines connecting the trap to the laser volume to enable the condensed impurities to be pumped out after the trap has been left without liquid nitrogen, to warm up to the ambient temperature during a period of inoperation.

In some cases the vapour pressure of one of the active components of the gas mixture will be below its required partial pressure at 77K. This is

particulaly true in the cases of the rare gases krypton and xenon. In this case it is necessary to provide some temperature control to the trap. A method for achieving this is outlined in figure 1.3. The condensation chamber is maintained at the required temperature by the electric heating coil, which in turn is controlled by an electronic circuit. The circuit uses thermocouples to sense the temperature of the block, compares this to the temperature set on the controller, and switches on the heater as required. The design of this type of temperature controlled cryogenic trap is patented by the Ministry of Defence, and manufactured under licence by Oxford Lasers Ltd.

All these investigations show that consideration of the materials used in the construction of laser of this type can have a large effect on the output performance of the laser. Care must also be taken to ensure that unwanted gases do not enter the laser envelope. These can be detrimental in themselves, or provide the precursors for other species after reactions within the discharge.

1.3.3 Optical materials

Absorption.

A major problem when trying to find suitable optical materials for use in the VUV region is optical absorption. Absorption is a problem not only for transmitting windows but also for reflectors, which can quickly form absorbing surface layer on exposure to the atmosphere (even for periods of less than 1 second).

The materials most widely used for windows in the VUV are lithium fluoride, magnesium fluoride and calcium fluoride. Crystalline quartz and saphire also have useful transmission for VUV at wavelengths longer than 160nm. Transmissions for samples of these materials are shown in figure 1.4. Absorption coefficients α, for the bulk material of the window are

related to these transmission figures by

$$T = \frac{e^{-\alpha t}(1-R)^2}{1-R^2e^{-2\alpha t}} \qquad 1.1$$

where α is the absorption coefficient, t is the window thickness and R is the Fresnel reflection coefficient at each surface in air, given by

$$R = \left\{\frac{n-1}{n+1}\right\}^2 \qquad 1.2$$

where n is the refractive index of the window material. The equation gives the transmission for parallel sided plates of the material with the light at near normal incidence. It takes into account full internal reflections, which are added non-coherently.

Transmissive materials for the VUV region

LiF has the shortest cutoff wavelength of 104nm, with MgF_2 at 115nm and CaF_2 at 125nm. However, as can be seen, above about 130nm MgF_2 has the higher transmission. The transmissions of the fluoride materials close to their cutoff wavelengths has been shown to decrease as the temperature of the material increases (Shishaskaya and Ryzhova, 1973). For VUV radiation of wavelengths shorter than 115nm it is necessary to use lithium fluoride. Use of this material, however, brings its own problems. LiF is a very soft material which makes polishing to a high degree of flatness extremely difficult. The VUV transmission of LiF is reduced by mechanical polishing so that thin optical plates are usually obtained by cleaving LiF crystals. Lithium fluoride is very soluble in water and is slightly hygroscopic. Exposure of the freshly cut surface of the crystal to moist atmosphere causes a degradation of the VUV transmission. The degradation is due initially to water adsorbed on the surface. After more prolonged exposure a layer of reaction products builds up on the surface due to the chemical reaction between LiF and water. Further reaction can then occur only if the water molecules diffuse through this layer. This leads to a saturation

of the decrease in transmission. The final transmission value varies between samples, but can be as high as 50% of the initial value. Transmission of LiF was studied by Patterson and Vaughan (1963), who measured a final level reduced by 15% at 121.6nm. The reduction was found to be greater for the shorter wavelengths. To minimise this loss of transmission the crystals should be stored in a dry environment.

In addition when exposed to high levels of short wavelength (74 to 115nm) radiation the tranmission in the band 104 to 120nm and 165 to 280nm is found to decrease markedly (Warneck 1965). The decrease was attributed by Warneck to the formation of colour centres. It is possible to recover the orginal transmission by annealing the crystal before use at 500°C for a few hours in a vacuum and then allowing it to cool slowly.

Magnesium fluoride is a harder material and is not so affected by atmospheric moisture. It is therefore an easier material to work with and is to be preferred for uses down to about 130nm.

Reflective materials for the VUV region

As stated above, there is also a problem in finding materials with suitable reflectivities in the VUV for use as mirrors and coatings for reflection gratings. Aluminium layers have a high initial reflectivity, but this reduces very rapidly on exposure to the air due to a rapid build up of an oxide layer. For instance, at 121.6nm a freshly deposited layer has a reflectivity of 63%. This reduces with time to 41% after 1 hour, to 36% after 1 day and to 27% after a month (Berning et al, 1960). Coatings of platinum, osmium and rhodium have been used, with the advantage over aluminium that they do not age. For example a 1% reduction in the reflectivity of osmium was measured after exposure to air for one month (Cox et al, 1973). However their reflectivities in the VUV region vary between only 20 and 50% for layers about 500 nm thick. Another disadvantage of osmium coatings is that they must be deposited onto substrates at 300°C, which prevents their use in some

circumstances.

The highest reflectivities in the VUV have been obtained using mirrors consisting of an aluminium layer overcoated with magnesium fluoride. Reflectivities about 85% at 121nm have been obtained using this method, and it is useful down to 110nm, below which the platinum metal group coatings provide better results. The magnesium fluoride layer performs a dual purpose. Firstly it prevents the build up of the aluminium oxide layer, and secondly it enhances the reflectivity of the aluminium through constructive interference of the reflections from the MgF_2-vacuum and the Al-MgF_2 interfaces.

The increased reflectance of the aluminium because of the overcoating of MgF_2 is due to the optical properties of aluminium in the VUV region. At 120nm it has a refractive index of 0.2, and an absorption coefficient of 0.85 (Berning et al, 1960). Coating the aluminium with MgF_2 (which has a refractive index of 1.7 at about 120nm and low absorption for wavelengths down to this value) with an effective half-wave layer causes constructive interference between the reflections from the Al-MgF_2 and MgF_2-air interfaces. The fact that there is an absolute phase change of 51^o on reflection from the aluminium-dielectric interface gives rise to an extended wavelength range over which this constructive interference will take place. The absorption coefficient of the MgF_2 coating is 0.1 at 110nm. With the increased absorption the reflectance of the coated aluminium is the same as for uncoated aluminium. Below 110nm the absorption coefficient for magnesium fluoride becomes so large that these coating lose their usefulness as protective layers because the total reflectance is very much reduced.

The thickness of the fluoride layer must be adjusted to suit the wavelength being used. Berning et al (1960), for instance, show a 25nm layer giving peak reflectivity at about 125nm, while a 38nm layer peaks at 138nm.

Hunter (1962) gives details concerning the conditions necessary for the fabrication of these high reflectance coatings. The aluminium layer must be

formed from very high purity aluminium, the substrate temperature below $50^{o}C$, ambient pressure less than 10^{-5} torr and very high deposition rates of the order of 100nm/s must be used to produce layers 50 to 200nm thick. As soon as possible after the Al layer has been laid down, and certainly within 30s, the MgF_2 evapouration must commence. The magnesium fluoride must be pure and thoroughly out-gassed, the low pressure must be maintained and deposition rates of 1-4nm/s should be used.

One limitation to the measured reflectivity of these dual layer coatings is the high absorption of the MgF_2 layer. Wood et al found this to be 10^4 greater than for single crystals in the range 105 to 160nm, and attributed it to absorption by the low energy tail of an exciton band and scattering from inhomogenieties at the surface and in the body of the MgF_2 film. They found that this absorption could be reduced by depositing the film onto high temperature substrates. However this would not work in the case of aluminium layers as they would be destroyed by the high temperatures. Despite this Al-MgF_2 reflective coatings are widely used for work in the VUV region.

1.4 LIFETIMES OF STATES AND PRODUCTION OF POPULATION INVERSIONS

1.4.1 Factors determining atomic and molecular lifetimes

The electron oscillator model for a classical atom gives rise to a transition rate, A_{ik} between an upper level, i, and a lower level, k, of

$$A_{ik} = \frac{16\pi^3 e^2 z_0^2}{3\varepsilon_0 h \lambda^3}, \qquad 1.3$$

where z_0 is the amplitude of oscillation of the electron.

The λ^3 factor in the denominator of this expression means that for the VUV wavelengths the classically allowed transition rates are very fast, leading to short lifetimes. For a value of λ of 150nm, and a value of z_0 of twice the Bohr radius (a_0, with a value of 5.29×10^{-11}m), equation 1.3 gives a classical transition rate of $6 \times 10^8 s^{-1}$, or a radiative lifetime for the upper

level of 1.7ns. This is typical for allowed transitions in the VUV region. The classical equation holds only for fully allowed transitions as it stands. In other cases it must be modified by a factor, the oscillator strength, to fit the particular transition. The oscillator strength depends on the transition dipole moment.

Quantum Mechanics allows the transition rate to be derived for any transition. The transition rate is now given by

$$A_{ik} = \frac{16\pi^3 R_{ik}^2}{3\varepsilon_0 h \lambda^3} \qquad 1.4$$

where R_{ik}^2 is the dipole matrix element connecting the two levels. The transition dipole matrix element is defined as

$$R_{ik} = \int u^*_k \, \underline{er} \, u_i \, dV \qquad 1.5$$

with $u_{i,k}$ being the total wavefunctions of the upper and lower levels.

In the case of transitions between electronic energy levels of a molecular species, the matrix element will depend on the electronic, vibrational and rotational wavefunctions. Now, the Born-Oppenheimer approximation allows the total wavefunction to be separated into a product of electronic, vibrational and rotational wavefunctions. For a molecular transition for which the Born-Oppenheimer approximation is valid, the matrix element can be written as

$$R_{ik}^2 = M(R_e) F_{vib} H_{rot}. \qquad 1.6$$

Taking these terms in turn, $M(R_e)$ is the electronic transition moment and depends only slightly on the internuclear separation and may be considered constant for all vibrational states. F_{vib} is the Franck-Condon factor for the transition and is the overlap integral of the two vibrational wavefunctions. H_{rot} is the Hönl-London factor and is the overlap integral of the rotational wavefunctions. It contains the wavefunctions of a rigid rotator, which are essentially spherical harmonics, and so this function can be readily calculated. These factors depend on which branch the transition belongs to and the total electronic angular momentum change ($\Delta\Lambda$) during the

transition. They are given in Herzberg (1963), for $\Delta\Lambda=0$, as

for an R branch transition,

$$S_J^R=(J+1+\Lambda)(J+1-\Lambda)/(J+1) \qquad 1.7$$

for a Q branch transition,

$$S_J^Q=(2J+1)\Lambda^2/[J(J+1)] \qquad 1.8$$

for a P branch transition,

$$S_J^P=(J+\Lambda)(J-\Lambda)/J \qquad 1.9$$

where J is the rotational quantum number of the lower level, and $\Lambda=1$ for a Π level.

In a laser system the lifetimes of the upper and lower levels are both important, as will be evident in the next section.

1.4.2 Conditions for a population inversion

Consider the two levels, i and k, in conditions where stimulated emission is negligible. Let the total rate of excitation to level i be S_i, and the total rate of decay be N_i/τ_i (which includes the decay due to the laser transition itself), where N_i is the population density in level i. Similarly for level k, S_k is the excitation rate to level k, including that from spontaneous decay of level i, and the total rate of decay is N_k/τ_k.

In the steady state the populations in each level remain constant, and

$$S_i = N_i/\tau_i \qquad 1.10$$

$$S_k = N_k/\tau_k \qquad 1.11$$

Therefore for a population inversion between levels of similar degeneracy ($N_i > N_k$),

$$S_i\tau_i > S_k\tau_k. \qquad 1.12$$

The inversion is most easily achieved if the pumping rate to the lower level is as small as possible compared to that for the upper level (a selective excitation mechanism), and the ratio of the lifetime of the upper state to the lower state is large (a favourable lifetime ratio).

However there is a minimum pumping rate to the lower level, due to the spontaneous decay of the upper level, thus

$$(S_k)_{min} = N_i A_{ik}. \qquad 1.13$$

This gives a minimum condition for a population inversion

$$N_i > \tau_k (S_k)_{min} \qquad 1.14$$

so from 1.13 the condition becomes

$$N_i > \tau_k A_{ik} N_i \qquad 1.15$$

which gives that

$$(A_{ik})^{-1} > \tau_k \qquad 1.16$$

Thus for a steady state population inversion a lower level lifetime shorter than the inverse of the spontaneous emission rate is needed. If this condition is not met then continous wave (CW) operation will not be possible. If it is fulfilled this does not necessarily imply CW laser action will be possible.

As an example of other consideratons for CW operation consider the ArF laser, one of the class of RGH lasers. This has a lower level lifetime of 10ps against dissociation, and so should be a CW laser. However in discharge devices it is limited to output pulses of about 10ns. This is due to the technological problem of obtaining a stable discharge in the ArF gas mixture. It is extremely difficult to get the glow phase of the discharge to last for more than 10ns before it constricts and then forms arcs. It is then no longer able to provide the conditions for excitation of the laser. The problem of discharge instability in RGH lasers implies a constraint on the circuits pumping the lasers. They must be able to acheive a population inversion in a time short compared to that on which the discharge constricts. In general, however, for CW lasers, where the upper level lifetime is longer than the lower level lifetime, there are no constraints on how fast the population inversion must be achieved.

In some cases the condition 1.16 is not met. Laser action may still be possible, but only transiently, giving rise to a pulsed output. The laser

action will feed the lower level more quickly than population relaxes from it. This build up of population means that there will no longer be a population inversion and the laser turns off. Lasers operating under these conditions are called self-terminating lasers, and include the nitrogen laser at 337nm and the hydrogen laser operating on the Lyman and Werner bands. The population inversion lasts for a time of order $(A_{ik})^{-1}$, which limits the duration of the output pulse. In these cases if the current rise time is slower than the time $(A_{ik})^{-1}$ inversions producing gains high enough to overcome cavity losses will never be obtained, and it will not be possible to achieve laser action. In the case of fully allowed VUV transitions $(A_{ik})^{-1}$ will be of the order of a few nanoseconds. Therefore the operation of self-terminating VUV lasers places severe constraints on the discharge circuitry, which must have nanosecond rise times for the excitation pulse.

1.4.3 Discussion of fast discharge circuits

To achieve nanosecond rise-time from electrical discharge circuits means that care must be taken to keep the capacitance and inductance of the circuit to a minimum. The smallest capacitance is limited to that which allows enough energy to be stored for the laser discharge. However the inductance is only present as stray circuit inductances and should be reduced as far as possible. This can be achieved by the use of strip line feeds rather than wires, multiple parallel feedthroughs into the laser envelope and minimising the loop areas between H.T. and earth lines.

The type of the discharge circuit is also important. Three types which have been used as the excitation sources for VUV lasers are Capacitor transfer, LC inverter and Blumlein circuits. These are described in detail in appendix 1.

1.5 CONCLUSION

In this chapter the VUV spectral region has been introduced. Problems connected with the production and detection of VUV radiation have been discussed, along with possible solutions. The context for these discusions was that of VUV lasers. Some applications of VUV lasers have been given. The condition necessary for the production of a population inversion was derived. For the case of a self-terminati ng VUV laser this indicated the need for a fast (nanosecond) rise-time for the excitation pulse.

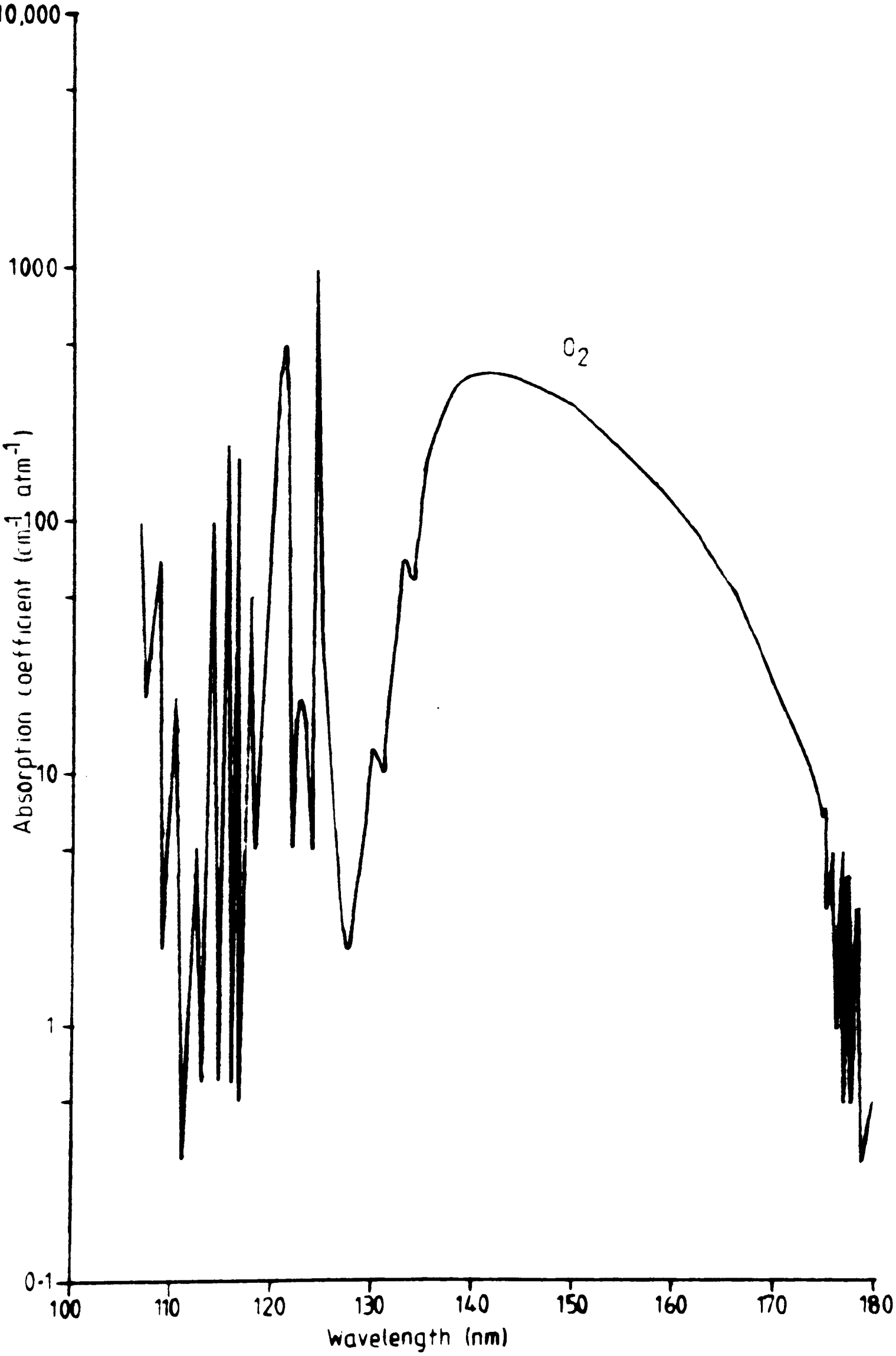


Figure 1.1 Absorption coefficient of oxygen

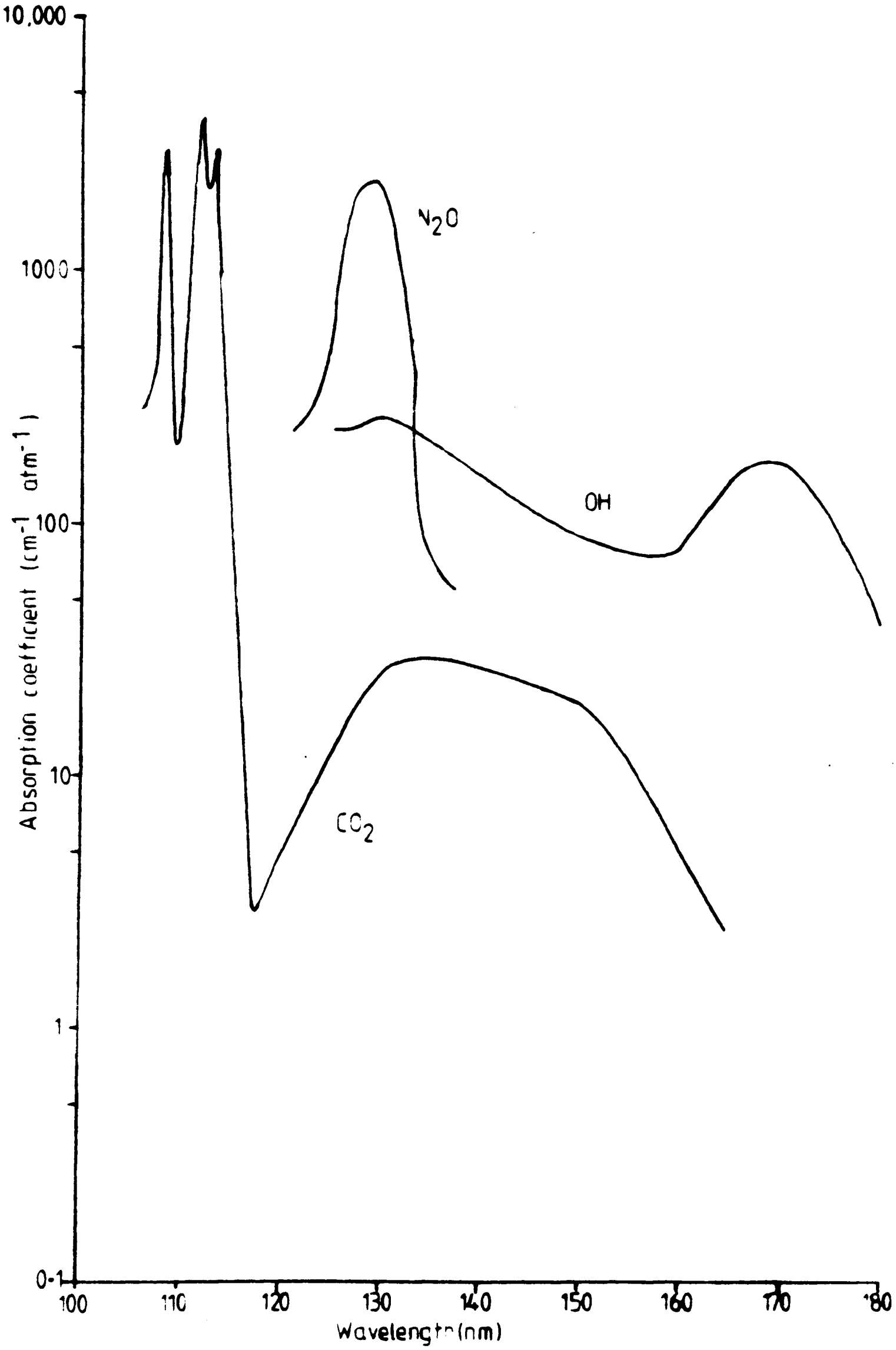


Figure 1.2 Absorption coefficients of gases

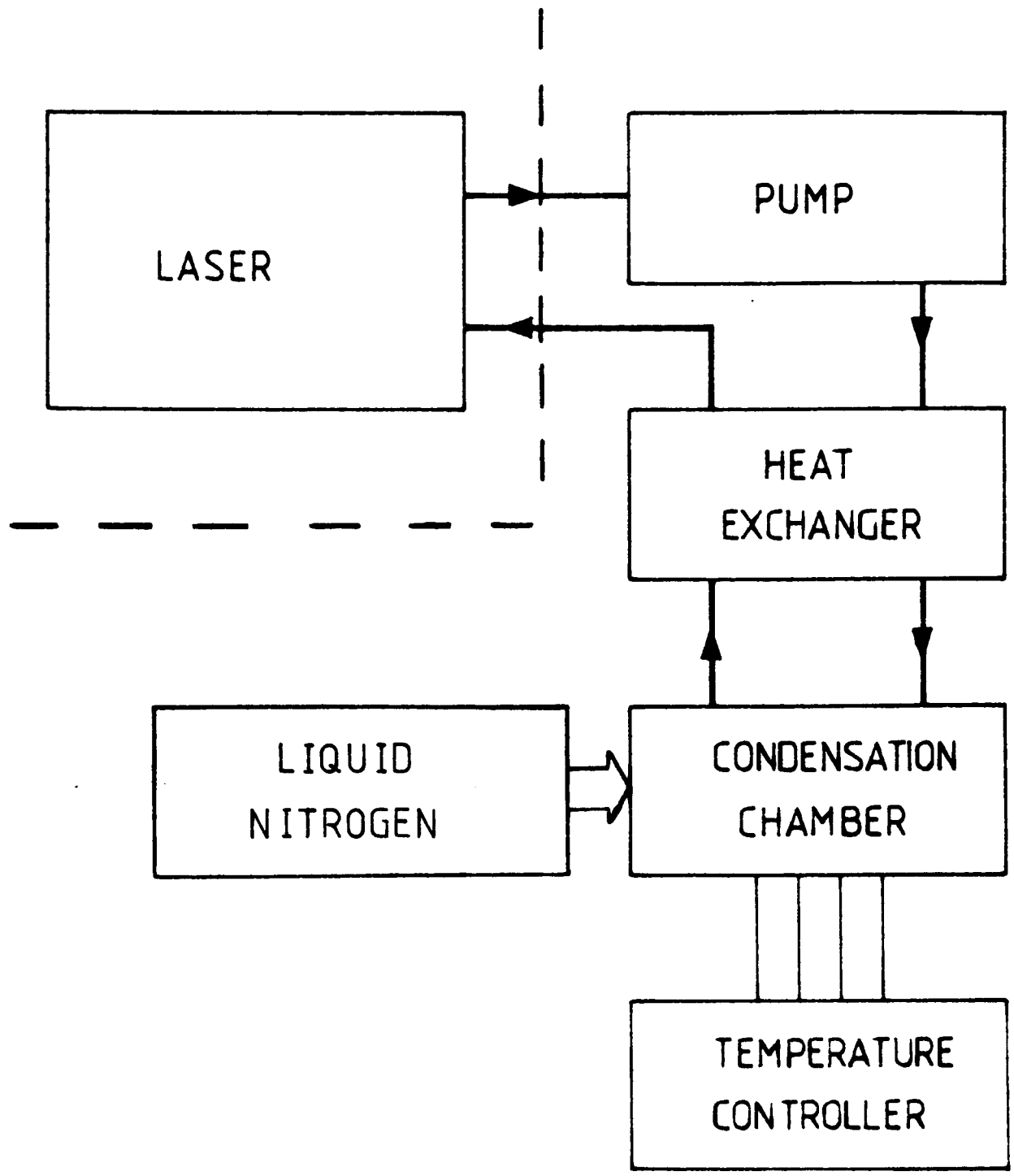


Figure 1.3 Block Diagram of Cryogenic Trap

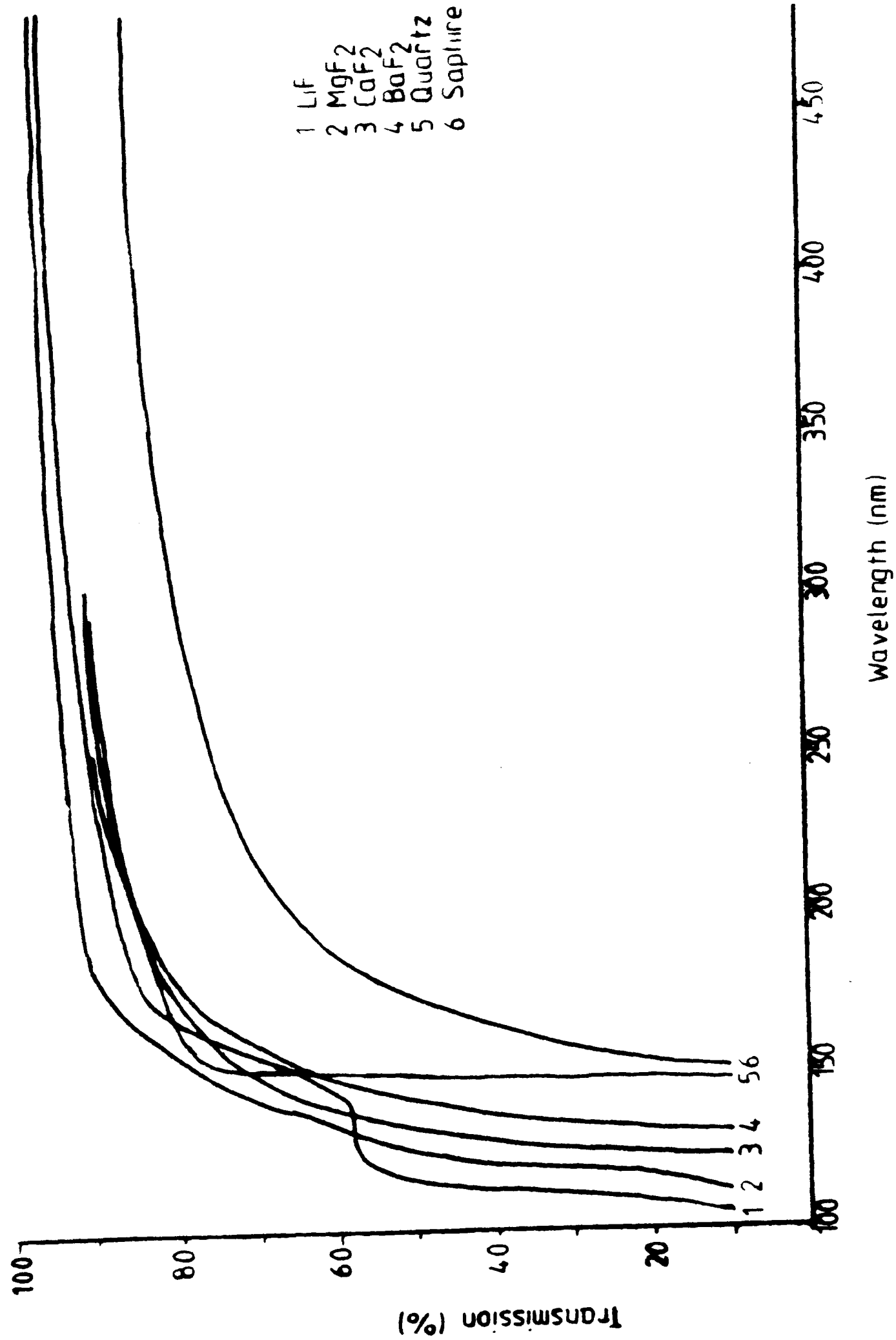


Figure 1.4 Transmissions of 3mm thickness of some solids in the VUV region

CHAPTER 2 : REVIEW OF VACUUM ULTRAVIOLET GAS LASERS

2.1 INTRODUCTION

In this chapter the various types of existing VUV lasers will be discussed. These are all based on molecular species. The chapter will be divided into two main sections. The first will deal with those lasers whose ground state is unstable and dissociates on a timescale of one vibrational period: a few picoseconds. These are the so-called bound - free transitions. The second half deals with lasers in which both the upper and lower levels are bound states of the molecule (bound - bound transitions). These are all self-terminating lasers. In most cases the lower laser level is an excited vibrational level of the electronic ground state. This leads to long lifetimes in the lower level, compared to that of the high lying upper level, and thus the condition for CW laser action, as discussed in section 1.4, is not met.

2.2 BOUND-FREE LASER TRANSITIONS

2.2.1 Argon fluoride laser at 193nm

The ArF laser belongs to the class of lasers called rare gas halide (RGH) lasers. In all of these lasers, the transition is between a bound excited state of the molecule, and the repulsive, or weakly bound, ground state (see figure 2.1). The inversion is formed by creating the molecules in the excited state. It was originally thought that the formation takes place through a harpooning reaction

$$Ar^{*} + F_2 \rightarrow ArF + F, \qquad 2.1$$

but later work (Kearsley, 1979) showed that the ion channel

$$Ar^{+} + F^{-} + M \rightarrow ArF + M, \qquad 2.2$$

in which M is a third body - typically a rare gas atom, will dominate in a

self-sustained discharge laser. The formation via the ion channel dominates by a factor of greater than ten, with the rate determining step for the formation of the RGH molecules being formation of the negative ion from the halogen donor. The upper laser level has a radiative lifetime of 4ns, and, at the pressures generally used, the vibrational levels of this electronic state will be essentially relaxed. Laser emission is at 193nm, in the tail of the oxygen absorption band, and so it can propagate through the atmosphere (see figure 2.2), but only with considerable attenuation.

The ArF laser is the most widely used of the known VUV lasers. Output energies of up to 500mJ and up to 250 pulses per second are obtainable from comercially available discharge excited systems.

The first observation of laser action from ArF was by Hoffman et al (1976). They used an axial electron beam depositing 3kJ into a gas mixture of 4Torr of fluorine and 1400Torr of argon, in a region 180cm long and 15cm in diameter. The maximum energy was 92J corresponding to an efficiency of 3%. Burnham and Djeu (1976) reported the first observation of discharge pumped laser action using an LC inverter circuit, with a pulse width of 40ns. Maximum energies of 80mJ were obtained with a mixture of 4.5Torr fluorine, 450Torr argon and helium to 1500Torr, the maximum pressure the apparatus could withstand. As part of their optical cavity was outside the gas envelope the laser spectrum showed structure attributed to absorption by the rotational lines of the (4,0) vibrational band of the Schumann-Runge system. More recently, workers at University of Hull (Andrew et al, 1984) have measured pulse energies of 2J at an efficiency of 0.5%. The device used by Andrew et al had a 0.5l discharge volume and used a charging voltage of 70kV across a 3.5cm electrode gap and a gas mixture of 10mbar fluorine, 200mbar argon and 5bar of a 1:1 mix of helium and neon. A gain of 15%cm^{-1} was also measured (Andrew and Dyer, 1985) from a mix of 10mbar F_2, 200mbar Ar and 3.5lbar He at a charging voltage of 40kV with a 2cm electrode spacing. This represents the highest reported gain for the ArF laser. However problems were

still encountered with decline in the signal amplitude with number of shots. This was attributed to loss of fluorine concentration due to reactions with the pressure vessel and a build-up of impurity species.

2.2.2 Argon chloride at 175nm

Oscillation on the ArCl band at 175nm (see figure 2.3) has only been observed once in a discharge pumped device. For that work (Waynant, 1977) a travelling wave Blumlein excitation circuit was used to power a device whose electrodes were 160cm long 2.5cm wide and with 1 - 7cm separation. The gas mixture comprised 1% Cl_2, 10% Ar with helium added to give a total pressure of 1bar. The output was 0.2mJ in a 10ns pulse and a small signal gain coefficient of 1.2% cm^{-1} was measured. The spectrum showed a broad (8nm) band peaking at 175.0nm and a secondary peak at 169.0nm. The primary band is due to a $B^2\Sigma^+_{1/2} - X^2\Sigma^+_{1/2}$ transition and the subsiduary peak is a $D^2\Pi_{1/2} - X^2\Sigma^+_{1/2}$ transition, both terminating on the unbound ground state. Liegel et al (1983) found that helium is preferable as the buffer gas, rather than an excess of argon, due to formation of Ar_2Cl at high argon pressures. Further, they pointed out that Cl_2 is to be preferred as the halogen donor over HCl because of quenching of the precursors of $ArCl^*$, which Liegel et al suggest is the lowest excited state of the chlorine atom.

2.2.3 Rare gas excimers

In the pure rare gas excimer laser systems, the laser transitions are between bound excited electronic states of the rare gas dimers, and the repulsive ground state (see figure 2.4). The wavelengths of the transitions are centred on 126nm for Ar_2^*, 147nm for Kr_2^* and 172nm for Xe_2^*. As the transitions end on dissociative lower states they are homogenoeusly broadened and thus the laser may be spectrally tuned without a large sacrifice of the output power. The useful tuning range is about 5nm, with linewidths of order 0.2nm (Hutchinson, 1980 and Uehara et al, 1985).

Oscillation on the rare gas excimer lasers has only been observed in electron beam pumped devices at high pressures. Hutchinson reports a xenon laser with 5MW peak power in a 3ns pulse at a pressure of 9 bar. A coaxial electron generator provides 5ns pulses of 500keV electrons into a 12cm long diode. A fused quartz prism was employed as an intracavity dispersive element to enable this laser to be tuned from 170 to 175nm. Uehara et al (1985) reported 2MW peak power from a tuned argon excimer laser at a pressure of 4MPa. Again a coaxial electron generator was employed. It gave a 90ns pulse of 700keV electrons into a 40cm diode. The laser pulse width was 5ns with a peak power of 2MW. A MgF_2 wedge was used to enable the laser to be tuned from 124 to 128nm with a linewidth of 0.3nm.

Pure rare gas excimer lasers are expensive to operate due to the high pressure of rare gas needed. It might be possible to operate these lasers in a discharge device using helium as a high pressure buffer to reduce the operating costs. The high pressures are necessary to enable the formation of the excimer from three body collisions. The fast electrons form atomic ions and excited atoms.

$$Xe + e \rightarrow Xe^{+} + 2e \qquad 2.3$$

$$Xe + e \rightarrow Xe^{*} + e \qquad 2.4$$

At high pressures the atomic ions form molecular ions, which undergo dissociative recombination to form excited atoms.

$$Xe^{+} + Xe + M \rightarrow Xe_2^{+} + M \qquad 2.5$$

$$Xe_2^{+} + e \rightarrow Xe^{*} + Xe \qquad 2.6$$

Due to collisions, all excited atoms relax to the lowest excited state. It is the collision of atoms in their lowest excited state, in the presence of a third body, which forms the excimers.

$$Xe^{*} + Xe + M \rightarrow Xe_2^{*} + M \qquad 2.7$$

The reaction rate coefficients for these formation reactions with helium as the third body are not so great as if the heavier rare gases are involved. Recent work in the Clarendon Laboratory (Sakurai, 1985) shows that

the use of krypton with helium as the buffer gas, compared to pure krypton, in a high pressure discharge reduces the efficiency by a factor of only two or three.

2.3 BOUND-BOUND LASER TRANSITONS

2.3.1 Molecular hydrogen on the Lyman and Werner bands

The theoretical possibility of laser action in molecular hydrogen, particularly on the Werner bands, was first proposed by Bazhulin et al (1965). The inversion was predicted to occur between vibrational levels of the $C(2p\pi\ ^1\Pi_u)$ state and excited vibrational levels of the $X(1s\sigma^1\Sigma^+_g)$ ground state (figure 2.5). Transition wavelengths are around 110 to 120nm. Due to the large magnitude of the vibrational quanta only the lowest vibrational level of the ground state is occupied at room temperature. The high energy electrons present in the first few nanoseconds following discharge breakdown populate the electronic levels much more efficiently than the vibrational levels of the ground state, hence an inversion can be achieved. Lasing is also possible on the Lyman bands, from the $B(2p\sigma^1\Sigma^+_u)$ level to excited vibrational levels of the ground state at around 160nm (see figure 2.6). These electronic levels have very short radiative lifetimes, 0.8ns for the 'B' state and 0.6ns for the 'C' state. The vibrational levels of the ground state will have long radiative lifetimes because hydrogen is a homonuclear molecule. Thus the laser must operate in a self-terminating mode, with pulse lengths of order 1ns. These short lifetimes dictate that the inversion must be formed in a time less than 1ns, which in turn means that the rise time of the discharge circuit must also be subnanosecond. The excitation may take place by direct electron impact, or via a short lived (10^{-16}s) negatve ion, $H_2^{-2}\Sigma^+_g$, which then decays to the upper laser levels. Direct excitation will lead to the vibrational levels of the upper states being populated according to the Franck-Condon factor connecting that level to the

ground state v"=0 level. The population in the ground state at room temperature will be distributed over the rotational levels J"=0,1,2 and 3 in the ratios 13:66:12:8 respectively. For the Lyman bands, the Franck-Condon factors suggest that v'=2 to 11 will be preferentially populated, and J"=2 will be the preferred rotational level from the selection rules and Hönl-London factors. Transitions to v"=9 to 14 are predicted to be the strongest, with the P3, R1 and P1 transitions the most probable. For the Werner bands calculations involving the upward and downward Franck-Condon factors predict the the v'-v" transitions 1-4, 2-5, 3-7, 2-6 and 0-2 will be the strongest. As most of the ground state population is in J"=1 then J'=1 and J'=2 will be most heavily populated, and based on the Honl-London factors the Q branch transitions will be the strongest. Thus the Q1 line of v'=1 - v"=4 is expected to be the strongest line on the Werner band laser.

Lasing was first observed by Hodgson (1970) on the Lyman bands on a number of P3 lines. A Blumlein discharge device with a solid dielectric switch and discharge volume of 120x1.2x0.04cm was used. Maximum energy of 3μJ in a 2ns pulse was obtained for a hydrogen pressure of 60 Torr. At almost the same time Waynant et al (1970) using a travelling wave Blumlein device (see appendix 1), with a wider channel, observed lasing on the Lyman bands between 156.7 and 161.3nm. The stimulated emission from the forward end of the travelling wave was found to be ten times that from the other end. They obtained 0.1mJ in a 1ns pulse.

Waynant (1972) first reported observations of gain on the Werner bands, using his travelling wave device. The lasing lines were Q1 (1-4) at 116.1nm and Q1 (3-7) at 123.0nm, each at about 5kW peak power and 1ns pulses, from hydrogen at 20Torr. Hodgson and Dreyfus (1972) employed a large electron beam generator, which delivered 5GW in a 3ns pulse, to excite the hydrogen at 20 to 100Torr. They measured peak powers of 500Wcm^{-2} on the Q1(1-4) line. Dreyfus and Hodgson (1974), with a 4GW electron beam generator of 1cm^2 cross section, obtained lasing on ortho- and para-hydrogen, deuterium and HD Lyman and Werner

bands. They observed stimulated emission at the shortest reported wavelength, on the R0(0-2) line at 109.8nm. Oscillation was optimised at hydrogen pressures of 25-30Torr. Pulse lengths of about 1ns were obtained with peak powers of 150Wcm^{-2} on the Werner bands and 60kWcm^{-2} on the Lyman bands.

Knyazev et al (1975) used a narrow waveguide channel (0.006x1x30cm) in their travelling wave Blumlein discharge circuit to produce the high current densities necessary for efficient excitation of the hydrogen laser. They found that the optimum hydrogen pressure was 100mbar, which gave 0.5mJ pulses of approximately 0.5ns duration, giving a peak power of 1MW. The energy stored in the line was 0.1J and the corresponding energy efficiency was 0.5%. Lines at much shorter wavelength, on the Lyman bands were observed, down to P3 (11,14) at 149.4nm, which ends on a level close to the dissociation limit.

Goldsmith and Knyazev (1977) studied the effect of the discharge channel width on the output power. Decreasing the channel width reduces the active volume and increases the diffraction losses, but it does increase the current density and pumping power density. At 100Torr hydrogen pressure they estimate current density of 10-100kA/cm^2 and pump power densities of 0.1-1GW/cm^3 are required. Their travelling wave Blumlein circuit was triggered by a miniature spark gap and would run at up to 100Hz for short periods, or sustained operation at 15Hz. Discharge thicknesses of 50, 100, 300 and 1000μm were investigated, with the highest power being achieved with the 300μm width: the length and electrode separation being held constant at 45 and 2.2cm respectively. Maximum energies of 20μJ were reported on the Lyman bands, from 45Torr of hydrogen flowing through the discharge channel at a charging voltage of 28kV, in a 0.5ns pulse.

Both these workers and Babis et al (1985) emphasise the importance of keeping the plates forming the channel accurately parallel over its length, and ensuring their flatness, as well as keeping the electrode separation constant. This is because the very narrow channel widths have a Fresnel

number much less than one, and a waveguide effect, based on grazing incidence reflections from the walls, will take place in the laser channel. Babis et al used a water cooling of the channel to achieve a repetition rate of 250Hz, and 30μJ pulses.

It is evident, therefore, that the VUV molecular hydrogen laser can be operated in "table-top" Blumlein excited devices with pressurised spark gaps to give multihertz operation. The pulse lengths are very short and offer the shortest laser wavelengths to date. However the pulse energies are low, about 20μJ, and offer little chance of scaling to higher energies because of the restriction in the width of the discharge channel, and thus active volume, necessary to achieve the high pump power densities.

2.3.2 Carbon monoxide at 181 to 197nm

Observations of VUV laser action in CO were first reported by Hodgson (1971). The laser emission was from the fourth positive system: the $A^1\pi$ - $X^1\Sigma^+$ transition (see figure 2.7). The scheme is similar to that of hydrogen in that the upper level is excited by direct electron impact, and an inversion is formed between excited vibrational levels of the 'A' state and excited vibrational levels of the ground state, which are initially unpopulated. A number of bands were observed from v'=2 and 3 to v"=6, 7 and 8 in the wavelength region 181 to 197nm. They are 181.1 nm (2-6), 187.8nm (2-7), 189.8nm (3-8), 196.0nm (2-8) and 197.0nm (3-9). Q branch transitions were found to be the strongest, with weak R branch lines being seen in stimulated emission, but no P branch. The R branch lines were also missing on the (3-9) band.

The excitation energy was provided by a Blumlein discharge circuit with a 0.05x1.2x120cm discharge channel and a solid dielectric switch. High purity CO at 60Torr was flowed through the channel. The output was in the form of superradiant pulses of 1.5ns FWHM and a peak power of 6W as measured with a photodiode. Hodgson suggests that the lower power of the CO laser is due to

electron losses to triplet molecular states which have energies slightly lower than the $A^1\Pi$ state.

2.3.3 Molecular fluorine at 157nm

The scheme for this laser is different from the two previous ones in that the laser transition is between vibrational levels of two excited electronic states, $D^3\Pi_{2g} - A^3\Pi_{2u}$ (see figure 3.2). This laser is commercially available, and is used in many of the VUV applications, as described in the previous chapter. In this work a significant improvement of the output energy of this laser was achieved. As a preliminary to a description of that work a description of the fluorine laser sytem and its historical development is given in the next chapter, with the results being presented in chapter 4.

2.4 CONCLUSION

In this chapter a number of discharge excited VUV lasers have been briefly reviewed. Apart from the molecular fluorine laser at 157nm and the ArF laser, operating just in the VUV region at 193nm, all the lasers operate at submillijoule pulse energies. At this time the fluorine laser seems the best candidate for a true VUV discharge excited laser with pulse energies in a regime useful for practical applications.

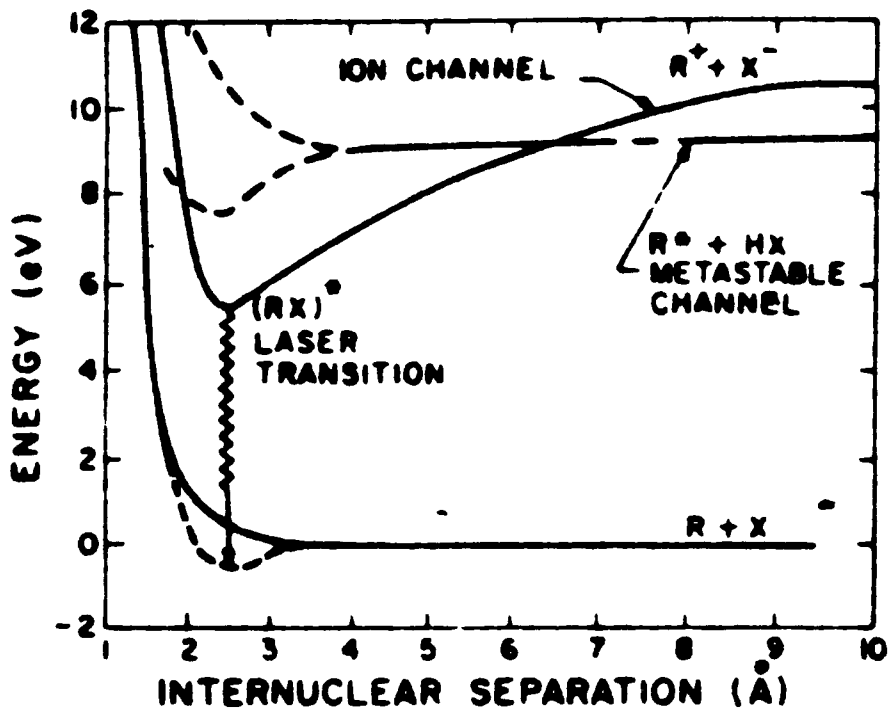


Figure 2.1 ArF Term Diagram

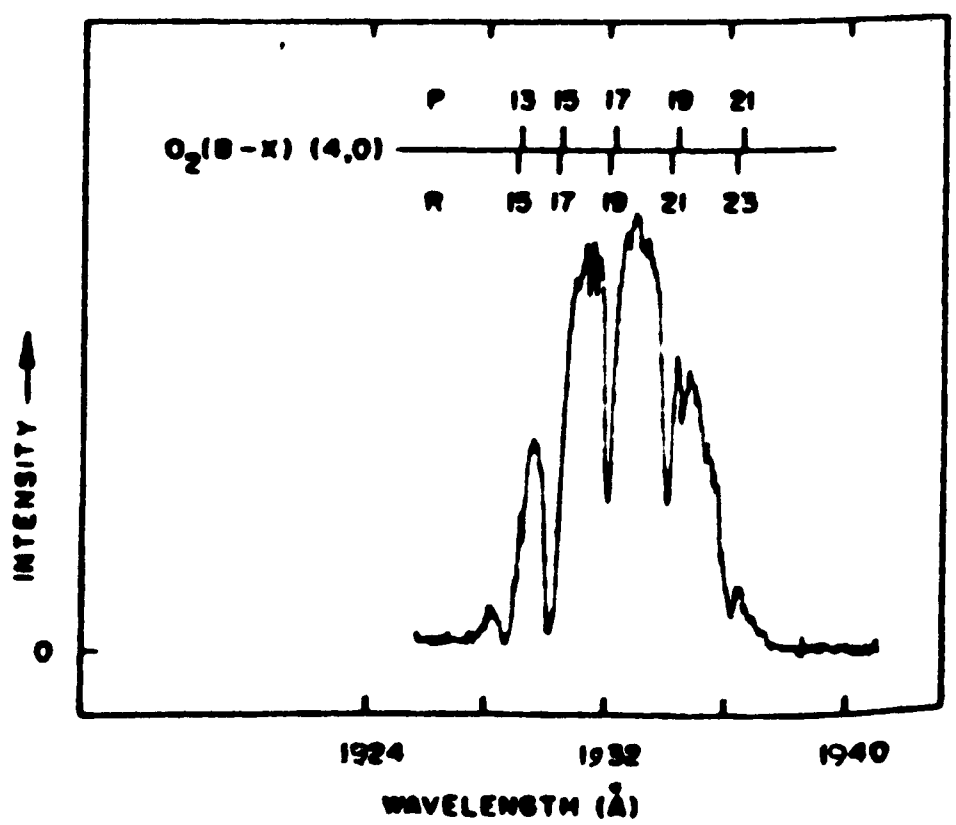


Figure 2.2 ArF Lasing Spectrum

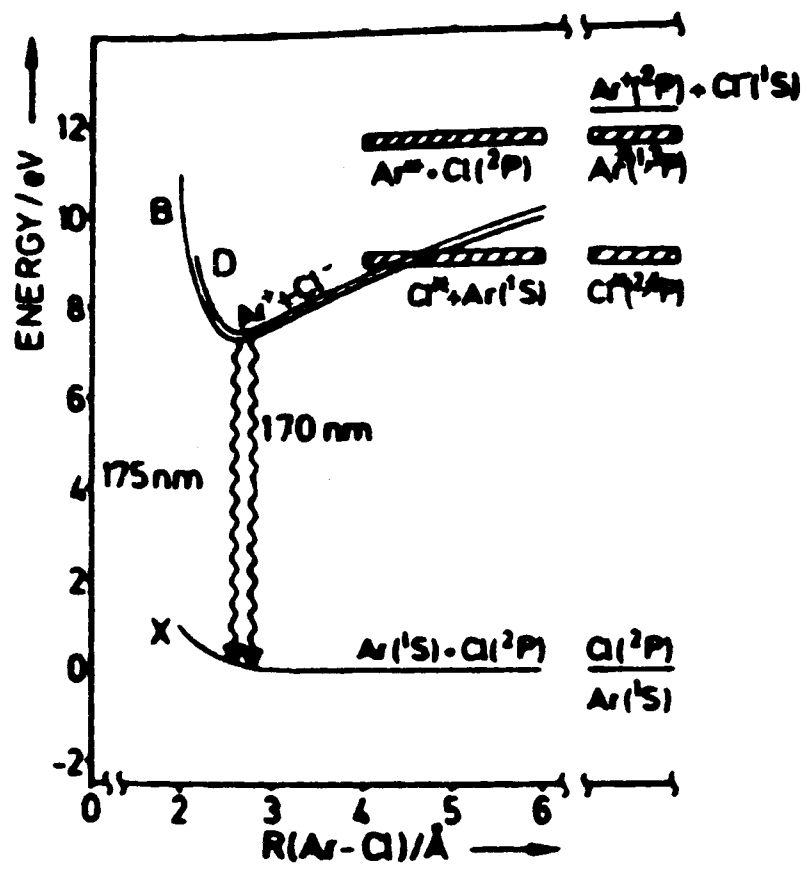


Figure 2.3 ArCl Term Diagram

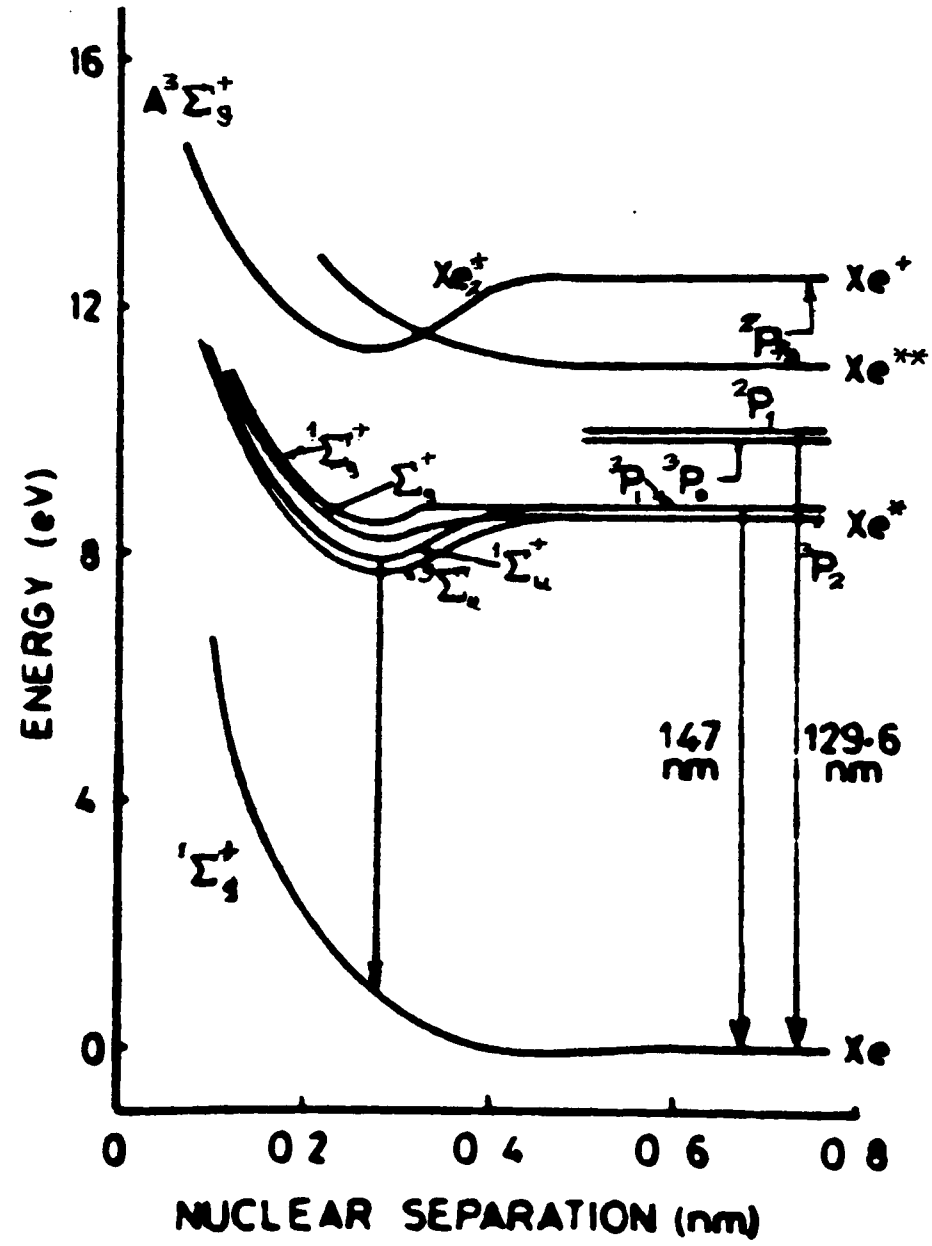


Figure 2.4 Xe_2 Term Diagram

HYDROGEN TERM DIAGRAM

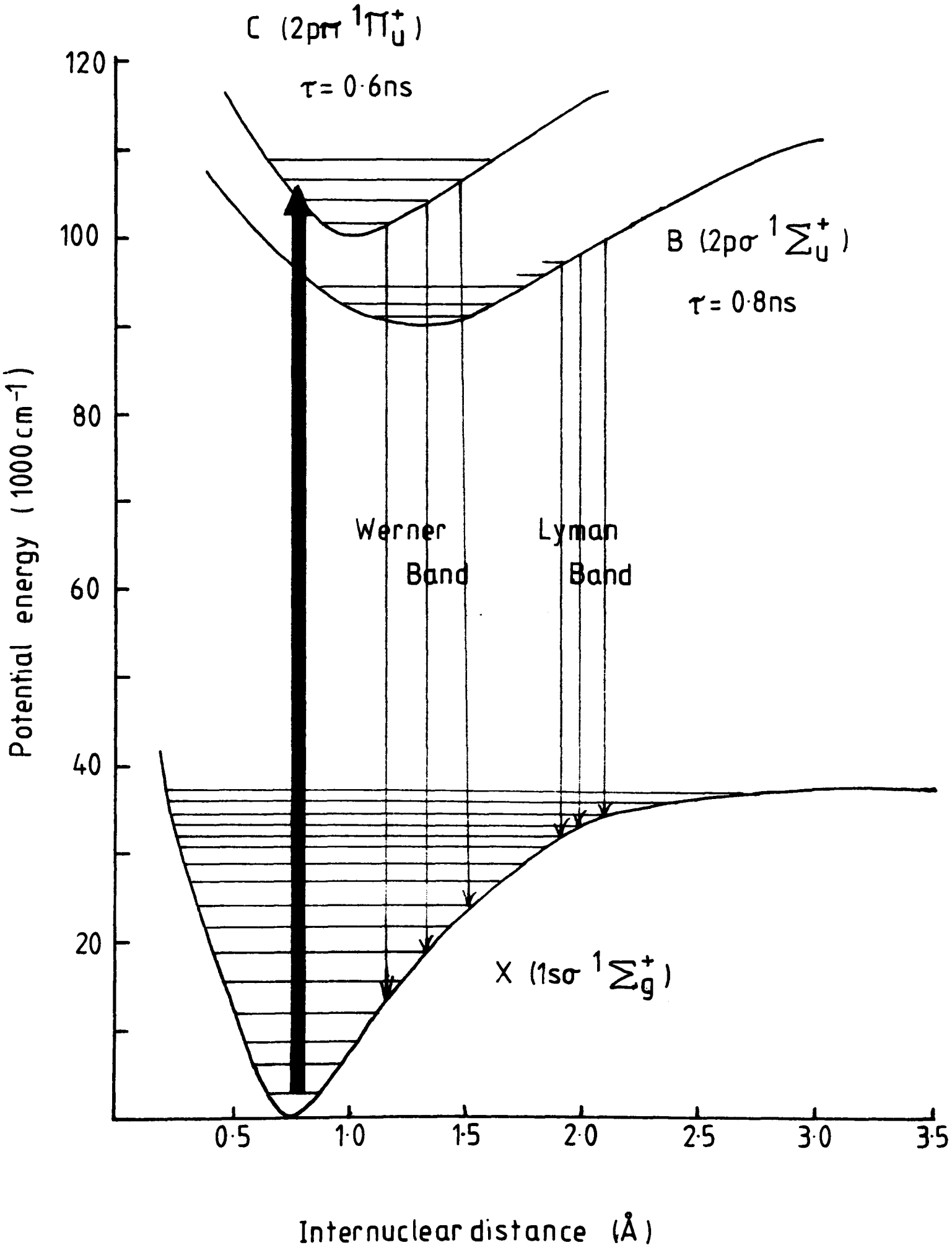


Figure 2.5 Hydrogen Term Diagram

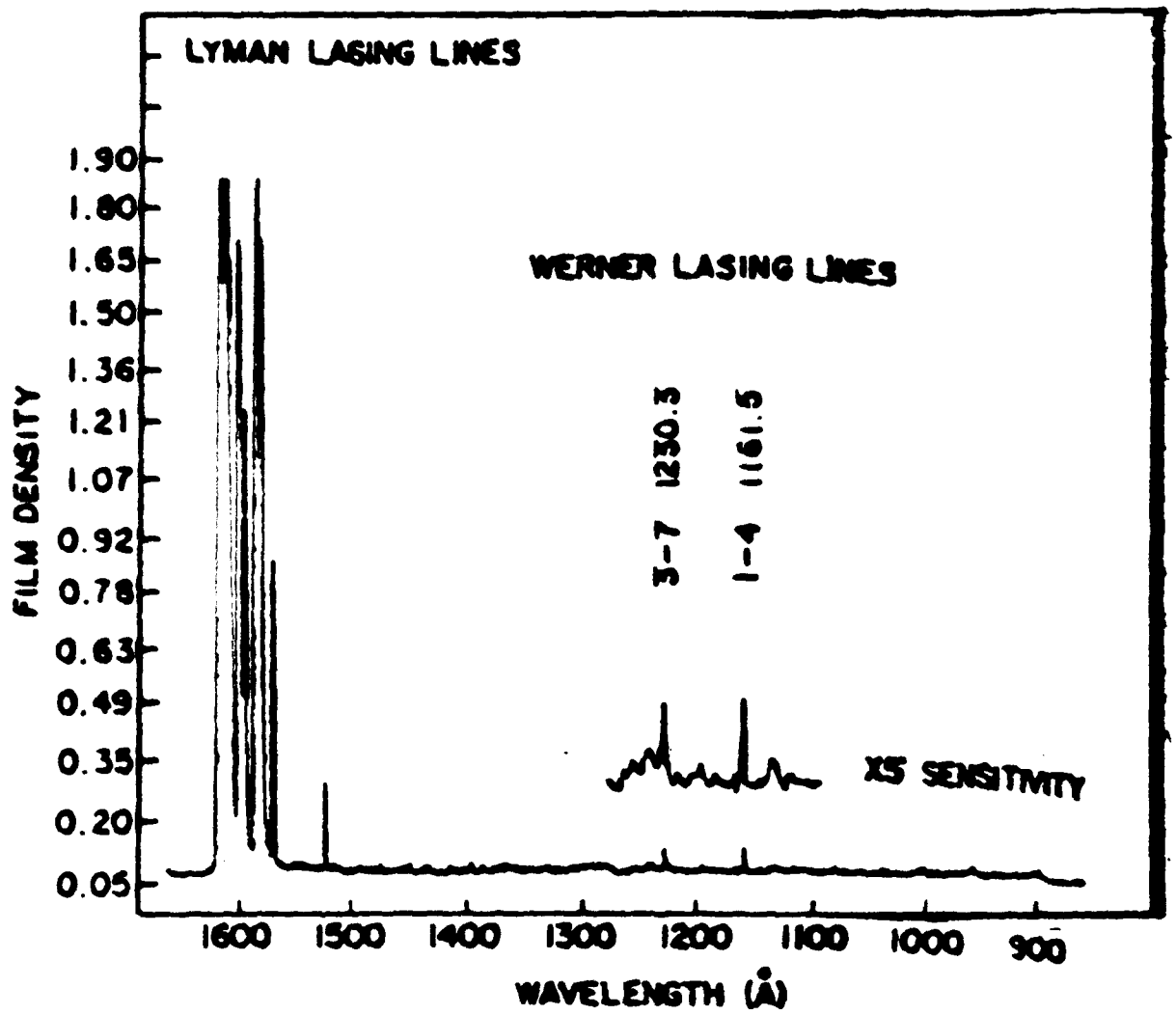


Figure 2.6 Lasing Lines of Molecular Hydrogen

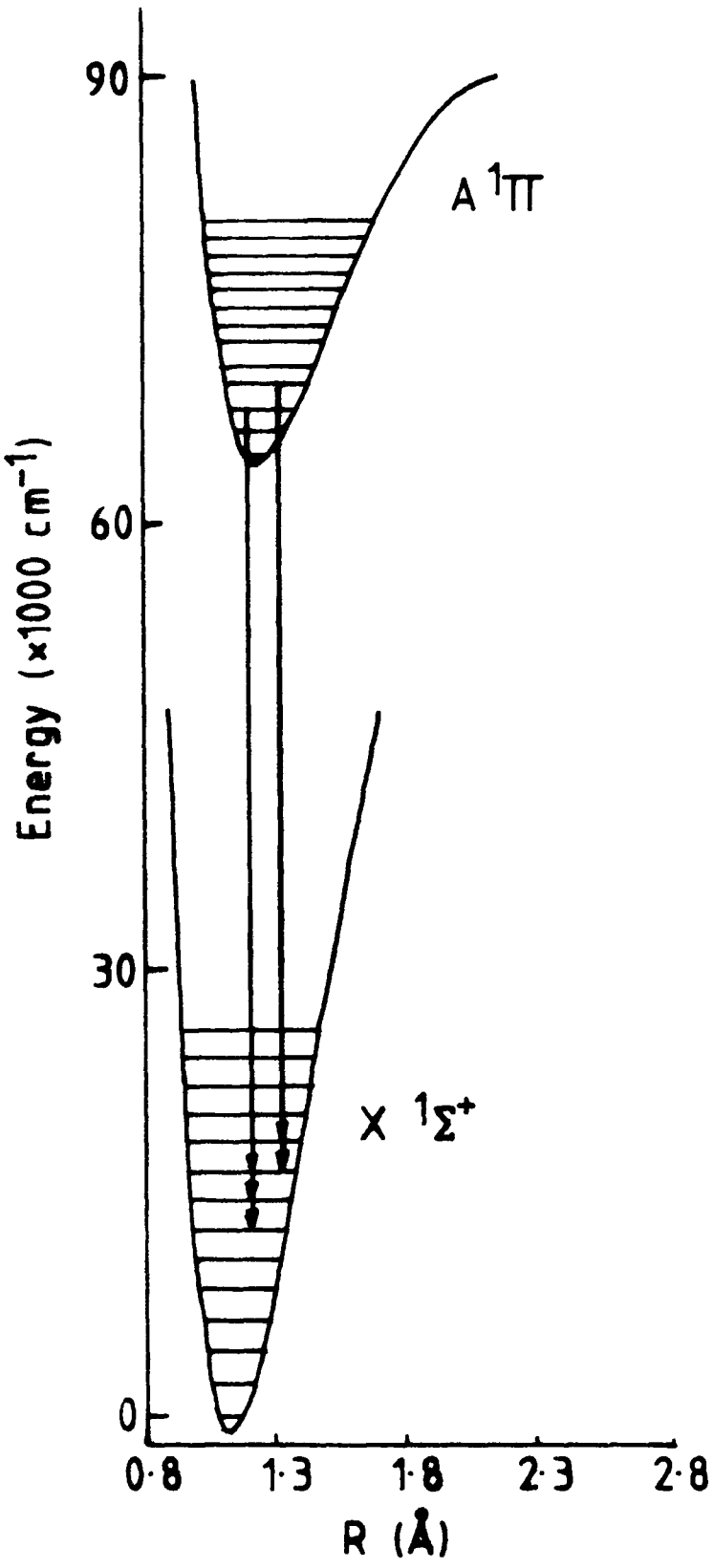


Figure 2.7 CO Term Diagram

CHAPTER 3 : MOLECULAR FLUORINE LASER

3.1 INTRODUCTION

As was concluded in the last chapter, the molecular fluorine laser shows most promise as a discharge excited VUV laser for practical applications. However, at the outset of the present studies, the fluorine laser had two severe disadvantages: a short gas fill lifetime and low pulse energy. The first of these would increase the down-time of the laser, and the second would reduce the range of its possible applications. The fluorine laser was thus studied in this work to try to overcome these problems.

The first part of this chapter reviews the historical development of the fluorine laser. Next, the physical processes of the laser are discussed. Finally the laser system developed for this work is presented.

3.2 HISTORICAL REVIEW OF THE MOLECULAR FLUORINE LASER

Laser emission from molecular fluorine at wavelengths around 157nm was first observed by Rice et al (1977). This original device used a large (4kJ) electron beam source to provide the excitation of the dilute mixture of fluorine in helium gas. Woodworth and Rice (1978) carried out further experiments with electron beam pumping, and found that high excitation fluxes (energy deposited per square centimetre per second) were essential to efficiently extract the energy from the fluorine laser. They also concluded that the best cavity consisted of high reflectivity rear mirror and an uncoated MgF_2 flat disc as output coupler.

Laser action on the same transition in a device pumped by discharge only was first reported by Pummer et al (1979). This device used a plastic-bodied gas envelope. Pummer et al noted a very rapid fall off in the laser energy with the number of shots. Also they were only able to achieve laser action

when they restricted the discharge volume, thus increasing the deposited energy density a result consistent with the findings of Woodworth and Rice. The maximum laser output pulse energy in the VUV achieved by Pummer et al was 8.5mJ. More recently Cefalas et al (1985) have made measurements of laser gain in a plastic bodied discharge tube, utilising a disconnected internal capacitor design. Again a rapid fall-off of energy with number of shots was observed. They attributed this to the build up of organic molecules, from the decomposition of the gas envelope,causing strong absorption in the VUV.

All of these devices operated with a gas mix of a few millibar of fluorine in a few bar of helium as buffer gas. Replacement of some or all of the helium with neon was found to be detrimental to the laser in terms of output energy and efficiency. In these publications, values for the optimum pressure ratio of $He:F_2$, and the optimum total helium pressure were found for the system. The optimum total pressure could not always be reached due to the gas envelope construction imposing too low a limit on the maximum pressure it could withstand.

3.3 LASER TRANSITION : SPECTROSCOPY OF THE FLUORINE MOLECULE

The laser spectrum was studied at a resolution of 0.03nm by Woodworth and Rice (1978). They found three lines at 157.48, 157.59 and 156.71 nm (see Figure 3.1). However, Pummer et al (1979) in their discharge pumped device only observed the transition at 157.5nm. They were unable to resolve this into two components at the available spectral resolution of their detection system. Woodworth and Rice assumed that the energy gap between the two lines at 157.5nm represents the energy of a rotational transition in fluorine; while the splitting between this set of lines and the line at 156.71nm represents the energy of a vibrational transition.

Recently McKee (1985) reported the laser emission spectrum, of a

commercial molecular fluorine laser, obtained using an 18m Eagle-mount vacuum spectrometer. The spectrum consisted only of two lines: a weaker one with a vacuum wavelength of 157.5233nm, and the stronger one at 157.6299nm. The published spectra does not extend to the wavelength of the 156.71nm line observed by Woodworth and Rice, and an implication of this could be that they did not observe laser emission at that frequency, as Pummer had not. The discrepancy between the vacuum wavelengths for the two laser emission lines measured by McKee and the wavelengths measured by Woodworth and Rice could be due to the latter authors quoting an effective air wavelength. This could arise from Woodworth and Rice having wrongly calibrated their evacuated spectrometer. The given vacuum wavelengths are both longer than the corresponding air wavelengths by a factor of the refractive index of the air (n=1.00029), to the quoted accuracy (+/- 0.01nm) of the measurements of Woodworth and Rice. It is expected that the wavlengths of McKee are reliable. It is the vacuum wavelength of the laser radiation that is the important quantity for applications of the fluorine laser in photoabsorption studies.

The laser transition has been identified (Tellinghuisen, 1977) as being of type $^3\pi_{2g} - {}^3\pi_{2u}$. This is analogous to the 342nm system in I_2, the 292nm system in Br_2 and the 258nm system in Cl_2. On all of these transitions laser action has been observed. In most cases the excitiation technique employed electron beam pumping. The laser transition has been marked on figure 3.2, which also shows the $^1\Sigma^+_g$ molecular ground state. Some information on the lower laser levels has been obtained from studies of electron energy loss spectra (Nishimura et al, 1979) and agrees well with the theoretical calculations of Cartwright and Hay (1979). The latter authors calculate the $^3\pi_u$ state to have a shallow potential well minimum with R_e=0.1881nm and a dissociation energy of 0.15eV. The vibrational frequency (ω_e) for this level is given as $303cm^{-1}$, and it is predicted to support five bound vibrational levels. At the equilbrium internuclear separation of the ground state

(0.142nm), the $^3\Pi_u$ state lies at 3.32eV.

The upper laser level was not observed in the electron energy loss measurements of Wang et al (1979) or Nishimura et al (1979). Nishimura et al postulate that this could be due to the upper state having a large equilibrium internuclear separation and therefore a small Franck-Condon factor for direct excitation from the ground state. Cartwright and Hay (1979) predict a group of states dissociating to $F^+(^3P) + F^-(^1S)$, among which will be the $2^3\Pi_g$ state, lying at 10eV above the ground state an R_e of 2.0 to 2.2Å. This state, because of its charge transfer nature compared to the essentially covalent bond of the $1^3\Pi_u$ state, should produce a strong $2^3\Pi_g$ - $1^3\Pi_u$ emission. These values, along with the calculated energy for the $1^3\Pi_u$ state at 2Å of 1.72eV relative to the ground state, gives an estimated value for the $2^3\Pi_g$ - $1^3\Pi_u$ transition energy as 8.3eV (λ=149nm).

Diegelmann et al (1982) used a high energy electron beam to excite a high pressure gas mix containing flourine, and an optical multichannel analyser to study the fluorescence spectra at a resolution up to 0.02nm. They noted a number of progressions with a measured sequential distance of 280cm^{-1}, in reasonable agreement with calculations of Cartwright and Hay. A sharp break-off of the band sequence at 149.7nm was observed. This would agree with the above calculation for the $2^3\Pi_g$ - $1^3\Pi_u$ transition into v"=0. These authors also calculated the molecular constants for the $^3\Pi_g$ state. The dissociation energy is 5.946eV, the equilibrium internuclear separation is 2.121A and the vibrational constant, ω, is 509cm^{-1}.

As stated before, lasing in molecular fluorine has been observed at 156.71, 157.48 and 157.59nm in high pressure binary gas mixtures. It has been suggested that the larger splittings (312 and 356 cm^{-1}) corresponds to different rotational lines for one pair of vibrational levels. From the quoted values, this splitting would seem to correspond best to that of the lower laser level. In the high pressure laser system the vibrational relaxation time due to collisions at a gas kinetic rate will be of the order

of a few nanoseconds. It therefore seems likely that under practical conditions the upper level is vibrationally relaxed before it undergoes the laser transition, and that all the laser lines start from v'=0. The fact that the measured laser wavelength is longer than that corresponding to the transition energy calculated above suggests that the laser transition terminates on an excited vibrational level of the $^3\pi_u$ state. It is reasonable to expect this state also to be vibrationally relaxed, and so any population in this state will be in the lowest vibrational level. It is therefore more likely that a population inversion will be achieved with respect to the higher vibrational levels, and reasonable to assume that the laser transition would terminate on an excited vibrational level. Furthermore, due to the weakly bound nature of this state with D_e=5kT, collision induced dissociation will also be a factor in maintaining the inversion. The $^3\pi_g$ state is the lowest of all the ionic states and is expected to be the one most populated under collision dominated conditions.

Thus, all of the available information points to the identification of the laser transition as $2^3\pi_g - 1^3\pi_u$ as being the correct assignment.

3.4 KINETIC MODEL

Detailed kinetic schemes to explain the excitation mechanism of the molecular fluorine laser have been proposed by Woodworth and Rice (1978) and Diegelmann et al (1982), both of whom used high energy electron beams for excitation. Woodworth and Rice used a 50ns exictation pulse, while Diegelmann et al produced their electron beam from a high voltage pulse lasting 5ns (FWHM).

The electrons in the high energy tail of the electron energy distribution collide with the helium atoms to produce helium metastables (He^*) and electron - ion pairs (He^+/e^-). Because of the relatively high pressures of the gas mixture there is a high probability that three body

collisions involving He^+ or He^* can take place to form molecular ions and rare gas excimers. The molecular ions can undergo dissociative recombination to form helium metastables. There are a number of possible reactions for these excited species with fluorine:

Exothermic charge transfer

$$He^+_n + F_2 \rightarrow F^+_2 + nHe \ (n=1,2,3...) \qquad 3.1$$

Penning ionisation

$$He^*_n + F_2 \rightarrow F^+_2 + e^- + nHe \ (n=1,2) \qquad 3.2$$

Dissociation

$$He_n + F_2 \rightarrow F + F^* + nHe \ (n=1,2) \qquad 3.3$$

This last reaction probably proceeds via a harpooning reaction to produce an excited rare gas halide (HeF^*), which then rapidly predissociates to give the excited fluorine atom.

Electrons of low energy undergo rapid dissociative attatchment to fluorine molecules via

$$F_2 + e^- \rightarrow F + F^-. \qquad 3.4$$

Electrons may also recombine with positive molecular fluorine ions via

$$F^+_2 + e^- \rightarrow F + F^*. \qquad 3.5$$

Excited fluorine atoms are also produced from collisions of F^- with F^+_2 or He^+_n. These excited atoms may be produced in many states, but rapidly decay to the lower levels of the ^2P and ^4P systems which are the lower laser levels for the red atomic fluorine laser transitions. Fluorine atoms in these states constitute a long lived energy reservoir because they have a long effective lifetime because of resonance trapping. They are able to undergo exchange reactions with fluorine molecules to form the ionically bound excited fluorine molecule,

$$F^* + F_2 \rightarrow F^*_2 + F. \qquad 3.6$$

It is expected that each helium metastable, or ion/electron pair,

originally produced will give rise to an excited fluorine molecule with negligible loss. Loss mechanisms for the excited $^3\Pi_{2g}$ states include spontaneous decay and collisional quenching

$$F^*_2(^3\Pi_{2g}) \rightarrow F_2(^3\Pi_{2u}) + h\nu(157.5nm) \quad 3.7$$

$$F^*_2(^3\Pi_{2g}) + e^- \rightarrow F_2 + e^- \quad 3.8$$

$$F^*_2(^3\Pi_{2g}) + F_2 \rightarrow 2F_2 \quad 3.9$$

As helium is not an efficient quencher of excited states it is not expected to play a large part in quenching the $F^*_2(^3\Pi_{2g})$ states.

The upper $^3\Pi_{2g}$ level for the laser transition at 157nm dissociates to an ionic pair, $F^-(^1S_0)$ and $F^+(^3P_2)$, whilst the lower laser level is covalently bonded. In this respect the molecular fluorine laser system is similar to that of the RGH lasers. In that case, Kearsley et al (1979a) have shown that the dominant formation rate is through the ion channel for conditions occurring within a fast discharge. It might be expected that similar mechanisms would play a part in the F_2 laser. The excitation kinetics would then be in accordance with the following scheme.

Transfer of energy from the electron swarm to the helium atoms forming ions and metastable states.

$$He + e \rightarrow He^* + e \quad 3.10$$

$$He + e \rightarrow He^+ + 2e \quad 3.11$$

Dissociative attatchment of electrons to the fluorine atoms.

$$F_2 + e \rightarrow F^- + F \quad 3.12$$

Production of positive fluorine ions via excited fluorine atoms.

$$He^* + F_2 + He \rightarrow F^* + F + 2He \quad 3.13$$

$$F^* + e \rightarrow F^+ + 2e \quad 3.14$$

Formation of excited fluorine molecules via three body recombination.

$$F^- + F^+ + He \rightarrow F_2^* + He \quad 3.15$$

The excited fluorine molecules are thus formed by ionic recombination in

the presence of a third body (a helium atom). The rate for the recombination reaction will increase with the helium pressure. Thus the F_2 laser is expected to operate most efficiently at high helium pressures.

3.5 LASER DESIGN

3.5.1 Design criteria

One major objective of the present work was to try to develop the molecular fluorine laser to a state where it could be useful as a laboratory and industrial tool for the sort of applications discussed in section 1.2. In this case, cost and size restrictions dictate that the device should be pumped by a discharge rather than by an electron beam since such devices are large and expensive. There is a need for a long gas fill lifetime to decrease the downtime for the laser and also to ensure good shot to shot reproducibility on a long timescale. Prior to this work commercially available fluorine lasers had pulse energies in the 10-15mJ range.

3.5.2 Gas envelope

As indicated by previous publications in the field, the decline of laser energy with number of shots occurs because of incompatibility of the gas envelope material with the fluorine-containing gas mixture, especially under discharge conditions. Therefore in this work care was taken in the selection of the materials within the gas envelope so that they should be fluorine compatible and unlikely to produce gaseous impurities in the presence of UV radiation from the discharge. A second approach prolonging the gas lifetime was also adopted: the gas mixture was circulated through a cryogenic trap. The action of the trap is to remove almost all organic impurities produced by the discharge, as well as those originally present in the gases.

It had been noted that in previous publications the laser output energy increases with increasing helium buffer gas pressure, but that the optimum

condition could not always be reached due to insufficient mechanical strength in the gas envelope. Therefore for the present work a gas envelope capable of withstanding high over-atmospheric pressures was used.

The basic laser head gas envelope consisted of a brass tube 620mm long with an outside diameter of 200mm. Flanges were hard soldered onto the ends of the tube so that end plates could be bolted on. These completed the gas tight envelope using an O-ring seal. As can be seen from figure 3.4, the laser ran with a discharge whose long axis was horizontal. The electrode assembly was supported by a base plate which carried the earthed electrode and was held fixed inside the tube. The top electrode was supported by four PTFE yokes along its length to maintain a constant electrode separation. The electrode length was 540mm.

The high voltage supply to the electrodes was brought in via four PTFE feedthroughs, to provide insulation of the central conductor from the case of the tube, which acted as the earth return for the circuit. The castellations along the sides of the feedthroughs provide a longer surface distance from the exposed end of the conductor to the tube body, and thus inhibits breakdown by surface tracking. The design of the electrodes themselves evolved throughout the course of this work, and will be described later. All the exposed metal surfaces within the laser body were coated with nickel to enhance their compatibility with the fluorine gas.

In spite of this it was still necessary to passivate the laser tube when new and after exposure to the atmosphere. The passivation proceedure involved evacuating the tube and then filling with about 10mbar of fluorine. The tube was left with this gas fill for a while, during which time the fluorine would undergo a reaction with the surface layer of the metal to form a layer impervious to further attack by fluorine. After passivation the first laser gas fill did not degrade extremely rapidly due to further fluorine loss.

The laser gas envelope was pressure tested to 11.5bar. This was felt to be more than adequate to achieve the optimum pressure for laser operation.

3.5.3 Gas handling

The laser head design described above embodied all of the features discussed earlier for prolonging the gas lifetime. In addition gas lifetime extension was promoted by circulating the laser gas mix through a cryogenic gas trap. The trap design has been described in section 1.5. A schematic diagram of the connections for this circulating loop is shown in figure 3.5. As discussed in section 1.5, oxygen has a very large absorption coefficient of $200cm^{-1}atm^{-1}$ at the fluorine laser wavelength. This means that besides taking care that the impurities due to decomposition of materials from which the laser tube is constructed are kept to a minimum, it is necessary to prevent air leaking into the tube, especially as it is evacuated between experiments. It is therefore a prime reqiurement that the entire gas handling system be made as free from leaks as possible. This will also enable the tube to be periodically cleaned out by pumping on it at a low pressure for an extended period to remove any impurities which have been adsorbed into the internal surfaces.

Initially, PTFE tubing was used in the circulation loop and connected via Swagelok compression fittings. However it was found difficult to obtain a satisfactorly low leakage rate with this method. Subsequently all the tubing was replaced with copper tubing. As many joints as possible were made by hard soldering the copper tubing into brass fittings. For the other necessary joints, mainly to allow the inclusion of taps in the system, compression joints employing O-ring seals which are specifically designed for vacuum operation were used. Even so, some of the Swagelok compression fittings were still needed. By these methods it was possible to achieve a leak rate of only $2.5x10^{-5}$ l atm min^{-1}.

3.5.4 Discharge excitation circuit

Woodworth and Rice (1978) pointed out that high energy excitation fluxes

were necessary for efficient operation of the fluorine laser. Thus, for discharge excitation a fast discharge circuit is necessary. A Blumlein circuit using transmission lines for energy storage would give a fast excitation pulse (see appendix 1). However to provide enough energy to effectively pump a large discharge volume at a high energy density the transmission line would be large and cumbersome and would not satisfy the reqirement for a bench-top laser. As a practical compromise it was decided to utilise a capacitor transfer discharge circuit (see appendix 1).

The physical arrangement of the fast discharge circuitry employed is shown in figure 3.4. It embodies the internal capacitor automatic preionisation technique introduced for rare gas haldide lasers by Kearsley et al (1979b). Placing the peaking capacitors close to the electrodes reduces the impedance of the final discharge loop and decreases the rise time of the excitation pulse. The peaking capacitors comprise sintered barium titanate "buttons" potted in epoxy to increase the tracking distance between their terminals to insulate them to the required working voltage. The epoxy cladding not only adsorbs many impurities which can be released into the laser gas, but also produces many cracking products when subjected to irradiation by the UV light of the discharge. The capacitors are therefore coated in PTFE before final assembly.

As shown, a gap of about 3mm is deliberately left between one terminal of each capacitor and a pin protruding through the the opposing high voltage electrode plate. As the voltage on the plate increases, after the main spark gap is triggered, the preioniser gaps break down forming arcs which allow the capacitors to charge. The UV light from the arcs irradiates the main discharge volume and ionises some of the species present to provide preliminary ionisation. As the peaking capacitors charge up, the voltage across the main gap increases until it eventually breaks down. This occurs at a higher voltage than the static breakdown voltage since the fast rising leading edge of the excitation pulse allows significant overvoltage to be

achieved. The peaking capacitors discharge via the small gaps and into the main discharge volume. The excitation of the laser gain medium lasts about 30ns before the discharge instabilities cause a termination of the glow discharge phase.

The electrical connections to and from the main storage capacitor were made via copper strip lines, rather than wires. The high voltage strip line was wide enough to be connected to all four high voltage feed-throughs into the laser head. The earth return was kept close to the high voltage strip line, separated by a Perspex insulating sheet, to reduce the area enclosed by the discarge loop. Reducing this area reduces the inductance of the larger discharge loop and further increases the rate at which the energy stored in the main capacitor can be deposited in the discharge volume.

3.5.5 Optics

The optical cavity employed for the fluorine laser consisted of a magnesium fluoride optical flat and a magnesium fluoride overcoated aluminium mirror. The magnesium fluoride flat was 20mm in diameter, and the pyrex substrate for the mirror was 25mm in diameter. Both were polished to a flatness of $\lambda/10$ in the visible region. The reflectivity of the mirror was not known exactly, and would in any case be a function of the age of the coating. However the MgF_2 coating was specified to give peak reflectivity at 157nm and its reflectivity would be approximately 85%. The output coupler was 3mm thick to give the desired mechancial strength to withstand the pressure difference across it at the highest working pressures (allowing a reasonable safety factor of 4). At 157nm, MgF_2 is calculated to provide a total reflectivity of 6% from both surfaces, and a transmission of 62%, allowing for absorption in the bulk of the material. The length of the optical cavity was 700mm.

The optics used for this laser were of a relatively delicate nature. Therefore, special window holders were designed which would hold the

optics onto an O-ring seal against the high pressure inside the tube, but would not allow them to be damaged by overtightening. These metal window holders were sealed onto the end flanges of the laser via another O-ring seal, and were held in place by four screws. The natural compressibility of the O-ring was used to enable the cavity mirrors to be aligned by adjusting the screws.

3.5.6 Radiation detection

The output pulse energy was measured using a pyroelectric detector (Gentec Model ED-200) with a sensitivity of 9.83V/J into 1MΩ. According to the manufacturer the calibration process is claimed to have an accuracy better than 10%. The only wavelength dependent element of the detector is the black absorption coating on which the pulse is incident. This has a constant low reflectivity of less than 2% down to 200nm, but at shorter wavelengths it starts to increase. Manufacturer's information on the reflectivity below 200nm is not precise, but at 157nm it is about 30%. Thus the actual calibration factor at 157nm is 6.9V/J to 10% accuracy.

Because of the strong absorption in air of the laser radiation, the detector was placed in a chamber that was sealed to the laser output window. Initially, the chamber was evacuated by a rotary pump, but it was found that at the lowest pressures attained a discharge would strike through the chamber and back to the pump. The discharge occurs because the "earthed" metal body of the laser can float up in volts transiently during the fast discharge pulse because of the inductance of its connection to earth. This discharge, close to the detector, produced spurious readings. To overcome the problem of the discharge in the detector chamber, helium gas was flowed through the detector chamber at a pressure of about 100mbar, which effectively prevented any discharge. The detector output was monitored on an oscilloscope.

3.6 CONCLUSION

In this chapter the molecular fluorine laser has been presented in detail. After a review of the historical development of the laser, a study was made of the energy levels of the fluorine molecule invovled in the operation of the laser, followed by the kine tic processes for the formation of the upper laser level.

The second part of the chapter concentrated on the laser system that was designed and built for this study and development of the VUV fluorine laser. Methods employed to increase the gas fill lifetime were discussed. The excitation system to be used for the laser was described. The performance of this laser is given in detail in the next chapter.

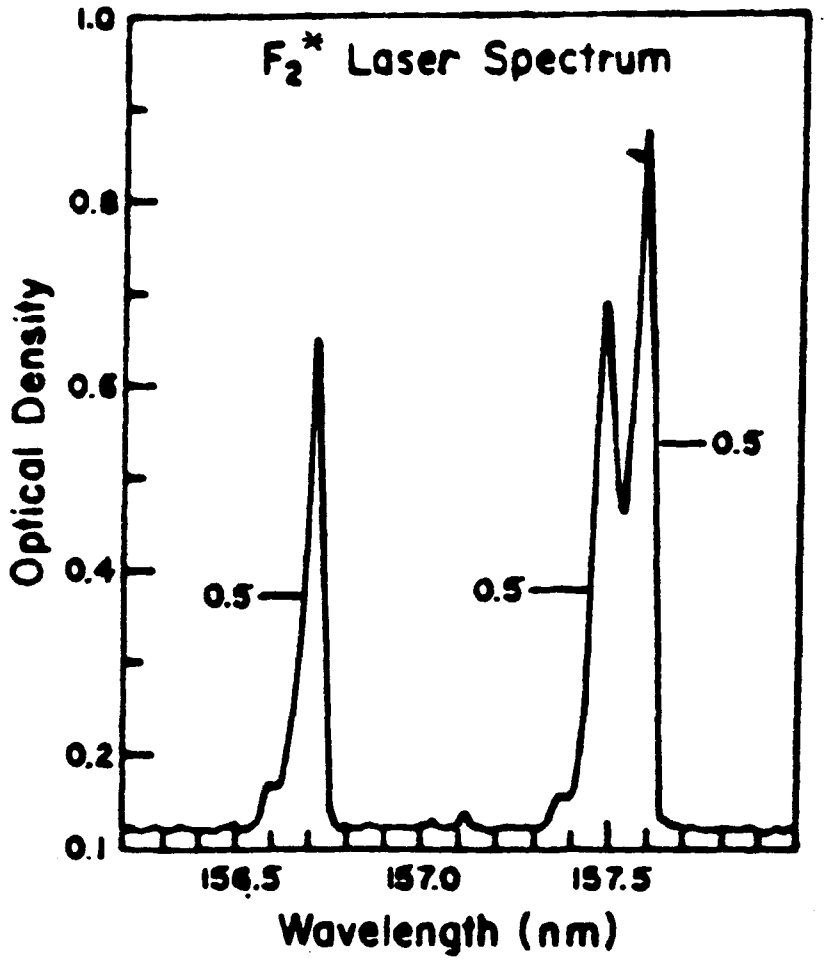


Figure 3.1 Fluorine laser spectrum

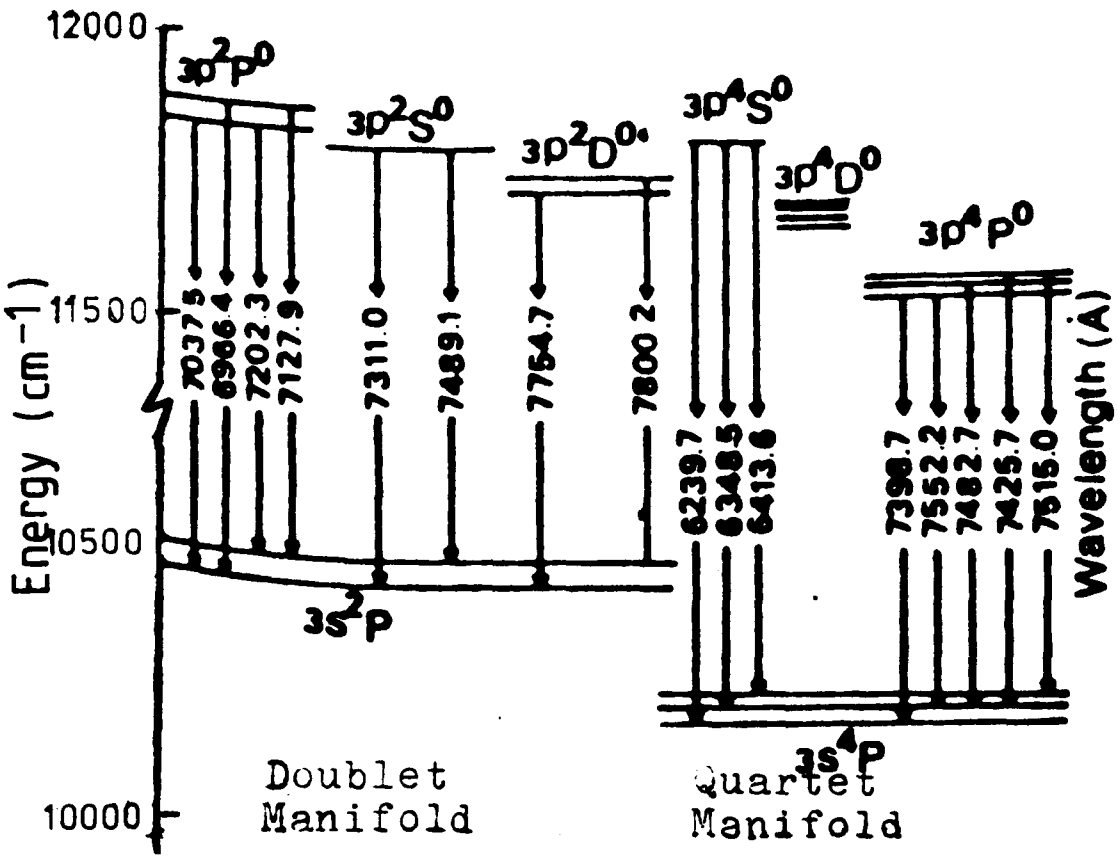


Figure 3.3 Atomic fluorine laser transitions

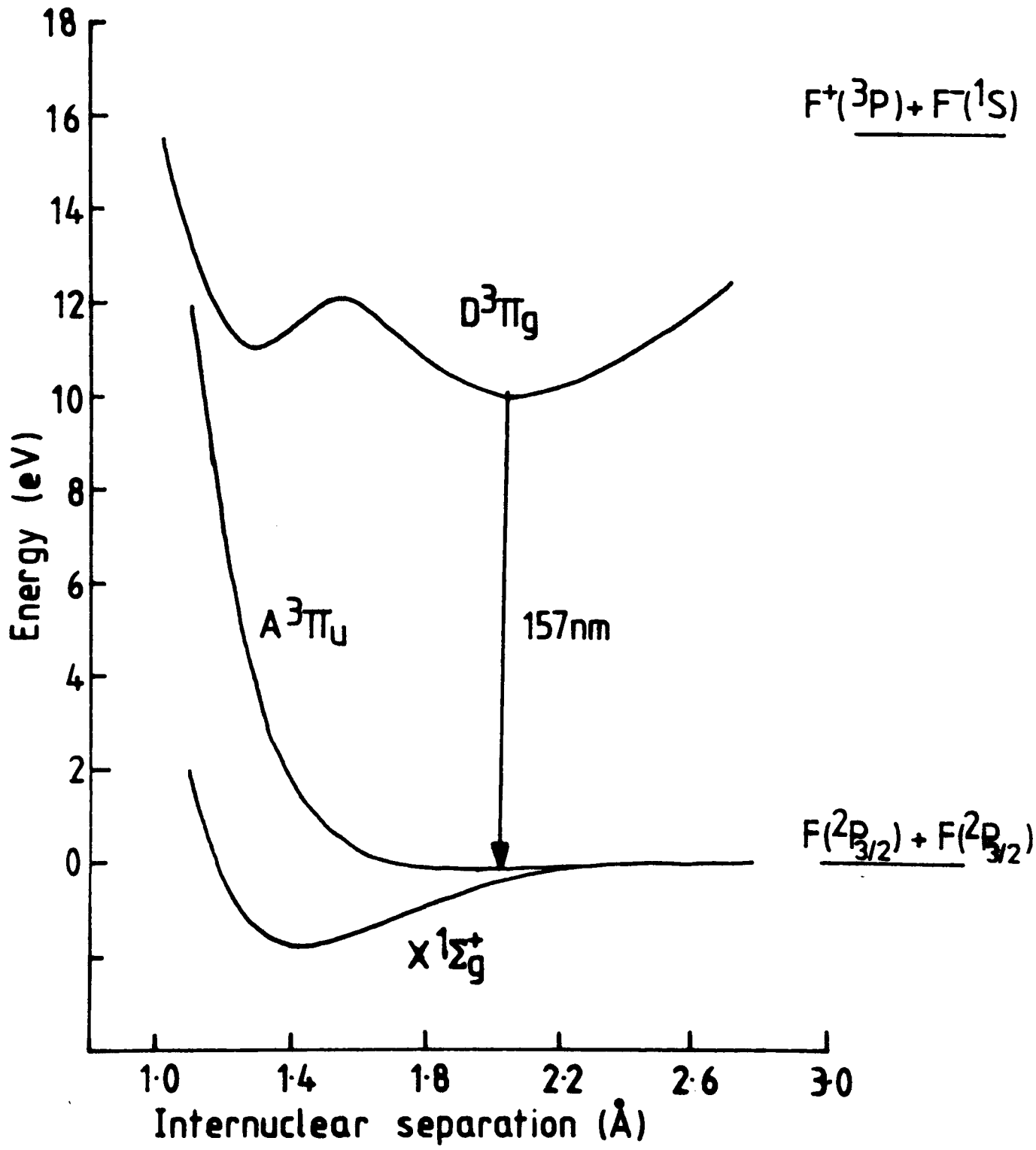


Figure 3.2 Fluorine partial term diagram

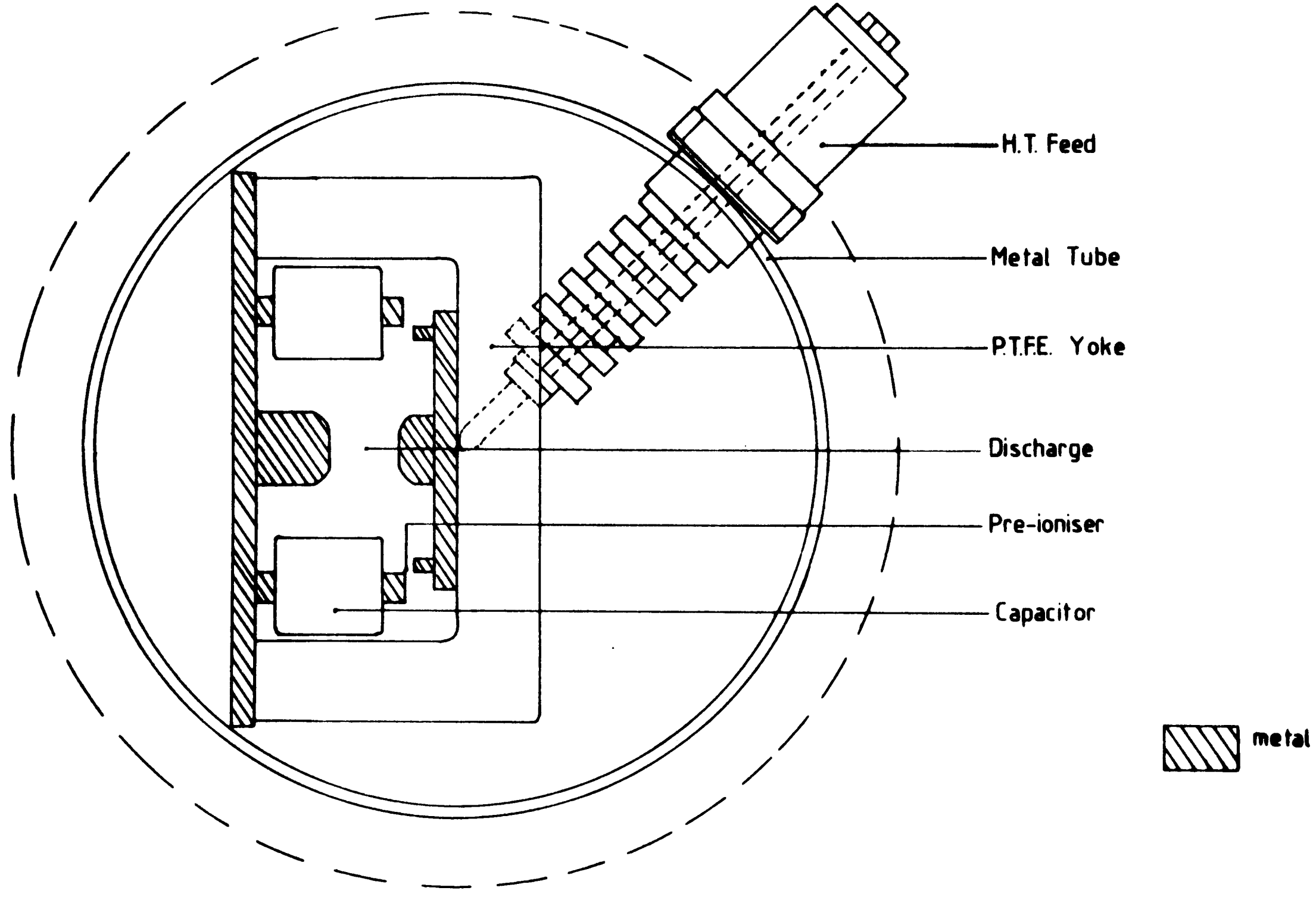


Figure 3.4 Laser tube structure

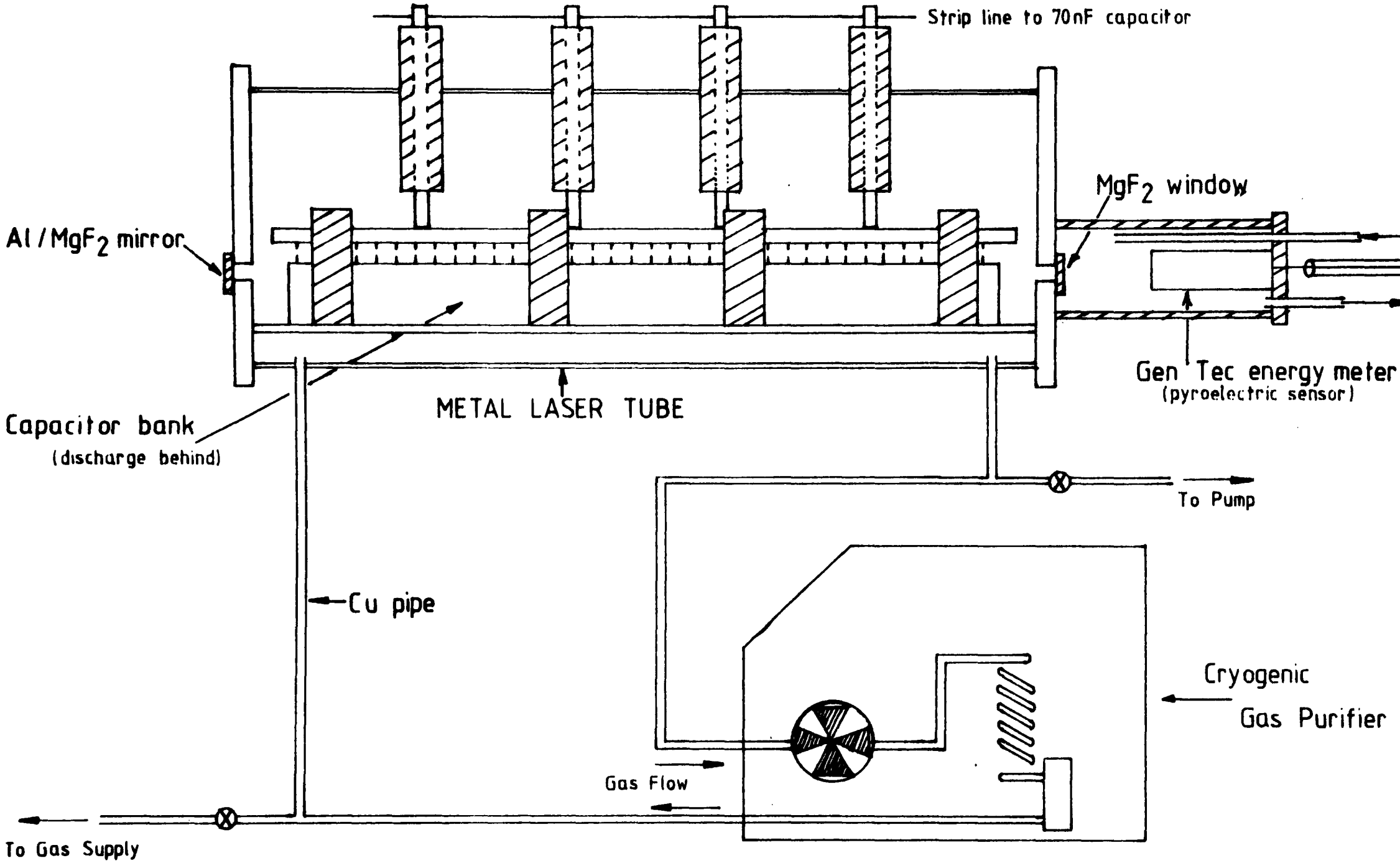


Figure 3.5 Gas circulation loop

CHAPTER 4 : OPERATIONAL PARAMETERS OF FLUORINE LASER

4.1 INTRODUCTION

In the previous chapters the fluorine laser has been introduced, and has shown to be a promising candidate for practical situations needing a VUV laser. In chapter 3 the design of a new laser system was presented for use in a study of the molecular fluorine laser. The aims of this investigation are to improve the perfomance of the fluorine laser in terms of efficiency, output pulse energy and gas fill lifetime. The details of this study are presented in this chapter, along with the results of the experiments characterising the operational performance of the laser.

4.2 INITIAL INVESTIGATIONS

The laser system was set up as described in the previous chapter. The internal peaking capac itance comprised 36 capacitors, each 625pF, giving a total of 22.5nF. The electrode profiles were half round, with a diameter of 12mm, and with a 3mm flat. Their spacing was 22mm. A circulation loop was arranged to purify the gas by circulating it through the GP2000 cryogenic gas purifier. The trap temperture was around 90K. The laser was passivated by circulating about 100mbar of a 5%F_2 in He mixture around the laser for 30 minutes. The cavity consisted of a MgF_2 output coupler and a MgF_2/Al mirror. The available optics limited the diameter of the output aperture to 15mm.

It was noticed that with gas mixtures comprising a few mbar of fluorine and up to about 2bar of helium, a red laser emission was produced. This emission was identified as the red and near infrared atomic fluorine laser. The excited atomic fluorine is produced by dissociative excitation of molecular fluorine on collisions with helium metastables (Sumida et al, 1979).

$$F_2 + He^* \rightarrow F^* + F + He \qquad 4.1$$

At pressures greater than 1bar, the populated upper laser level will belong to the quartet manifold (Sumida et al, 1979). The most likely transition is $3p^4S_{3/2} - 3s^4P_{3/2}$, with a wavelength of 634.85nm. There could also be some IR transitions at 740-750nm from a $3p^4P - 3s^4P$ system (see figure 3.3).

In the experiments for this work all these lines would be detected together by the energy meter (Gentec ED200) and would be indistinguishable. However the red and infrared lines could easily be distinguished from the VUV radiation by admitting air into the detector chamber. The air prevents the VUV from reaching the detector. Although the red lasing was no longer visible at total pressures above 2bar, a visible/IR component was measured on the energy meter for pressures up to 4.5bar. The red/IR contribution to the pulse energy did not alter much over a wide range of pressure and voltage values, and was always found to be in the 1.5-2.5mJ range. Thus, when measuring the VUV laser energy, this IR contibution could be eliminated by subtracting it from the readings taken. The red lasing was useful in the initial aligning of the laser system. The laser emission on the red atomic fluorine lines was used to fine tune the optical alignment of the laser cavity, and also as a guide in positioning the detector so that it would gather all the laser radiation.

Preliminary experiments showed that laser energy increased with voltage and pressure of helium for a given partial pressure of fluorine. A maximum of 12mJ was obtained in this arrangement with 4mbar F_2 and 3.4bar He at 45kV.

The effect of the cryogenic trap in extending the working lifetime of the gas was investigated. During one experiment the circulation compressor was turned off. The laser pulse energy fell from 13.6mJ to 8.7 mJ in 18 minutes. The compressor was then turned on again and the energy rose to 11.4mJ in 2.5 minutes and then gradually fell to 10mJ over the next 35 minutes. The experiments were performed at a pulse repitition frequency of 1

Hz.

4.3 IMPROVED PERFORMANCE

One method which might be expected to increase the laser energy is to increase the discharge volume. This was done by changing one of the electrodes for a 12x6mm bar with two shoulders of 6mm radius milled onto it giving a 'D' shaped profile. To effectively pump this discharge volume the number of internal capacitors was increased to 62, giving a peaking capacitance of 38.75nF, and the storage capacitor was changed to one of 69nF capacitance. The extra internal capacitors were placed as another row, offset and further from the discharge than the existing ones. Extensionswere made to the top terminal of these capacitors so that the preionising gaps through which they were charged up were in between the existing preionisers. Thus the number of preionisation arcs was almost doubled, giving a more uniform preionisation of the discharge volume.

To check the uniformity of the discharge the tube was filled with a KrF laser mix of 125mbar Kr, 175mbar F_2 and 3bar He, after changing the optics for 50mm diameter quartz ones (flat output coupler and an aluminium backcoated mirror). It was seen from the laser burn pattern that the discharge was split (fish tailing) towards the narrow electrode: the field enhancement at the corners of the electrode was encouraging the discharge in that region. This effect was independent of the polarity of the charging supply. To overcome this problem, the flat section across the top of the wide electrode was reprofiled so that it gradually curved away from the discharge region. The electrode was replaced as the high voltage electrode, and the narrow electrode became the earthed one. The electrode separation was 25mm. The KrF laser mix at 46kV now gave 0.4J . The burn pattern was recorded on Polaroid film and was seen to be rectangular with dimensions 25x12mm.

The MgF_2 optics were replaced on the laser, with the holder for the

output coupler redesigned so that it had a 16mm clear aperture. However, from simple geometrical arguments it can easily be shown that this aperture will only pass 57% of the energy contained in the 25x12mm beam.

The laser tube itself had been pressure tested to 10bar. The 3mm thick MgF_2 window clamped over a 16mm aperture (sealing onto an O-ring), is calculated to be able to withstand a 6.5bar pressure difference across it, with a safety factor of 4. It was thus considered safe to operate the laser at total pressures of up to 4.5bar, although in practice the maximum pressure was limited by the compressor in the purifier circulation loop.

To try to further increase the purity of the gases the helium was admitted to the laser tube via a BOC purifier (Model RGP III). This consists of a molecular sieve, and heated tubes containing copper oxide and titanium granules. It was found that the laser energy could vary between gas mixtures of the same proportions. This was taken as an indication that impurities were being carried in with the gas fill. Precautions used against this were to flush through all the gas lines from the cylinders before filling the laser tube, and the use of copper pipe lines as much as possible in preference to PTFE. It was felt that water and other undesirable substances might be able to permeate through the walls of the PTFE pipe in small quantities.

The laser was operated in this configuration with different gas mixtures and charging voltages to establish its optimum working conditions by monitoring the output energy. The energy values presented in figures 4.1 to 4.7 are the mean of a number of energy readings taken for each set of conditions. The voltage output from the GenTec meter was monitored on an oscilloscope. This value was then converted to an energy using the calibration factor for the meter (6.9V/J in the VUV), and scaled to the full beam value allowing for the limiting output aperture. As mentioned the IR component did not alter much with the varying conditions. This component is included in the the following results, but an upper limit of only 3mJ can be placed on it. For this series of experiments the trap temperature was in the

range 90-95K.

4.4 ENERGY SCALING RESULTS AND DISCUSSION

The results of laser VUV energy as a function of fluorine partial pressure, helium pressure and charging voltage are shown in figures 4.1 to 4.7.

As can be seen from the graphs the general trend is for the laser energy to increase with increasing helium pressure and increasing charging voltage. The turn-over in energy at high pressures appears to be due to incomplete breakdown of the gas at that pressure for the given applied voltage. This was particularly evident for some of the high pressures and low charging voltages, and could be visibly and audibly observed as the laser discharged. Another explanation for the turnover could be that at higher pressures in a helium discharge, e^-/He^+ pair production dominates over metastable production, and that the electrons then quench the excited molecular fluorine states. This argument was recently put forward by Cefalas et al (1985) to explain the results of their gain measurements. However, the former explanation is the more likely in view of the direct observations and the electron production not being expected to increase to such an extent that it grossly affects the electron density in the pressure range over which the effect is observed.

The increasing laser pulse energy as a fuction of the helium pressure probably reflects the faster reaction rates at higher buffer gas density, leading to an increased excitation rate for the excited molecular fluorine states, through a reaction such as equation 3.15. Helium is an inefficient quencher of the excited molecular fluorine states, and also of the precursor excited atomic fluorine states. Therefore increasing the helium pressure will have a overall beneficial effect on the upper laser level population.

Molecular fluorine itself is, however, an efficient quencher of the

excited molecular fluorine states. It would be expected that there would be an optimum partial pressure of fluorine in the laser gas mix to give maximum output energy. This will be because of the competing effects of increasing the fluorine concentration: on the one hand it will lead to an increase in the density of the upper laser level states due to increasing their rates of formation, and on the other hand there will be a reduction in their density due to increased quenching.

From the experimental results it is seen that, for a given helium pressure and charging voltage, there is a broad maximum in the output energy around a fluorine partial pressure of 7mbar. This agrees with results previously published. Woodworth and Rice (1978), in a electron beam pumped device, observed a broad maximum at a fluorine pressure of 9mbar, at a total helium pressure of 8.5bar. Pummer et al (1979), in their discharge pumped device found a broad maximum with a peak for a pressure of 6mbar, in 2.2bar of helium. Thus the optimum fluorine pressure would seem to be very much device independent, with little variation over a wide range of total pressures.

As the fluorine partial pressure is increased another effect is noticed: the helium pressure for which there is the turnover in energy, as a function of pressure, is reduced. This is due to the extra fluorine altering the characteristics of the discharge, and givng it a greater tendency to constrict.

4.5 CONCLUSION

It has been shown that it is possible to produce VUV lasing in fluorine with pulse energies of up 50mJ. This was achieved in a compact and relatively simple bench-top device without the need to resort to large electron beam devices.

However it is seen that for these devices to operate reliably extreme care must be taken to ensure that the impurity levels within the system remain

at low levels. This involves using high purity gases and ensuring that the gas system is suitably gas tight, as even a small quantity of air in the laser will drastically reduce its performance. In order to stop the build-up of impurities as the laser is running, attention must be paid to the materials used for the construction of those components in contact with the laser gas mix, especially if they are near the discharge area. Finally to remove any discharge products a cryogenic trap in a circulation loop has been shown to enable the laser to operate for considerable times on a single gas fill.

These properties of high energy and long gas lifetime means that the fluorine laser is now an effective proposition as a VUV laser source for a number of commercial and experimental operations.

This work indicates that further increase of the pulse energy of the fluorine laser is achievable by increasing the total pressure of the helium within the tube. The construction of laser tube used here would allow this. The circulation compressor could be changed for a high pressure rotary vane circulator, if one compatible with the fluorine containing gas mixture were available commercially.

The higher pressure would necessitate the use of higher charging voltages. This in turn might necessitate a slight increase in the overall size of the system to accommodate components rated for these voltages, and also to reduce the possibility of breakdown from the high voltage points. Alternatively, from the graphs it can be seen that by doubling the pressure, in the linear region, the pulse energy is approximately doubled. Thus the electrode separation could be reduced by half, and the tube pressure doubled to give the same energy from a smaller device, as the capacitances could be halved to keep the energy deposited in the discharge constant for the given charging voltage.

At present the molecular fluorine laser seems the most promising device for effectively producing VUV laser radiation.

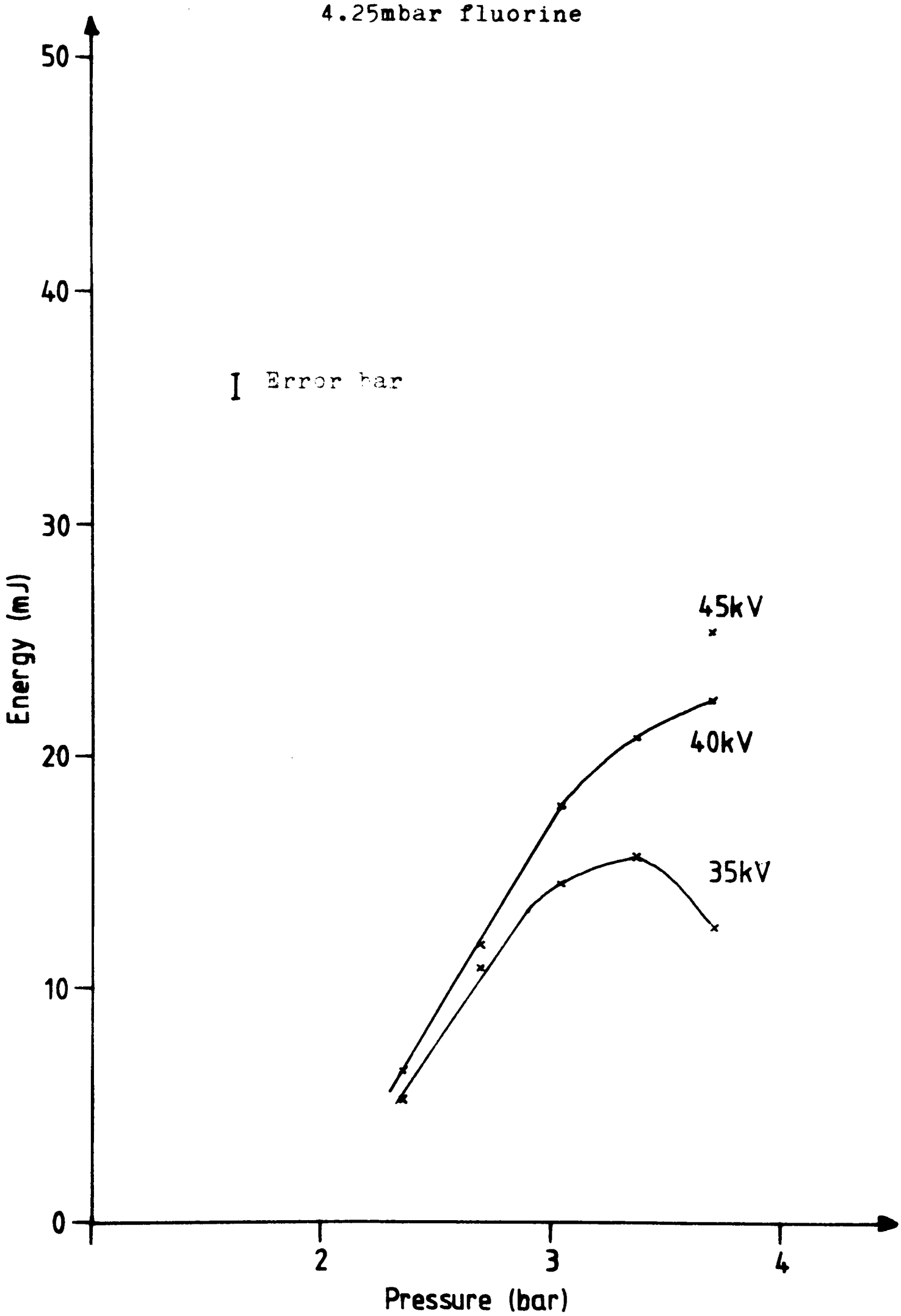


Figure 4.1 Laser energy as a function of helium pressure

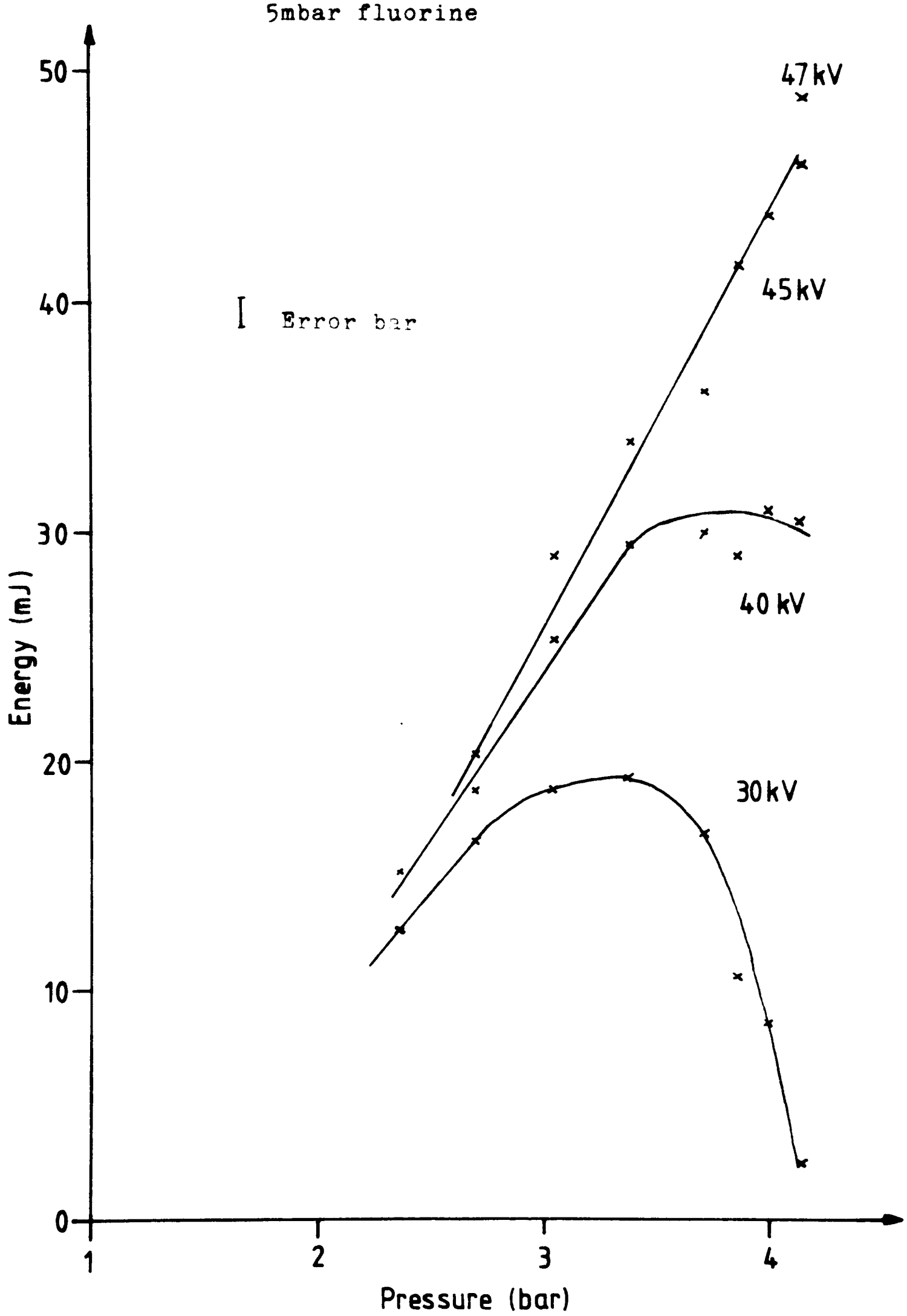


Figure 4.2 Laser energy as a function of helium pressure

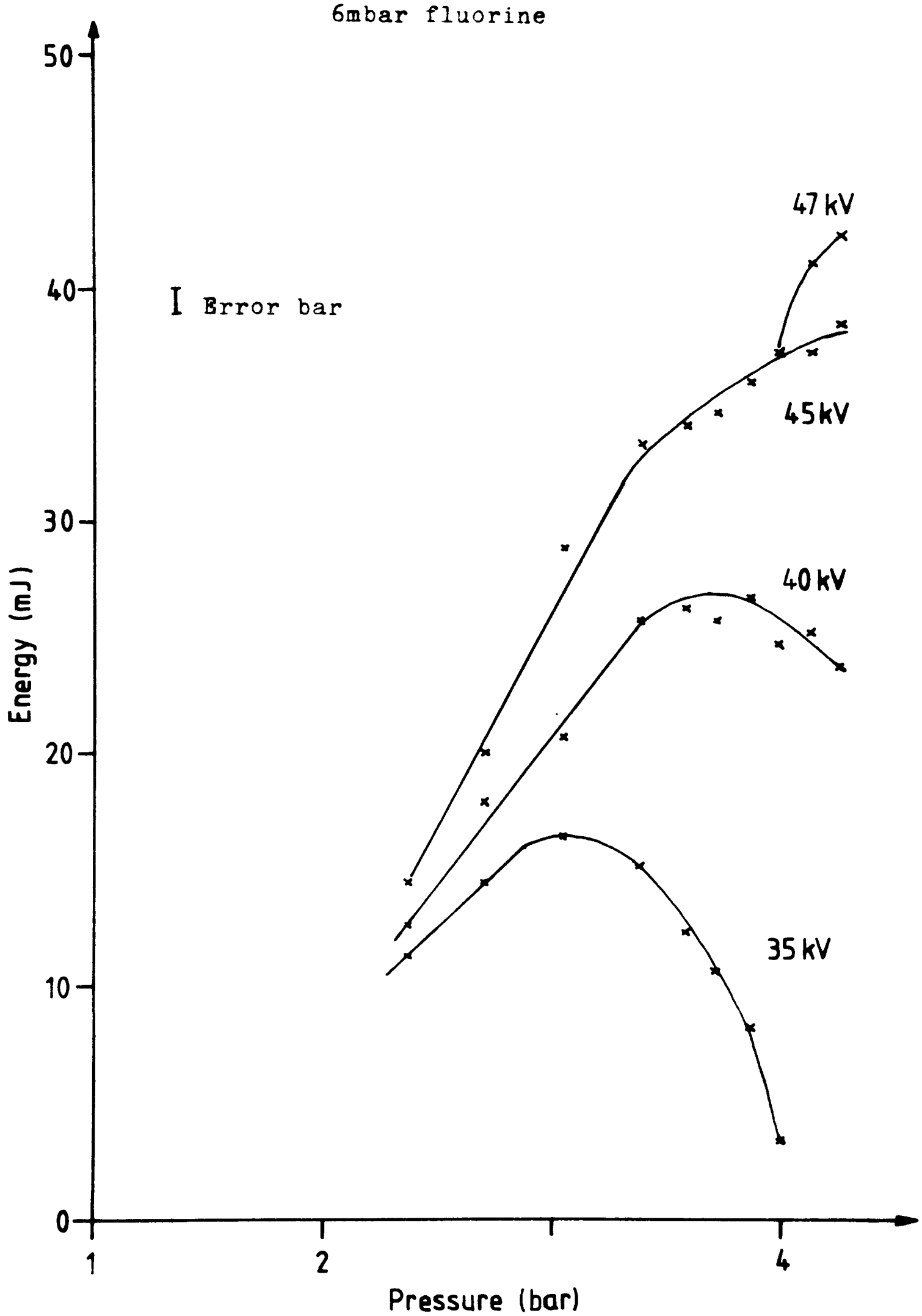


Figure 4.3 Laser energy as a function of helium pressure

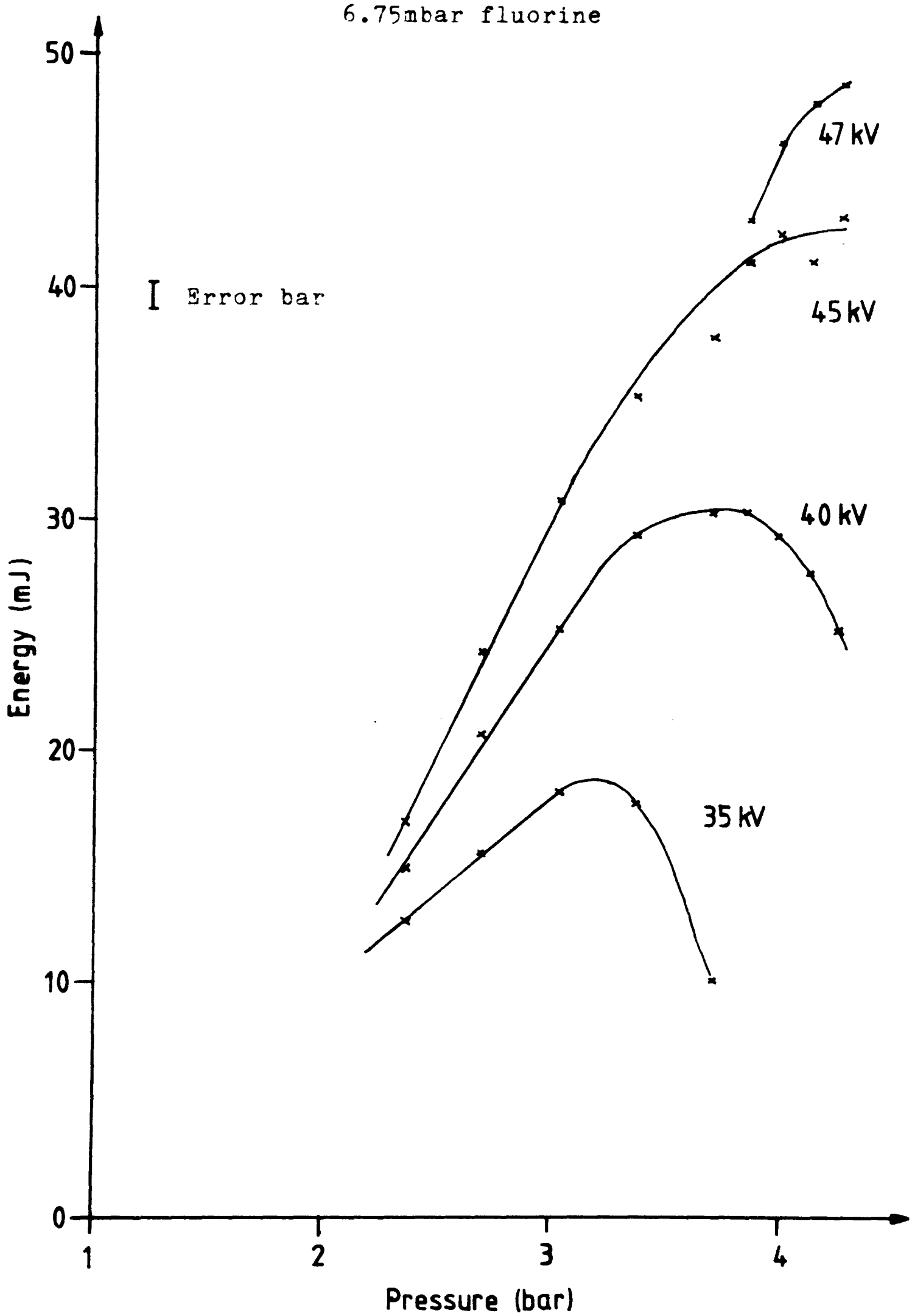


Figure 4.4 Laser energy as a function of helium pressure

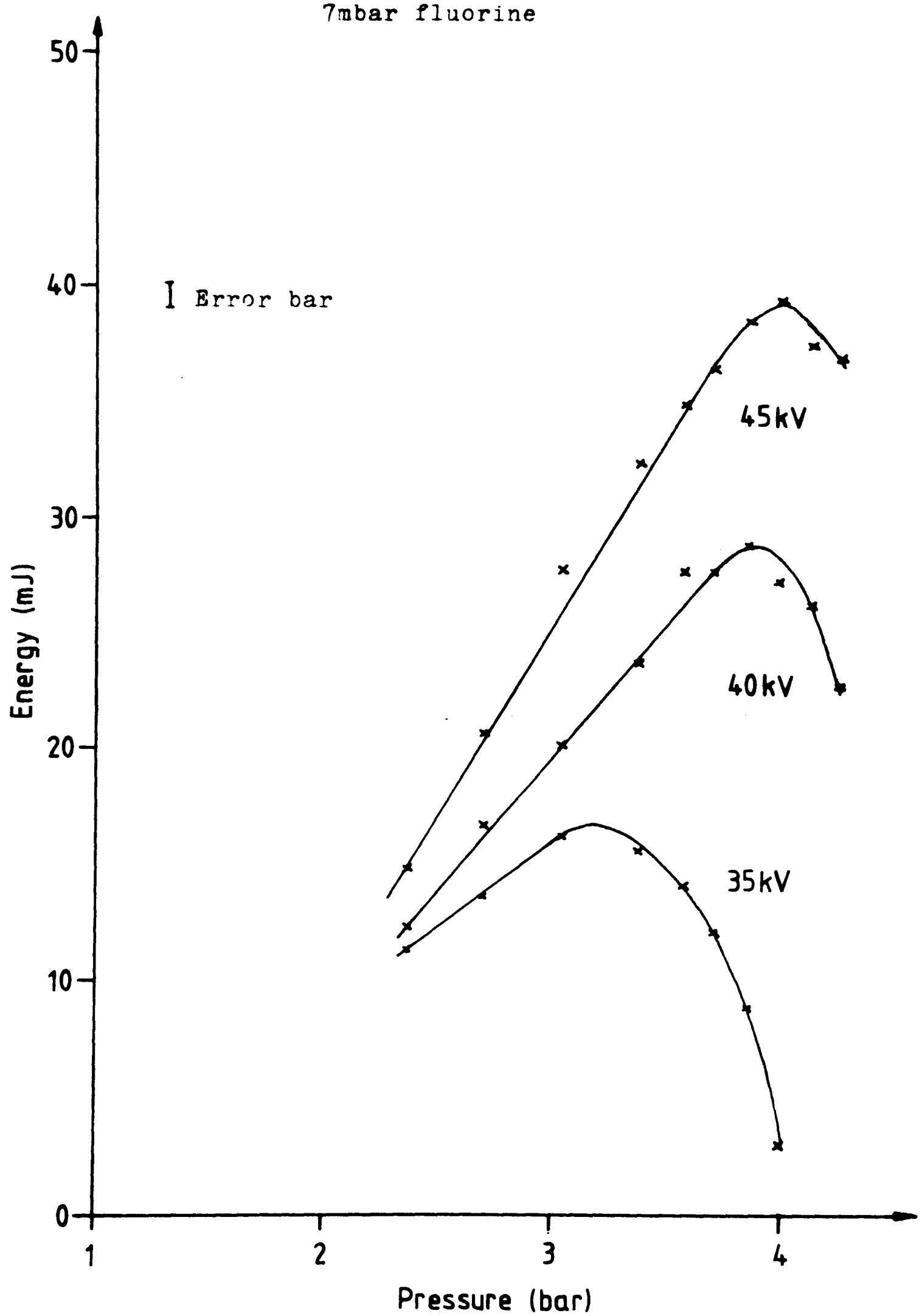


Figure 4.5 Laser energy as a function of helium pressure

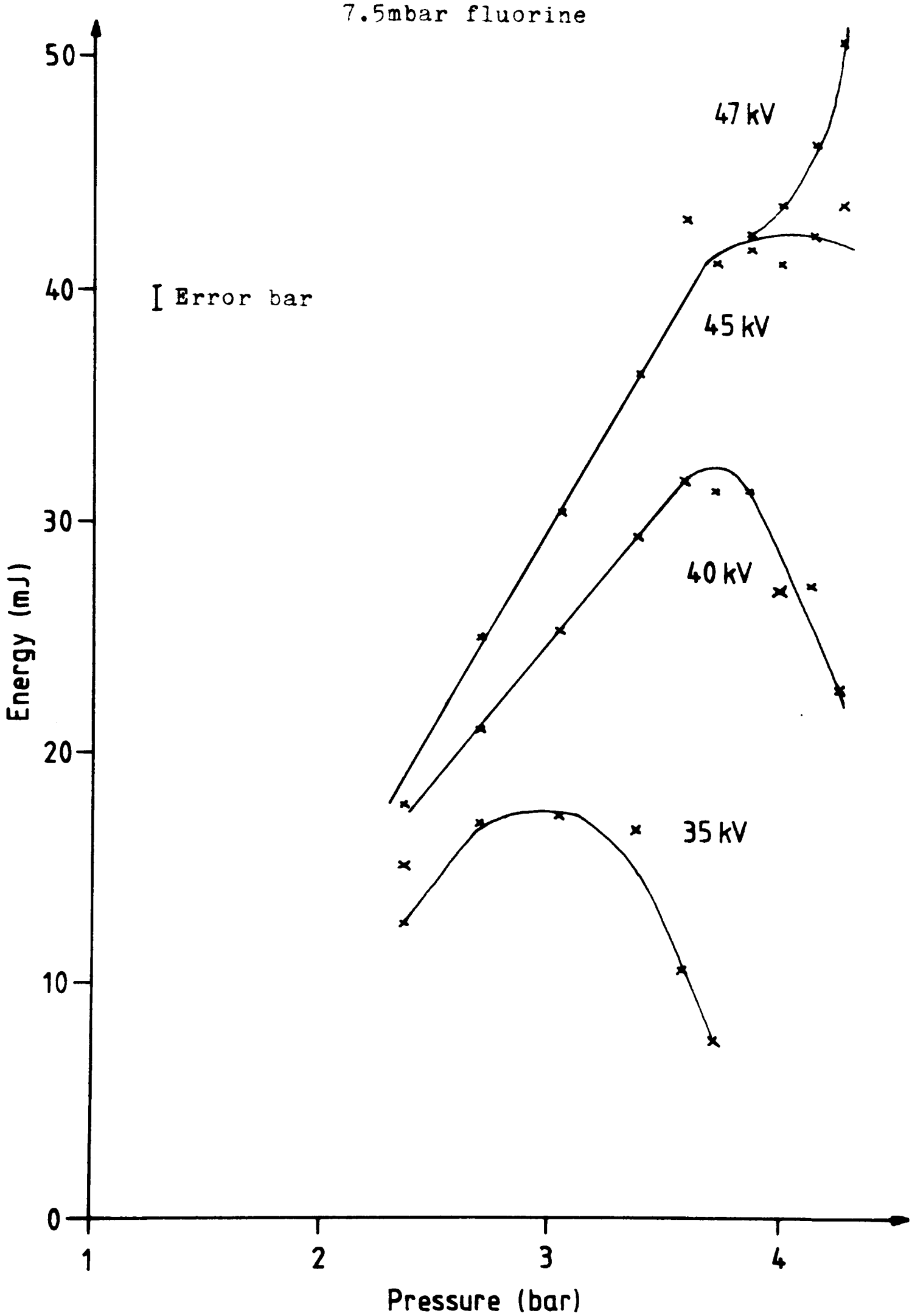


Figure 4.5 Laser energy as a function of helium pressure

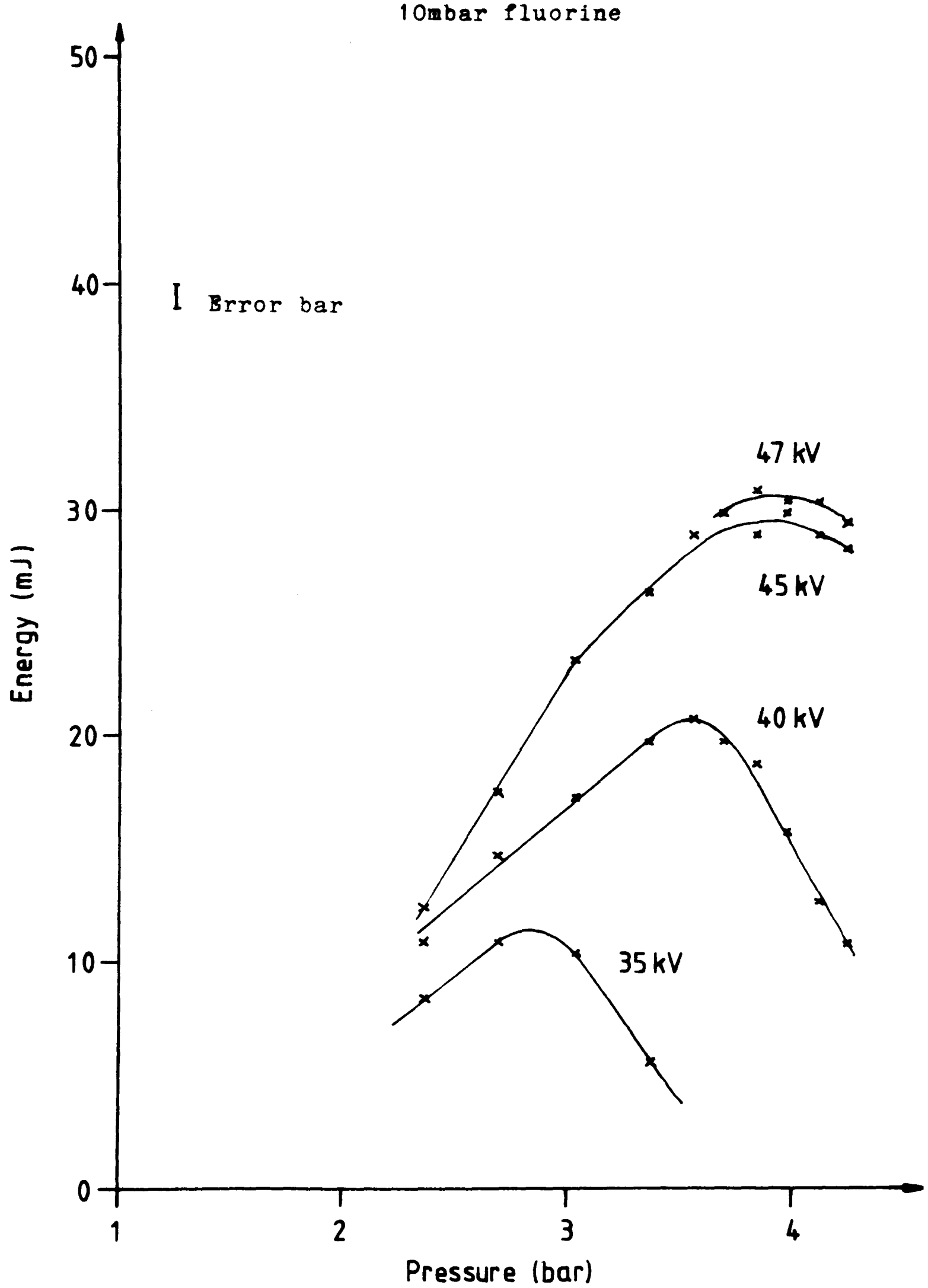


Figure 4.7 Laser energy as a function of helium pressure

CHAPTER 5 : PROPOSED NEW LASER SYSTEM IN NITROGEN

5.1 INTRODUCTION

In this chapter a new scheme for a VUV laser is presented. The scheme involves a two stage pumping scheme using an electric discharge and absorption of UV laser radiation. The scheme is outlined and then individual aspects studied in turn in the following sections. The production of the intermediate metastable state, the transfer of population to the proposed upper laser level using the UV laser, and the build up of population in the lower laser due to the discharge are all investigated.

Ideally, for a new VUV laser system to have practical potential for those applications requiring high energy photons, it should be efficient, be capable of scaling to an appropriate size to enable the output to meet the reqiurements of the application, and yet maintain a degree of simplicity of construction and component parts. Existing sources of short wavelength VUV radiation certainly do not meet all of these requirements.

Molecular hydrogen lasers operating on the Werner bands emit between 110 and 120nm, but at low energies. Their pulse energies cannot be increased by enlarging the discharge volume due to the necessity of providing an extremely fast rising edge on the current pulse (less than 1ns) together with a high current density (see chapter 2). Argon excimer lasers produce radiation around 126nm with reasonably high energies (20mJ), but require electron beam pumping. Electron beam generators to provide the currents of tens of Amps at accelerating potentials of up to 1MV are necessarily large, cumbersome and have very low pulse repetition frequencies. Thus, present devices do not fulfill all the postulated system requirements.

In devising a new system the above system requirements must be borne in mind, along with another obvious condition which must be fulfilled: the gain medium must be transparent to the emitted radiation. This would probably

limit the choice of material to simple diatomic or monatomic gases; as indicated by the systems reviewed in chapter 2.

In the original proposal for this research project (SERC No GRC/30771) it was proposed to look for emission on the analogue, in nitrogen, of the Lyman and Werner bands of molecular hydrogen: that is the main resonance electric dipole transistions from $^1\Sigma_u$ and $^1\Pi_u$ states to the $^1\Sigma_g^+$ ground state. However, because these states are connected to the ground state by fully allowed deep VUV transitions they have short radiative lifetimes. The level on which the transition terminates is an exicted vibrational level of the electronic ground state. Nitrogen is a homonuclear molecule for which radiative transitions between vibrational levels are not allowed. Even for heteronuclear diatomic molecules, with fully allowed radiative transitions between vibrational levels, the lifetime of the vibrational levels will be of the order of 10μs. The nitrogen molecules will thus tend to be collisionally, rather than radiatively, relaxed under practical conditions. The condition for CW laser action as derived in section 1.4 would not then be satisfied, and the laser will belong to the class of "self-terminating" lasers. Because of the fast transition rate from the upper level the excitation to the high lying levels must have a short rise time. If the excitation is to come from a discharge then the current pulse will have to have a short rise time, which will lead to the same problems as the H_2 laser with regard to its scalability.

It was suggested by Dr D J Bedwell that this problem could be overcome if a fast laser pulse were used to transfer population optically into the upper level of the potential nitrogen laser transtion. The upper level in nitrogen would have to be pumped via an excited intermediate level so that overall the system would represent a means of up converting the "transfer" laser radiation by a linear process.

A block diagram of the proposed scheme for a new VUV laser in molecular nitrogen is shown in figure 5.1. A discharge is used to excite nitrogen molecules to a metastable level. Population is then transferred from this

metastable state to the proposed upper laser level by absorption of radiation from the "transfer" laser. This creates a population inversion between the upper laser level and vibrationally excited levels of the electronic ground state of nitrogen. Transitions to these levels in the VUV region are the proposed laser transitions.

Since the lower laser level has a much longer lifetime than the upper level, the laser will operate in a self-terminating mode. The fast excitation to the upper level at a rate sufficient to produce a population inversion is provided by the fast laser pulse. It is only necessary for the discharge to excite population into the intermediate level on a relatively long timescale (of order 100ns).

However, the potential efficiency of this system would not be realised if it were necessary to use a frequency doubled dye laser to provide the "transfer" radiation. In that case the conversion efficiency of any initial pump laser radiation to dye laser energy is no more than about 15% (Telle 1981). Further the SHG process itself has a low effiency of less than 5% (Dewey 1976, Dunning 1973). Thus, overall, the system would be 100 times less efficient then it would be if the initial laser used to pump the dye could be directly employed to excite the VUV gain medium. A search was conducted for coincidences of the emission wavelengths of known UV laser and transitions between excited states of molecules with potential as VUV gain media. This search proved successful. An overlap was found between the RGH $XeCl^*$ laser emission at 308nm and the rotational-vibrational bands of the $b(^1\Pi_u)$-$a(^1\Pi_g)$ levels in molecular nitrogen, one of the Gaydon-Herman (GH) singlet systems. The study of the proposed VUV laser system based on these concepts will occupy most of the rest of this thesis.

5.2 OUTLINE OF THE PROPOSED SCHEME FOR A VUV LASER

In figure 5.2 is shown the term diagram of the relevant levels in

molecular nitrogen. The intermediate level (labelled a) has the same symmetry as the molecular ground state (labelled X). As g-g transitions are strictly forbidden by the electric dipole selection rules the 'a' state is only connected to the ground state by electric quadrupole and magnetic dipole transitions. These transitions comprise the Lyman-Birge-Hopfield (LBH) system. The ratio of the transition probabilities of the quadrupole to magnetic dipole radi ation (Q/D) for the a-X transition has been studied by a number of workers. Originally, Wilkinson and Mulliken (1957) tentatively proposed a value of 0.15 from poor photographic plates. Vanderslice et al (1965) obtained a value of 0.33, but their result is probably not very accurate due to the use of long absorption path lengths which put the spectra in the region of strong absorption. Because of the limited dynamic range of the photographic film this would tend to increase the ratio Q/D as measured by comparing the strong mixed transition lines to the weaker quadrupole only lines. Although Shemansky (1969), using photoelectric recording, did not resolve the rotational structure, the values he arrived at (0.08 to 0.1 for various vibrational bands) are certainly the most reliable now available. Thus we shall take the ratio Q/D as 0.1 as a representative value. The fact that some of the radiation observed is electric quadrupole, giving rise to S($\Delta J=+2$) and O($\Delta J=-2$) branch rotational transitions, as well as the dipole Q, P and R($\Delta J=0,+1,-1$) branches has led to this state being re-designated $^1\Pi_g$ rather than $^1\Pi_u$ as originally thought (Gaydon 1944). The state has a long radiative lifetime of about 0.14ms (Shemansky 1969), although collisionally induced transitions imply that under conditions of practical interest the effective lifetime is much shorter than this (see section 5.1). Since the 'a' state is metastable, it is a good candidate for an intermediate energy storage level, assuming the level can be populated (see sect. 5.3). Transfer of population to the 'b' state is accomplished by absorption of 308nm XeCl laser radiation. As the 'b' state has fully allowed transitions to the ground state, the Birge-Hopfield (BH) system, it has a

short (2.6ns) radiative lifetime (Zipf and Gorman 1980). A discharge pumped XeCl laser pulse typically has a rise time of 3-5ns and so can be used to transfer population to the 'b' state on a timescale comparable to that on which the population decays by radiation.

Emission from the 'b' state on both b-X (BH) and b-a (GH) transitions has been observed from the vibrational levels, v'=1, 5 and 6 only. In absorption, rotationally resolved lines to other vibrational levels are diffuse to varying degrees (Carroll and Collins 1969). These two factors point to the likelihood that other vibrational levels of the 'b' state are significantly depopulated by predissociation. That this predissociation affects different levels to varying degrees suggests that it is due to another state crossing the b state, with the strength of the predissociation depending on the overlap integral of the two wavefunctions. Carroll and Collins (1969) and Dressler (1969) propose the c'$^3\Pi_u$ state is the most likely candidate to cause the predissociation. Although this interaction would involve a spin-forbidden transition, there is a strong interaction between these states as they arise from the same electronic configurations (Carroll and Collins 1969, Pratt, Dehmer and Dehmer 1984). The potential energy curve for the c' state proposed by Carroll and Mulliken (1965) cuts the 'b' state curve at about the equilibrium internuclear separtion for the 'b' state and so will strongly predissociate v'=0 due to the large wavefunction overlap. By a similar argument it will not cause much predissociation to v'=1. If this qualitative argument is continued to higher levels, then from the shape of the curve (Fig. 5.1) it would not be inconsistent with the maximum observed predissociation at v'=3. Zipf and Gorman (1980) give, for the 'b' state as a whole, the predissociaton branching ratio as 92%. The c' $^3\Pi_u$ state asymptotes to a pair of nitrogen atoms $[N(^4S)+N(^2D^0)]$ as its dissociation limit at 97940cm^{-1} and thus, as this is a repulsive state, electron impact excitation of the b $^1\Pi_u$ state is an efficient means of producing metastable nitrogen atoms. Calculated absolute transition probabilities on the b-X(v'=1 - v")

progression show a maximum for the vibrational level in the 'X' ground state v"=2, and a subsidiary maximum for v"=10, corresponding to transitions from the two stationary points of the vibrational wavefunction. Thus in looking for the possibility of gain from this system, transitions terminating on v"=2 and v"=10 and the ones around them, would be the most likely candidates. However, to achieve a population inversion, the ground electronic state must be vibrationally cold. This aspect is further considered in section 5.5.

5.3 EXCITATION OF NITROGEN MOLECULES TO THE INTERMEDIATE 'a' STATE

5.3.1 Discharges and afterglows

Cartwright et al (1977) produced values for the cross sections for the excitation by electron impact of the a $^1\Pi_g$ state of molecular nitrogen by integrating the differential cross sections from electron energy loss data. The results show that direct excitation of this state by electron collisions would be expected to show similar behaviour to that of the C $^3\Pi_u$ state (see figure 5.3). The C $^3\Pi_u$ is the upper level of the Second Positive emission system, and of the familiar UV nitrogen laser at 337.1nm. Thus, one would expect the emission from the 'a' state to be similar to the Second Positive emission. As will be shown later however, in time resolved emission studies carried out as part of this work, the LBH emission appears at much later times in the discharge afterglow than the Second Positive emission. Cartwright et al (1977) compare their cross-sections with those devised by previous workers (Brinkman and Trajmar 1970, Ajello 1970, Borst 1972, Finn and Doering 1975). Although the earlier cross-sections show a similar dependance on electron energy, the absolute cross-section values are some 30-50% higher. This was attributed by Cartwright et al to cascade from other levels, but they did not specify which other states might be

contributing. Freund (1971) points out that cascade on the GH bands will be weak. He shows that there is strong coupling between the vibrational levels of the $a^1\pi_g$ state and the $a'^1\Sigma_u$ and $w^1\Delta_u$ states. Indeed MacFarlane (1966a,1966b) observed stimulated emission on the a'-a and w-a bands, but pointed out that all of these levels are populated throughout the afterglow.

Berkowitz et al (1956) proposed a new mechanism for the production of active nitrogen in discharge afterglows. Their scheme was for the production of B $^3\pi_g$ states through the stabilisation of a collision complex involving two ground state nitrogen atoms. These form nitrogen molecules on a $^5\Sigma^+_g$ curve from which the complex is transferred to the 'B' state by a collision induced radiationless transition near the intersection of the two curves. Bayes and Kistiakowsky (1960) extended this line of argument to the a $^1\pi_g$ state, whose curve also crosses that of the $^5\Sigma^+_g$ state. Carroll (1962) used data from afterglow measurements of the predissociation of the 'a' and 'B' states in order to construct a potential curve for the $^5\Sigma$ state. He suggested that only the $^5\Sigma$ v=0 level, at 77940cm^{-1}, was active in the afterglow, and that the $^5\Sigma$ state had a dissociation energy of only 870cm^{-1}. Young (1960) found support for this mechanism in that the LBH and First Positive Band systems show the same decay rates in the afterglow. This mechanism would populate v=6 of the 'a' state preferentially, though other lower levels would be populated through collision induced vibrational relaxation. On the basis of Young's data, approximately 50 gas kinetic collisions are needed to transfer 'a' state molecules in the vibrational levels v=4,5,6 to v<4 for pressure above 1 Torr. The scheme proposed by Berkowitz and refined by Young can thus be represented as:

$$N(^4S) + N(^4S) + M \rightarrow N_2(^5\Sigma^+_g) + M + \Delta E\ (774cm^{-1}) \qquad 5.1$$

$$N_2(^5\Sigma^+_g) + M \rightarrow N_2(a^1\pi_g, v=5) + M + \Delta E\ (926cm^{-1}) \qquad 5.2$$

$$N_2(a^1\pi_g, v=5) + M \rightarrow N_2(a^1\pi_g, \text{lower v levels}) + M \qquad 5.3$$

where M represents a nitrogen molecule. Vibrational relaxation is a stepwise process, with most of the population ending up in the v=0 level of the 'a' state. As the $^5\Sigma$ to $^1\Pi$ radiationless transition involves a change of $\Delta S=2$ this might account for the relative weakness of the LBH bands compared to the First Positve emission from $B^3\Pi_g$. Golde and Thrush (1972a) showed that the dependence of the rate of formation of the 'a' state on the density of nitrogen atoms was consistent with a reaction

$$N(^4S) + N_2(B^3\Pi_g) \rightarrow N_2(a^1\Pi_g) + N(^4S) \qquad 5.4$$

favouring population of v=0,1 of the 'a' state. These workers suggested that the formation of $N_2(a^1\Pi_g)$ from two nitrogen atoms occurred as the result of an inverse predissociation, rather than as a stabilisation in the $^5\Sigma$ state. Indeed, the existence of a weak predissociation in the emission spectrum of $N_2(a^1\Pi_g)$ above v'=6 is well established, with the $^5\Sigma$ state being the predissociating state.

5.3.2 Optical methods of excitation

Population of N_2 molecules in the 'a' state can also be accomplished using two photon absorption techniques. Filseth et al (1977), using only about 0.1mJ of UV radiation from a frequency doubled dye laser with a fundamental wavelength around 520nm, were unable to detect the LBH signal directly from excitation by two photon absorption. Instead, they used a sensitised fluorescence technique depending on the close energy match between the vibrational levels of the nitrogen 'a' state and those of the $A(^1\Pi)$ state of carbon monoxide. Collisions induced exchange of energy from the $a^1\Pi_g$ state of nitrogen to the $A(^1\Pi)$ state, which is then detected by emission, of the Fourth Positive System, as it decays to the ground state. Van Veen et al (1982) detected the LBH emission directly by two photon absorption to excite the 'a' state, using about 1mJ of UV radiation from a frequency doubled dye laser. They used time resolved detection of this emission to study the decay of the 'a' states as a function of time at various pressures.

5.4 ABSORPTION OF RADIATION FROM THE "TRANSFER" LASER

5.4.1 Absorption linewidths

On considering the optimum conditions for absorption of the pump laser radiation it is necessary to consider the linewidths of the rotational-vibrational transitions of the $a^1\pi_g - b^1\pi_u$ band. There are three mechanisms that act to broaden an emission line; natural broadening, Doppler broadening, and collision, or pressure, broadening. These will be examined in turn for the transition of interest here.

Natural Linewidth

The natural linewidth is given (Corney, 1977) as

$$\Delta\bar{\nu} = 1/(2\pi c\tau) \text{ cm}^{-1} \qquad 5.5$$

For the 'b' state in molecular nitrogen the radiative lifetime, τ is 2.6ns, which gives a natural linewidth of 0.002cm^{-1}.

Doppler Broadening

The broadening of a transition line due to the Doppler effect is given (Corney, 1977) as

$$\Delta\bar{\nu} = 7.16\text{x}10^{-7}(T/M)^{1/2}\bar{\nu}_0 \qquad 5.6$$

in which T is in Kelvin, and M is in a.m.u. In the case of interest T is approximately 300K and M is 28, giving

$$\Delta\bar{\nu} = 2.34\text{x}10^{-6}\bar{\nu}_0 \qquad 5.7$$

For the b-a transition centred around $32{,}500\text{cm}^{-1}$ a Doppler linewidth is expected of

$$\Delta\bar{\nu} = 0.076\text{cm}^{-1}. \qquad 5.8$$

Collision broadening

The effect of collisions between molecules also acts to broaden the linewidth of the emitted radiation. The linewidth is given by Corney (1977) as

$$\Delta\bar{\nu} = 1/\pi c\tau_0 \qquad 5.9$$

where τ_0 is the mean time between collisions, given by

$$1/\tau_0 = n\sigma(8RT/\pi M)^{1/2} \qquad 5.10$$

Taking, T=300K and $\sigma = 1.6\text{x}10^{-14}\text{cm}^2$, the collision broadening cross-section as given by Shemansky (1969), and n as the number density of molecules at 1mbar of $2.7\text{x}10^{16}\text{cm}^{-3}$ then

$$1/\tau_0 = 2.06\text{x}10^{7}\ \text{s}^{-1}. \qquad 5.11$$

The pressure broadened linewidth at 1mbar is then,

$$\Delta\bar{\nu} = 2.18\text{x}10^{-4}\text{cm}^{-1}. \qquad 5.12$$

In summary, the various broadening mechanisms give,

Natural linewidth : 0.002cm^{-1}

Doppler linewidth : 0.076cm^{-1}

Collision linewidth : 0.0002cm^{-1}

Thus it is seen that at moderate pressures most of the line broadening is effectively due to Doppler broadening.

Each rotational transition will have a linewidth of the order of 0.1cm^{-1}, and for efficient absorption the "transfer" laser radiation should either a) have a linewidth of this magnitude, or b) the individual rotational lines of the absorption band should have a separation not much larger than their full width at half maximum intensity (FWHM) so that neighbouring lines overlap significantly, and broadband radiation can be absorbed on a number rotational of lines simultaneously.

5.4.2 Overlap of 'a'-'b' absorption band with "transfer" laser radiation

Little work has been carried out at high spectral resolution to resolve the individual rotational emission lines from the appropriate singlet levels in nitrogen. Carroll and Collins (1969) have carried out a study at high resolution of the BH emission, from which it is possible to fix the rotational levels in this state relative to v"=0, J=0 of the $X^1\Sigma_g^+$ ground state. Similarly, Miller (1969) studied the LBH bands and gave energies of the rotational states for low vibrational quantum numbers of both the ground

state and the $a^1\Pi_g$ state. From this data it is possible to find the transition energies for the rotational lines of the b(v'=1) to a(v"=0) transition. Rajan (1974) observed this transition directly in a discharge at low pressure. Low pressure was used in order to reduce the relative intensity of the overlapping 3-2 and 4-3 bands of the Second Positve System. Rajan also worked at liquid nitrogen temperature thereby reducing Doppler widths as a further aid to unravel the complex structure. Rajan himself checked the accuracy of his work against that of Carroll and Collins and of Miller by comparing the values for the rotational levels in the 'b' state as deduced from the b-X emission to values obtained by finding the energies of the levels of the a (v=0) state and adding the energies of the b-a transitions. These results agree to the quoted accuracy of the VUV measurements ($0.8cm^{-1}$). Rajan's results are shown in figure 5.5, where it can be seen that, except near the R branch band head, the lines are considerably further apart than their Doppler width. Thus it would seem that for optimum energy transfer of pump laser radiation the laser output would have to be of a narrow linewidth.

Spectral scans of the output from untuned and tuned $XeCl^*$ lasers have been published in the literature (Tellinghuisen et al 1975, Sze and Scott 1978, Corkum and Taylor 1982, Takahashi et al 1985). These show four main bands due to transitions between the v'=0 level in the 'B' state and v"=0,1,2 and 3 levels of the 'X' state (ground state). These bands all degrade to shorter wavelengths. By probing the XeCl discharge with a frequency doubled dye laser, Corkum and Taylor (1982) found a low level of gain (about 20% of that at the peak) to shorter wavelngths due to population in higher vibrational levels of the B state. The overlap of the $XeCl^*$ B-X radiation with the 'a' - 'b' absorption transition of nitrogen is also shown in figure 5.5.

5.4.3 Absorption intensity on rotational lines

For optically thin absorbing layers, the intensity of radiation absorbed by a transition between an upper level i and a lower level k, for the case where the probe beam has a larger bandwidth than the transition linewidth, is given by

$$\Delta I_{ik} \propto N_k \rho_{ik} B_{ik} hc\nu_{ik} \Delta x \qquad 5.13$$

where ρ_{ik} is the radiant energy density at the transition frequency ν_{ik}, N_k is the density of molecules in state k, and

$$B_{ik} = (8\pi^3/3h^2c\ )R_{ik}^{\ 2} \qquad 5.14$$

is the Einstein B coefficient connecting the two levels, with $R_{ik}^{\ 2}$, being the matrix element for the transition. For transitions between levels of molecular species, in situations where the Born Oppenheimer approximation is valid, the matrix element can be separated into a number of factors. These were disscussed in section 1.4.

To calculate the population in the lower level of a particular transition the Boltzmann factor is used to give the population in each rotational level relative to the population of the lowest vibrational level in the electronic ground state. In the case of 'b' -> 'X' in nitrogen, Λ=1 and there is no level with total angular momentum, J, equal to zero. To refer to the total number of molecules in each level consider that N is proportional to the sum of the Boltzmann factors over all states, remembering that each rotational level has a degeneracy of 2J+1. This sum is referred to as the partition function, Q, and is given by

$$Q_k = \sum(2J_k+1)\exp(-F(J_k)hc/kT) \qquad 5.15$$

where

$$F(J) = BJ(J+1)-DJ^2(J+1)^2 \qquad 5.16$$

is the term energy relative to the J=0 level, and T is the rotational temperature for that state. So the population in level k is given by

$$N_k = [(2J_k+1)\exp(-F(J_k)hc/kT_k)]/Q_k \qquad 5.17$$

Thus the absorbed intensity for the radiation is given by

$$I_{ki} \propto [S_J\nu(2J_k+1)\exp(-F(J_k)hc/kT_k)]/Q_k \qquad 5.18$$

where J_k is the rotational quantum number for the lower level, and the other terms have been taken into the proportionality as they are constant for all the rotational transitions. By a similar argument the spontaneous emission intensity is given as

$$I_{ik} \propto [S_J \nu^4 (2J_i+1) \exp(-F(J_i)hc/kT_i)]/Q_i. \qquad 5.19$$

Using values of B and D for the a $^1\pi_g$ (v=0) of B=1.6079cm^{-1} and D=6x10^{-6}cm^{-1} (Miller 1970) and for the b $^1\pi_u$ (v=1) level of B=1.4086cm^{-1} and D=16.4x10^{-6}cm^{-1} (Carroll and Collins 1969) with the band origin for the v'=1 - v"=0 transition as 32,500.33cm^{-1} (Rajan 1974) it is possible to calculate numerically the relative intensities of the absorption and emission for the rotational transitions, for a given vibrational temperature, T_v for each level. A computer program was written (see appendix 3) to enable these calculations to be performed. This provides an indication of the transitions on which strongest absorption would be expected. The expected absorption is indicated on figure 5.5, where the height of the rotational line represents the strength of the absorption for T_v=700K. A value of T_v which is higher than the 300K wall temperature was used because on fitting the emission intensity to the spectrogram published by Rajan (1974) the best fit in that case was obtained for T_v=180K. Now Rajan used a discharge tube cooled to 77K at the walls. Not suprisingly, the rotational temperature in the discharge that is deduced from his results is somewhat higher than the ambient temperature. However it would be expected that the gas temperature in Rajan's case would conform more closely to the wall temperature than is to be expected in any of the cases used in this study. This is because a low pressure and small tube radius were used in Rajan's studies, leading to a molecular mean free path of comparable length to the tube radius. Thus a value of 700K would seem appropriate here. Referring to figure 5.5 it is evident that the optimum overlaps of pump laser intensity and absorption strength occur between the R branch transitions from J"= 16 and 17 with the peak in the XeCl emission on the 0-0 vibrational transition and J"= 21 and 22 with the 0-1 XeCl emission

peak. Also between the P branch transitions from J"= 7 and 8 with the 0-1 peak and for J"= 11 and 12 with the 0-2 peak. This implies that to tune the "transfer" laser output to the frequencies corresponding to these transitions would give the maximum absorption.

5.5 LOWER LEVEL POPULATION

To achieve gain on the proposed b-X transition it is necessary for the lower laser level to have a smaller population than the upper level. This means that, as the lower level is a vibrational level of the molecular ground state, it is necessary for the nitrogen to be vibrationally relaxed. It would then be possible to obtain gain on transitions to higher vibrational levels, especially to those around v"=10 where there is a high transition probability.

5.5.1 Vibrational excitation of the $X^1\Sigma^+_g$ ground state by electron collisions

At ambient temperatures almost all the nitrogen molecules are in the v=0 vibrational level with a very small fraction, given by the Boltzmann factor, in the v=1 level.The primary cause of vibrational excitation of the molecular nitrogen ground state is caused by inelastic collisions of v=0 nitrogen molecules with electrons with energy about 2eV. Measurements of inelastic cross-sections as a function of electron energy show an onset about 1eV, peaking around 2.3eV and rapidly falling off, so that above 4eV the cross-sections have decreased by about two orders of magnitude from the peak value. These values also show a resonant structure, which does not correspond to the vibrational structure of the ground state. Schulz (1964) performed the first experiments with an energy resolution high enough to resolve this structure. He suggested that the excitation from the ground state is achieved via a resonance state, in this case a compound negative ion, $N^-_2\ ^2\pi_g$. This state has a lifetime of order one vibration time (10^{-14}s), after which it

decays into an excited vibrational level of the ground electronic state.

The resonance arises from the temporary capture of an electron into the lowest vacant orbital of the nitrogen molecule. The nuclear wavefunction propagates across the N^-_2 potential well in such a way that only one reflection of the wavepacket is important, because it is almost completely annihilated by autoionisation at the end of the first cycle. Thus only one outgoing and one reflected wave need to be considered. The superposition of these two waves produces a standing wave whose nodal positions depend on the incident electron energy. The energy dependence of the vibrational excitation cross-sections then comes about because of the overlap between this standing wave and the wavefunctions of the vibrational states of the neutral molecule.

The extra electron enters and departs by tunnelling through a centrifugal potential barrier, which therefore leads to the relative cross-sections having a dependence on the probabilty of penetration through the barrier. For high states it can be shown (Schulz 1976) that the probability of penetration will vary with E, the energy of the departing electron, as $E^{5/2}$. The value of E corresponds to the difference of the incident electron energy and that of the final vibrational level (which is simply the threshold energy for excitation of that particular level). If the incident electron energy at the peak of experimentally determined cross-sections are compared it is evident (Allan 1985), that their excess over the threshold energy decreases with increasing vibrational quantum number (see figure 5.6). Thus a rapid decrease of the excitation cross-section to higher vibrational levels is expected, even though the overlap integrals are varying slowly with vibrational quantum number.

A number of workers have studied the inelastic cross-sections for the vibrational excitation of nitrogen. Detailed experimental cross-sections as a function of energy and vibrational level have been measured as relative values, while absolute measurements have been made either for the total cross-section over all states, or for one particular vibrational level. The

relative cross-sections have then been normalised to these data at one point only.

Recent relative measurements of Allan (1985) agree well with relative calculations of Dube and Herzenberg (1978) using the model of a short lived negative ion resonance. This is called the "boomerang model" as the nucleii only execute a single vibrational cycle during the lifetime of the N^-_2 ion. Jung et al (1982) obtained an absolute cross-section value by integrating the differential cross-sections over all angles, and summing over rotational transitions for v"=0 to v'=1. If it is assumed that the angular distributions are the same for all vibrational levels, then the relative data can be normalised to this value of $5.41 \times 10^{-16} cm^2$ at the peak of the v'=1 excitation curve at 2.25eV. This asumption is justified as can be seen from the angular distributions of Dube and Herzenberg (1978), and also because, as the cross-section maxima are in the resonant region, the angular distribution is a function of the final electronic state and not the vibrational one. Peak cross-sections for excitation to vibrational levels greater than eight are smaller by two orders of magnitude than for the first excited level, and so excitation to these levels can be effectively neglected.

Thus far, only excitation from the ground state has been considered. Theoretical studies by a number of workers (Chen 1964, Chandra and Temkin 1976, Dube and Herzenberg 1978) have also examined excitation from excited states and also by superelastic collisions - those removing vibrational quanta. Although these workers used different models (Chen - factoring resonant contribution from electronic and nuclear parts, with nuclear part fitted to agree with ground state resonant structure, Chandra and Temkin - hybrid model, Dube and Herzenberg - boomerang model) their results agree to within a factor of two. It is a feature of all these studies that the cross-section for single quantum jumps caused by inelastic collisions, are much larger (factor of two) than any others and that the cross-sections decrease very rapidly with Δv greater than two.

The superelastic cross-sections for v'=v to v"=0 are generally about twice as large as the excitation cross-section v"=0 to v'=v. Again superelastic collisions with single quantum jumps are favoured.

The cross-section resonances mentioned above occur for electron energies in the range 1 to 4 eV. The exact value at which the cross-section peaks depends on the exit channel. Outside the range 1 to 4eV the cross-sections are down by two orders of magnitude. However 1 to 4eV is the energy range in which most electrons in a typical nitrogen discharge lie. Therefore in considering the vibrational populations in the discharge it would be necessary to consider all these inelastic and super-elastic collsions, for the populations of levels up to v"=8. The absolute rates for transitions will depend on the populations in each level, but due to the relatively large up rate for single quantum jumps it would be expected that the populations in the higher levels would grow during the discharge pulse due to stepwise excitation.

5.5.2 Electron energy distribution function

In general the electron energy distribution function (eedf) in a low pressure gas discharge will be non-Maxwellian. Molecular gas discharges are characterised by mean electron energies in the 0.5-3eV range. The distribution reflects the form of the dominant electron-molecule energy exchange interactions; in this case due to vibrational and electronic exctiation of the molecule. Theoretical calculations of the eedf for nitrogen were first carried out by Nighan (1970) and more recently by Capitelli et al (1981). Their results show that, relative to a Maxwellian distribution, there is a defecit of high energy electrons above 2eV, and that this is more pronounced for the discharges with low values of E/N. This is due to the large vibrational excitation cross sections discussed in the previous section effectively removing electrons when their energy reaches about 2eV. As the value of E/N is increased the energy input into the gas is increased and the

electrons are able to penetrate this barrier, giving rise to a high energy tail. For an eedf with mean energy around 2eV, typical of most gas discharges, the electron-molecule energy transfer is approximately evenly divided between vibrational excitation of the first eight levels, and electronic excitation, to levels in the 8 to 14eV region. For higher mean energies electronic excitation is favoured.

When the nitrogen vibrational levels become significantly populated it is possible for superelastic collisions to take place, and to return energy to the eedf. Such collisions have the effect of increasing the numbers of electrons in the high energy tail of the distribution. This effect is particularly noticeable in the post-discharge regime, and these portions of the distribution can be increasing out to 10 or 100ms after the discharge.

5.5.3 Vibrational distribution

The population distribution across the vibrational levels in the molecular nitrogen ground state in a discharge will not generally follow a Boltzmann distribution, indeed it can show very marked deviations. A single vibrational temperature cannot therefore be used to descibe the population in all levels, but a characteristic "temperature" can be defined as

$$T' = (E_1 - E_0)/(k \ln N_0/N_1), \qquad 5.20$$

the "temperature" over the lowest two levels given by the ratio of the population in the lowest levels.

Besides the previously discussed mechanism of electron collisions giving rise to populations in excited levels it is also possible for collisions between molecules to cause the exchange of vibrational populations between states. These collisions can be of two main types; Vibration-Vibration (V-V) processes in which vibrational quanta are exchanged between two molecules, and Vibration-Translation (V-T) processes when vibrational quanta are removed from the nitrogen and the energy is transferred to the translational energy of the gas (heating). Due to the anharmonic nature of the vibrational level spacing,

the V-V processes are not exactly resonant: the energy defect being supplied by the translational modes. These energy defects are greater for the higher levels which leads to the V-V rates being much greater (by orders of magnitude) for the lower levels. Single quantum jumps are much more likely than multiple quantum exchange, because the expression for the transition probability contains the two matrix elements for the transitions in the two molecules. The V-T rates increase with vibrational quantum number as the translational mode then has to carry off less energy, for these single quantum jumps, because the vibrational spacing decreases for higher vibrational quantum numbers. For levels up to v=20 and gas temperatures below 2000K, the V-V rates are several orders of magnitude greater than the corresponding V-T rate. The rotational temperature will be in equilibrium with the translational temperature. Highly excited molecules colliding with lower level molecules will be non-resonant, and so will be more likely to undergo V-T processes, whereas among the lower levels V-V exchange processes will domminate. This effectively gives rise to two time scales in the evolution of the vibrational population.

Firstly, a fast exchange of vibrational quanta among the lower levels to produce a quasi-steady distribution on a timescale of a few microseconds.

Secondly, V-T transitions, which take place on a much longer timescale of order of milliseconds, cause this distribution to come into equilibrium with the heat bath via a series of quasi-steady states. Among the upper levels however a Boltzmann distribution is achieved due to the higher rate of V-T transitions.

These quasi-steady distributions were first investigated by Treanor et al (1967), who derived the resulting distribution in the form of a Boltzman distribution modified to account for the anharmonicity of the vibrational spacing. The form he derived for the population in a level with vibrational quantum number v is

$$N_v=N_0\exp(-vE_1/kT')\exp((vE_1-E_v)/kT), \qquad 5.21$$

where T is the translational temperature, and T' was defined in equation 5.20. For low values of T this distribution shows a minimum in the region v=5-10 depending on the value of T' Under conditions where the vibrational temperature is larger than the translational temperature there will be preferential transfer of energy to the higher levels, the anharmonic pumping effect.

5.6 TIMING CONSIDERATIONS

The proposed N_2 VUV laser system depends on the transfer of population from the intermediate 'a' state to the upper laser level, 'b' state, at a time when it will produce a maximum population inversion with respect to the lower levels, which belong to the vibrational manifold of the nitrogen $X^1\Sigma$ ground electronic state. The separate functions of producing molecules in the intermediate states by the discharge, and the use of an XeCl laser to cause transfer to the upper level, means that the time at which transfer is induced can be independently chosen to optimise the magnitude of the inversion.

In a previous section the production of the intermediate $a^1\pi_g$ state was discussed. It was shown that N_2 molecules in the $a^1\pi_g$ level is produced predominantly via recombination of two nitrogen atoms. The newly created N_2 molecules are predominantly in a vibrationally excited state, with v=6. These then relax to the lowest vibrational level of the 'a' state on a timescale of 1 microsecond at 10mbar pressure (Young 1960, Golde & Thrush 1972a). This relaxation rate is an order of magnitude faster than the rate of decay from the $a^1\pi_g$ state due to collisionally-induced radiative transitions determined by Van Veen et al (1982). Quenching of the electronic $a^1\pi_g$ state by electrons is expected to be slow compared to vibrational quenching, so that throughout the duration of the discharge pulse a steady build-up of population in the intermediate state can be expected. However, the higher vibrational levels of the ground electronic state are also being populated directly by electron

collisional excitation and by anharmonic pumping. To a first order approximation we may consider electron collisional excitation to be responsible for governing the gross population of vibrationally excited molecules, while V-V relaxation governs the distribution of the vibrational population within the populated states. The rate for the first process increases linearly as the number density of nitrogen molecules, while the rate for the the latter process goes as the square of the number density. Treanor (1967) gives the transition probability for low vibrational quantum number states at 500K as 2×10^{-2} per collision. Assuming typical values of hard sphere collision cross sections, this implies that the characteristic time for the transition is about 2 microseconds. If this is compared to the sub-nanosecond time for electron collisional excitation, it is seen that during a discharge pulse lasting less than 1 microsecond there will not be time for the vibrational distribution to reach any quasi-steady distribution governed by V-V rates, and all of the vibrational population movements can be regarded as being caused by electron collisions. Nevertheless, electron collisions can bring about large populations in highly excited levels on these short timescales. Therefore to achieve maximum inversion, it would seem to be advantageous to wait for about 0.5 microsecond after the discharge starts before attempting to transfer the molecules to the b $^1\Pi_u$ proposed upper laser level by absorption of the short pulse of radiation from the "transfer" laser. This is in order to allow for vibrational relaxation of the population in the intermediate 'a' state to its lowest vibrational level, while minimising the time for build-up of population in the ground state excited vibrational levels.

5.7 CONCLUSION

In this chapter a new system with potential as a VUV laser has been proposed and described. It effectively allows the up-conversion of radiation

from an XeCl laser without the need for non-linear processes. It should be noticed that because of the two stage pumping, the conditions for the first stage can be optimised to populate the intermediate level on a relatively long timescale. The subsequent transfer of population to a reasonably high energy state, and the final stage, involving relaxation within the upper laser level, can be completed on a short timescale, governed by the rise time of the XeCl laser pulse, at a time chosen to produce maximum gain. The system has some prospect of being scaled to higher energies by increasing the interaction volume with the "transfer" laser. This would hardly be possible if the excitation process required a very fast discharge or if the conversion was via a non-linear process requiring high pump energy densities.

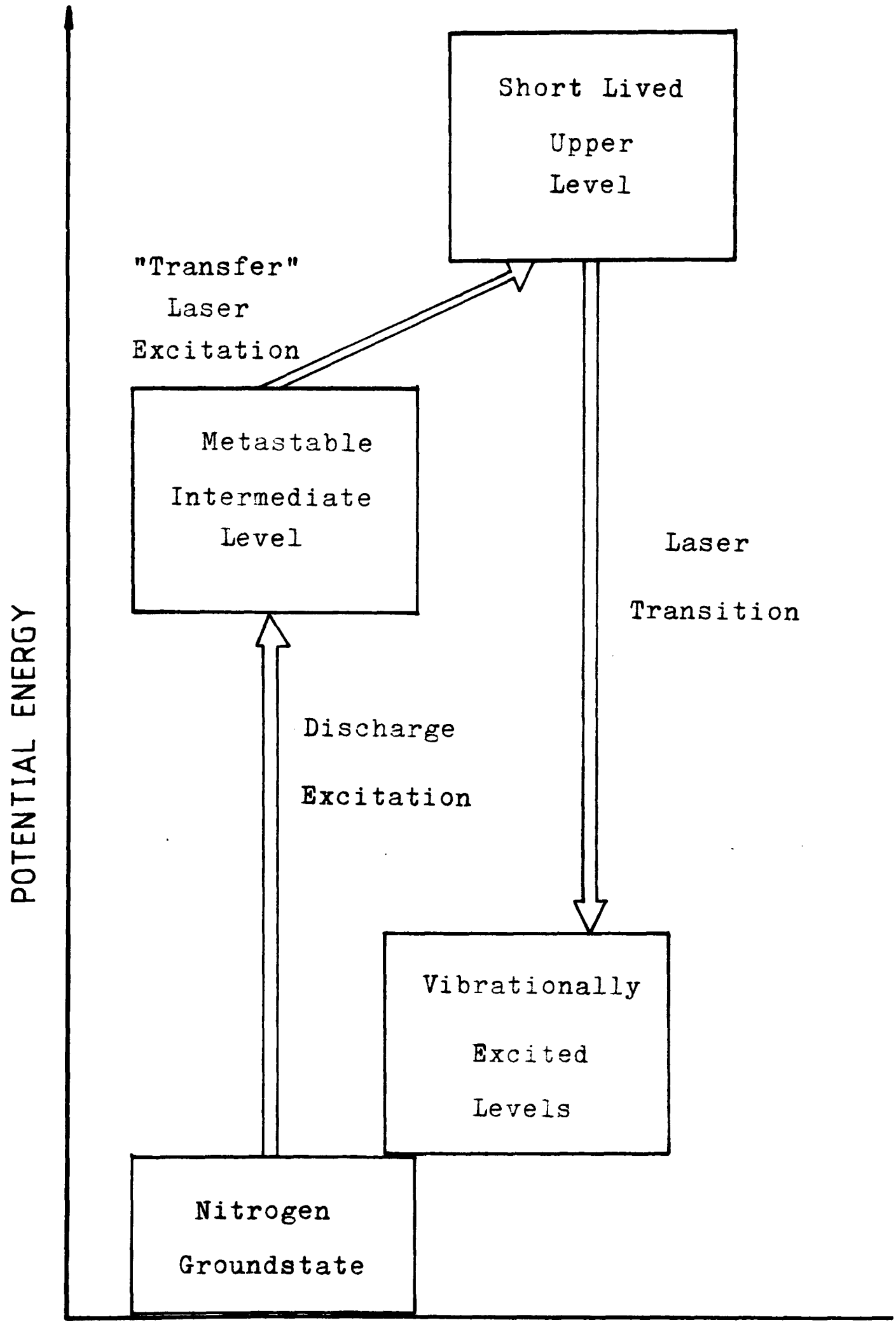


Figure 5.1 Simplified scheme of proposed laser

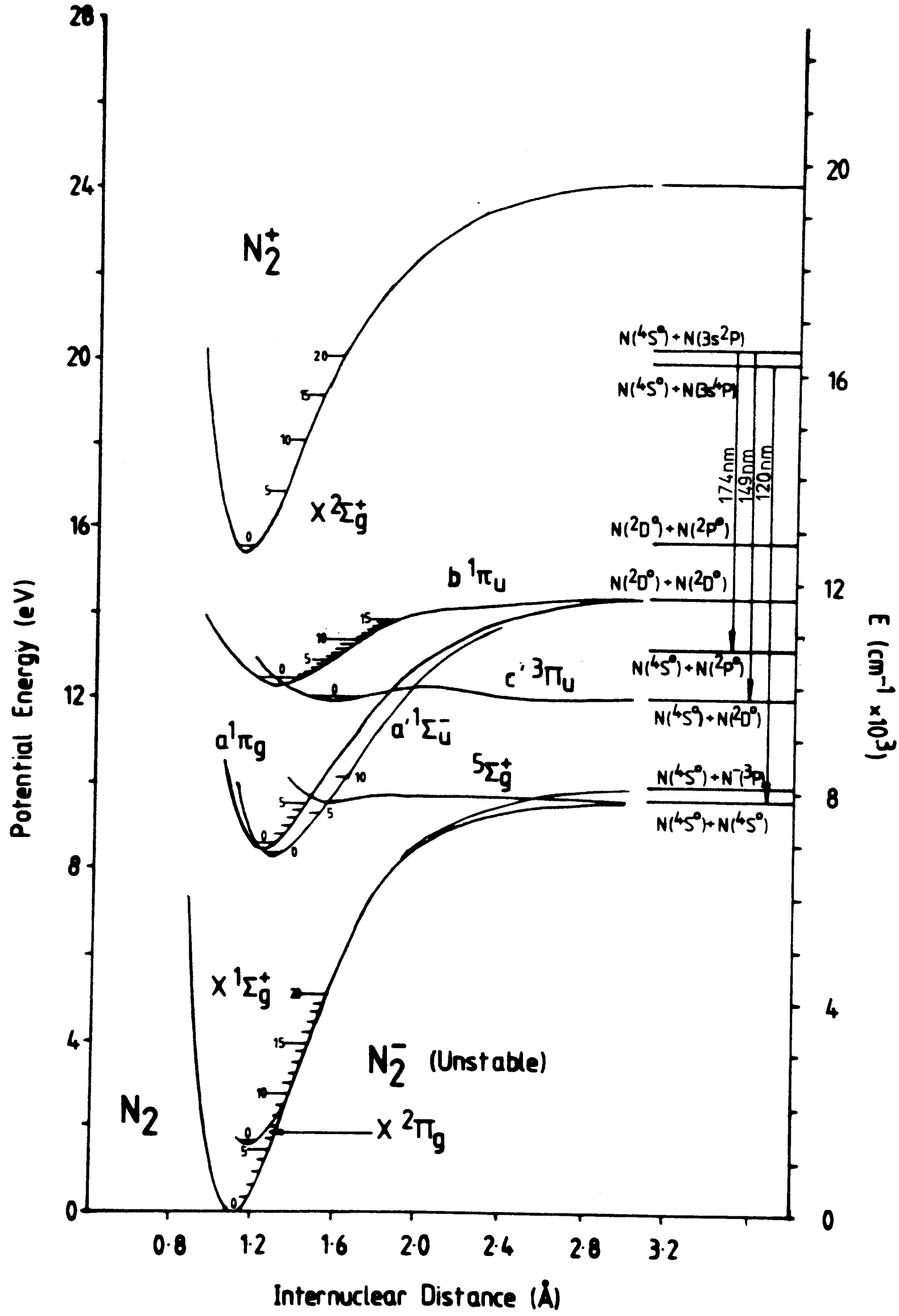


Figure 5.2 Selected Potential Energy Curves for Nitrogen

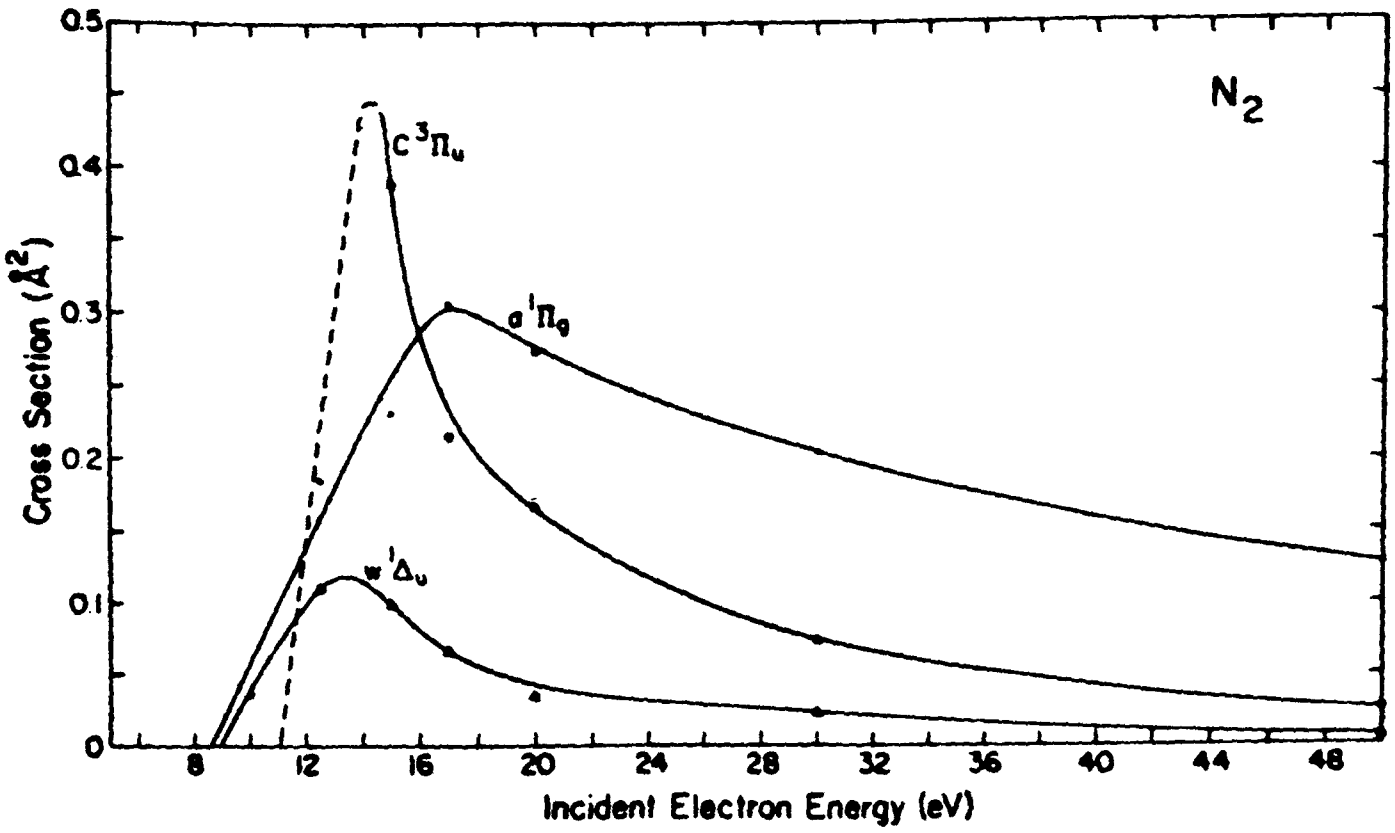


Figure 5.3 Electron impact excitation cross sections

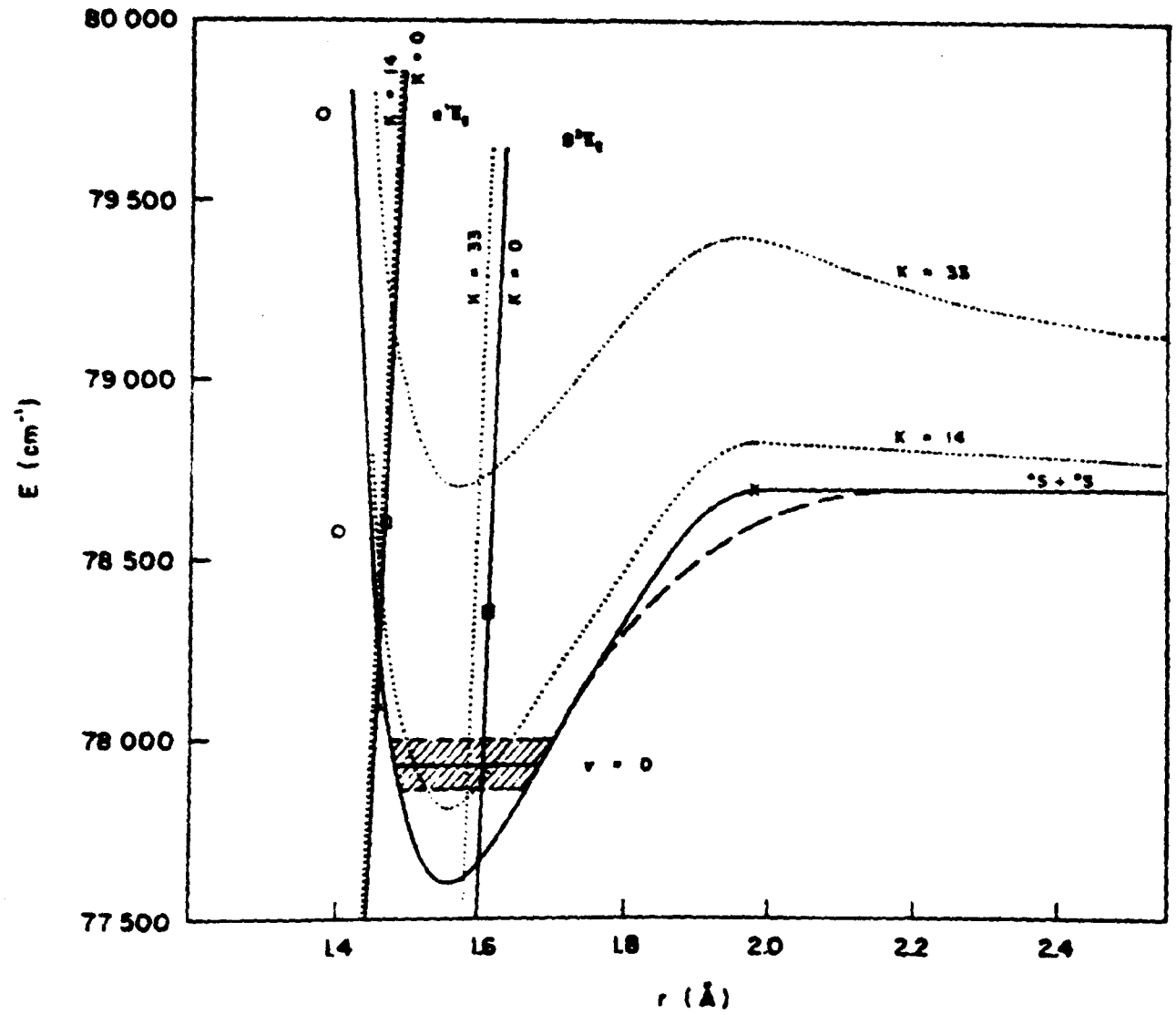
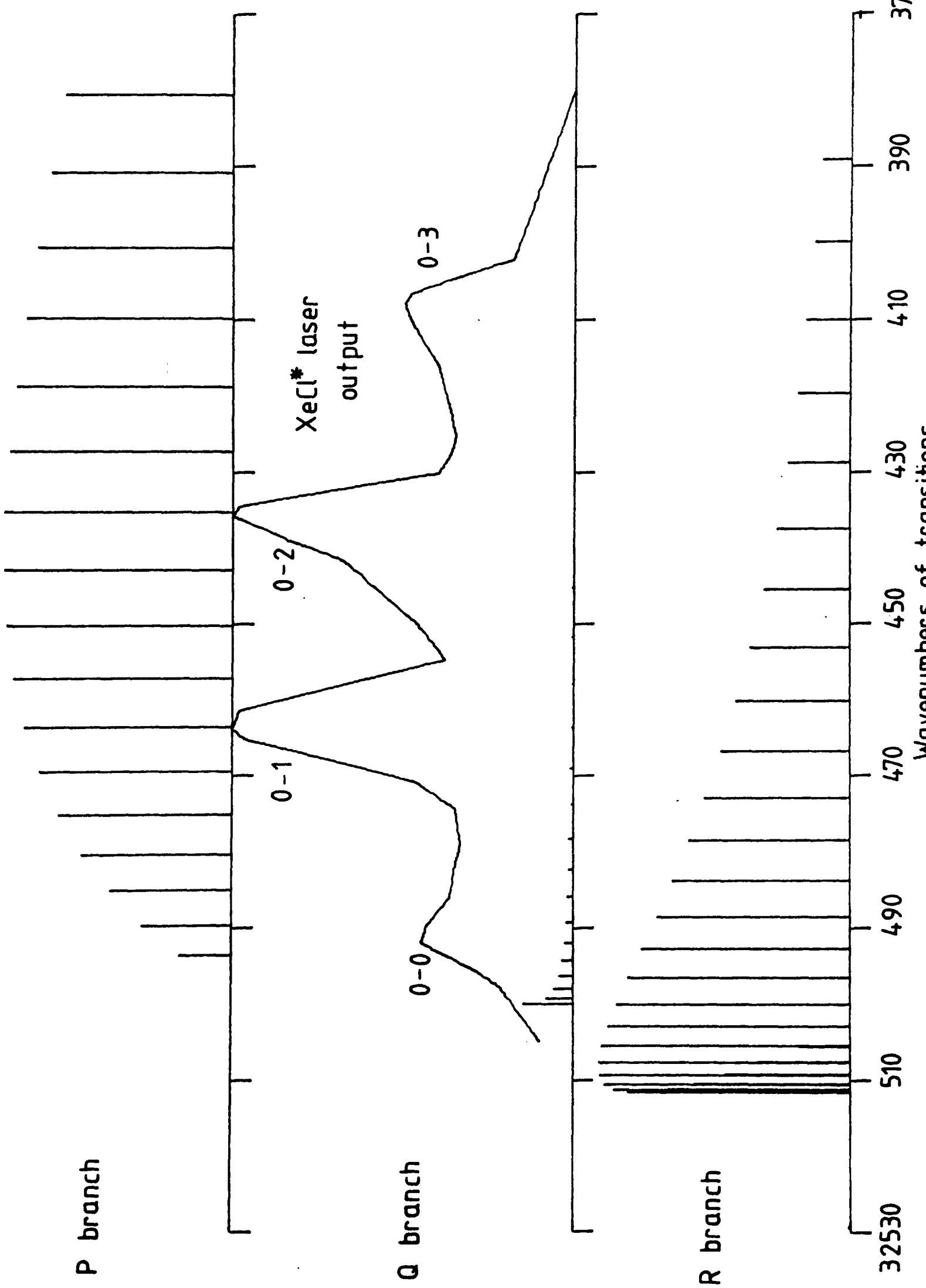


Figure 5.4 Curve crossing partial term diagram

Figure 5.5 Rotational transitions of the $b^1\Pi_u(v'=1) - a^1\Pi_g(v''=0)$ band



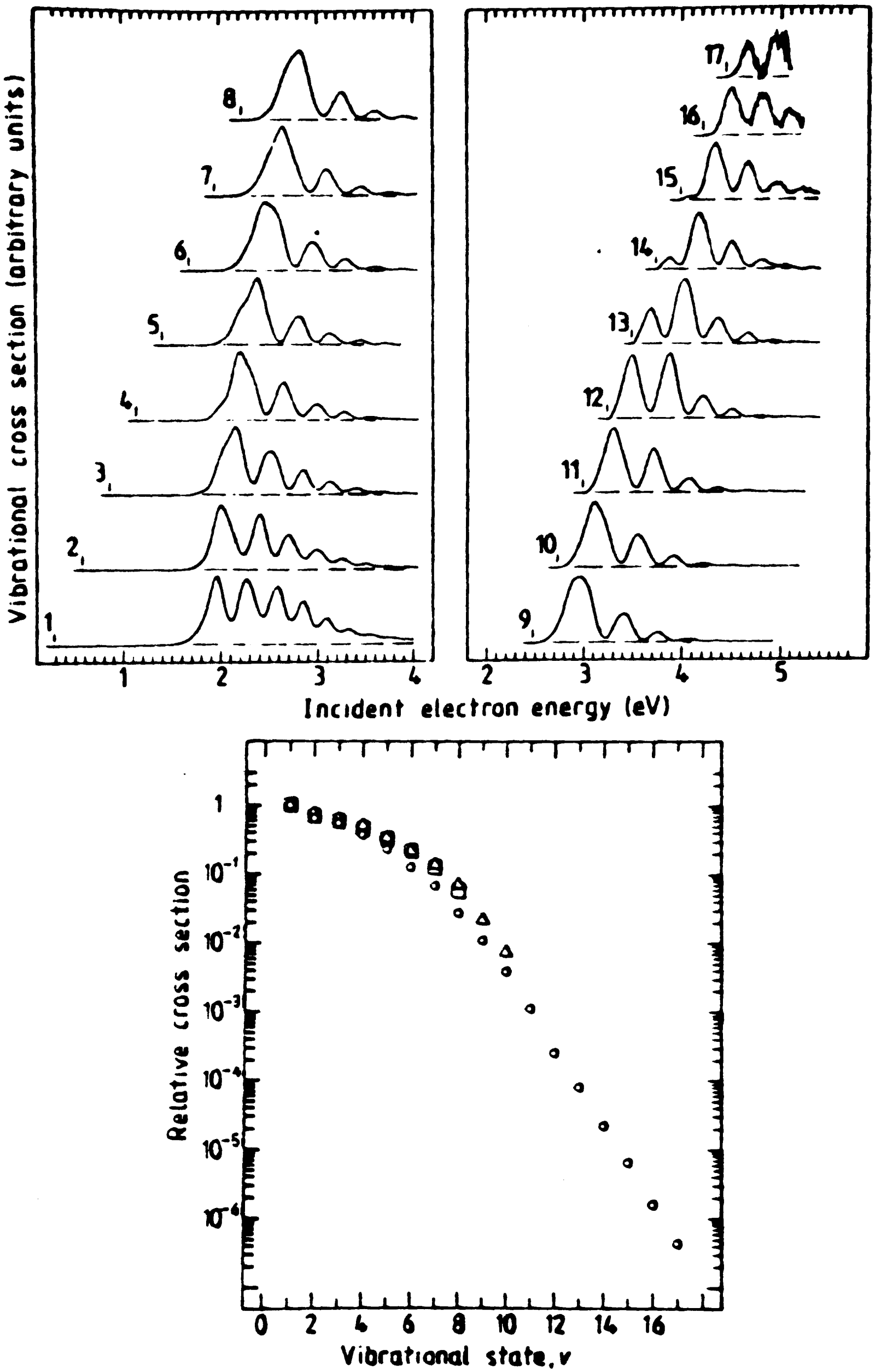


Figure 5.6 Vibrational excitation cross sections

CHAPTER 6 : XENON CHLORIDE TUNED LASER

6.1 INTRODUCTION

In the previous chapter a novel scheme was proposed for a VUV laser. The second stage of the excitation process requires that radiation from a xenon chloride laser should be absorbed by molecules in an intermediate metastable state. In this chapter, the design of a xenon chloride laser suitable for "transferring" the population to the upper level of the proposed VUV laser medium is described. Details of the performance of the xenon chloride laser are presented.

The xenon chloride laser belongs to the class of lasers called Rare Gas Halide (RGH) lasers. As their name suggests, the lasing species is an excited complex formed from a rare gas atom and a halogen atom. These molecules are weakly bound or dissociatively unstable in the ground state, but have bound excited states. By forming these "dimers" in an excited state (excimer), an inversion is achieved with respect to the dimer ground state, which is empty due to its unstable nature. Thus it is possible to achieve lasing action on the transition connecting the excited state to the ground state. The fluorides and chlorides of argon, krypton and xenon have all lased in self - sustained discharges (although ArCl is a special case, see chapter 2). They oscillate at a number of VUV and UV wavelengths; 175nm (ArCl), 193nm (ArF), 222nm (KrCl), 249nm (KrF), 308nm (XeCl) and 350nm (XeF) all on the B-X molecular transition.

As mentioned earlier, the XeCl laser is of interest in this work because of the coincidence of its output photon energy with the $b\,^1\pi_u - a\,^1\pi_g$ transition energy in molecular nitrogen.

The ground state of XeCl is weakly bound with a dissociation energy of 255 +/-10 cm^{-1} (Tellinghuisen et al, 1976) (figure 6.1), with a vibrational spacing of about $20cm^{-1}$ among the lower levels. Under the multi-atmosphere

conditions at which the laser operates, vibrational quenching of the upper state is very rapid down to the lowest vibrational level. Thus the laser output consists of a number of transitions from v'=0 in the 'B' state to v"=0,1,2,3 in the 'X' state (see figure 5.5). These bands show an asymmetric nature: they are violet degraded because of the various rotational transitions. However the individual rotational lines, separated by a few tenths of a wavenumber, are not resolved in the laser output due to pressure broadening and the isotope shift between transitions of ^{37}Cl and ^{35}Cl.

In a discharge-excited XeCl laser a typical gas composition would be a few millibar of hydrogen chloride gas (the preferred halogen donor), a few tens of millibar of xenon and a few bar of buffer gas, usually helium or neon. The kinetic processes which take place during the discharge are complicated, but the important ones for the dominant mechanism for the formation of excited XeCl are summarised below.

$$HCl + e \rightarrow H + Cl^- \qquad 6.1$$

$$Xe + e \rightarrow Xe^+ + 2e \qquad 6.2$$

$$Xe + e \rightarrow Xe^* + e \qquad 6.3$$

$$Xe^* + e \rightarrow Xe^+ + 2e \qquad 6.4$$

$$Xe^+ + Cl^- + He \rightarrow XeCl^* + He \qquad \text{ion channel} \quad 6.5$$

The 'B' state of XeCl lies close to another excited state, designated 'C', $130cm^{-1}$ away. The populations of those states are fully mixed due to fast collision induced transitions. This gives the 'B' state an effective lifetime of 40ns. Quenching of the 'B' state, predominantly by HCl and Xe, means that its lifetime is an estimated 5ns. It is seen that for effective production of a large population of XeCl (B) an excitation pulse is needed which rises fast on this timescale. This is provided by the fast "internal capac itor" discharge circuit. In this work the same discharge circuitry and laser tube were used as for the molecular fluorine laser, detailed in chapter 3. The only major changes were in the optical cavity employed, as described in a later section.

6.2 LASER DESIGN

Under normal operating conditions the oscillating transition of XeCl is quite well homogeneously broadened, due to the high buffer gas pressure, and comprises a number of transitions all from the XeCl(B,v'=0) vibrational level. As is seen from figure 5.5 the laser output of a discharge excited XeCl laser operating in a normal cavity with broad band mirrors covers approximately $100cm^{-1}$, and overlaps a number of rotational transitions in nitrogen. Because of the narrow linewidth of the individual rotational lines most of the laser energy cannot possibly be absorbed by the nitrogen. To use the laser energy efficiently it is necessary to concentrate the laser oscillation into a narrow band of frequencies so that it can interact with a single rotational transition in nitrogen. It is also desirable for the centre frequency of the laser to be tuneable so that interaction with one selected rotational transition is possible.

By allowing the laser cavity to have a high Q value only at the desired wavelength it is possible to suppress laser action at the other wavelengths because of high cavity losses. As there is reduced competition for the available population inversion for the desired laser output wavelength there is a strong build up of oscillation at this wavelength. Thus, most of the inversion feeds oscillation at the required output wavelength, and the energy is concentrated into this region. Such an approach is far superior to any technique of extra-cavity wavelength selection, e.g. a monochromator, where the energy at the undesired wavelengths is thrown away.

In producing a narrow bandwidth tunable laser there is a trade-off between bandwidth and pulse energy: generally the narrower the bandwidth the lower the energy. Either an intra-cavity etalon, or an arrangement with a grating as the rear reflector can be used as the tuning element. The etalon is tuned by rotating it around an axis perpendicular to the optic axis of the

cavity. The grating can be used in a number of configurations, as shown in figure 6.2. Since the resolving power of a grating depends on the the number of lines which are effectively illuminated, there are various schemes to expand the lateral extent of the grating which is illuminated.

1. Grazing incidence grating

The grating is arranged so that the beam has a very large angle of incidence. A mirror is used to reflect one of the diffracted beams of low order number back to the grating and thus through the laser medium.

This method will give very narrow linewidths, but with low energies due to high reflection losses. These increase rapidly if the angle of incidence is above about 87 degrees due to scatter into grating grooves.

2. Grazing incidence grating with beam-expanding prism

By using a prism to provide some beam expansion, the grating is filled even when the angle of incidence is about 80 degrees, when grating losses are more reasonable.

This can increase the extremes of the tuning range, but is rather more complicated to align.

3. Littrow grating

This system has a low loss and so gives a large energy output and wide tuning range. But the linewidth is quite large and the high power densities on the grating can easily exceed its damage threshold.

4. Littrow grating with beam expanding prism

Here again the beam is expanded by passing it through a prism at a high angle of incidence. This leads to a reduced bandwidth, with a moderate loss of energy. The tuning range will also be reduced slightly.

For this work it was decided to use a Littrow mounted grating with beam expanding prisms. With this tuning arrangement it is not possible to use the whole width of the discharge gain medium, as a path with a narrow angular spread needs to be defined through the cavity for wavelength selectivity. This is achieved by placing apertures at each end of the cavity. However, this means that only a fraction of the gain region is used to produce the output beam. In an effort to use the available energy to maximum efficiency and to achieve as high an output energy as possible, the output beam of the oscillator was fed back through the gain region, as a single pass amplifier (figure 6.3). This arrangement was used rather than a folded cavity, of twice the length, as it allowed more cavity round trips during the gain period. The light thus passes through the wavelength selective elements more often, which gives a better spectral discrimination as undesired wavelengths see a greater loss. The gain period is limited by the time for which a stable glow discharge can be maintained. As the discharge constricts, and possibly collapses to an arc, the voltage across the gap collapses and the electron temperature falls such that it is unable to adequately pump the laser medium. The spatial uniformity of the medium is broken up and the current flows through only a few channels. This happens in a typical RGH mix after a few tens of nanoseconds. Local inhomegeneities of the electron density cause increased current flow and locally deplete the HCl concentration thus reducing the attatchment rate per electron and further increasing the electron density and current (Coutts and Webb, 1986).

To achieve a suitably narrow linewidth it is necessary to illuminate a large portion of the grating, whilst allowing only a narrow range of angles diffracted off the grating to pass through the cavity. The slits, placed at the ends of the cavity, define the beam's angular divergence, and the slit furthest from the grating restricts the accepted angles from the grating. As more lines are illuminated the resolving power of the grating increases, and so a narrower range of wavelengths is allowed to pass through the slits. To

expand the beam it is passed through a prism, with a grazing angle of incidence onto the hypotenuese face. As the angle of incidence is increased the beam is expanded by a greater factor, but the reflection losses, particularly from the hypotenuese, are increased. So the penalty to be paid for a narrower linewidth is reduced energy in the oscillator beam and a compromise must be found between the desired linewidth and an acceptable energy level.

Both the reflection losses from the beam and its expansion factor as the beam passes through a prism can be calculated. The expansion factor is calculated from geometrical arguments. The path of the beam is traced through the prism by applying Snell's Law at each interface, to give the deviation in the direction of the beam. The reflection losses at each face are found from Fresnels equations, once the incident and refracted angles have been ascertained for each plane of polarisation. Using a computer, the reflection energy losses and expansion factors were calculated as a function of the angle at which light is incident onto the prism. This was done in order to investigate the best arrangement regarding the number of prisms, and their required angular orientation. The results of this calculation are shown in Table 6.1 and displayed in figures 6.4 and 6.5, as a function of the incident angles on two beam expansion prisms.

It should be noted that the calculation has been performed for an initially unpolarised beam. This is appropriate to the case of a laser where the number of cavity round trips during the gain period is sufficiently small that the favoured polarisation will not have built up an intensity greatly outweighing the unfavoured polarisation.

It can be seen that, for a given beam expansion factor, the reflection losses using two prisms are less than if a single prism is used. This arises because at the reduced angle of incidence needed with two prisms the loss is sufficiently reduced that, even with the extra number of interfaces, the losses overall are smaller than with one prism. Further there is a broad

minimum of reflectivity around the symmetrical arrangement, when the radiation is incident on both prisms with the same angle. So to achieve a desired expansion factor the best arrangement would appear to be to have to prisms with the same angle of incidence for the radiation on each.

When setting up the prisms in this arrangement it is necessary to know the angle at which the light comes out of the first prism. If the incident angle is known this angle can be easily calculated. For incident angles around 80 degrees, the beam emerges from the prism at around 5 degrees to the normal of the emergent face.

The radiation incident onto the prisms can be considered as consisting of two orthogonal polarisations. Let the planes containing the electric field vectors for these two polarisations be parallel to and perpendicular to the plane containing the normal to the prism face and the incident ray. These are designated p-polarised and s-polarised repectively. The magnitude of the reflection coefficient from a dielectric surface depends on the plane of polarisation, and so these two cases will have different reflection losses when they pass through the beam expanding prisms. The p-polarisation suffers less reflection loss, and for an 80 degree incident angle on both prisms it is only 57% of the s-polarisaton loss. This figure only takes into account the forward, beam expanding pass through the prisms.

The grating itself will have a higher efficiency for radiation polarised with the electric field vector perpendicular to the grating lines. In the arrangement used in this work, with the grating lines vertical, and tuned by rotation around a vertical axis, the maximum efficiency will correspond to the p-polarised light from the prisms. Thus the cavity will have a lower loss for the p-polarised light and it is expected that the output will be dominated by this polarisation, which corresponds to horizontally polarised light.

The higher cavity Q factor for the p-polarisation over the

s-polarisation could be further enhanced by antireflection coating the prisms for the p-polarised light. This was done in the later stages of this work, when the xenon chloride laser was used to pump the excited molecular nitrogen. However in the initial stages when the XeCl system itself was being investigated the prisms were left uncoated so that the reflectivity would not be such a fast function of the angle of incidence onto the prisms. Then when the optimum angular orientation of the components had been found the prisms were coated to minimise their reflectivity at this angle.

6.3 OPERATIONAL CHARACTERISTICS OF THE XeCl LASER

6.3.1 Untuned oscillation

The xenon chloride laser was initially operated using a plane-plane cavity consisting of an aluminium coated mirror and a quartz flat as output coupler. The discharge circuit had a 69nF storage capacitor, and a total of 39nF capacitance for the internal peaking capacitors. The discharge volume was 600x25x12mm. The GP2000 cryogenic gas purifier was connected to the laser tube as part of a gas circulation loop.

The laser tube was filled with a gas mix as follows; 6mbar HCl, 35mbar Xe and to 3bar with He. In this configuration the laser output energy was measured for different values of the charging voltage, using a GenTec pyroelectric energy meter. The results obtained were:

30kV	142mJ
35kV	167mJ
40kV	188mJ.

With these values obtained for comparison purposes the cavity optics were changed to allow line narrowed tuned operation.

6.3.2 Initial tuned configuration

The laser was arranged with two 45^{o}-90^{o}-45^{o} quartz prisms to expand the

radiation onto a Littrow mounted grating (1200 1/mm blazed at 750nm). Another quartz prism was used to turn the oscillator beam back on itself for injection into the amplifier side of the discharge (see figure 6.3). The cavity was formed between the grating and a quartz flat , at the far end of the discharge, whilst at the end near the grating the gas envelope was completed with a quartz window, placed 5^{o} off axis. In this first arrangement 0.5x12mm slits were placed to define the cavity dimension of the oscillator side only. This led to the output being dominated by double pass amplified spontaneous emission (ASE) from the amplifier side, with a small tuneable contribution superimposed on it. This problem of an untuned background radiation from the amplifier section would have to be taken into account in all future measurements of the performance of the tuned laser. To reduce the amount of ASE falling on the dectection system another set of slits were fabricated. These had two 1x12mm slits and one set were placed at each end to define both the oscillator and amplifier paths. Also, off axis windows were fitted at both ends of the discharge, and the oscillator cavity output coupler became the retroreflecting prism. These measures helped to reduce the amount of ASE, but could not remove it entirely. This was in part due to the arrangement of the oscillator and amplifier in that they could not be adequately decoupled to prevent the amplifer side from double pass lasing off the oscillator side output coupler, without significantly increasing the complexity of the optical arrangements.

6.3.3 Optimisation of performance

In order to operate the laser under the best conditions the gas mixture fill was varied over a wide range to determine the optimum. This was done using only the output from the oscillator side so that effects of amplification would not be involved. The laser was flled with 5mbar HCl and 25mbar Xe and with the GP2000 trap at 139K and a charging voltage of 30kV, the energy was measured as a function of the total pressure in the tube as more

helium was added. For each pressure the average energy was found both with the grating covered and with it uncovered, the first value being taken as an indication of the background value of untuned radiation component in the output energy. The results are shown in the following table and figure 6.6.

Table 6.2 Laser energy vs. pressure

Pressure (p.s.i.)	Energies (μJ)		
	Grating		
	Covered	Uncovered	Difference
18	60	16	44
20	70	17	53
22	78	21	57
24	87	26	61
26	96	29	67
28	106	32	74
30	113	34	79
32	116	36	80
34	116	36	80
36	118	36	82
38	119	36	83
40	87	33	54
42	83	35	48

These results show a broad maximum around 35p.s.i. total pressure.

To find the optimum value of the partial pressures of xenon and hydrogen chloride the ability to alter the temperature of the cryogenic trap was used. An excess of these two gases was placed into the laser tube and circulated through the trap. Then the actual partial pressures of the gases would correspond to the vapour pressure of the gases at the temperature of the trap. Again the oscillator energy was monitored, this time as a function of the trap temperature for a constant total pressure of 36p.s.i., and charging voltage of 30kV. The values obtained are as shown in figure 6.7. This shows a maximum for a trap temperature around 130K, corresponding to vapour pressure of 32mbar Xenon and 3.5mbar Hydrogen Chloride. In future the operating parameters will correspond to those giving maximum energies in this series of experiments.

6.3.4 Gain measurements

Measurements of gain were made under a number of different system configurations to establish the effectiveness of the amplifier side the laser. The gain was taken as the ratio of the output energy from the amplifier side, with injection of the oscillator beam, to that from the oscillator alone , after making due allowance for the untuned background radiation.

1. With slits only around the oscillator side of the discharge and the beam expansion prisms set so that the beam is incident at an angle of 80^{o}, the following results were obtained (see figure 6.8). In this experiment the effect of ASE was avoided by moving the detector far from the laser so that the laser radiation and ASE were spatially separated. To ensure that only the tuned energy fell on the detector a lens was used to focus the radiation onto a small aperture high sensitivity energy meter (GenTec joulemeter type ED100). The ASE was also reduced by running the laser with below-optimum gas mixture: 2mbar HCl, 20mbar Xe and 31p.s.i. He.

Table 6.3 Energy vs. charging voltage

Charging volts (kV)	20	22	24	26	28	30	32	34	36
Amp. energy (mJ)	0.31	0.71	0.92	1.07	1.12	1.22	1.27	1.32	1.32
Osc. energy (mJ)	0.02	0.07	0.09	0.10	0.11	0.12	0.14	0.14	0.15
Gain	15.5	10.1	10.2	10.7	10.2	10.2	9.1	9.4	8.8

2. In this experiment the two beam expansion prisms were set to angles of 75^{o} and 80^{o}. The laser was tuned to the peak of the 0-2 vibrational transition. The gas fill was 5.5mbar HCl, 37mbar Xe and 36p.s.i. He, with a trap temperature of 132-135K. The gain values have standard deviations of 10% due to pulse to pulse variations of the energies.

Table 6.4 Gain vs. charging voltage

Charging volts (kV)	25	30	35
Osc. energy (μJ)	71	127	158
Amp. energy (μJ)			
Grating uncovered	1090	1480	1650
Grating covered	180	290	340
Difference	910	1190	1310
Gain	12.8	9.4	8.3

3. The prism angles were changed so that the angles of incidence were 78^{o}

and 77°, and the laser tuned to the 0-1 vibrational peak. A gas mix of 5mbar HCl, 37mbar Xe and 36p.s.i. He., with the trap at 130K. The gain measurements have a variation of about 3%.

Table 6.5 Gain vs. charging voltage

Charging volts (kV)	25	30	35
Osc. energy (μJ)	138	170	192
Amp. energy (μJ)			
Grating uncovered	1370	1790	1970
Grating covered	400	520	570
Difference	970	1270	1400
Gain	7.0	7.5	7.3

4. As a comparison the tuning elements were altered so that there was a grazing incidence angle of 85° onto the grating, with a mirror to complete the cavity. This used the same conditions as above in 3. The tuning range was restricted to just the two strongest lines of the XeCl emission. The gain values have deviations of 15%, mainly due to large variations in the oscillator energies.

Table 6.6 Gain vs. charging voltage

Charging volts (kV)	25	30	35
Osc. energy (μJ)			
Grating uncovered	80	192	248
Grating covered	40	142	206
Difference	40	50	42
Amp. energy (μJ)			
Grating uncovered	812	1350	1625
Grating covered	400	650	800
Difference	412	700	825
Gain	10.3	14.0	19.6

6.3.5 Linewidth measurements

To enable the linewidth of the tuned laser output to be measured a Fabry-Perot interferometer was used. Its plates were mounted on piezoelectric transducers so that, by applying a slow voltage ramp to them, the etalon spacing could be scanned through a number of free spectral ranges. The laser beam was expanded onto a ground quartz diffusing plate, placed in front of the Fabry-Perot plates, using a 100mm lens. The light transmitted through the interferometer was focused onto a pinhole (0.1mm diameter) placed at the focus of a 750mm focal length lens, behind which a vacuum photodiode was placed to

detect the radiation. The plates were flat to 1/60 wavelength at 308nm, and had a reflectivity of 95%, giving a finesse of 61. The mean plate separation was 0.91mm, giving a free spectral range of $5.49cm^{-1}$. In this case the etalon finesse will contain a contribution due to the plate flatness, with an effective finesse of 30, (Jacquinot, 1960). According to Jacquinot, this gives the effective etalon finesse of 24. Thus the interferometer linewidth was $0.2cm^{-1}$. The interferometer was aligned initially using a beam expanded HeNe laser to illuminate the plates whilst viewing the circular fringes on a screen and adjusting the plate tilt for maximum definition of the fringes.

The laser output was studied either by tuning it to a fixed wavelength and the scanning the separation of the Fabry-Perot plates, or by holding the plate separation constant and adjusting the grating position to tune the laser wavelength. A signal averager (Lambda Physik Fotometer) was connected to the output line from the photodiode. The signal was averaged over three pulses and the mean pulse energy recorded on a chart recorder, from which measurements of the linewidth could be made from a knowledge of the free spectral range (fsr), by dividing the peak width by peak separation and multiplying by the fsr. Figure 6.9 shows the results of one such scan.

Due to the presence of broadband background radiation the intensity between orders does not become zero, and so a suitable baseline must be establised when looking for the half height width of a peak. This was taken to be the transmitted intensity with the grating tuned well away from the lasing position. Because the separation of the orders measured from the charts was not always constant, the value used for a particular peak was the mean value for the separation of its two adjacent peaks, although for those peaks at the ends of a scan only one value of a separation would be available. In some cases the amplified beam was measured, and in others the oscillator beam was picked off, before it would be injected into the amplifier side, and investigated with the Fabry-Perot.

A table showing the results of these experiments is given below. The

scan speed is the time in minutes to change the etalon plate separation by its maximum travel allowed by the piezoelectric tranducers. The prism angles given are those incident angles on the hypotenues face of each prism, or for the case of grazing incidence on the grating, when no prisms are used, it is the incidence angle on the grating. The energy values are calculated from the peak heights on the chart recordings, knowing various scaling factors of the instruments and making comparisons to actual energy measurements where available. They are accurate to 40%. The errors in the linewidth measurements come from the spread of values obtained for each run. The values will include a contribution from the Fabry-Perot linewidth, estimated at $0.2cm^{-1}$. All measurements are taken at a charging voltage of 30kV, and with the cryogenic trap at 130K, unless otherwise stated.

Table 6.7 Linewidth measurements summary

Expt. No.	Beam	Scan Type	Scan Speed	Prism Angles	Energy mJ	Linewidth cm^{-1}	Notes
A	AMP	GRT		15,10	1.3	2	
B	AMP	F-P	100	"	1.5	2	
C	AMP	F-P	20	"	2.1	2	
D	AMP	GRT		"	2.5	2	
E	OSC	GRT		"	0.16	1	
F	OSC	GRT		"	0.32	2	
G	OSC	F-P	100	"	0.32	3	
H	OSC	F-P	100	12,8	0.17	1	
I	AMP	F-P		"	1.27	2	
J	AMP	F-P	100	"	1.47	2	27.5kV
K	AMP	F-P	100	"	1.2	3	
L	AMP	F-P	100	"	1.35	2	25kV
M	AMP	F-P	50	"	1.69	2	
N	AMP	F-P	50	"	0.23	1	114.5K
O	AMP	F-P	50	"	0.05	1	110K
P	AMP	F-P	50	10,5	1.17	2	
Q	AMP	F-P	50	"	1.23	3	
R	OSC	F-P	50	"	0.03	1	
S	OSC	F-P	50	"	0.03	1	125K
		GRAZING INCIDENCE GRATING					
T	AMP	F-P	20	85	1.47	3	
U	AMP	F-P	100	"	1.47	2	
V	AMP	F-P	50	>85	1.26	3	

Although within each run the peak heights varied, as did the peak linewidths, to within the experimental error there was no correlation between peak height and the width to spacing ratio within a run.

6.3.6 Tuning range

When the oscillator output was fed back through the discharge and amplified, it was possible to produce tuneable laser radiation on all four vibrational transitions across a wavelength range of 1nm, as shown in figure 6.10. However if only the oscillator output was used it was only found possible to detect lasing when the grating was tuned to the region around the two more intense peaks (0-1 and 0-2). A similar restriction to the tuning range occured if the grazing angle incidence grating arrangement was used.

6.4 CONCLUSION

In this chapter the design of a xenon chloride laser, suitable for use as the "transfer" laser of the new VUV laser scheme proposed in the previous chapter, has been presented. The operating characteristics of the XeCl laser have been described.

It has been shown that it is possible to obtain about 1.5mJ of tuneable laser radiation with a bandwidth of about $2cm^{-1}$, and a tuning range of over $100cm^{-1}$. This has been achieved in a device of relatively straight-forward design involving minimum change to an existing wide discharge XeCl laser. By choosing a suitable optical arrangement it has been possible to create both an oscillator and an amplifier stage within the same discharge. The operation of a laser with the oscillator and amplifier utilising the same discharge is simplified because there is no need to strictly control the relative breakdown of two separate discharges.

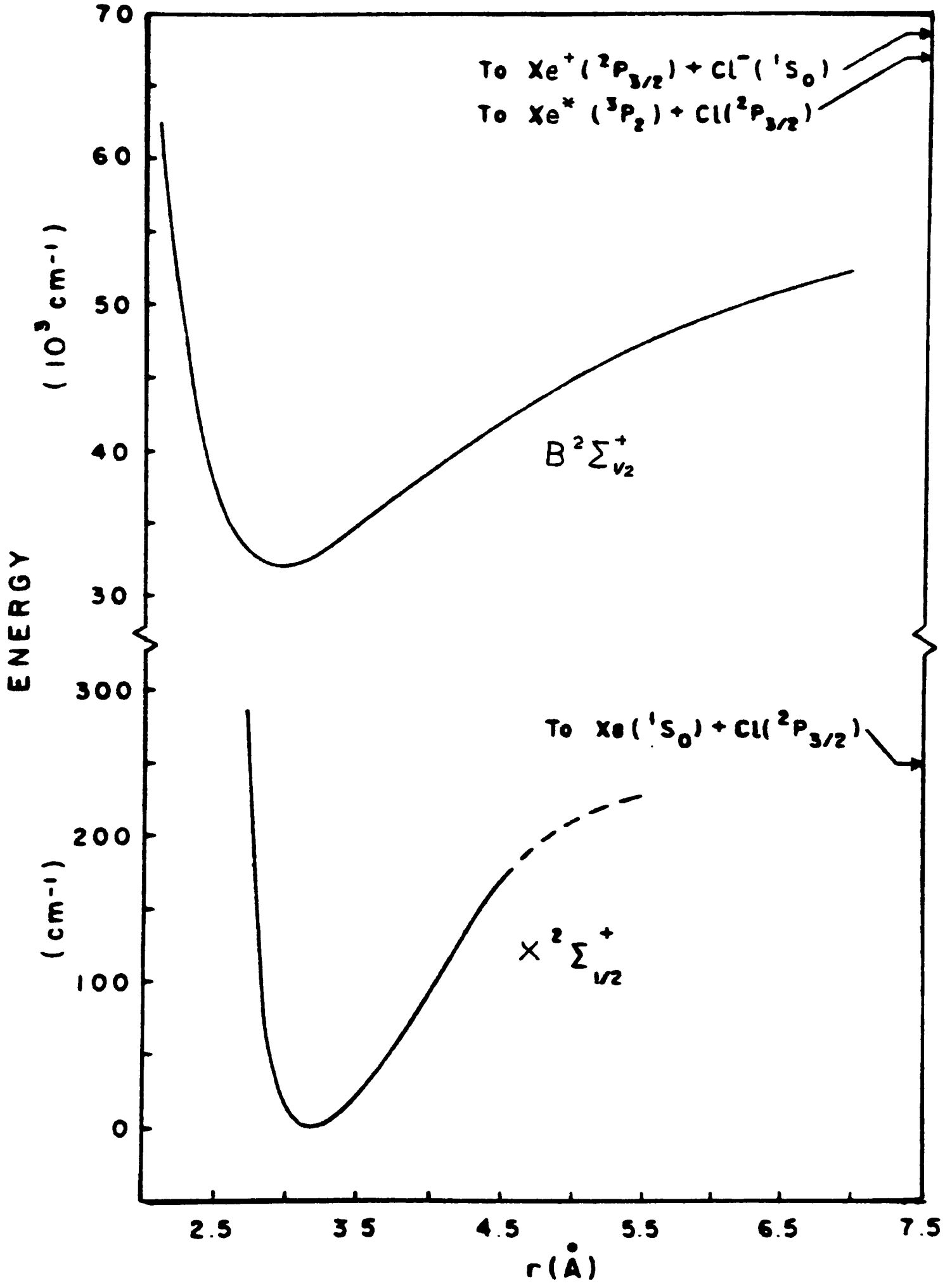
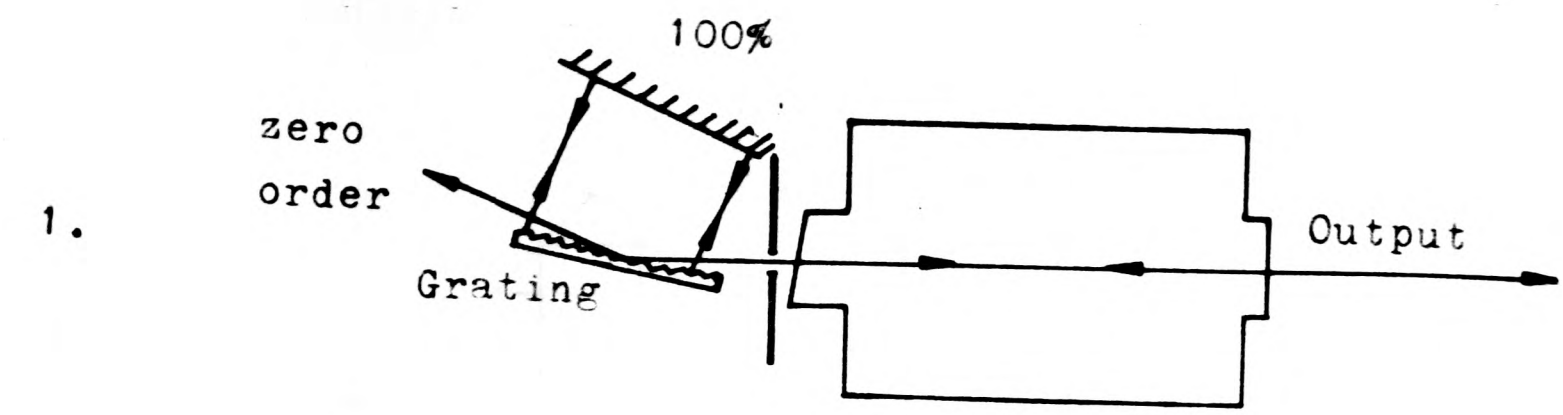
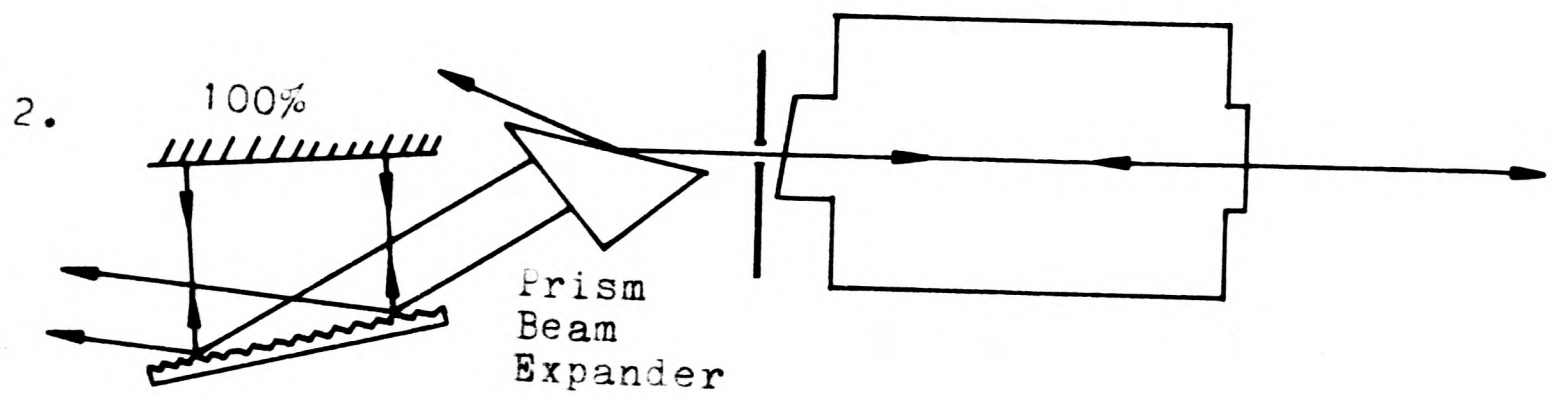
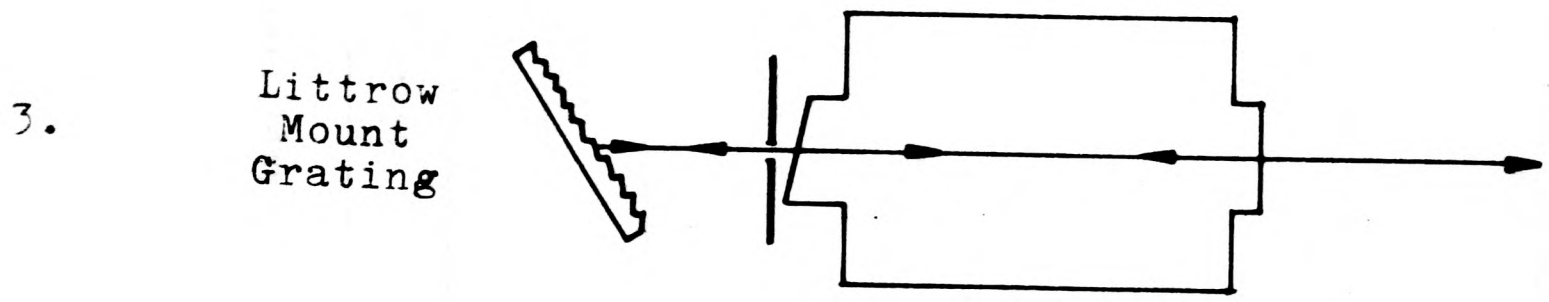


Figure 6.1 Potential energy curves for XeCl

Note: Different scales for upper and lower curves.







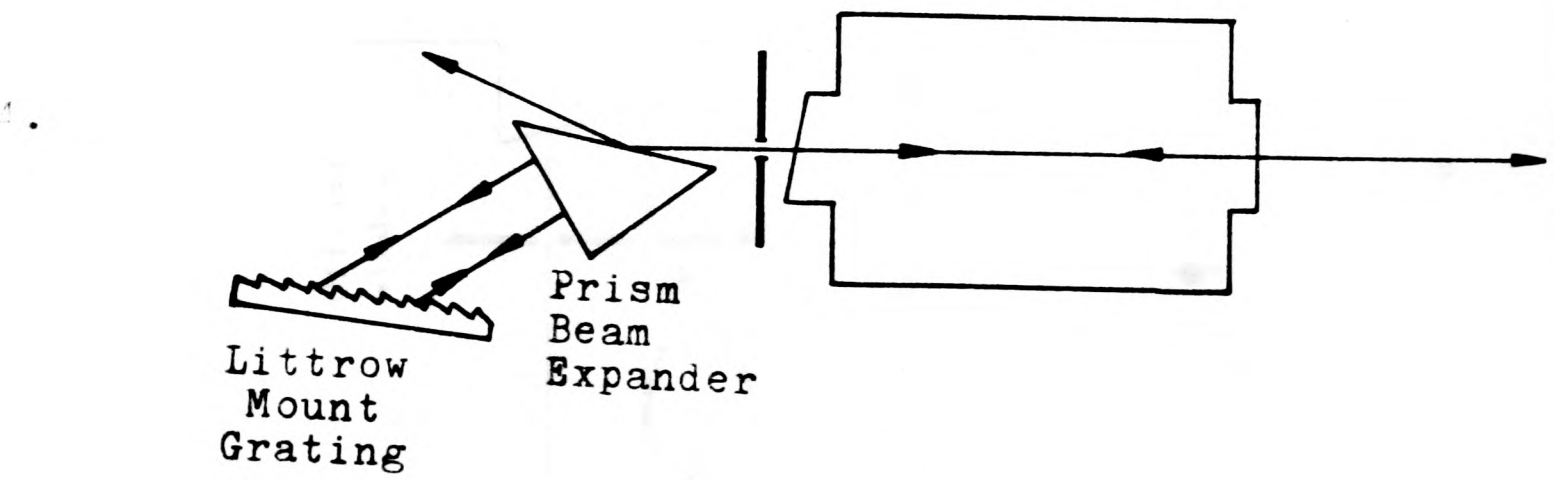


Figure 6.2 Tuned XeCl Laser Cavities

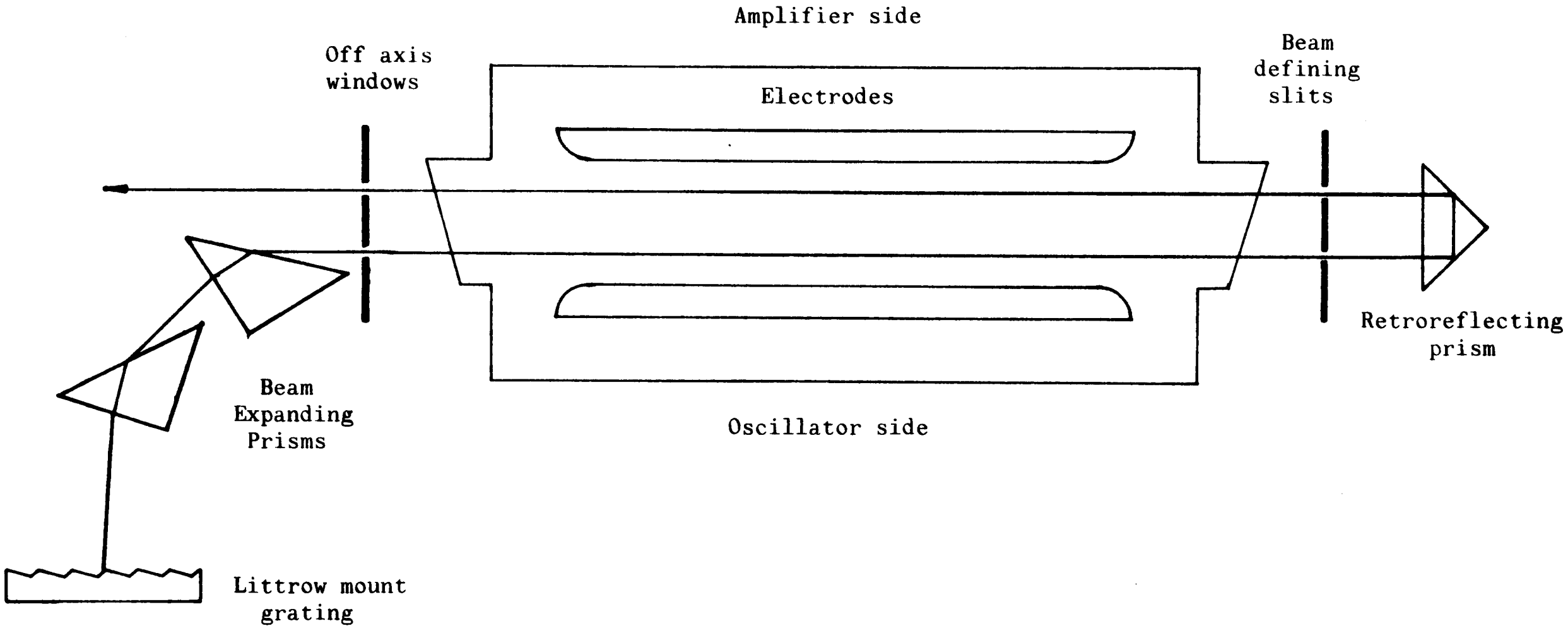


Figure 6.3 Oscillator/amplifier arrangement for tunable XeCl laser

	One Prism	74	75	76	77	78	79	80	81	82	83	84	85	86
74	26	43	45	46	48	50	52	54	57	60	63	67	71	75
	3	7	8	8	9	9	10	11	13	14	16	19	23	29
75	28	45	46	48	49	51	53	56	58	61	64	68	72	76
	3	8	8	9	9	10	11	12	13	15	17	20	24	31
76	30	46	48	49	51	52	54	57	59	62	65	68	72	77
	3	8	9	9	10	11	12	13	14	16	19	22	26	33
77	32	48	49	50	52	54	56	58	60	63	66	69	73	77
	3	9	9	10	11	12	13	14	15	17	20	23	28	35
78	35	50	51	53	54	56	58	60	62	64	67	71	74	78
	4	9	10	11	12	13	14	15	17	19	21	25	30	38
79	38	52	53	55	56	58	59	61	64	66	69	72	75	79
	4	10	11	12	13	14	15	16	18	20	23	27	33	41
80	41	54	56	57	58	60	61	63	65	68	70	73	76	80
	4	11	12	13	14	15	16	18	20	22	26	30	36	45
81	44	57	58	59	60	61	63	65	67	69	71	74	77	81
	5	13	13	14	15	17	18	20	22	25	29	33	40	50
82	48	60	61	62	63	64	66	67	69	71	73	76	79	82
	5	14	15	16	17	19	20	22	25	28	32	37	45	56
83	52	63	63	64	65	67	68	70	71	73	75	78	80	83
	6	16	17	19	20	21	23	26	29	32	37	43	51	64
84	57	66	67	68	69	70	71	73	74	76	78	80	82	85
	7	19	20	22	23	25	27	30	33	37	43	50	60	75
85	63	71	72	73	73	74	75	77	78	79	81	83	85	88
	8	23	24	26	28	30	33	36	40	45	51	60	72	90
86	69	76	76	77	78	79	79	80	82	83	84	86	88	90
	11	29	31	33	35	38	41	45	50	56	64	75	90	112

Table 6.1 Expansion factors and reflection losses

Row headings refer to angle of incidence on prism 1
Column headings refer to angle of incidence on prism 2
Top figures are reflection losses
Bottom figures are expansion factors for the given prism arrangements

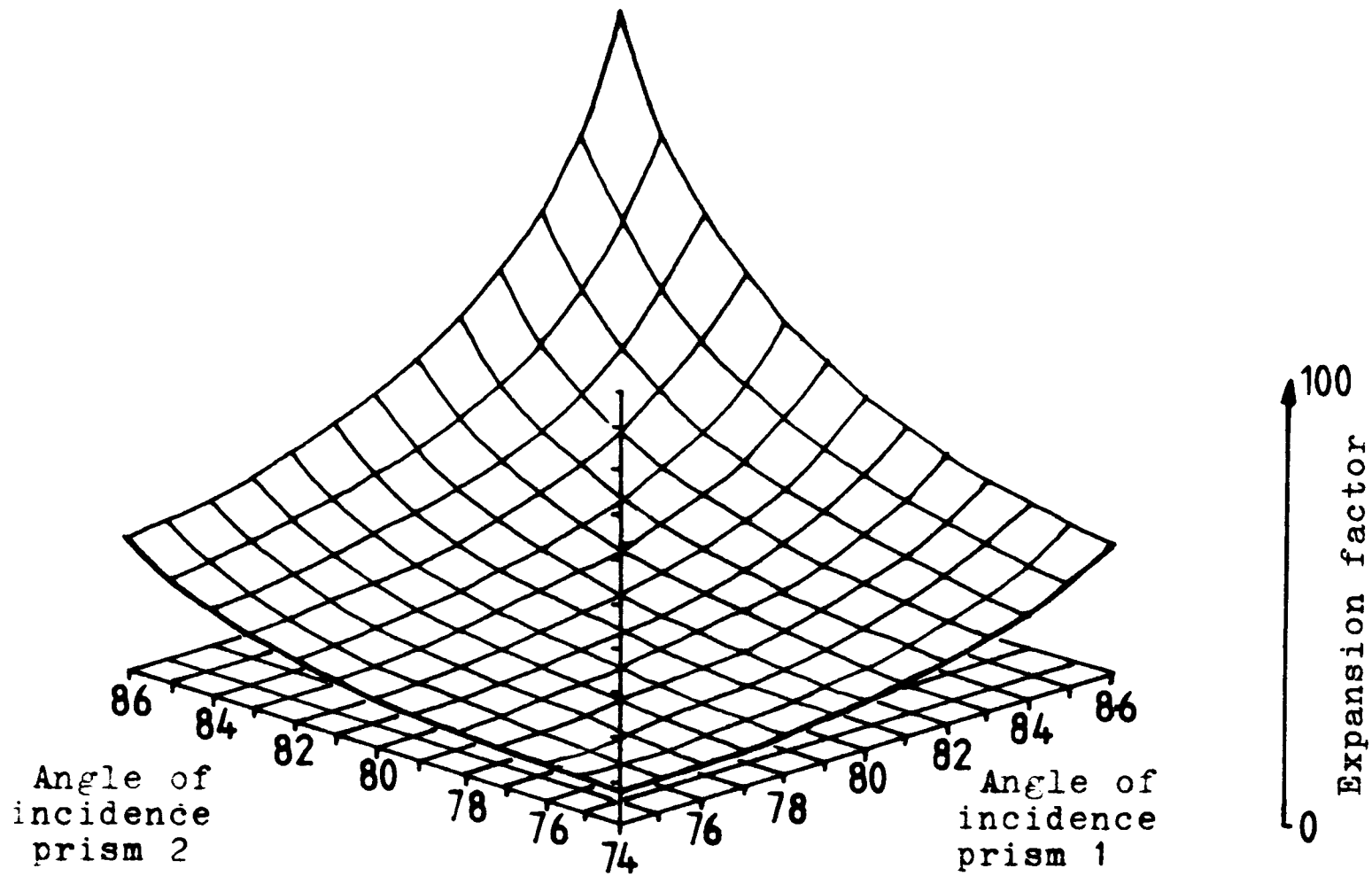


Figure 6.4 Beam expansion factors as function of prism angle

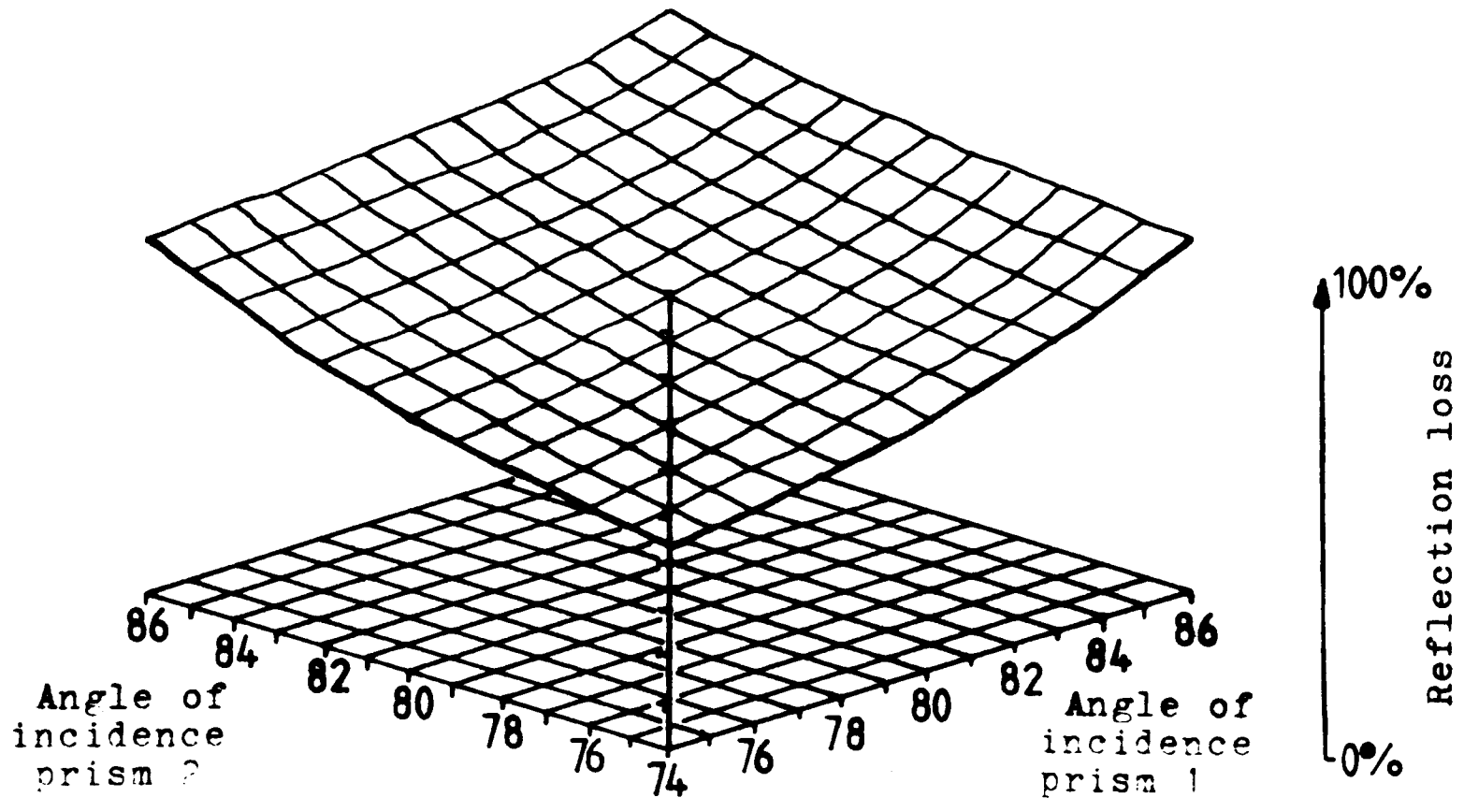


Figure 6.5 Total reflection losses as a function of prism angle

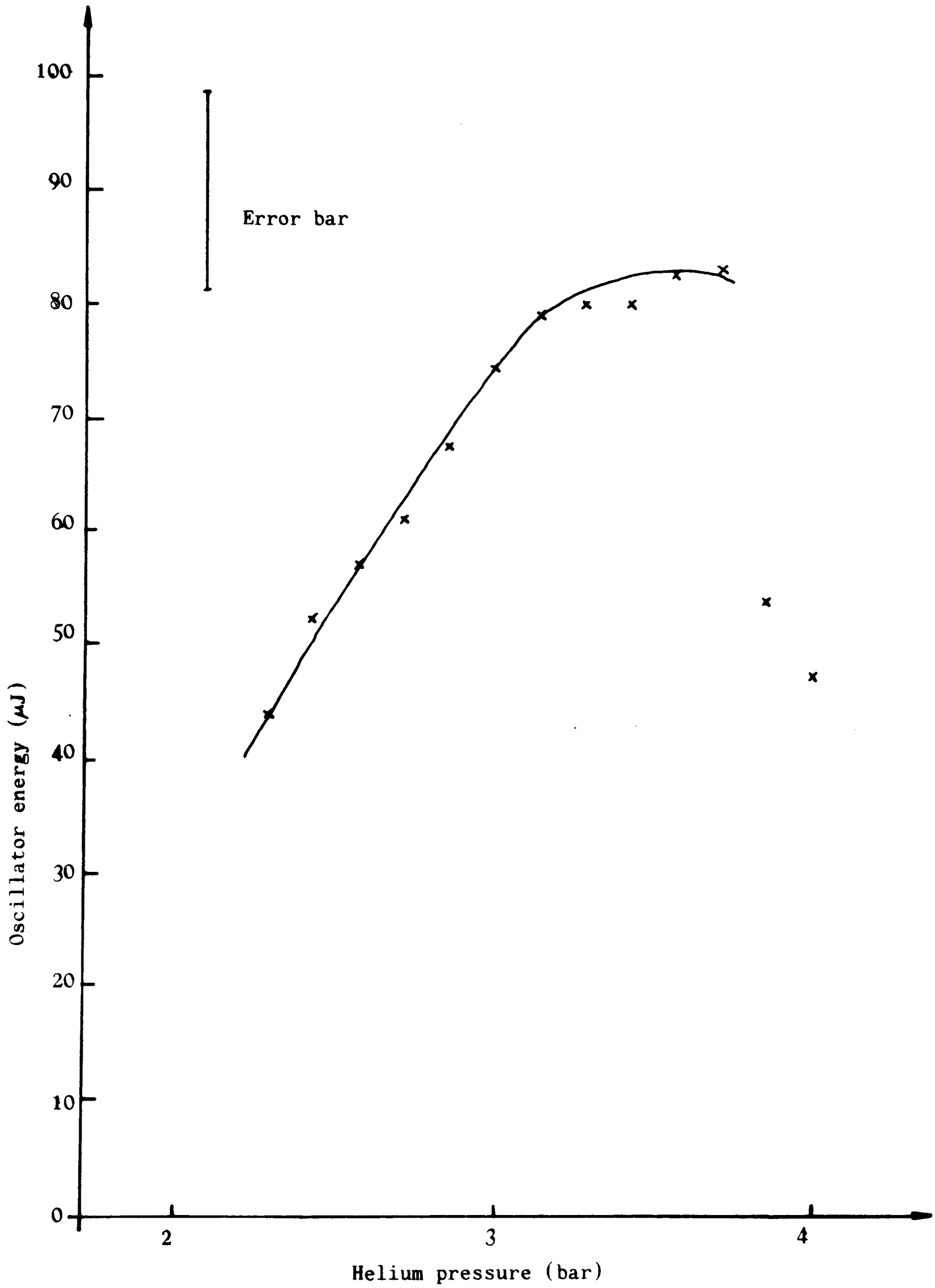
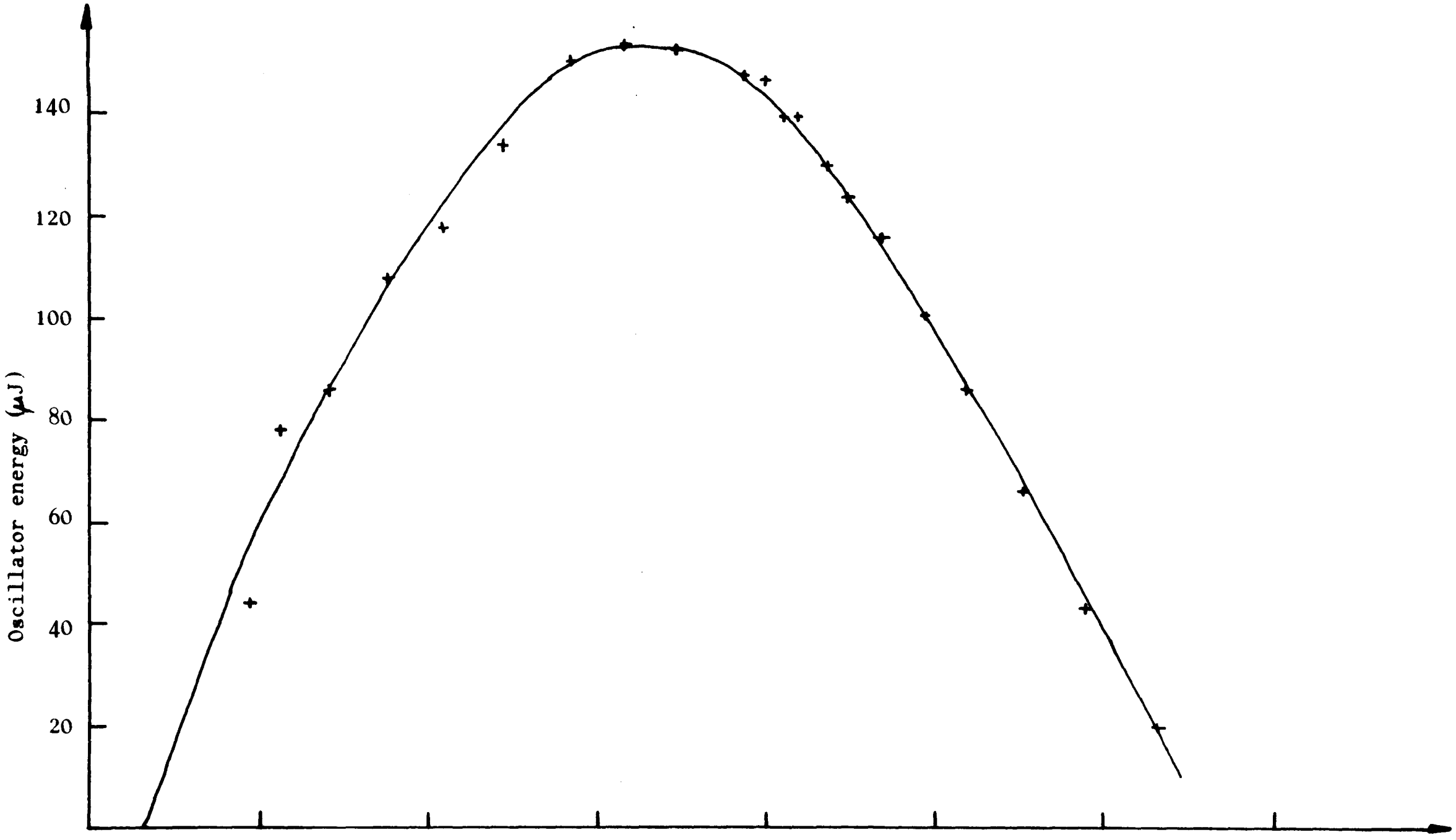


Figure 6.6 Oscillator energy as a function of helium pressure



Trap temperature (K)	120	125	130	135	140	145	150
HCl vapour pressure (mbar)	0.9	2.1	4.6	9.2	17.8	34.2	56.6
Xe vapour pressure (mbar)	12.4	23.7	42.1	73.7	126.3	267.9	328.9

Figure 6.7 Oscillator energy as a function of cryogenic trap temperature

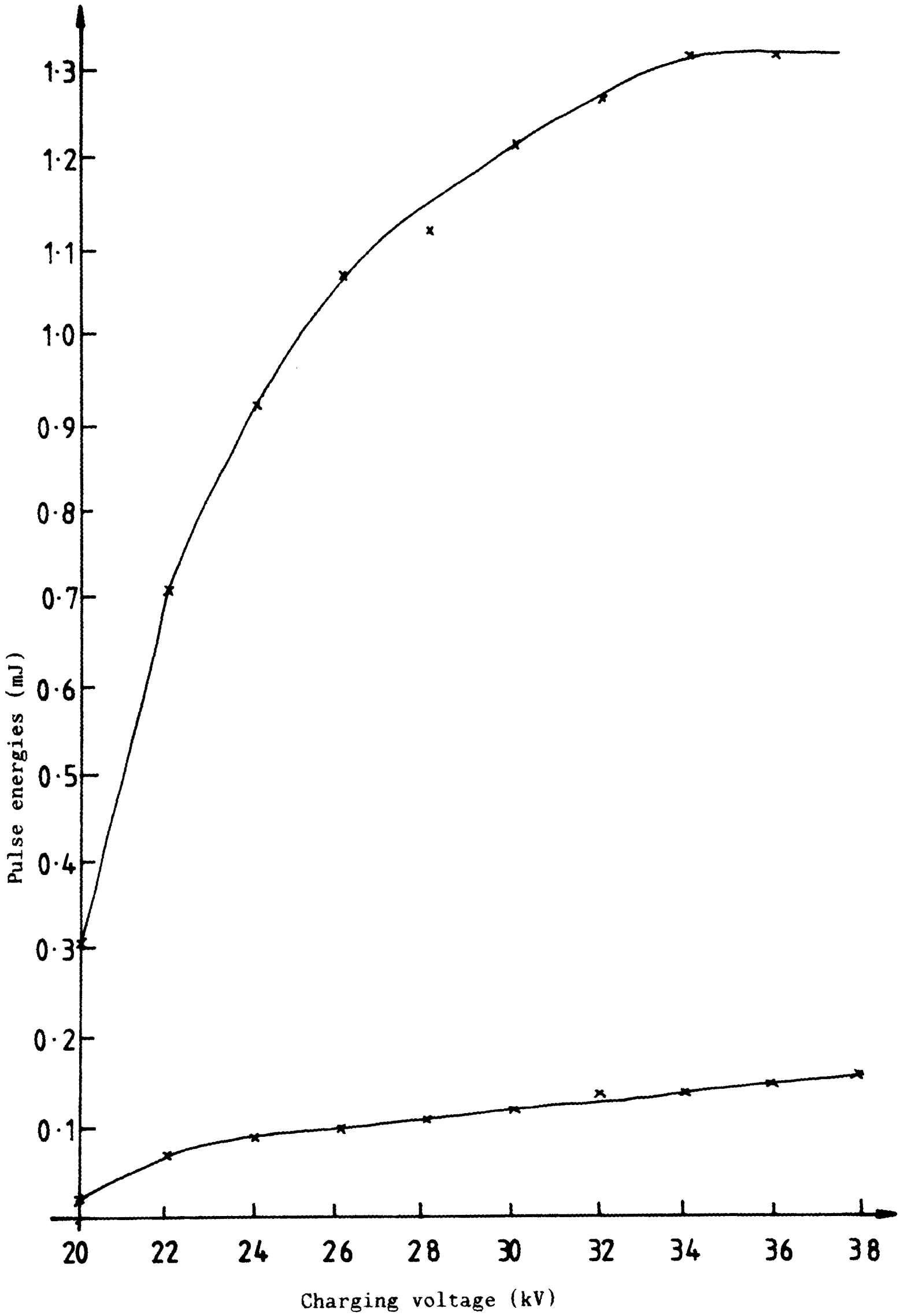


Figure 6.8 Comparison of oscillator and amplifier pulse energies

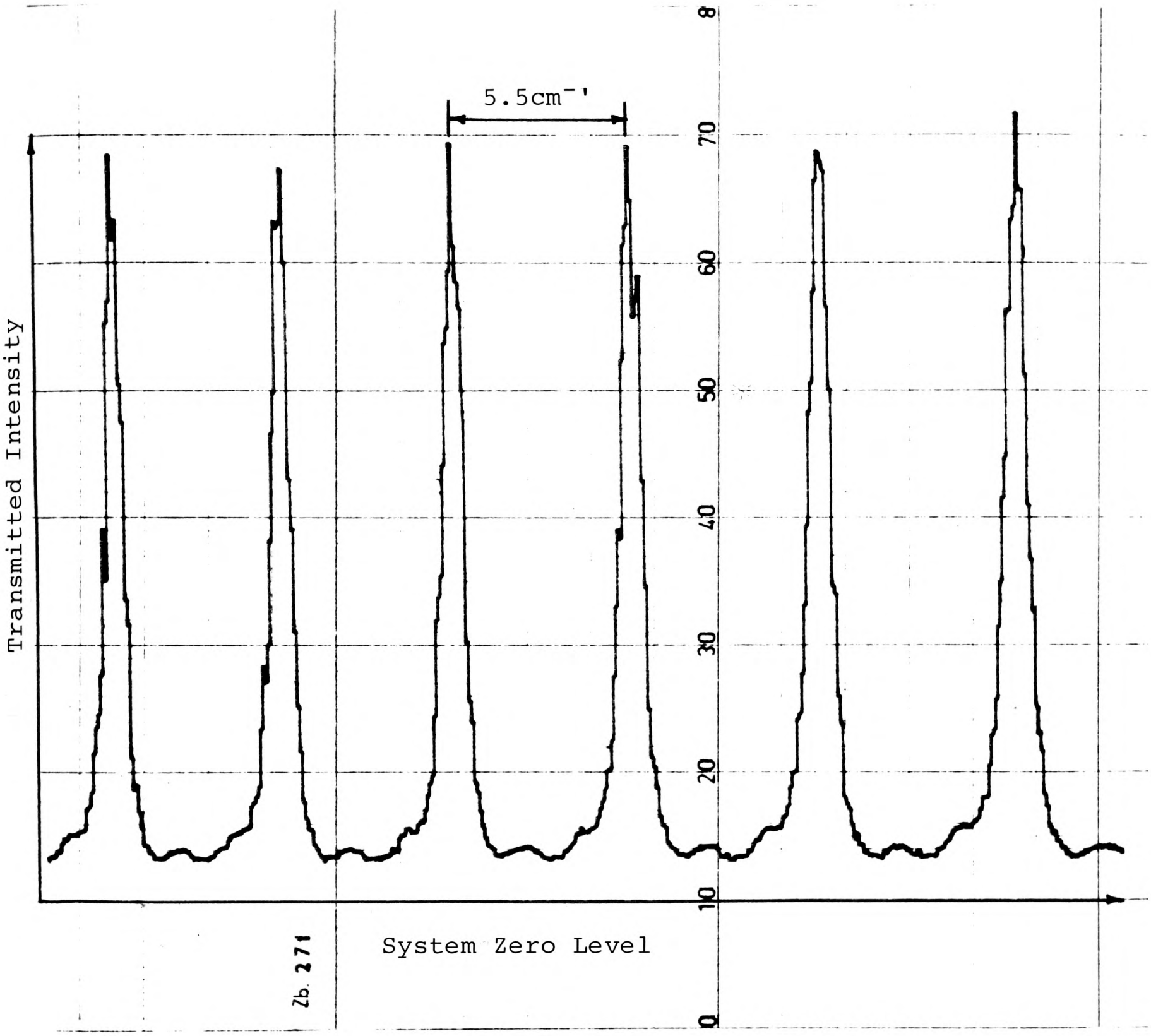


Figure 6.9 Fabry Perot etalon scan of oscillator output

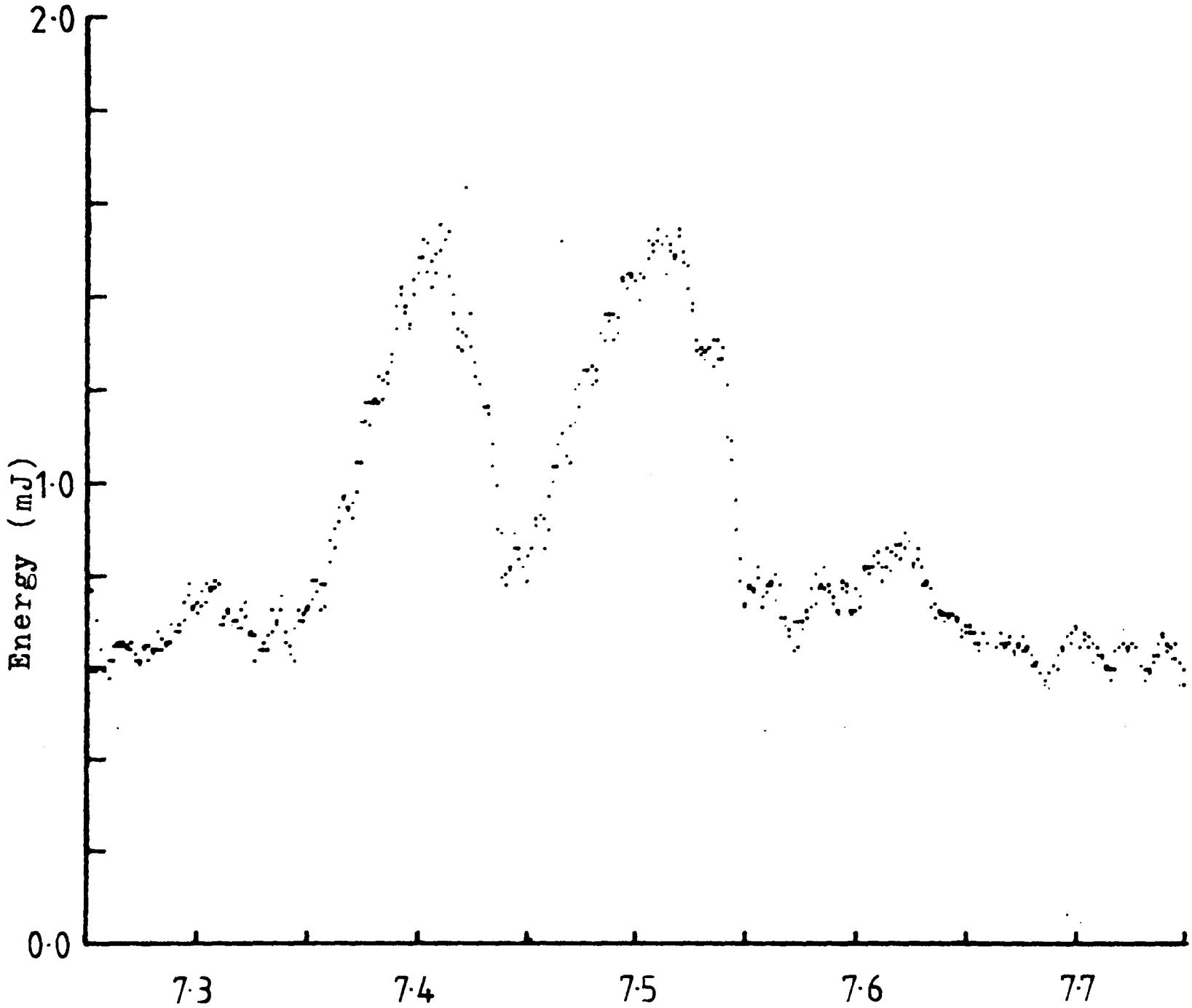


Figure 6.10 Tuned amplified output of XeCl laser

CHAPTER 7 EXPERIMENTAL ARRANGEMENTS FOR PRELIMINARY INVESTIGATIONS OF THE PROPOSED NITROGEN VUV LASER SCHEME

7.1 INTRODUCTION

In previous chapters, a new scheme for a VUV laser has been presented. In this chapter, the equipment used for the experimental investigations necessary to realising the potential of that system in practice is discussed.

The first part of the chapter concentrates on the detection of the VUV radiation. In the second part there is a discussion of the techniques for the interfacing of the experimental apparatus to a microcomputer.

7.2 EXPERIMENTAL APPARATUS

7.2.1 General

The work described in this chapter concerns the general problem of detecting visible, UV and VUV radiation emitted from gas discharges. In many cases the light is of a very low intensity. It was therefore necessary to employ photoelectric detection, together with sensitive electronic recording apparatus. However, pulsed gas discharges inevitably produce electromagnetic fields of large amplitude and high frequency. Such radio frequency fields are detrimental to the recording of the data for two main reasons.

Firstly, they can cause sensitive recording apparatus to give spurious results, and even cause them permanent damage in some instances.

Secondly, the RF noise is picked up on the signal cables causing a considerable reduction in the signal to noise ratio, even if coaxial cable is used exclusively to provide interconnections between parts of the detection system. To overcome the first problem the electronic equipment was sited well away from the vicinity of the discharge. The effectiveness of the spatial

separation was enhanced by enclosing the discharge within a Faraday cage: the walls and floor of the room containing the discharges were covered with copper sheet, which was firmly earthed. All detection equipment was housed in a separate, but adjacent room: the quiet room. All shielding within the Faraday cage was connected to the wall earth, including the signal cable braids as they passed through the wall to the quiet room, in which was the recording equipment. Care was taken that a piece of equipment was only connected to earth via one route, to avoid the formation of unwanted ground loops, which would enhance the pickup of noise.

The apparatus for the experiments described here consists of three main elements: an electric gas discharge producing emission, a system for detecting this emission and producing an electrical signal output, and a recording system for storing these signals and processing them in an understandable and permanent way. Some form of control is also necessary to coordinate the various elelments.

For the moment the discharge tube and its associated vacuum eqiupment and circuitry will not be disscussed in detail as it underwent a number of evolutionary changes which will be dealt with in the next chapter. The emitted light was detected using a VUV monochromator and a photomultiplier tube, and the signal recorded either directly or on an oscilloscope or via a boxcar integrator. Coordination of the experiments was under the control of a microcomputer. These various elements of the detection system will be discused in the following sections, and are shown in diagrammatic form in figure 7.1.

7.2.2 Vacuum and gas handling considerations

In this section some points concerning the vacuum and gas handling system of the discharge tube and VUV monochromator will be discussed.

As stated previously, when studying emission in the VUV region it is necessary to have a system free of impurities which would act to absorb the

radiation, and even, perhaps, to quench the emitting species. This imposes strict requirements on the maximum leak rates allowable for the vacuum vessel, and limits the choice of materials available for its construction. It was found that any plastic materials within the system (even if kept well away from the discharge region but exposed to the hard UV radiation) had a detrimental effect. This was not at first realised, and the flange coupling the discharge tube to the monochromator was initially fabricated from PVC. This was later changed to brass when the PVC was seen to be degrading where exposed to the radiation. For most of the experiments described here the VUV monochromator was part of the gas envelope, as there was no suitable window material when investigating the region below 110nm.

To keep the gas clean, a number of gas purification techniques were used. A cryogenic trap was placed in the circulation loop and operated at the temperature of liquid nitrogen (77K). A chemical trap was also used for some of the experiments. This consisted of a narrow bore tube of copper which had been heated to red heat in air and thus had a layer of copper oxide on its surface. It was placed in the gas circulation loop and run at a moderate temperature (500K). This had the effect of oxidising any impurities in the gas. It was particularly used for converting CO to CO_2, by the reaction

$$CO + CuO \rightarrow Cu + CO_2, \qquad 7.1$$

which could then be removed in the cryogenic trap. In some of the later work a flow of clean gas was maintained through the discharge region from the cylinder.

7.3 RADIATION DECTECTION SYSTEM

7.3.1 Monochromator

To select the individual VUV emissions a McPherson 0.2m VUV scanning monochromator was used. Originally this was provided with an osmium coated grating, although for the later work the grating was replaced by an

aluminiumized grating with a magnesium fluoride overcoat. Both gratings were holographic gratings with 1200 l/mm. The monochromator's speed was f/4.5, the grating size being 40x45mm. The resolution of the monochromator was quoted by the manufacturer as 0.1nm, and it had a linear dispersion of 3.37nm/mm at 100nm. Its wavelength accuracy was specified by the manufacturer as 0.1nm, but, as will be seen, its linearity was better than this. Grating efficiencies for the osmium grating were given as 22% at 121.6nm, and 29% at 161.0nm. However such values are believed to be much greater than the ones obtained in these experiments because of the aging of the grating and its previous history of use. Later measurements were made with the new grating, when the given efficiencies of 6.6% at 121.6nm and 3.4% at 161.0nm can be expected to be essentially correct.

The scanning control of the monochromator was connected to a stepping motor to facilitate computer control of the wavelength setting. From data taken over the whole wavelength range of the monochromator, the scanning calibration was found to be 200 steps/nm. Although no specific check was made on the linearity and wavelength independence of this calibration, cross-checks of spectra produced with published wavelength values agreed well. As this calibration represents an average over the whole range (0-500nm) of the monochromator, and typically only the range 100-200nm was used in this work, it is fair to assume that this calibration will hold over the range of interest.

7.3.2 Scintillator and photomultiplier tube

Having isolated the VUV emission of interest by imaging it onto the exit slit of the monchromator there are two basic options as to how the VUV radiation can be converted to an electrical signal. Either a "solar-blind" VUV Photomultiplier Tube (PMT) can be used, or a scintillator can be employed to convert the VUV to radiation at a wavelength at which another PMT is sensitive.

The first method has the advantage that the PMT is only sensitive to the radiation of interest because of the material used for its photocathode, and will not detect any radiation scattered inside the monochromator (e.g that emitted on some of the strong bands of nitrogen such as the Second Positve bands at around 300nm). This method has the disadvantage that a "solar-blind" PMT will have a lower gain because of the lower quantum efficiencies of such photocathodes compared to those in conventional tubes. In addition, extra care must be taken in the operation of such a tube. The window into the tube, through which the VUV passes, is sealed over the exit slit of the monochromator. The working voltage must not be then applied to the photocathode until the monochromator is properly evacuted otherwise there can be a breakdown from the photocathode to any nearby earthed point, destroying the PMT. For normal PMT operation at 2 to 3kV, the pressure distance product for the distance from the photocathode to the nearest earthed point at the pressure in the monochromator, must be greater than 25mmHg cm, or less than 0.1mmHg cm, the latter being the condition for normal usage. The precaution means that the PMT is never operated in conditions near the Paschen curve minimum appropriate to the gas in the monochromator.

There is also the problem, when operating at the shortest wavelengths, that the lithium fluoride windows of the "solar-blind" PMT do not transmit the incident radiation, as they have a cutoff wavlength of 105nm.

The disadvantages of using a "solar-blind" PMT were thought to outweigh the advantages and for this work the combination of a sodium salicylate scintillator and a PMT with a visible response were used. It was accepted that there might be a wavelength independent background on the signals detected due to light scattered within the monochromator.

Sodium salicylate has a constant quantum efficiency from the near UV down to about 60nm. Mesurements made on the absolute quantum efficiency vary (Samson, 1967), but a mean value of 60% seems reasonable. For the shorter wavelengths, the efficiency depends very much on the history of the

scintillator since its preparation. The efficiency falls off very rapidly in the first few hours, but then degrades more slowly over the next weeks. This degradation is enhanced by exposure to the moisture in the air. The fluorescent output from the sodium salicylate is in the blue part of the visible spectrum, centred at 420nm with a 30nm bandwidth.

The photomultiplier tube chosen for this work was an EMI 9893B/350. The bialkali photocathode has a quoted peak quantum efficiency of 22% at 400nm, which decreases to about 20% at 420nm. The specified gain is $2x10^7$ at 2000V. However, the photocathode diameter is reduced to 0.35in because of internal focussing which gives a negligible cathode dark count, at room temperature, of typically 40 counts per second. The tube has a 2.5ns rise time, a transit time for electrons to the anode from the cathode of 45ns, and an output pulse width of 4ns. It is extremely important to take into account the finite transit time in searching for overlap between signals from the PMT and other detectors monitoring events from coincident sources.

The detectors employed in the present work were prepared as follows: sodium salicylate crystals were dissolved in methanol to make a saturated solution. A few drops of this solution were placed on a 1 inch diameter glass disc, and the methanol was allowed to evaporate, leaving a thin opaque coating on the scintillator. The disc was used as the output window of the monochromator, with the scintillator placed towards the grating and the disc sealed to the exit port of the monochromator with an O-ring seal. To measure the absolute efficiency of the scintillator in situ (including any scattering effects) the monochromator was tuned to 380nm. According to the manufacturer, at this wavelength the PMT has the same response as at 420nm, the peak of the sodium salicylate fluorescence. Further, the scintillator should have the same efficiency at 380nm as in the VUV region. There is also a strong emission from nitrogen at 380nm on the Second Positive band. A discharge was run in nitrogen under steady conditions. With the scintillator in place the output from the PMT was measured and recorded. Next, the scintillator was

removed, keeping all other conditions constant, and again the PMT signal was recorded. The ratio between these two values can only be due to introducing the scintillator. It was found that the efficiency of the sodium salicylate was 21%.

7.4 SIGNAL RECORDING SYSTEM

7.4.1 Boxcar integrator - general

Signals from the PMT were processed by an EG&G Princeton Applied Research Corporation (PARC) Model 162 Boxcar Averager fitted with dual Model 164 Gated Integrators. The averager was fitted with circuits to compare as a ratio the outputs from the two integrators. It was also provided with digital storage to allow accurate operation at low pulse repetition frequencies. Figure 7.2 shows a block diagram of the system (only one channel has been shown for clarity).

7.4.2 Timing considerations

The basic cycle of operation of the boxcar integrator starts when a trigger pulse is applied to the trigger input (figure 7.3). After an initial delay from the time when the trigger input signal reaches the predetermined voltage at which the trigger level is set, the gate to the integrator is opened for a specified time, called the Aperture Duration (t_{AD}). The gate then closes and the stored charge on the capacitor of the input stage, proportional to the applied signal voltage, is retained until the next trigger pulse. At low pulse repetition frequencies (prf) there will be some droop and loss of charge from the capacitor between pulses. To overcome this the digital storage board digitises the voltage across the capacitor and then applies an analogue voltage to maintain the charge on the capacitor at the correct level. The initial delay between the trigger pulse and the gate opening can be varied to any time within the specified Aperture Delay Range

(ADR). The actual initial delay depends on a number of factors.

Firstly, there is a nominal minimum delay of 75ns to allow the electronics to respond to the trigger. This can be further complicated as the minimum trigger level is 0.5V, with an input impedance of 50kΩ, which means a fast trigger pulse is required. This must be taken into account when deciding on a suitable trigger source if the system is to be able to gate on the early part of the signal. When triggering from sources almost coincident with the signal it was found necessary to delay the signal by passing it along a length of transmission cable.

Secondly, the aperture opening time depends on the setting of the "% initial delay" dial: this gives the fraction of the ADR before the gate opens, and allows various parts of the signal to be studied.

Lastly, the position of the gate depends on the scan ramp. This is used to move the gate through the ADR by a small increment each pulse. The rate at which the gate is moved is set by the user, and it allows the time resolved structure of the signal to be built up over a number of shots.

Most of the discharges producing the emission to be studied were pulsed. They were initiated by the firing of a pressurised spark gap. A sample of the light emitted by these spark gaps was fed along optical fibres, to the detection system outside the Faraday cage and onto a fast vacuum photodiode (ITL TF1850). The output from the photodiode was used as the trigger source for the boxcar integrator. The emission from the discharge occurred at a time of the order of 100ns after the onset of the light from the spark gap. As mentioned earlier this was insufficient to allow the boxcar integrator electronics to respond, so the signal from the PMT was normally delayed by passing it along a 15m length of coaxial cable, giving 75ns delay.

A pulse coincident with the aperture is provided from the integrator module. This was used to check for coincidence between the gate and the required portion of the signal.

7.4.3 Averaging

The averaging procedure appplied by the boxcar integrator can be carried out in one of two modes: linear or exponential. In the linear mode the output is the average of N repetitions, where N is the actual number of individual pulses with all repetitions contributing equally. As this mode was not employed for the present work it will not be described further. In the exponential mode, the output signal asymptotically approaches G times the input signal over a number of sampling periods, where G is the gain of the system and has the value of 100 in this case (figure 7.4). To the incoming signal in each period is added a fraction of the stored value. The output signal therefore represents a weighted average with the most recent samples having the greatest influence on the output. It is the correct mode to use when scanning the input signal continuously as a function of either wavelength or time. After the output signal has reached its steady state value, say after five time constants, it can be said to be equivalent to averaging $2TC/t_{AD}$ repetitions of the signal, where TC is the time constant of the integrator. Note that, because there is a factor of 100 attenuation in the feedback loop and 6 times gain in the summing line, the actual value of RC of the integrator is about 17 times smaller than the selected time constant within the boxcar integrator.

The averaged signal output from the gated integrators (M164) are fed to the mainframe processor (M162). Here any ratioing or subtraction of the signals from the two channels is performed before the signal is passed to the outputs via a smoothing filter. This does not perfom any further averaging, but provides some additional smoothing at the expense of degraded output signal rise time, which must be taken into account at rapid scan rates if the loss of signal resolution is not to be too high.

7.4.4 Time constants and aperture duration

As stated above, time constants can be selected for both the integrator

module and the mainframe processor. These time constants will be designated TC and MPTC respectively. For exponential averaging, a time of one TC is needed for the signal to reach 63% of its steady state value. It is important to realise, however, that this sampling time, equivalent to TC, is that for which the aperture into the boxcar integrator is open. The actual time taken to acquire this data will depend on the aperture duty factor: the ratio of the time the aperture into the boxcar integrator is open to the time it is closed. Thus it is convenient to define an Observed Time Constant (OTC) as

$$OTC=TC/(AD \times pfr) \qquad 7.2$$

such that the signal output will approximately reach its steady state value (to within 1%) when the experiment has run for five observed time constants.

When scanning the data signal, the resolution will depend also on the MPTC as well. These two can be combined to give an Effective Time Constant defined as

$$ETC = [(OTC)^2+(MPTC)^2]^{1/2}. \qquad 7.3$$

When scanning the signal in time, the Minimum Scan Time (MST) to move the gate through the ADR, so that there will not be an unacceptable loss of time resolution, is given by

$$MST = ETC \times ADR/AD, \qquad 7.4$$

i.e. at least one ETC must be allowed for the gate to be scanned through one aperture duration.

Besides affecting the duration of the experiment, the aperture duration also has an effect on the time resolution and signal to noise ratio of the final results. If the aperture duration is made too great then it will have the effect of smearing out the signal, equivalent to a lower time resolution, and reducing its amplitude (figure 7.5). Note also that the signal has undergone an apparent time shift for large aperture durations. These points must be borne in mind when selecting the appropriate aperture duration for a particular set of experimental conditions.

7.4.5 Accuracy

Quoted accuracy ranges of the signal throughput for the various components are given below. All the errors will be compounded throughout the system.

Gated integrator (M164) 2%

Digital Storage board

Encode accuracy 0.1%

Short term hold 0.2%/min

Ratioing board 0.7%

After zeroing and gain calibrating, the system is linear to 0.1%.

Another source of error on the final signal will depend on the accuracy with which the position of the opening of the gate can be achieved.

Jitter on gate opening 0.05% of Aperture Delay Range.

When scanning through signals in time the accuracy of the time measurements will depend on how accurate the Aperture Delay Range can be set,

Aperture Delay Range accuracy 2%

7.4.6 Oscilloscope

An oscilloscope was used for recording the relative timing of various signals, and also observing for the time signature of signals on a single shot basis. The model used was a Tektonix 466 storage oscilloscope. This has a 100MHz bandwidth, which gives it a 3.5ns rise time.

7.5 COMPUTER AIDED EXPERIMENTING

7.5.1 General considerations

The use of a microcomputer to control the experimental apparatus has several important benefits. It relieves the experimenters of the necessity to spend time on the automatic parts of each experiment, and frees them to concentrate on the specific design of each experiment.

The microcomputer should be capable of interacting easily with the outside world: both sending signals out and receiving data. It must also have a means of storing the data for future use. For the present work it was decided to use a BBC microcomputer, because this machine is well equipped to handle the input and output (I/O) requirements. For the input signals it has a four channel analogue to digital converter (ADC). This is referenced to 1.8V and comprises a 10 bit converter with a 10ms encode time. For signal output the computer is provided with a User Port (UP). This is an 8 bit port connected to a VIA6522.

The 6522 is a versatile chip which can be programmed either for input or output, or a mixture of both, on any of its eight data lines. The lines can source 1mA, and sink 1.6mA. Data is latched by the 6522 from the internal bus for output, or from the input device, until required. For this work the UP was used only for output, and none of the handshaking or timing properties of the 6522 were needed. Thus the programming of the 6522 was relatively straightforward. The output data latch can be thought of as an 8 bit number. Writing to this latch with a one in a certain bit causes that line to be held high, e.g. writing 140, or 10010110 in binary, pulls lines 1,2,4 and 7 high (the rightmost bit is bit 0). For the BBC microcomputer system an output or input line is high (logic level 1) when at 5 volts and low (logic level 0) for 0 volts

Storage of the data was on 5.25in floppy discs, with a single drive, giving 400k storage per disc. The one drawback with the BBC microcomputer is the size of its internal memory. This problem was outweighed by the advantages of the system and was overcome in the way in which the data was stored as it entered the computer, as described in a later section.

The computer was required to initiate each cycle of the experiment by causing the discharge to be fired. It would then interrogate the data recording device, generally the boxcar integrator, to find the new value for the data and store this. Lastly it might be necessary to command the stepper

motor to move on to enable a different wavelength to be investigated. The interpulse timing was also controlled by the microcomputer. The implementation of these various tasks will be discussed below from the point of view of the electronic connections needed, and also of the programmes written.

7.5.2 Hardware

Discharge triggering

As mentioned previoiusly, triggering of the discharge was achieved by triggering a pressurised spark gap. The triggering electrode (an ordinary car spark plug) was pulsed to approximately 20kV. This pulse was derived from a car ignition coil, which was itself provided with a 2kV pulse from an electronic trigger circuit. This circuit could either be left free running at a preset repetition rate, or could be provided with externally generated synchronisation pulses. External synchronisation pulses needed only to be of 200ns duration provided they had an amplitude of 3V or greater. In order to prevent pick up of RF noise from the pulse generating circuits and the discharge from causing catastrophic failure of the microcomputer it was necessary to isolate the signal line to the trigger circuit from the output of the microcomputer. The circuit used is shown in figure 7.6. When line 1 (PB1) is held low, the optoisolator is turned on and the line to the trigger circuit is pulled high.

Stepper Motor Control

Also shown in figure 7.6 are the connections which enable the stepper motor to be moved. The stepper control box accepts optical inputs on optical fibre to cause it to advance the motor one step. Two inputs are required, one to trigger the movement and another to govern the direction. The pulse must be 200 microseconds long. Two lines were buffered so that enough current could be sunk to drive the LEDs which provided the input to the stepper

control. PB0 was used for the step command. When PB2 was high the motor was commanded to run in reverse, as for rewinding after a scan.

Boxcar integrator interfacing

From the BBC microcomputer three other output lines were used. These were connected directly to the output connector of the boxcar from the top three lines of the UP. PB5 was connected to Signal Reset (pin 41) on the boxcar integrator: holding this line low sets the instrument integrators to zero and clears the digital storage board. PB6 was connected to Scan Reset (pin 42): holding this pin low causes the position of the aperture to be reset to the value set by the "% initial" dial. PB7 was connected to Scan Hold (pin 40): holding this pin low stops the aperture position from advancing. These last two connections were only needed when the aperture was being scanned through input signal on succesive shots to build up the time resolved structure of the signal.

When the signal was being scanned in time it was necessary to know what point in the scan had been reached when a particular piece of data was recorded. This was achieved by monitoring the channel A (pin 8) and channel B (pin 44) scan ramps. These pins have a linear ramp voltage on them from 0 to 5V, corresponding to the position of the aperture in time from 0 to the limit of the ADR. Because the ADC is referenced to 1.8V a 1:3 potential divider was used to bring the scan ramp voltages into the right range. These were connected to channels two and three of the ADC as shown in figure 7.7.

Finally, it was necessary to bring the averaged data output from the boxcar into the microcomputer. This is presented on pin 4, and will be in the range 0-10V. In fact, as the PMT used to detect the radiation gives a negative output, the output from the boxcar is also negative. Thus to bring this signal into the correct range for the ADC it needs to be inverted and reduced in amplitude. This was achieved by using an inverting amplifier with a gain less then unity. Two different gain values were provided (giving

reductions by factors of two or five) to enable the input into the microcomputer to be in a sensible range for different input voltages to the boxcar integrator. It will be noticed from figure 7.7 that channel 0 is connected to the ADC refence voltage (1.8V). By comparing all the converted data to the conversion on this channel an allowance can be made for any drift of the reference voltage.

By interfacing the microcomputer to the PMT output via the PARC boxcar integrator, all the necessity to operate at high speed is removed from the computer. Its relatively slow inbuilt ADC can be used to digitise the data in the interpulse period of typically a few tenths of a second, giving it ample time to complete its task. The accuracy of the ADC (0.1%) is better than the 2% of the gated integrator and so will not degrade the experimental data.

7.5.3 Software

The series of programmes written for use in the present experiments have two main purposes: they must enable the experiment to be easily controlled, and in addition they must facilitate the storage of the data for future use, processing and comparison. In use they must be friendly towards the user, and compatible amongst themselves. As a large amount of data would need to be stored and manipulated it was decided that it would be an uneconomic use of the available memory, if the data was stored using one computer integer for each number. This is because in the BBC microcomputer each integer is stored as four bytes, but as the ADC are only 10 bit converters two bytes will suffice to store the data, thus doubling the amount of data that can be stored. Compressing the data in this manner wil also halve the data transfer time to disc.

All the programmes disscussed here have documented listings in appendix 3. The main control programme comes in two forms: one when the wavelength is to be scanned, the other when the time resolved structure is to be studied. As the data is read into memory it is stored in a contiguous block,

and also displayed on the monitor screen. At the completion of the run there is an option to save the data onto disc for future reference, along with information concerning the conditions used for that experiment. A low resolution hard copy of the data sufficient for immediate inspection purposes could be obtained by using a screen dump to a dot matrix printer. Other programmes, not listed, were written to display the data in a more complete form with the associated infomation. A programme was also written to enable one spectrum to be subtracted from another, mainly for use when a background spectrum was present.

To enable the indentification of spectra produced a program was written to synthesise the expected spectrum from the species under investigation. Known wavelengths and relative intensities of the transitions are supplied to the program, which then produces the spectrum, allowing for the resolution of the experiment. A hard copy of the synthesised spectrum could be used as an overlay for the experimental results.

7.6 CONCLUSION

In this chapter the experimental apparatus for the investigation of the proposed laser system in nitrogen has been described. The philosophy and practical considerations involved in integrating the various pieces of equipment and bringing them under the control of a microcomputer have been discussed. The software specially written for this project has been outlined.

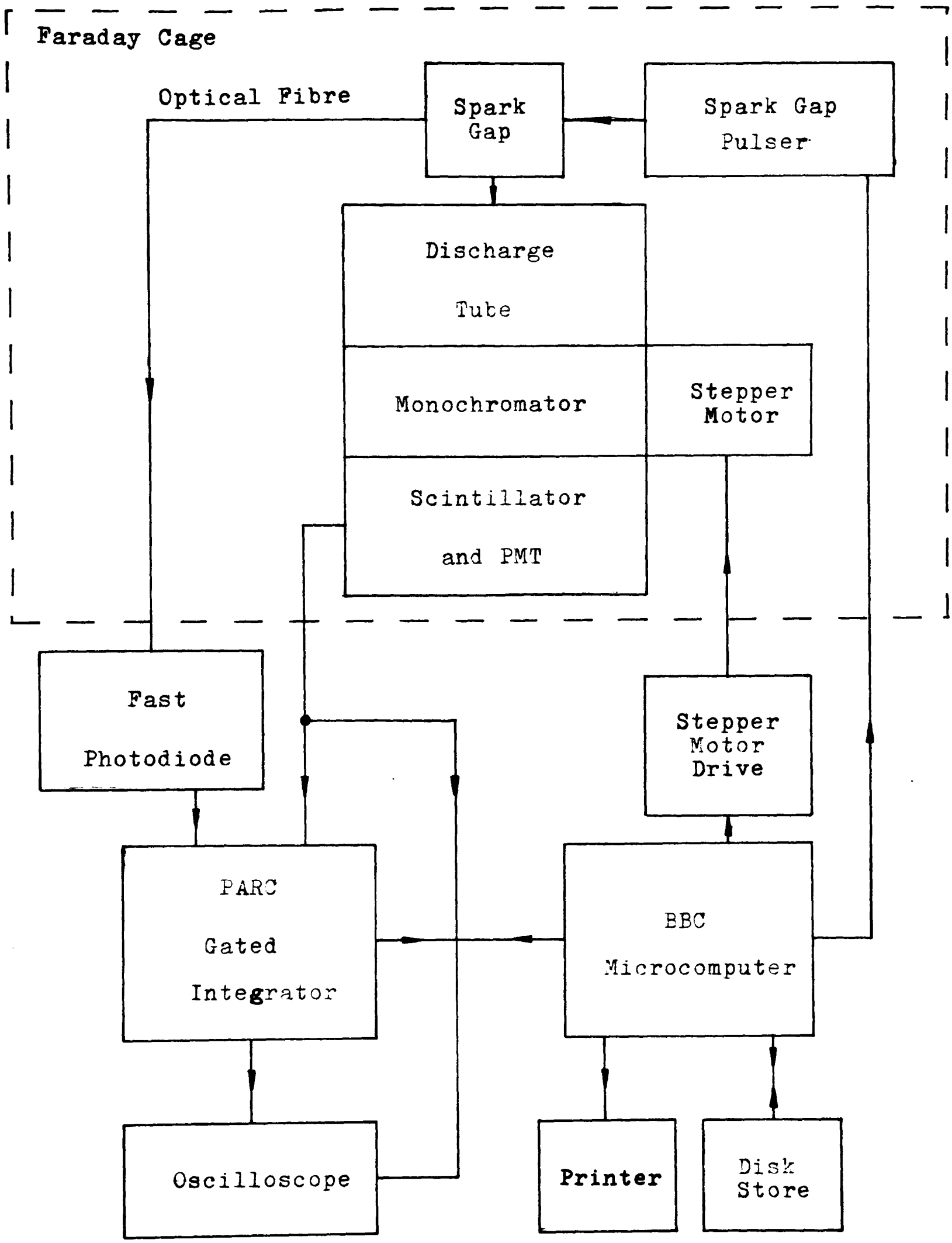


Figure 7.1 Block diagram of detection system

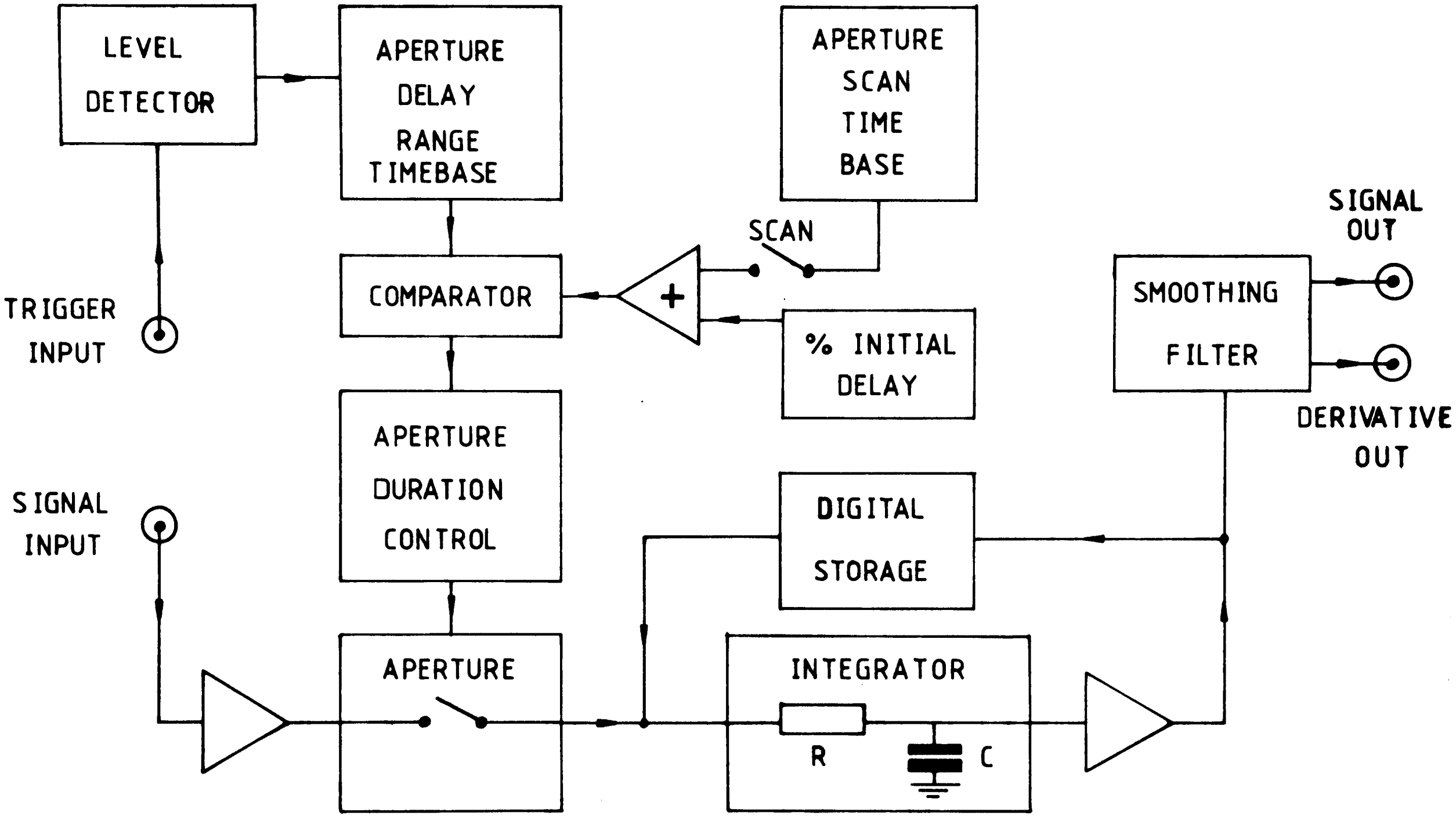


Figure 7.2 Simplified block diagram of gated integrator

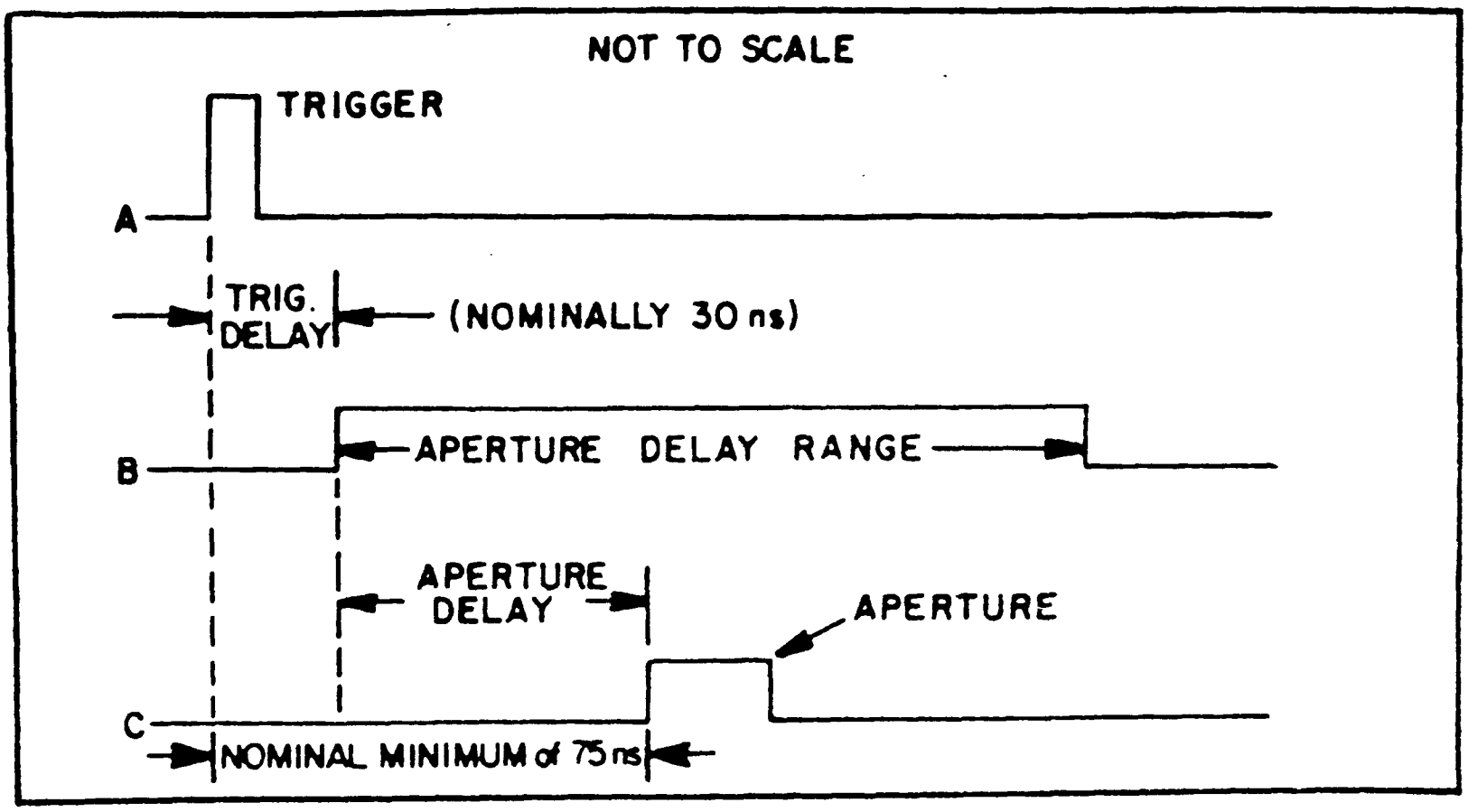


Figure 7.3 Timing Relationships

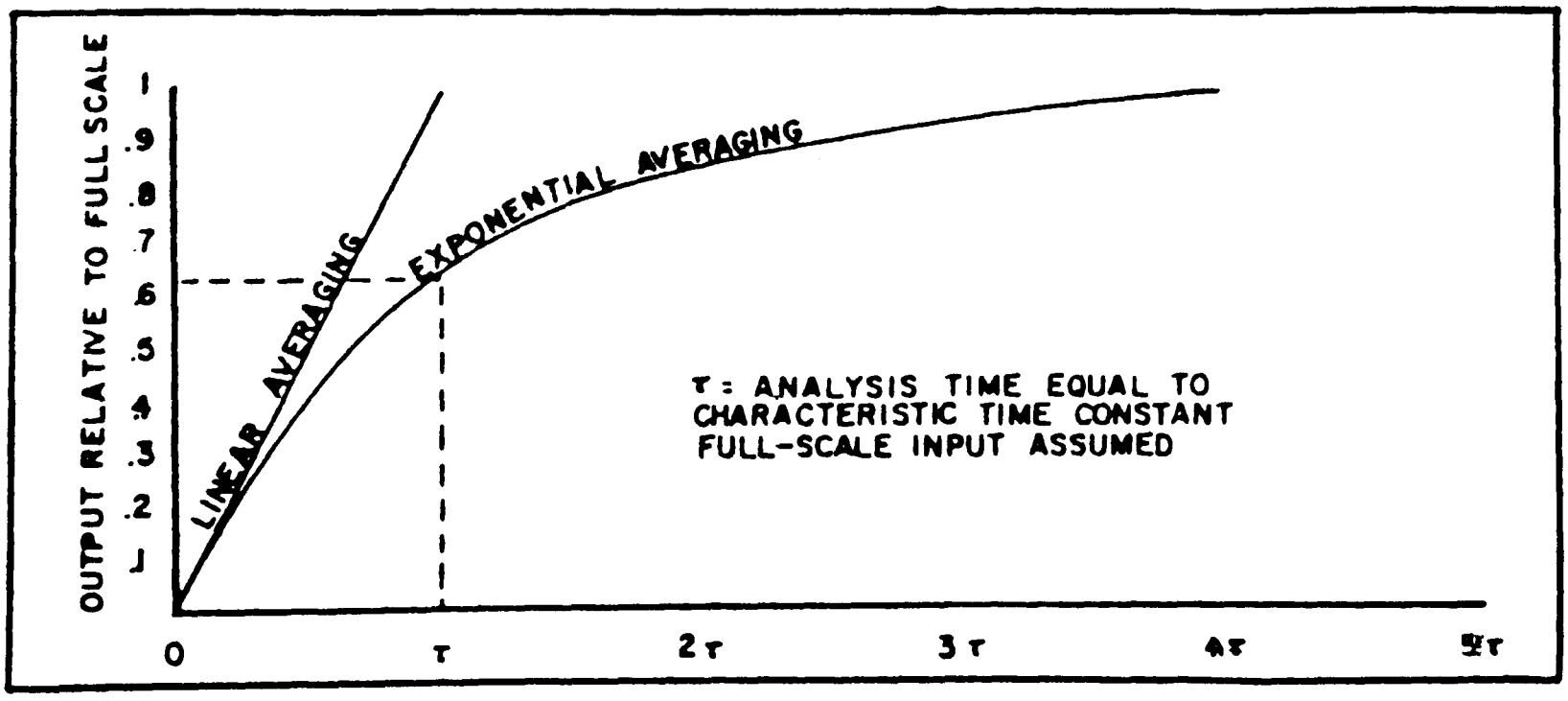


Figure 7.4 Comparison of Linear and Exponential Averaging

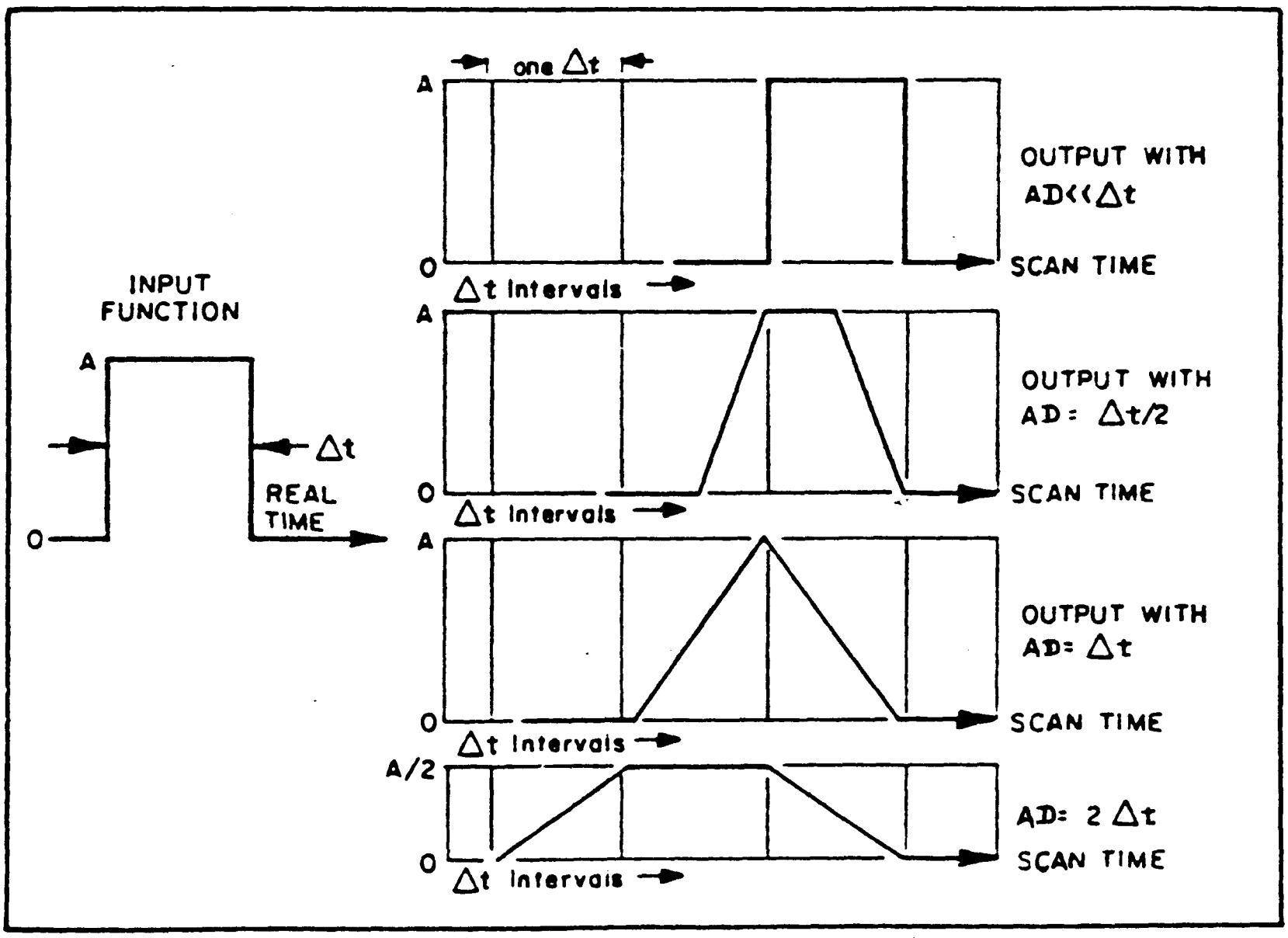


Figure 7.5 Effect of changing the Aperture Duration

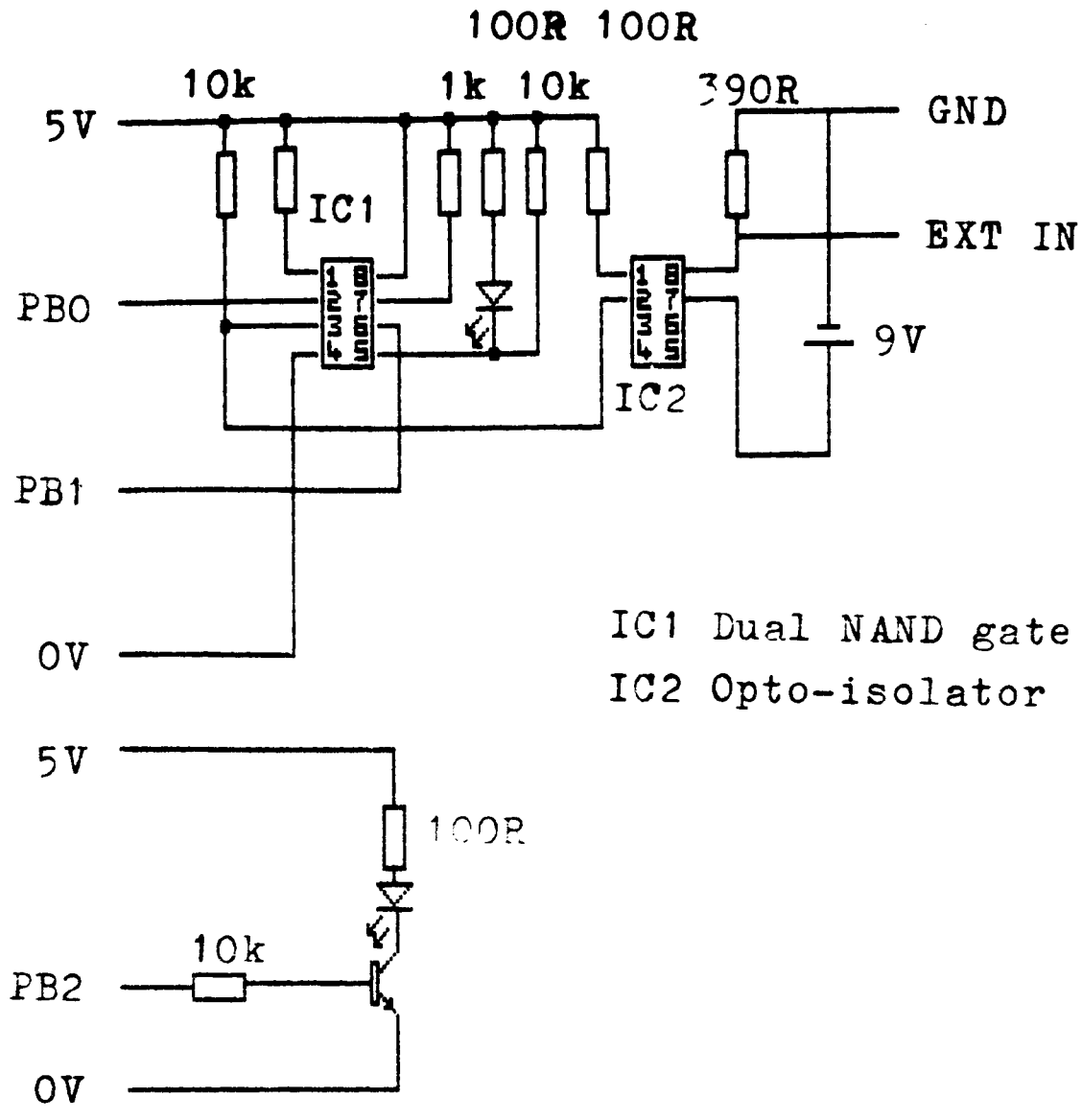


Figure 7.6 Connections: User Port
to trigger unit and stepper motor

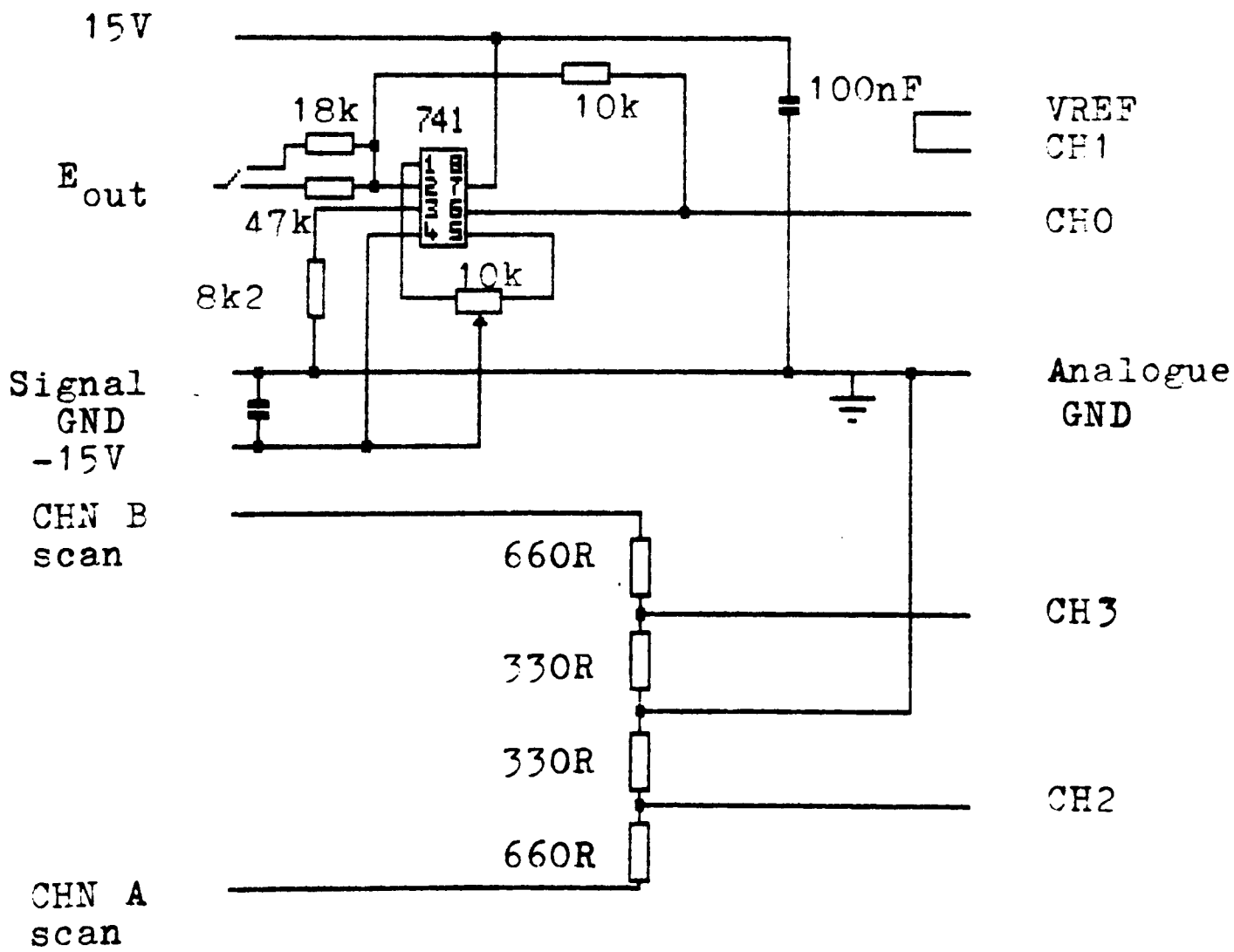


Figure 7.7 Connections: Boxcar integrator to
ADC port

CHAPTER 8 : INVESTIGATIONS OF THE PROPOSED NITROGEN VUV LASER SYSTEM

8.1 INTRODUCTION

In previous chapters a scheme for a new VUV laser has been presented and the experimental apparatus to be used for an investigation of that propsed laser scheme was discussed. In this chapter the experiments themselves are detailed.

The work was divided into two stages corresponding to the two stage excitation scheme of the proposed laser system. Firstly, the production of nitrogen molecules in the intermediate metastable level was investigated. Secondly, the further excitation of these molecules to the upper laser level by means of the absorption of radiation from the "transfer" laser.

The state of the nitrogen molecules is monitored by detection of the radiation emanating from that state. An equation is derived to enable an estimate of the population density of the molecules in the state under investigation to be made from a knowledge of the intensity of this radiation.

8.2 INITIAL INVESTIGATIONS

8.2.1 Discharge tube

For the investigation of the optical and electrical excitation of nitrogen, a discharge tube (DT I) of similar design to that used for the XeCl laser was made (figure 8.1). As can be seen that, apart from it having smaller dimensions, the major difference is the addition of a cross-piece in order to allow the sidelight emission from the discharge to be viewed directly. The internal structure carried the electrodes and peaking capacitors. There were 22 internal capacitors in parallel each of 0.625nF capacitance. There was a 2mm gap separating one terminal of each from its

high voltage pin to provide a preionisation arc as each capacitor was charged up. The upper, high voltage electrode was a flat plate, and the lower earthed electrode had a 1cm diameter semicircular profile.

The tube was made from brass, and for this work it was not thought necessary to nickel plate it as it was not envisaged that any corrosive gases would be used in it. However all the internal insulating mounts were made from PTFE to improve the system's cleanliness, and the capacitors were also sealed in PTFE.

One side of the cross-piece was sealed over the input slits of the monochromator with a MgF_2, window to isolate the monochromator from the discharge and yet pass the short wavelength radiation into it. The other side of the cross-piece and the two ends had 8mm clear apertures with quartz windows sealed over them.

8.2.2 Laser induced fluorescence of hydroxyl radical

The small discharge cell (DT I) was used to excite nitrogen over a range of pressures and a search was made for absorption of the tuned radiation from the XeCl laser. The XeCl laser radiation was detected, after it had passed along the length of the nitrogen discharge, by letting it fall on the sodium salicylate coated ends of a plastic fibre optic cable. The fibre optic passed out of the Faraday cage and allowed the light transmitted by it to fall onto a photodiode situated in the "quiet room" next door. The amplitude of the output from this photodiode was recorded via the gated integrator. The prisms for the tuned XeCl laser were set to angles of incidence of 75^{o} and 80^{o}, thus giving a linewidth of about $2cm^{-1}$ and a pulse energy of 2mJ.

With 250 mbar of nitrogen in DT I and a 30kV discharge a strong absorption feature was observed on the short wavelength side of the 0-2 vibrational transiton of the XeCl laser output. It was possible to detect the absorption for a range of pressures (50mbar to 250mbar). This feature was not present without the discharge in nitrogen, nor if the gas was circulated

through the liquid nitrogen cryogenic trap. The absorption was also present if the discharge was in "pure" helium, and so was obviously not due to absorption on the $a^1\Pi_g - b^1\Pi_u$ transition in nitrogen, as needed for the proposed laser system. The feature was identified as an absorption band of the hydroxyl radical (OH). The absorption is due to rotational lines of the v'=0 to v"=0 transition on the $X^2\Pi - A^2\Sigma$ band (see figure 8.2), around 308.1nm to 308.3nm. The vapour pressure of water at 175K is 1.5×10^{-5}, so the precursor for the OH radical would be effectively removed by the trap. Adding distilled water to the DT I caused a large increase in the absorption, making the discharge opaque to the XeCl radiation (see figure 8.3).

An attempt was made to look for this transition in emission, by evaporating water into DT I and running a discharge buffered with helium. The transition was readily observed, being optimised for an estimated partial pressure of 0.5mbar of H_2O in 1bar of He. It was then an obvious next step to investigate whether any laser induced fluorescence (LIF) was produced by the absorbed XeCl laser radiation. It was necessary to ensure that the aperture of the gated integrator was open over the time interval of signal due to the laser pulse. To allow detection of the laser pulse a silica fibre was placed such that the XeCl pulse fell on it, after traversing DT I. The fibre was bent in a curve so that the radiation was sent into the monochromator, across the DT I cross-piece (see figure 8.4). The monochromator was tuned to 308.2nm and the signal from the photomultiplier tube (PMT), due to the laser radiation was fed into a fast storage oscilloscope. The marker pulse for the gated integrator aperture opening was also fed into the oscilloscope and the gated integrator delay adjusted so that its sensitive aperture period overlapped the XeCl laser pulse. In this way any effect due to the finite transit time of the PMT would be cancelled, and the gated integrator would accept the signal from the time the XeCl pulse passed through DT I. The silica fibre was now removed and the monochromator left set to 308.2nm, in the middle of the OH emission band. The XeCl laser was adjusted to the lasing wavelength. The

signal recorded by the gated integrator is shown in figure 8.5. Here the effect due to LIF is easily seen. Note that figure 8.5 shows the emission intensity as a function of the XeCl laser wavelength only. The background emitted intensity is due to the disharge excited emission of the 'A' - 'X' transition in the OH radical.

These experiments have shown that the system designed for this work is able to produce, and detect, LIF from discharge excited species. In this instance the species is the OH radical formed from the dissociation of water in the discharge.

8.2.3 Carbon monoxide fluorescence

An attempt was made to observe in emission from DT I the radiation on the Lyman-Birge-Hopfield (LBH) bands of nitrogen. Indeed a signal was detected at 166nm, clearly belonging to a band system in the same spectral region as the LBH bands. A check was made that this was indeed due to incident VUV radiation (and not some background non-VUV or laser radiation component being scattered inside the monochromator) by admitting air into the monochromator. The signal was no longer detected, indicating that the detected signal was indeed VUV radiation. When a new gas fill was put into DT I, the signal was not initially detected, but it increased as a function of time. Further investigation revealed that the 166nm signal was present for a number of gas mixtures of nitrogen in helium, as well as pure nitrogen, in the range 20 to 120mbar. In all cases the signal intensity increased as a function of the time the discharge was on, and seemed to saturate after about 100 minutes. If the gas mixture was circulated through the cryogenic trap the intensity rapidly fell to a low level, but would recover in about 10 minutes if the circulation compressor was switched off again. From these observations it was concluded that the signal was coming from an impurity species whose concentration was increasing as a function of the time since the discharge was switched on. One possibility was NO, formed in the discharge by a reaction of

nitrogen and oxygen. Oxygen might enter as an impurity with the gases, or from small air leaks into DT I. Another possibility was CO. This would either be formed by the dissociation of CO_2, which would enter by the same means as oxygen, or by a reaction of oxygen with carbon formed by a cracking reaction of the hard UV radiation on the organic insulating materials placed near the discharge.

To distinguish between these possibilities a high resolution wavelength scan of the region of interest was performed. The wavelengths of the peaks detected agreed well with the published values for the CO fourth positive system (Read, 1934). In the region 219nm to 251nm emission on the CO^+ first negative system was also observed. It was thus concluded that the emissions overlapping the region of the LBH bands were from carbon monoxide. As a further check the DT I was filled with a mixture of 5mbar CO in 95mbar He, and the same wavelength scan was run. Peaks were detected at the same wavelengths, but with greater intensity, thus confirming the above conclusion. Although CO has a vapour pressure of 500mbar at 77K, the effect of the cryogenic trap was to remove some precursor for the production of CO by the discharge. Emission detected from CO is shown in figure 8.6.

It is known (Filseth et al, 1977) that adding CO to a N_2 discharge can be used as an indication of the production of the metastable $a^1\Pi_g$ state of nitrogen due to increased fluorescence on the CO fourth positive bands, $A^1\Pi - X^1\Sigma^+$. This "sensitised fluorescence" is due to the collision induced reaction

$$N_2(a^1\Pi_g,\ v'=5) + CO(X^1\Sigma^+, v''=0) \rightarrow N_2(X^1\Sigma^+_g, v'') + CO(A^1\Pi, v'<10). \qquad 8.1$$

There is a high probability of this reaction occurring due to the close coincidence of the excited CO and N_2 levels.

It was hoped initially that this effect could be used to aid in the detection of any molecules in the 'a' state produced in the nitrogen discharge. However the increase in fluorescence detected on addition of nitrogen to discharges of CO in He was not very great. The largest increase

was found to be 20% on the addition of 12mbar of N_2 to a mixture of 1mbar of CO in 1bar of He.

It was therefore decided that the nitrogen molecules in the 'a' state would be best detected directly. To avoid the LBH band signals being masked by the stronger CO fourth positve bands it would be necessary to keep the CO concentration in the discharge to very low levels. The cryogenic trap removed a large proportion of the CO from the discharge, but left a small background component. To remove this a copper oxide oven, as described in the previous chapter, was introduced into the gas circulation loop. With the copper oxide heated to between 100°C and 200°C it was possible to totally remove any detectable trace of CO from the discharge.

8.3 EXCITATION OF MOLECULES TO THE $a^1\Pi_g$ STATE

8.3.1 Conditions needed for production of N_2 in the 'a' state

Before further attempting to investigate the effect of the XeCl laser in transferring population from the 'a' to 'b' states in nitrogen, a study was made of the conditions under which the production of the 'a' states was optimised. The DT I, with the electrode configuration as described in the foregoing sections, was used with a range of nitrogen pressures. However no emission from the 'a' state could be observed. It was felt that 'a' state emission would be more probable at lower pressures, when the quenching rate of the 'a' state by ground state nitrogen molecules would be reduced. The original internal electrode structure of DT I was not appropriate for low pressure discharges, since it relied on confinement of the discharge path between the electrodes - a feature which is characteristic of high pressure operation. Thus a new electrode arrangement was used, designated DT II. It had a "finger" electrode as shown in figure 8.7. The "finger" electrode was connected via the cross-piece of the discharge tube opposite the monochromator slits. The other electrode was 25mm diameter copper tube in an earthed brass

disc, placed in the other arm of the cross-piece, allowing radiation into the monochromator.

At this time the plate carrying the MgF_2 window, isolating the monochromator from DT II was removed. This allowed the monochromator to act as a gas ballast volume, and also removed the absorption of radiation near the cutoff wavelength of the window as it passed through it. The discharge circuit used with DT II is also shown in figure 8.7. The high voltage to drive the discharge is applied across the discharge and a current limiting (or "ballast") resistor in series.

Different discharge conditions were tried, but no LBH emission was observed. The value of the ballast resistor was varied, and it was found the larger values gave a less luminous but more noise-free discharge. This corresponded to a longer current pulse, and so a DC discharge was used to further improve the signal to noise ratio of the observed signal. This did not produce immediate results. However by flowing the gas in through the monochromator and out of a pumping port at the end of DT II, emission on the LBH bands was identified (see figure 8.8). The emission was greatest if the finger electrode was held at positive volts relative to the earthed plate. By various tests, in which parts of the discharge were shielded from the detection system, it was established that the LBH emission was emanating from the pink positive column part of the discharge.

The grating in the monochromator was changed at this stage as it showed obvious signs of degradation. The new grating had an efficiency of 3.4%, according to the manufacturer's calibration. Using the new grating at once led to an increase in the signal by a factor of about two. A side effect was that the efficiency of the sodium salicylate scintillator seemed to decrease more rapidly with time, perhaps as a consequence of the increased photon flux on it.

A new discharge tube (DT III) of a simpler design was introduced, as shown in figure 8.9. It was then possible to flow the nitrogen directly along

the discharge region, thus removing any impurities as they built up. On searching again for emission from a pulsed discharge it was hoped that the higher currents possible would lead to larger populations in the 'a' state. For these experiments the pin was pulsed negative, and was viewed by the monochromator through the positive column. It was possible to detect the LBH bands with this system. Various values of the current limiting resistor were tried in order to study their effect on the LBH emission. It was found that the emission followed closely the time evolution of the current through the discharge, for a constant external capcitance of 20nF. A comparison of the current pulse RC time and the decay constant of the LBH emission are given below.

Table 8.1 Decay constant vs. ballast resistor value

Resistor (kΩ)	RC time (μs)	LBH decay constant (μs)
10	200	250
1	20	26
0.1	2	2.7

The smaller values of resistance gave the more luminous discharges. However there was a greater pulse to pulse variation, which made it more difficult to observe the LBH signal. Either the recorded trace was more noisy, or if more averaging time constant was applied by the gated integrator to smooth the signal the scan times were prohibitively long. A resistance of about 100Ω was found to be the best compromise.

Using the experimental arrangement DT III the emission from the $a^1\pi_g$ state of nitrogen on the LBH bands was detected (see figures 8.10 and 8.11). The emission was visible under a range of nitrogen pressures, and did not vary in intensity a great deal in the range 8mbar to 20mbar. Helium was added to the nitrogen in the discharge to produce a more stable discharge, and reduce the quenching of the 'a' states by enabling lower nitrogen partial pressures to be used. However the LBH emission was no more intense under these conditions, but the emission on the atomic lines of nitrogen, and carbon was accentuated.

It will be noticed that the relative intensities of the vibrational transitions of the LBH bands do not agree with the published data. This is perhaps because of absorption from vibrational levels of the ground state populated due to the high vibrational temperature in the discharge.

8.3.2 Estimate of number density of the $a^1\Pi_g$ molecules

To enable the effectiveness of populating the $b^1\Pi_u$ state from the 'a' state to be estimated the magnitude of the population density of the 'a' state is needed. This can be calculated from the intensity of the radiation on a particular vibrational transition of the LBH band, if the transition probability for that transition is known.

It is also necessary to know what fraction of the photons emitted on this transition are detected. This depends on the efficiency of the detection sytem, including that of the grating, the sodium salicylate scintillator and the quantum efficiency of the PMT at the emission wavelength of the sodium salicylate (420nm), and the fraction of photons reaching the grating. The efficiencies are given in manufacturer's data, or, in the case of the sodium salicylate, are calibrated as described in the previous chapter . The fraction of photons reaching the grating is found by calculating the solid angle subtended by the grating for each volume element of the discharge, making due allowance, in some cases, for the obstruction caused by the edges of the input slits. The fraction required is then the ratio of these calculated solid angles summed over all elements of the discharge, to 4π steradians. These calculations for each element of the discharge, and the final summation were performed by a computer programme (see appendix 3). This was written in Pascal to shorten the runtime. The size of the exit slits of the monochromator did not affect the number of photons reaching the PMT for this work. The slit width used was 0.1mm, giving the monochromator a resolution of 0.4nm. In this case the emission on both the LBH and the BH bands in molecular nitrogen of an individual vibrational transition is seen as

a line source. The rotational lines of these transition extend over approximately 0.2nm.

The programme also calculated the density of molecules in the 'a' state following the method below. Let F represent the ratio of the number of photons reaching the grating to those generated, as discussed above and calculated by the computer using geometrical arguments. The efficiency, E, of the detection system, represents the product of the efficiencies of the three components; grating, sodium salicylate and PMT. The sodium salicylate efficiency was found to be 20%. The grating efficiency was given in the manufacturer's data as 3.4% at 160nm, and 6% at 121.6nm. As the grating was relatively new, it is expected that these figures will be reasonably reliable. The quantum efficiency of the bialkali photocathode is given as 25%, although this figure is subject to variations.

Now each photoelectron produced by the photocathode of the PMT gives rise to a pulse of electrons at the anode of the PMT and when the anode is connected to an oscilloscope it is this pulse which is detected. For the PMT tube used here the pulse appears with a half-width of about 5ns, and an amplitude of 15mV to 20mV. When observing the LBH bands the individual photoelectron pulses can be counted, due to the low transition frequency. The average number of counts in a period of a few microseconds thus gives the rate of production of photoelectrons. Let this be N counts per second, the transition rate for the particular vibrational transition be A s^{-1}, and the number density in the state $a\,^1\Pi_g$ (v'=0) be n cm^{-3} in a discharge of volume V cm^3. Then by equating the number of photons reaching the grating from the discharge to that number needed to give rise to the number of photoelectrons counted, the following equation is obtained

$$n\,A\,V\,F = N / E, \qquad 8.2$$

which gives the population density as

$$n = N / (E\,A\,V\,F). \qquad 8.3$$

Using this method a rough estimate for the population in the $a\,^1\Pi_g$ (v'=0)

of $1x10^{11}$ cm^{-3} was made for a 5mbar nitrogen discharge.

This process of counting the individual photoelectron pulses from the PMT was not practical for the other transitions as the photon flux was so great that the pulses overlapped. To extend the density estimate to the results recorded on the printout from the microcomputer, the response of the microcomputer/printer system was calibrated by feeding known signals into the gated integrator and measuring the height of the recorded trace on the printout. The response was found to be linear and reproducible. If the applied pulse did not fill the aperture duration of the gated integrator, then the output signal was reduced proportionally. However, for this work the signals from excited nitrogen all filled the aperture durations used, and had very little change in intensity in this period. The electron pulses from the PMT were converted to analogue voltage signals by integration at the input resistor, R, of the gated integrator. The value of the resistor was usually 50Ω. The gain, G, of the PMT was available from the manufaturer's calibration data supplied with the PMT. The PMT calibration was supplied for certain specified values of the voltage applied to the PMT. For this work the tube was always operated at one of these voltages (usually 2kV), enabling the gain of the PMT to be known to the manufacturer's individual tube calibration error. Thus N photoelectrons per second emitted from the photocathode would produce a voltage, v, at the gated integrator of

$$v = N\ G\ R\ e \qquad 8.4$$

where e is the electronic charge ($1.6x10^{-19}C$). Thus with the printout calibration as K m/V and a height for a particular peak of H m, the eqivalent number of photoelectrons would be

$$N = H\ /\ (K\ G\ R\ e), \qquad 8.5$$

so the number density in the $a^1\pi_g$ (v'=0) would be, from 8.3 and 8.5,

$$n = H\ /\ (K\ G\ R\ e\ E\ A\ V\ F). \qquad 8.6$$

The uncertainties in some of the quantities in equation 8.6, especially G, E and F, are difficult to quantify. Therefore this equation will give only an order of magnitude estimate of the population density. However this is the only calculation that can be made to obtain a value for the population density.

As an example of the use of this method the data collected from a 9kV DC discharge in 9mbar of nitrogen, using the simple flowing gas discharge tube, gave an estimate for the 'a' state population of $6 \times 10^{12} cm^{-3}$. Further uses of this method for estimating the population density in particular molecular states are given in chapter 9 for a variety of conditions.

Thus it has been shown that an appreciable population is being produced in the metastable nitrogen state.

8.4 EMISSION FROM $b^1\Pi_u$ STATE

Concurrently with the investigation into the production of the metastable $a^1\Pi_g$ state a study was made of the emission on the BH bands from the $b^1\Pi_u$ states. The transition rates for the BH bands are very much larger than for the LBH bands, and hence the emission was observable for much smaller populations in the 'b' state. It is not surprising, therefore, that the BH emission was seen in cases where the LBH bands were not seen.

The BH bands could not be detected, however, when using the internal capacitor electrode structure of DT I. There are a number of reasons for this.

Firstly, this arrangement is equivalent to running the other pulsed discharges without any ballast resistor. At the low pressures used the preioniser gaps were seen not to breakdown, and hence the internal capacitors would not charge up. These conditions would lead to a discharge with large pulse to pulse variations which would make it difficult to detect the BH emission.

Secondly, the thickness of the discharge which the monochromator views is very much thinner in the case of the internal capacitor discharge, perhaps 1cm compared to 10cm in the case of the long discharges of DT II and DT III. Although the transverse discharge extends laterally, the limited acceptance angle of the monochromator meant that this did not increase the light falling on the grating.

In an attempt to increase the stability of the discharge the nitrogen was buffered with helium. However this had the effect of increasing emission on the lines of neutral atomic nitrogen, and also those of carbon which is always present as an impurity. It was found that while buffering leads to stable discharges it does not increase the emission on the desired bands.

On recording the time resolved emission of the BH bands and comparing them to the LBH emission, it is seen that the former has a shorter decay constant (see figures 8.12 and 8.13). By pulsing the XeCl laser at a time delayed from the start of the nitrogen discharge, when looking for the effect of transferring the population from the 'a' to 'b' state, it was possible to reduce the effects due to the population in the 'b' state arising from direct excitation, by the discharge. From the time resolved scans it can be seen that delaying the XeCl pulse about 100ns from the time at which the emission on the BH bands is maximum there is still be an appreciable population in the 'a' state, but the population in the 'b' state will have decayed significantly by this time. However there is still a background component in the emission which is not related to the effect of the transfer laser.

Figures 8.14 and 8.15 show some of the wavelength resolved scans made of the emission on the BH bands. These were made under a variety of conditions as shown. Also observed are some transitions on the $b'^1\Sigma^+_u - X^1\Sigma^+_u$ (v'=1 - v"=n) system, which overlap the b-X (v'=1 - v"=n) transitions

It was noticed that the intensity distribution of these traces was not in agreement with the published transition probabilities for the vacuum vibrational bands (Zipf and Gorman 1980). For example the v'=1 - v"=1 peak is

relatively more intense than the v'=0 to v"=0 band. The relative intensities of the transitions were investigated as a function of the time since the start of the discharge. It was found that at later times, after 400ns, the transitions to levels v"=8-12 were more intense than those to v"=0-4, although their transition probabilities were about an order of magnitude smaller. It was postulated that this was due to self-absorption as the low lying vibrational levels became populated in the tail of the discharge pulse.

An inference from this is that self-absorption on the transition to v"=0 would be expected at all times. The absorption cross-section for the X-> b (v"=0 - v'=1) transition in nitrogen is $6x10^{-17}cm^2$ (Zipf and Gorman 1980). The path length through the monochromator to the sodium salicylate scintillator is 50cm. At 8mbar this gives an absorption coefficient-length product of kl=648. Thus no radiation on this transition would be detected by the PMT due to massive self-absorption.

However, there is something emitting almost exactly at the same wavelength as the v'=1-v"=0 transition. Using the assignments of Dressler (1969) and the data from Tilford and Wilkinson (1964), this transition has been identified as being between a Rydberg state and the molecular ground state, $c'_4\ ^1\Sigma^+_u$ (v'=3) - $X^1\Sigma^+_u$ (v"=4), at 98.505nm. The b-X (v'=1 - v"=0) transition is at 98.565nm. The c'_4 (v'=3) state perturbs the b'(v'=7) state (Dressler,1969) and so population from the b' state can undergo transitions on the c'_4-X transition due to state mixing. Due to a reasonably large Franck-Condon overlap of the b'(v'=7) state with the nitrogen ground state it would be expected that this state will be populated. Hence the relative intensity of the transition at 98.5nm would not be expected to fit in with the rest of the progression as it does not belong to that progression.

Observations of the BH bands in emission have therefore acted as a check that the system is sensitive to detecting radiation at these short wavelengths, so that the more technically difficult task of investigating the effect of the radiation from the "transfer" laser could then be undertaken.

8.5 LASER INDUCED FLUORESCENCE FROM $b^1\Pi_u$ STATE OF NITROGEN

8.5.1 Method of detection of laser induced fluorescence

Having established that it was possible to produce the intermediate $a^1\Pi_g$ states, it was decided to look for evidence of laser induced fluorescence (LIF) from the $b^1\Pi_u$ state using the radiation from the xenon chloride laser. As spontaneous emission had been previously seen from the 'b' state under discharge conditions giving rise to production of the 'a' state, the LIF would be evidenced by an increase in the emission on the BH bands at the time when the XeCl laser passed through the discharge. Due to the longer lifetime of the 'a' states, the difference could be enhanced by pulsing the XeCl laser in the afterglow of the nitrogen discharge, when the intensity of the LBH emission due to discharge excitation was decreasing as a function of time.

To enable the effect due to the LIF to be isolated it would be necessary to perform two experiments for each set of operational parameters; one with the XeCl laser radiation passing through the nitrogen cell, and the other with it blocked. These experiments were run under the control of the microcomputer, which also stored the data collected in the standard format. This meant that a program could be written which would enable a point by point subtraction of the control data from that containing the LIF component, in order to isolate the effect due to LIF (see appendix 3).

8.5.2 Relative timing considerations of discharges and detection system

The timing between the two discharges was controlled by causing the firing of one spark gap to send a high voltage pulse along a coaxial cable, which then became the trigger pulse for the second spark gap (see figure 8.16). By varying the length of the cable, and choosing appropriately the circuit which had the master spark gap, the XeCl laser pulse could be made to occur at any desired time delay and pass through the nitrogen discharge at any

required time. Various minimum delays must be allowed for, for the XeCl laser discharge the laser pulse occurs 250ns after its spark gap breaks down, while the corresponding time for the nitrogen discharge is about 75ns.

The trigger pulse for the gated integrator was taken from the spark gap of the XeCl laser. The end of a fibre optic cable was sealed into the translucent body of the spark gap. The light incident on the fibre was fed along it and onto a photodiode situated in the "quiet" room (see figure 7.1). The photodiode output signal was used as the trigger pulse for the gated integrator. It was decided to use this signal, derived from the firing of the XeCl laser, as it was most important that the aperture of the gated integrator was synchronised accurately with the XeCl pulse. There was some uncertainty in the relative times at which the two discharges broke down, because, at the low nitrogen pressures used, the exact time of the breakdown of the nitrogen cell was uncertain. Thus if the gate was opened at a fixed delay relative to the nitrogen discharge the effect of the radiation from the XeCl laser might have been missed on some shots because the aperture might have been opened too soon. However, on a timescale of a few tens of nanoseconds, the position of the XeCl laser pulse, relative to the discharge pulse in nitrogen, would not have a great effect on the LIF signal.

To accurately set the position of the gated integrator aperture over the XeCl pulse it was necessary to set the monochromator to 308.2nm and observe the laser radiation passing through the nitrogen cell being scattered into the monochromator. The signal from the PMT was fed to a fast storage oscilloscope, and the gated integrator triggered as described above. The gate marker signal from the gated integrator was also fed into the oscilloscope, and the initial delay on the gated integrator altered to bring the two signals into coincidence as observed on the oscilloscope. By this method any delay due to the transit time of the PMT would be taken into account in ensuring that the signal occuring from the correct time period of the discharge is observed. If the XeCl laser signal was taken directly from a photodiode

placed in the beam, and the gate set up on this signal, it was found that the signal admitted to the gated integrator from the PMT came from a period in the discharge before the XeCl laser pulse had passed through it.

A 75ns delay was still used between the trigger pulse and the PMT signal entering the gated integrator to enable time for the gate opening electronics, within the gated integrator, to respond to the trigger.

8.5.3 Discharge tube and circuit

For this series of experiments a final variation on the discharge tube design, designated DT IV, was used. This is shown in figure 8.17. This design should keep the discharge away from any of the seals, and hence reduce the likelihood of impurity build up within the tube. The flat quartz windows allowed the UV laser radiation to be passed easily through the tube, without distortion. This meant that some experiments could be done with the XeCl laser pulse retroreflected back through the nitrogen discharge to increase its total interaction length.

The discharge circuit used a copper sulphate ballast resistor rather than the previously used carbon film resistors which experienced catastrophic failures in use due to the large voltages and currents applied to them. The resistance of the liquid reisistor was measured on an "Avo" meter on the $\Omega/100$ range as 90Ω. The $\Omega/100$ range is used so as to minimise the effect to the resistor of the measurement process. In DT IV the pin electrode was pulsed to negative volts and the anode was at earth potential - physically a copper sleeve reaching from an earthed plate in front of the monochromator slits almost to the cross arms in the tube. To minimise the nitrogen excitation circuit impedance, in order to give as fast a rise time to the current pulse as possible, and also reduce the jitter in the time at which the discharge breaks down, the earth return was an aluminium sheet laid along the top of the discharge tube. This did produce a faster current rise time, but had the effect of causing the most luminous part of the discharge to be concentrated

in a 4mm thick segment along the top part of the tube.

8.5.4 Experimental investigations

A series of experiments were performed to establish the best conditions for the LIF signal. They involved varying the gas pressures, charging voltages in the nitrogen discharge as well as the relative delay between the nitrogen discharge and the XeCl laser and the amount of line narrowing on the XeCl laser.

Consideration of XeCl laser linewidth

Experiments with the XeCl laser as a narrow-band tuned source failed to produce any LIF signal for any position of the tuning grating. If the slits were removed from one end of the laser tube it was found that a small LIF signal could be obtained, but that this was independant of the position of the grating. In this case the linewidth of the XeCl laser was estimated to be about $40cm^{-1}$. From this it was concluded that the XeCl laser was transferring population from the $a^1\Pi_g$ to $b^1\Pi_u$ state via a number of the rotational transitions.

As the laser is line narrowed two effects occur. Firstly, its spectral brightness increases, but secondly, the number of rotational transitions excited is reduced. From the results just presented, the latter effect has the more dominant role, and the efficiency of the pumping decreases as the laser is line narrowed. It was therefore decided to run the XeCl laser untuned with a cavity consisting of an aluminium coated quartz mirror, and a flat quartz output coupler.

The pulse energies used for the experiments were monitored after the they had passed through the (undischarging) nitrogen cell. For all experiments they were found to be in the 15-20mJ range, with little effect on the LIF signal for changes in energy within this range.

Optimisation of pressure and voltage of nitrogen discharge

To investigate the variation of the LIF signal as a function of pressure and voltage, a series of experiments were undertaken. The light at 108.3nm was monitored as a function of time from the start of the discharge, with and without the beam of the XeCl laser passing through the discharge. The laser pulse was launched through the discharge at 350ns after the peak of the directly excited BH emission. The results of these experiments are shown below. For various charging voltages and pressures the peak intensity of the directly excited BH emission and the peak intensity of the LIF signal (after subtracting the background direct emission) are given, in arbitary units.

Table 8.2 Conditions for optimising the LIF intensity

Voltage (kV)	Pressure (mbar)	Peak of discharge emission	Peak of LIF
12	2	195	30
	4	52	35
	8	23	22
	17	22	18
15	2	155	35
	4	70	26
	8	24	20
	17	26	10
18	2	210	0
	4	44	32
	8	30	23
	17	65	17

In general it is seen that the most intense LIF signal occurs at the lowest pressures, as does the most intense discharge excited emission. For 2mbar pressure the LIF signal produces only a small variation on a large background, so that values of the LIF intensity must be regarded as very unreliable under these conditions. At 4mbar a reasonable signal was obtained when a long time constant (10μs) on the gated integrator to average the large pulse to pulse variations in the discharge was used. However when investigating the wavelength dependance of the emission by scanning the monochromator, such a large time constant meant that prohibitively long run times were needed. Because of this, and the relatively small signal variation between 4mbar and 8mbar, in later experiments a pressure of nitrogen of about

8mbar was used.

Investigation of relative timing of nitrogen discharge and XeCl laser

Having established the discharge conditions for optimum LIF signal the signal was investigated as a function of the delay between the discharges. An arbitary zero for the relative timings was taken to be that at which the peak intensity of the discharge excited BH radiation occured. These experiments were with 10mbar of nitrogen and a charging voltage of 20kV. The data were taken with a flow of nitrogen entering the discharge tube, and leaving via the monochromator. It was noticed that even if the nitrogen discharge tube was sealed off it was still possible to see the LIF signal for up to 45 minutes. This was taken as an indication that a clean system had been developed which is not susceptible to build up impurity species.

The results are shown in figures 8.18 to 8.20. These results are discussed in detail in the following chapter. Note that the same attenuation factor between the signal from the PMT and the height recorded on the chart was not used for all these figues so that the relative scales are not comparable. Also the trace obtained at the shortest time delay is obtained from a small difference from a large background, when the background emission is most intense. The other conditions for the experiments are 50ns aperture duration at 150ns delay from the gated integrator triggering. A time constant of 1μs was used with a 1s smoothing time constant on the gated integrator output. The monochromator slits were set at 100μm and the scan rate was 0.03nm/s. The PMT had was operated at an overall voltage of 2kV

The attenuation factors in each case are as follows in table 8.3.

Table 8.3 Attenuation factors for LIF results

Delay (ns)	50	75	250(1)	250(2)	350
Attenuation	250	50	100	150	50

In figure 8.21 are shown photographs of the PMT output displayed on an oscilloscope. The LIF signal is clearly seen as a large increase of the output at the time at which the XeCl laser pulse passes through the discharge.

As observed from the results of the emission from the 'b' state excited purely by the discharge, the relative intensities of emissions to different lower level vibrational states does not agree with the published values of the transition probabilities. The transition probabilities would indicate that the shorter wavelength transitions should be more intense by a factor of about nine, than those to vibrational levels in the ground state with vibrational quantum number greater than six. It should be remembered that all these transitions come from the same upper level. This effect is not fully understood, but could be due to a build up of population in the $v''=1,2,3$ levels leading to self absorption of these transitions, or due to a wavelength dependence in the efficiency of the detection system. This point is discussed further in the next chapter.

8.6 CONCLUSION

In this chapter the results of experiments investigating the practicality of the proposed VUV laser scheme have been presented.

The conditions necessary for efficient production of the intermediate metstable level in molecular nitrogen have been investigated. A method of estimating the population in a particular state from a measure of the intensity of radiation from that state has been given.

This work has also shown that it is possible to transfer population from the excited metastable states in nitrogen to higher lying electronic states using UV laser radiation. The LIF signals observed represent the shortest wavelength LIF effect originating on excited levels seen to date.

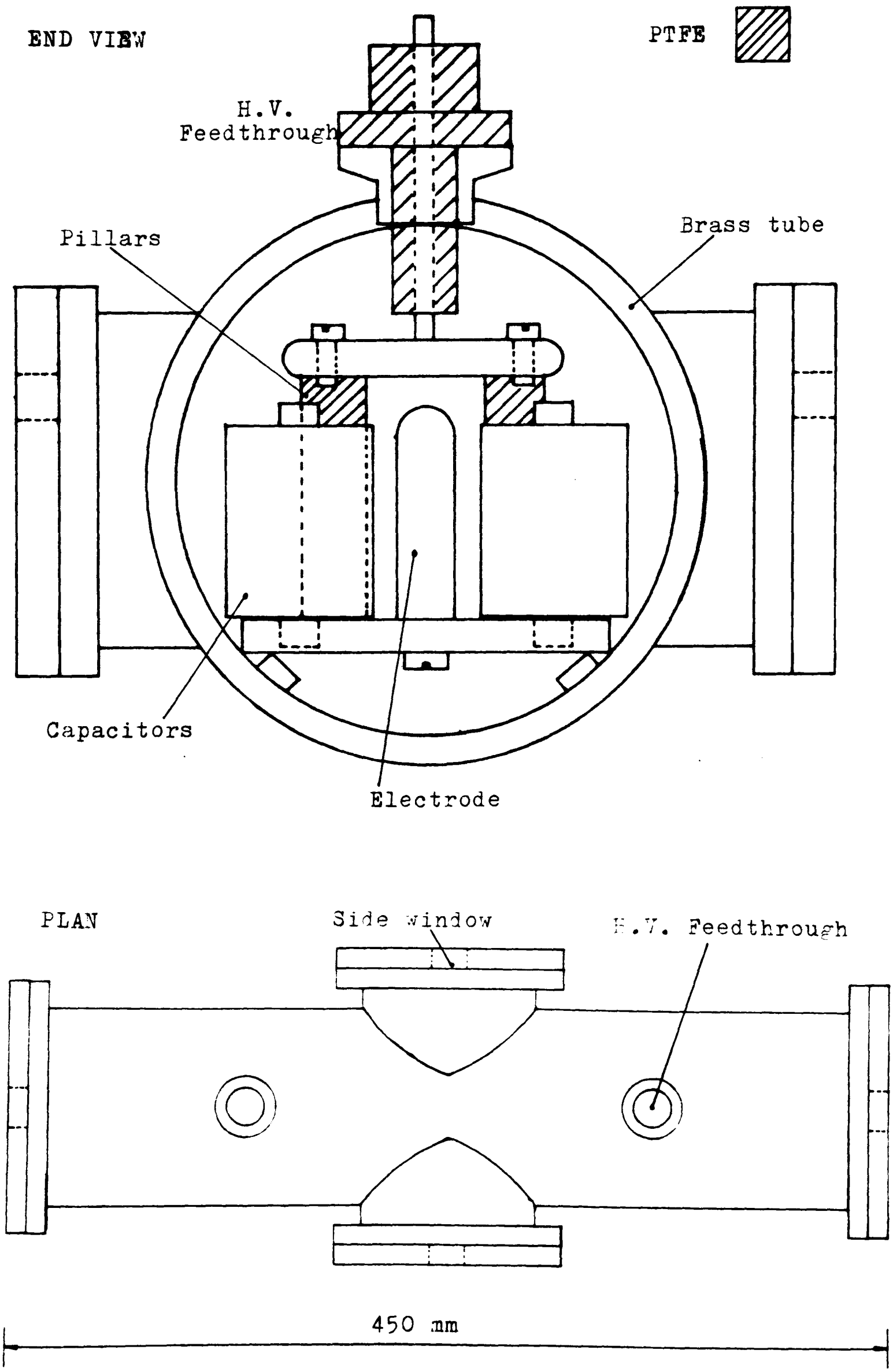


Figure 8.1 Brass bodied internal capacitor discharge tube (DT I)

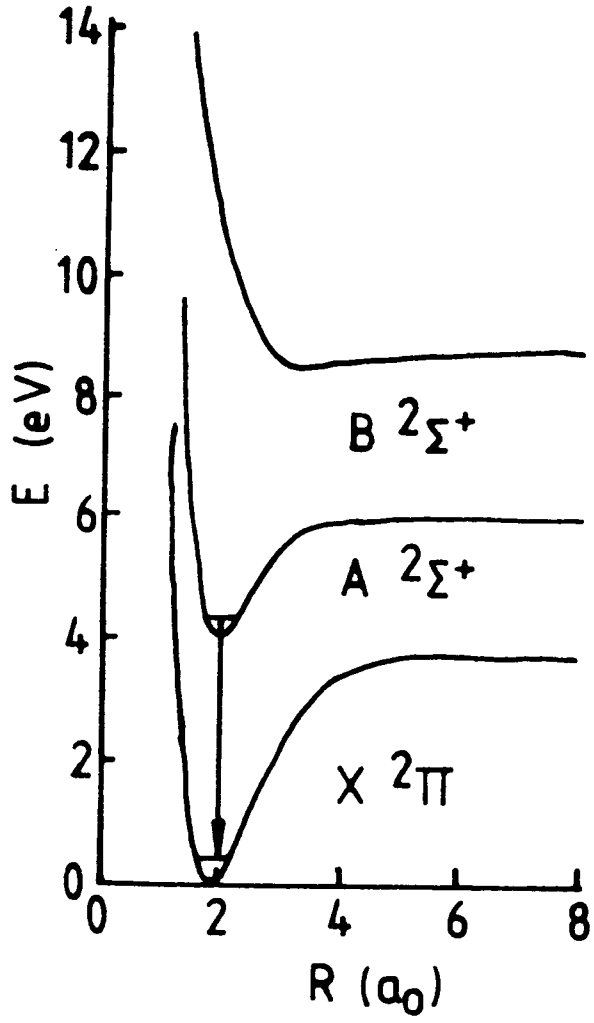
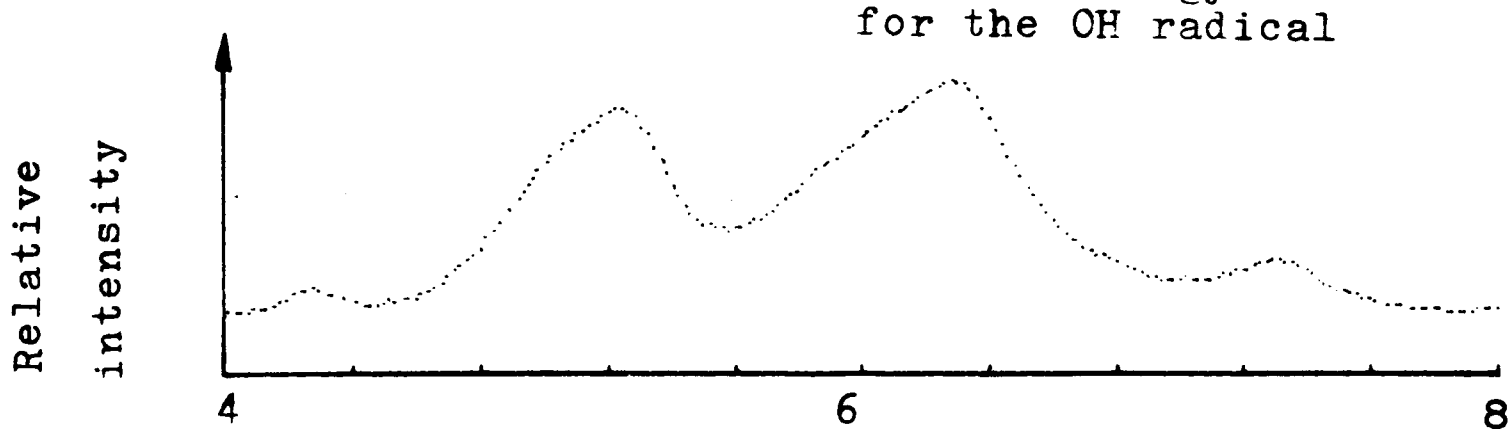
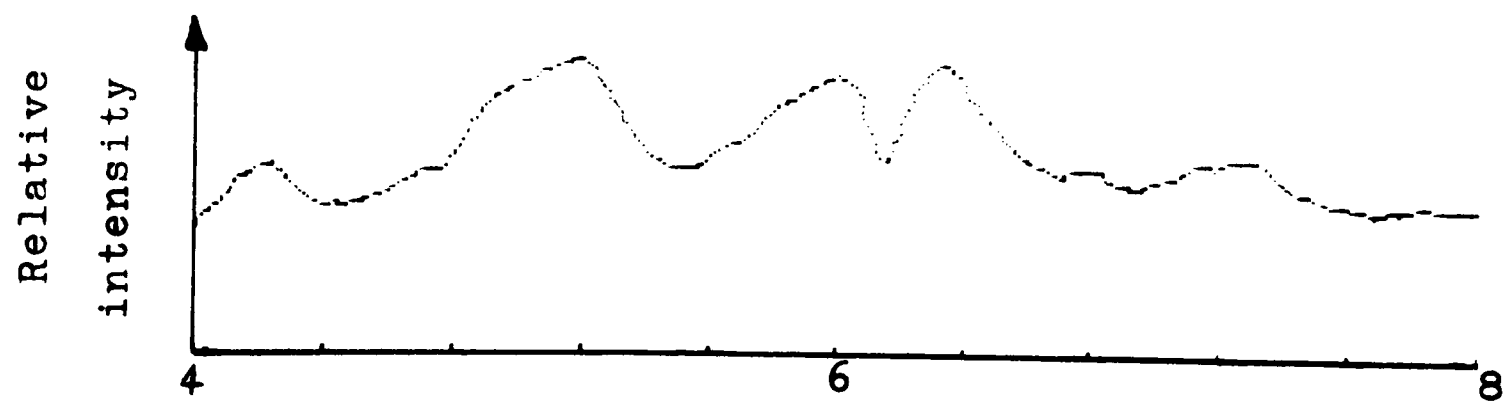


Figure 8.2 Potential energy curves for the OH radical



XeCl laser tuning curve from grating rotation



As above with discharge in H_2O/He mixture showing absorption of XeCl laser radiation.

Note: Monochromator set to 308.2nm throughout both the above experiments.

Figure 8.3 Absorption of XeCl laser radiation by 'A'-'X' band of OH radical

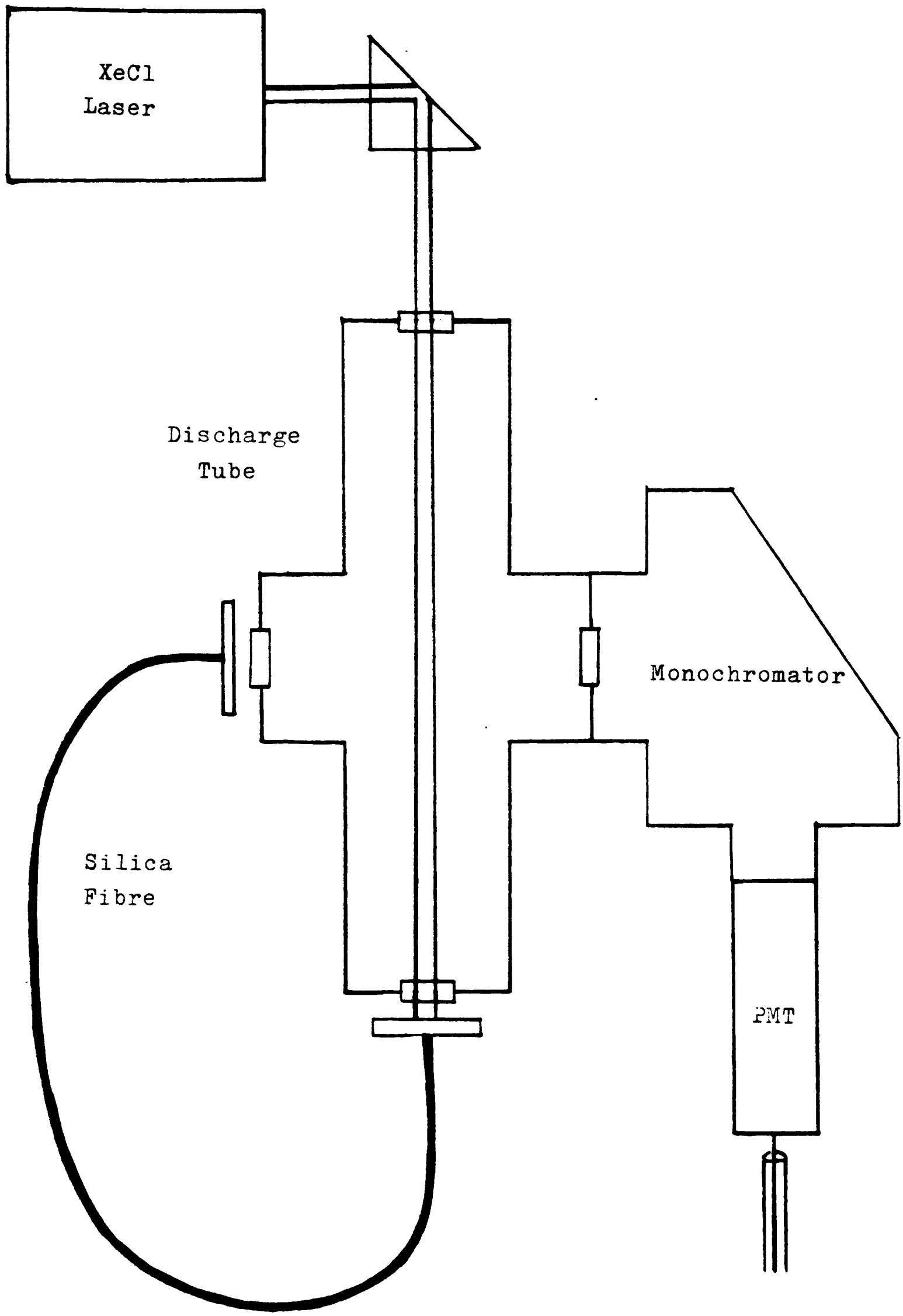
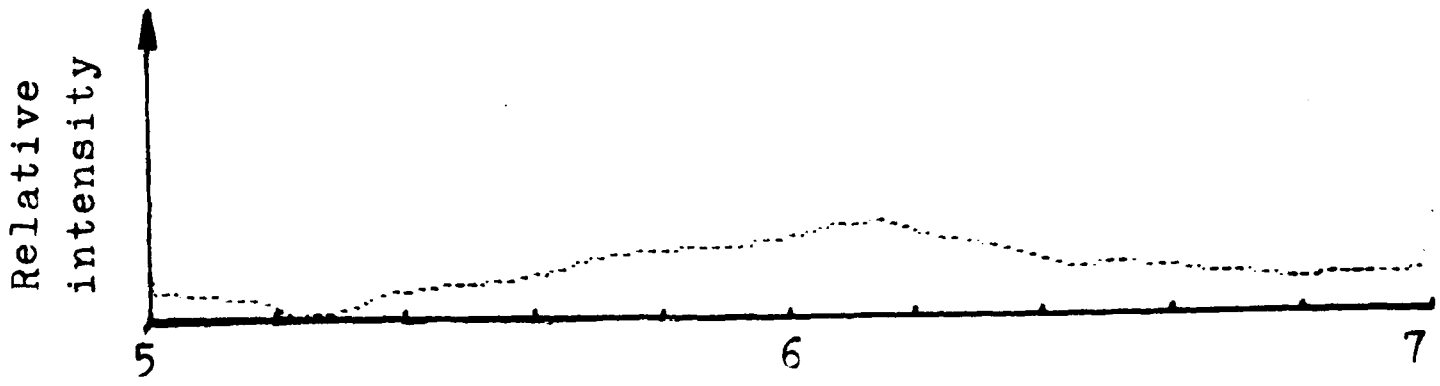
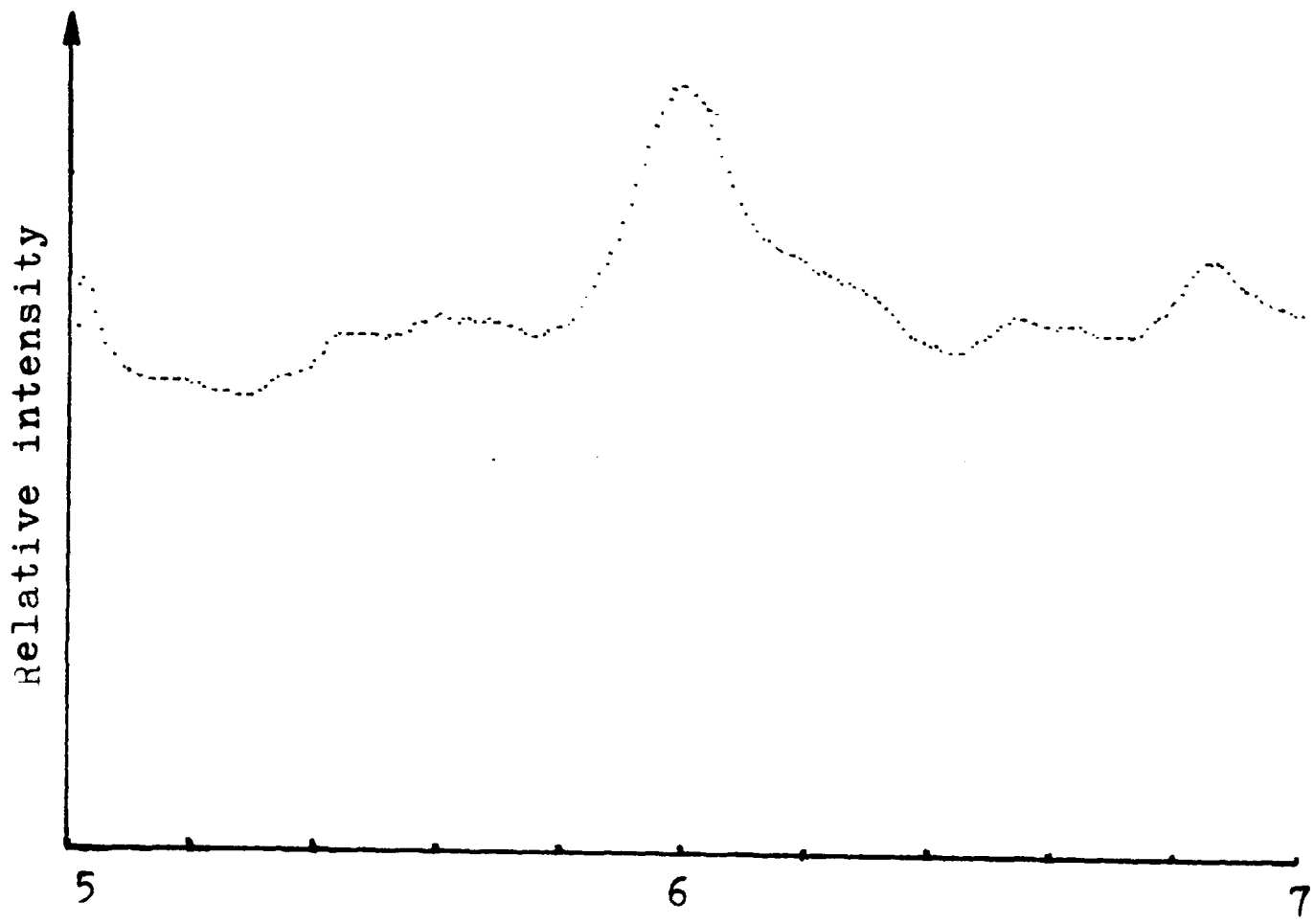


Figure 8.4 Arrangement for injection of XeCl Laser radiation into Monochromator



XeCl laser radiation scattered into monochromator



XeCl laser grating position

Radiation detected with a discharge in a gas mix of 0.5mbar H_2O / 1bar He showing LIF

Notes: 1) Monochromator set to 308.2nm throughout both above experiments.
2) Range of XeCl laser grating tuning is less than in figure 8.3

Figure 8.5 LIF on 'A'-'X' band of the OH radical

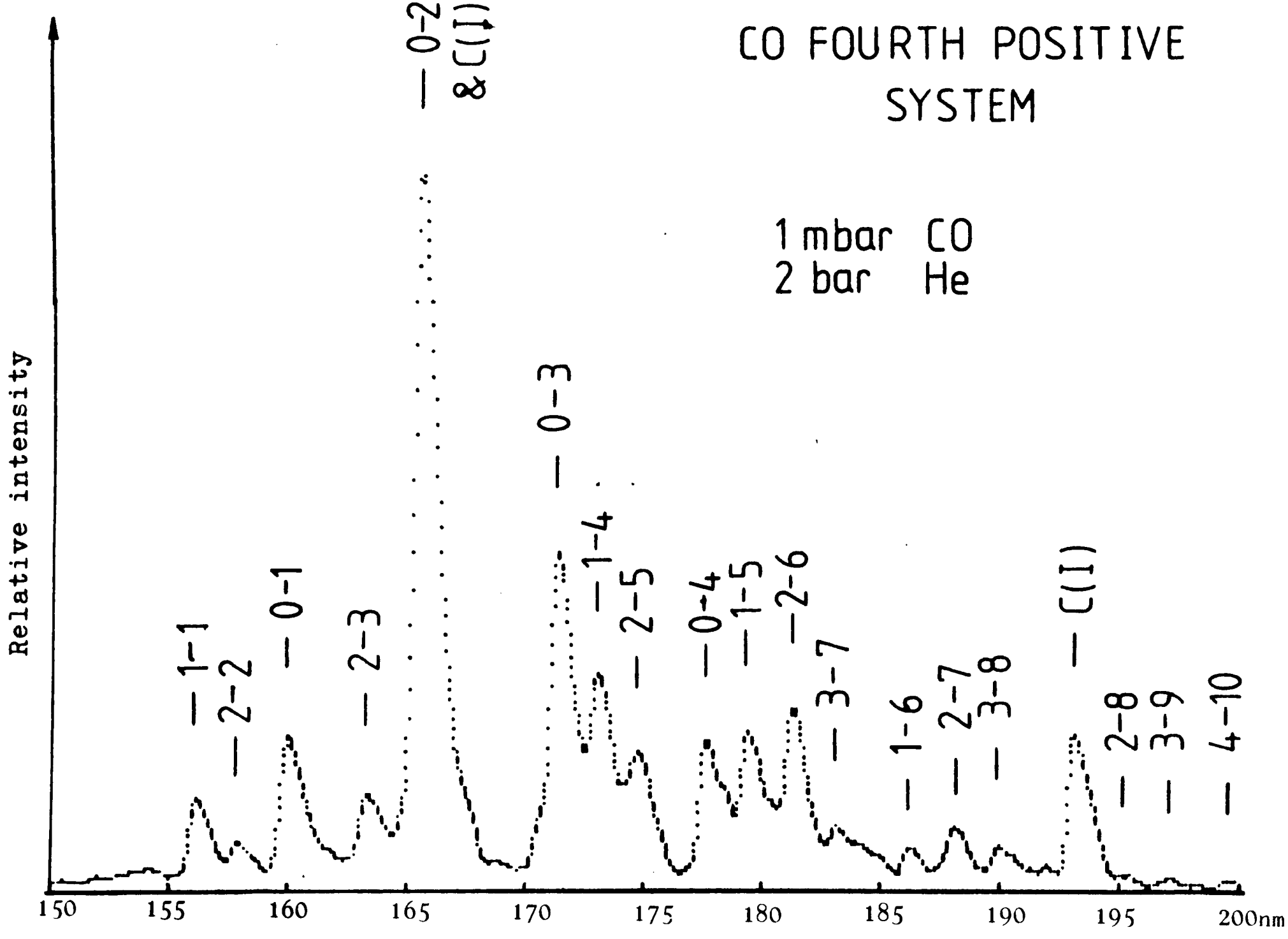


Figure 8.6 Emission on CO fourth positive band

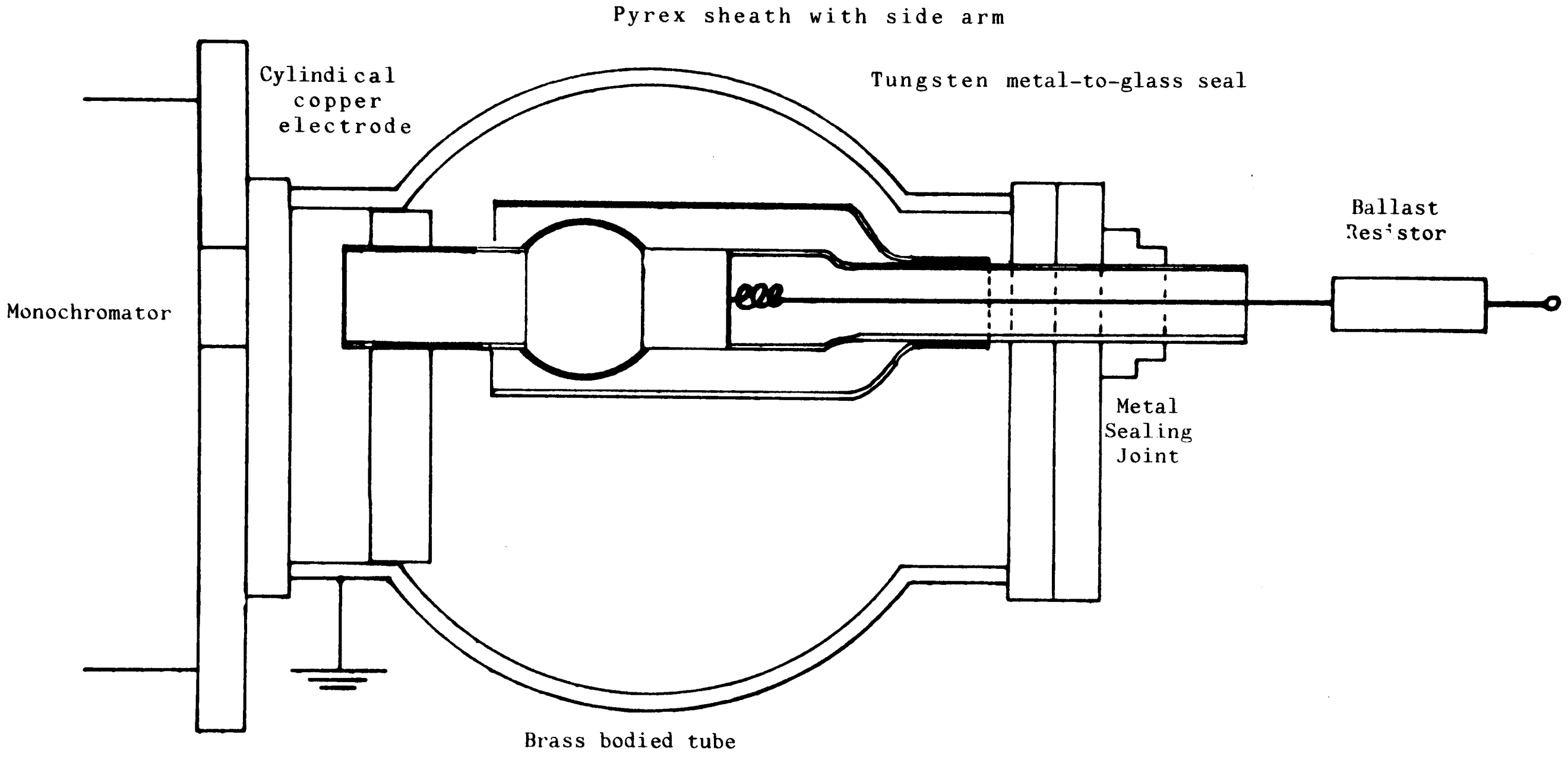


Figure 8.7 "Finger" electrode (DT II)

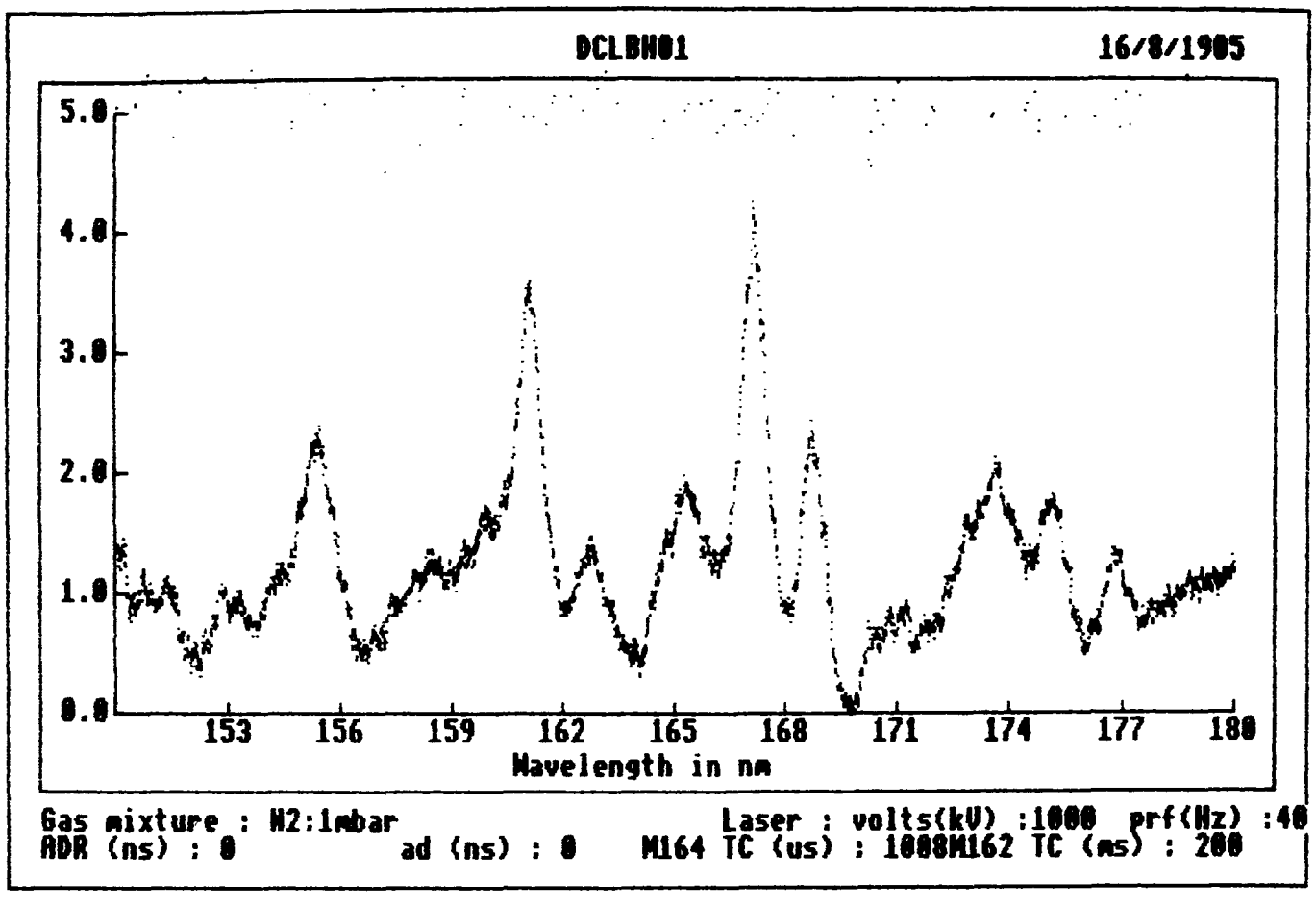


Figure 8.8 LBH emission from dc discharge

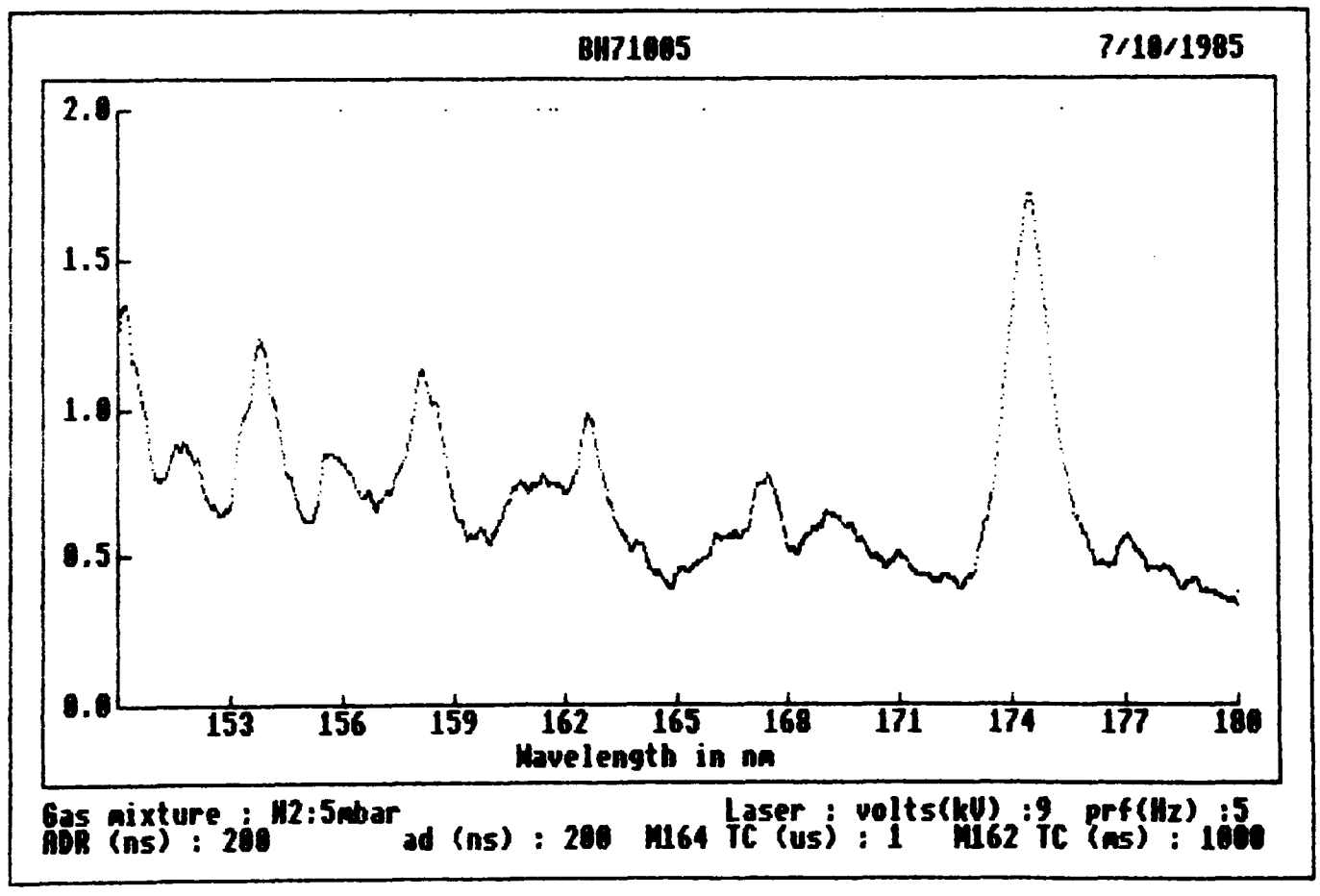


Figure 8.10 LBH emission from pulsed discharge

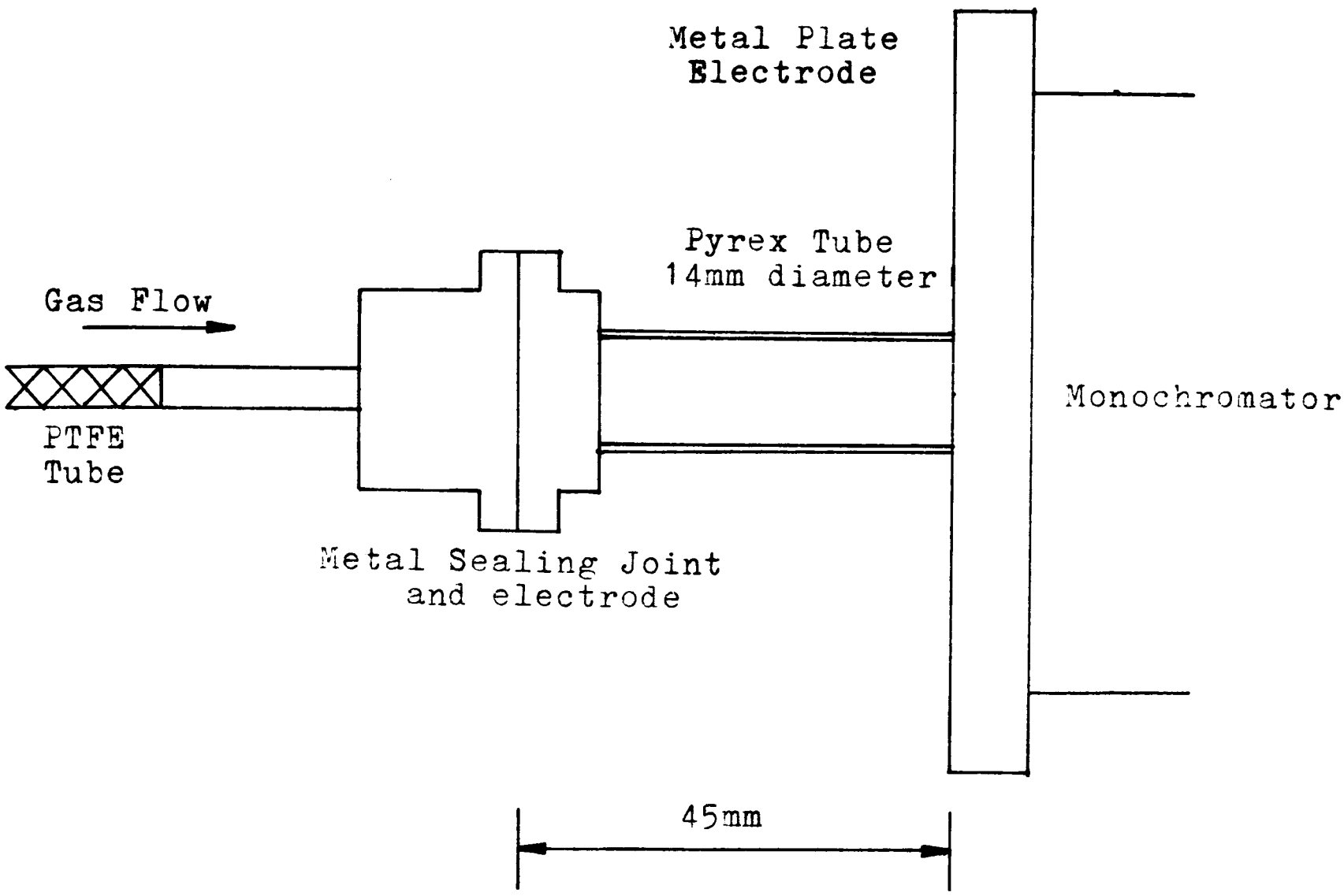


Figure 8.9 Discharge Tube DT III and circuit

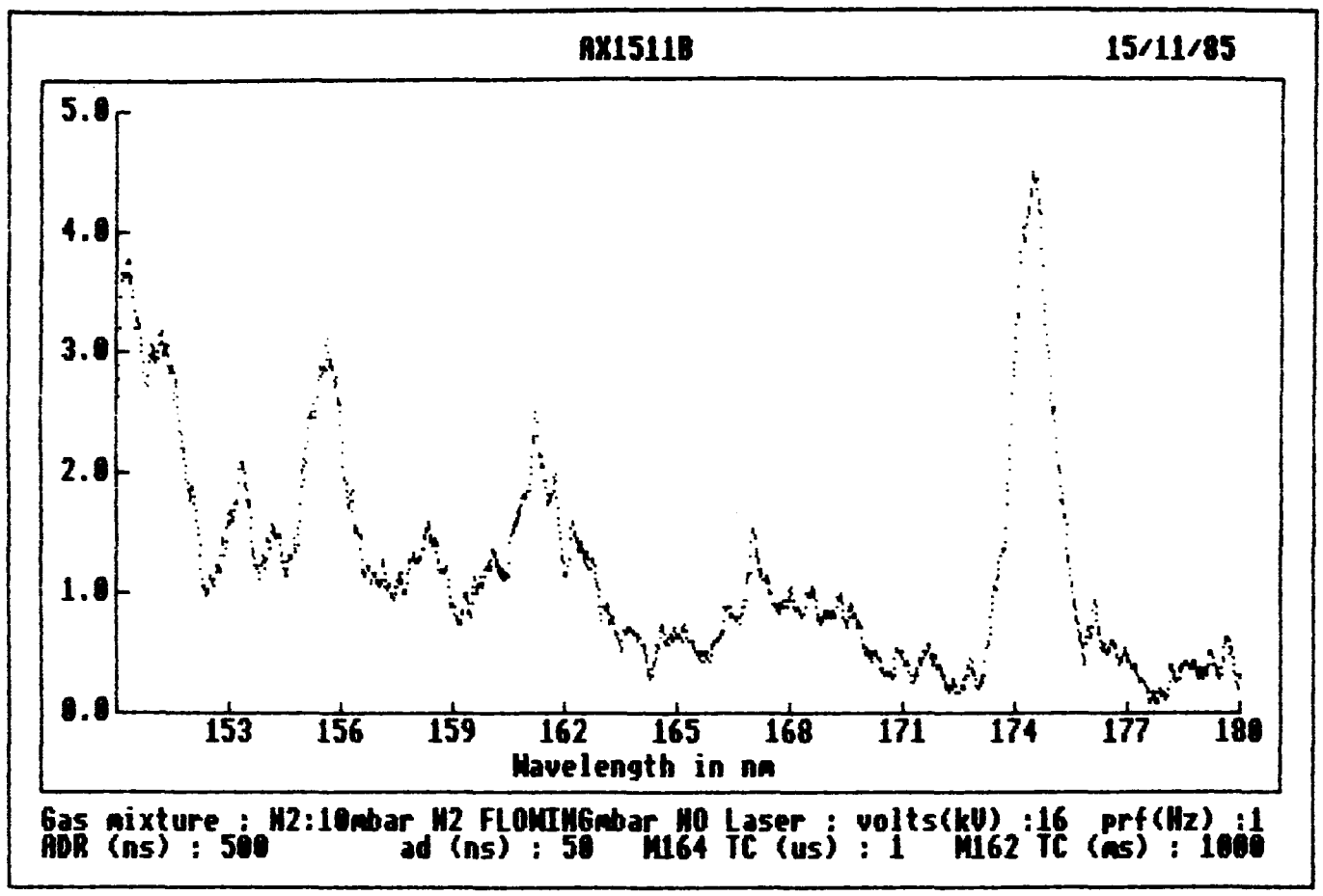


Figure 8.11 LBH emission from pulsed discharge

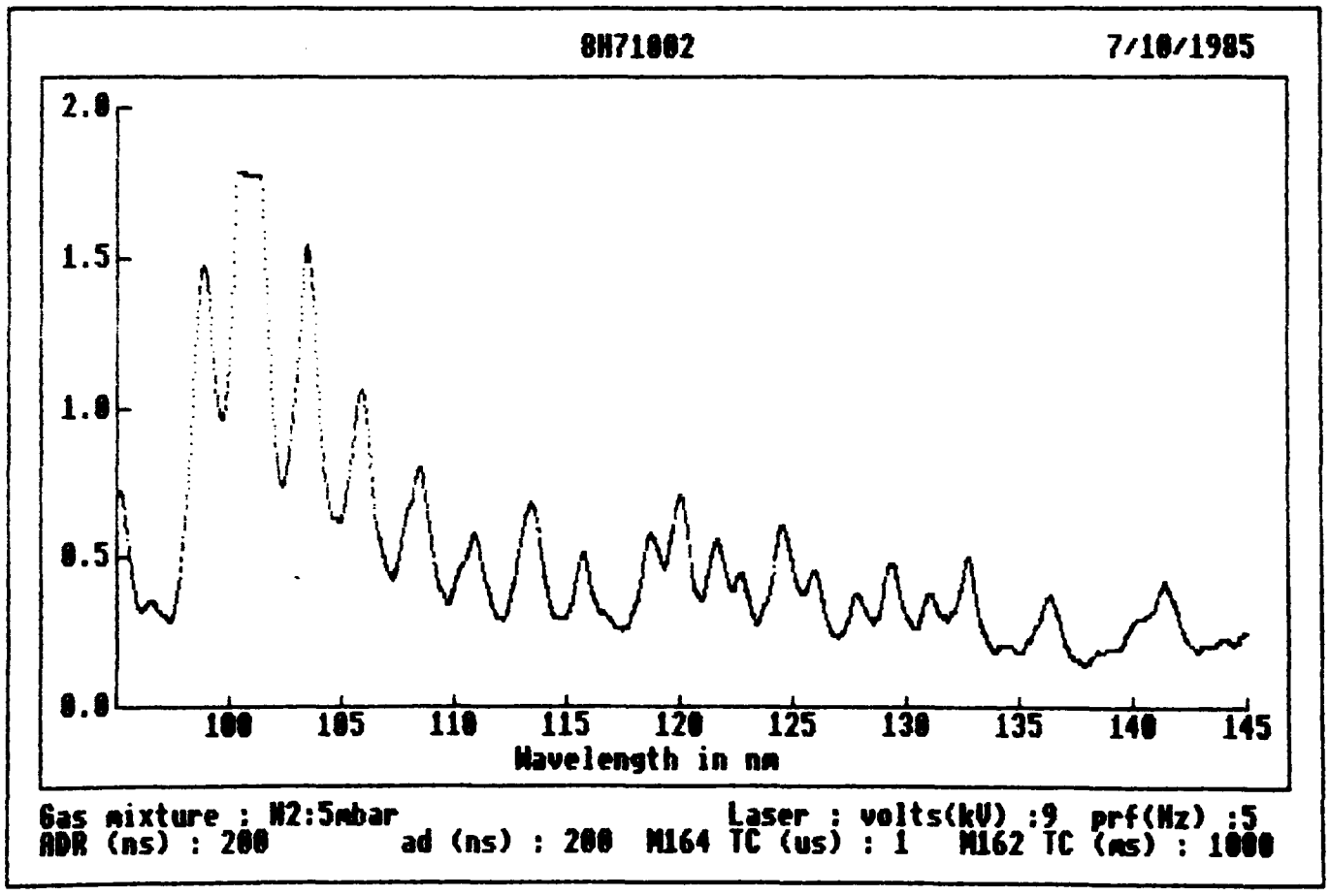


Figure 8.14 BH emission

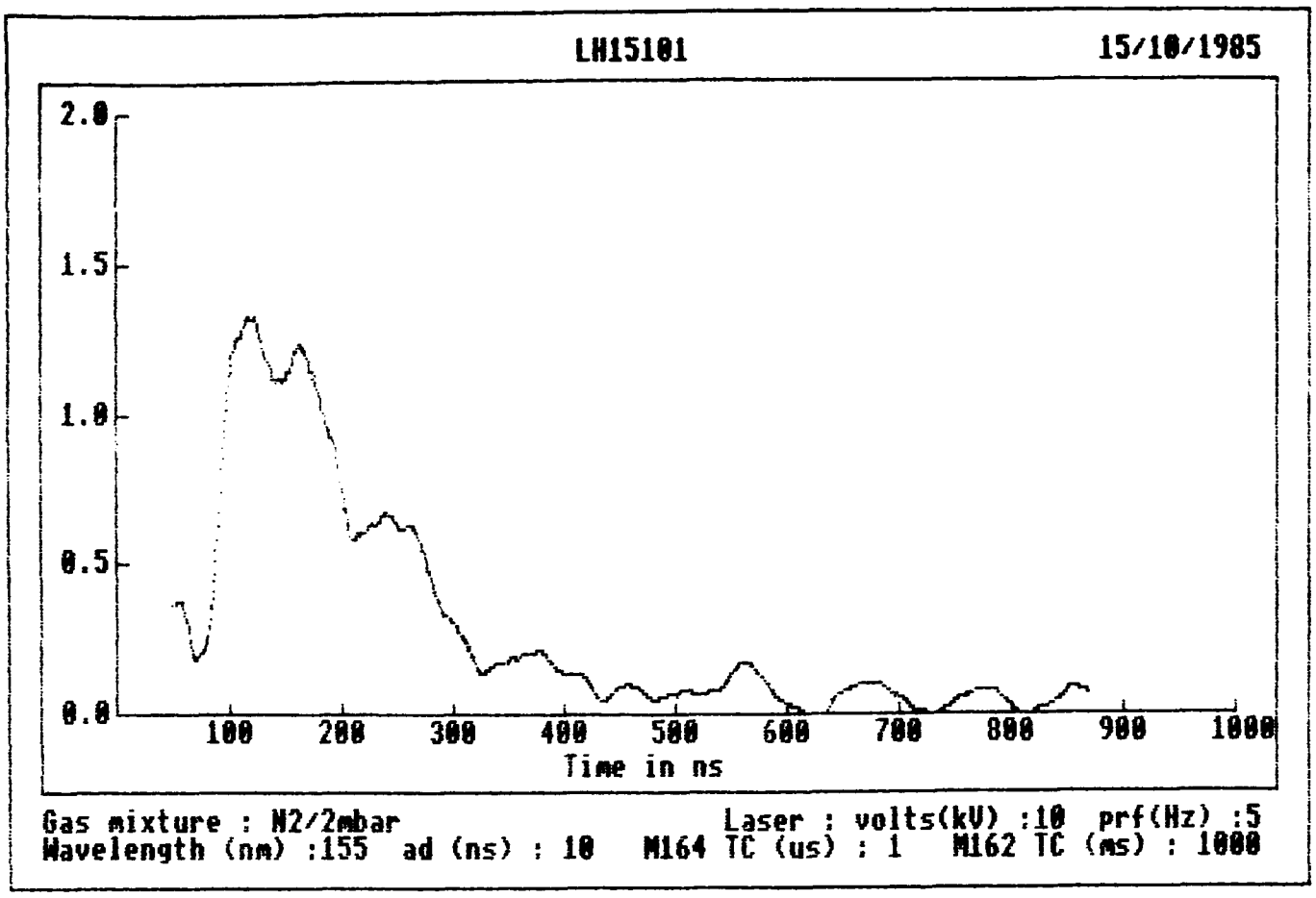


Figure 8.12 Time resolved emission on the LBH band

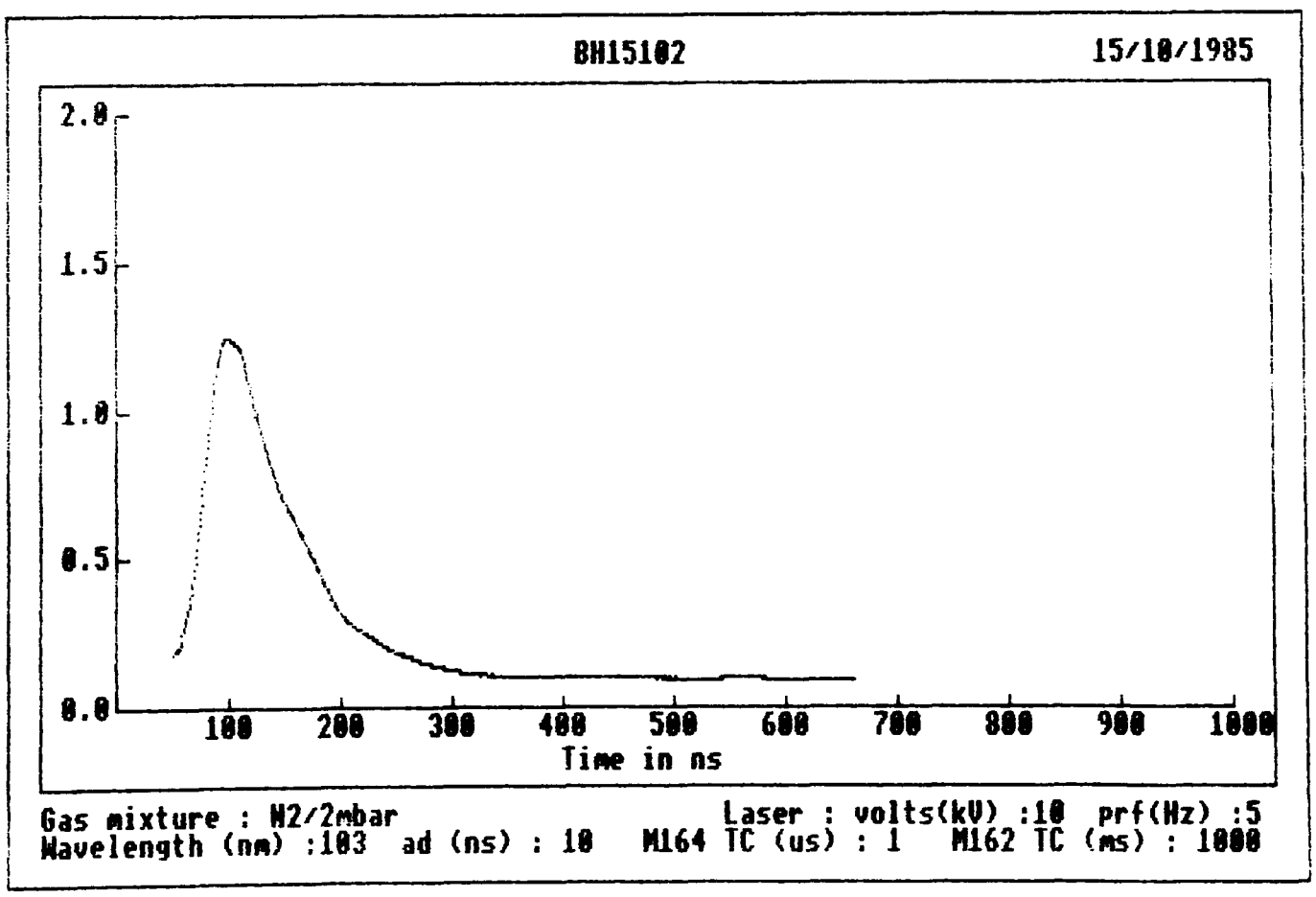
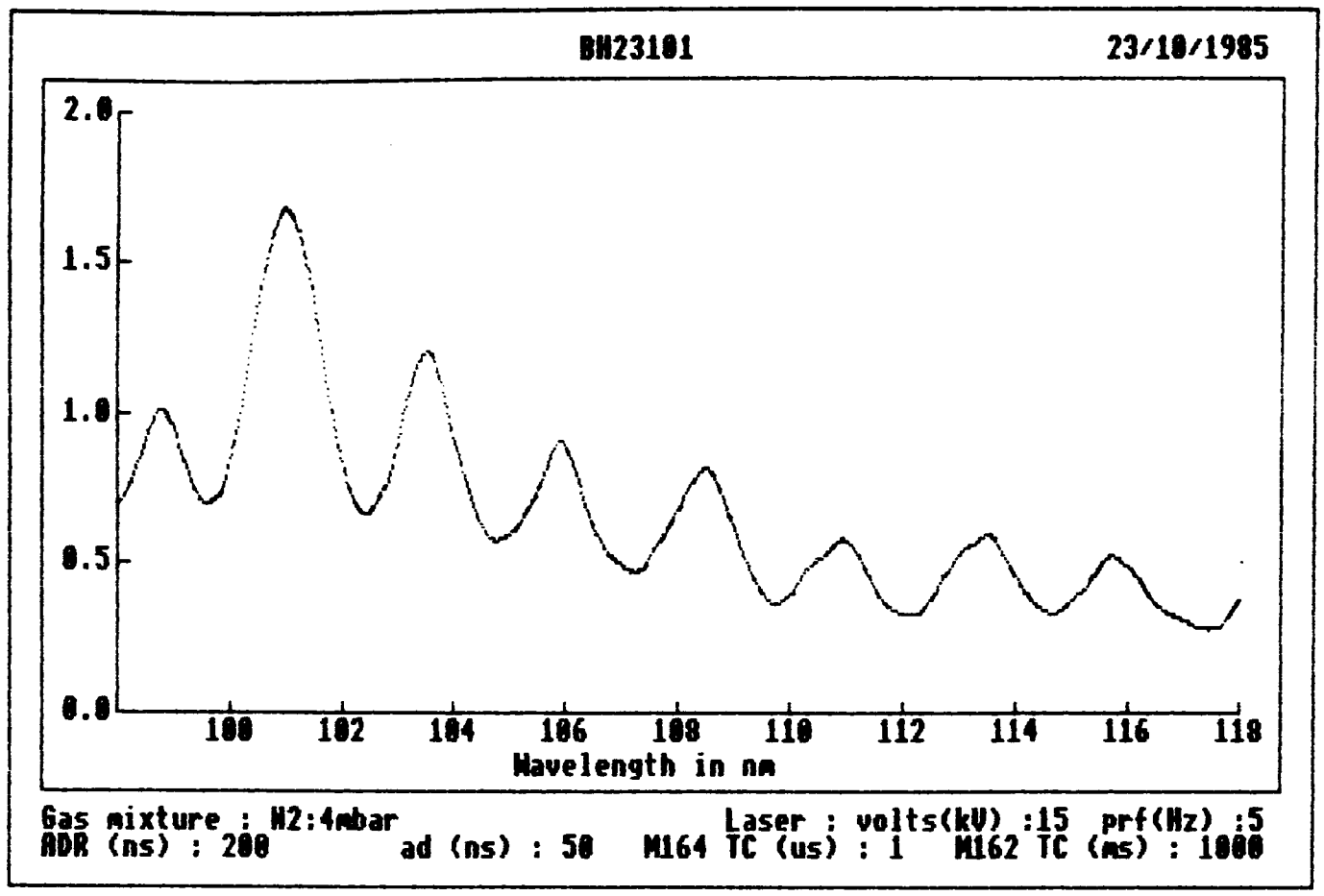


Figure 8.13 Time resolved emission on the BH band



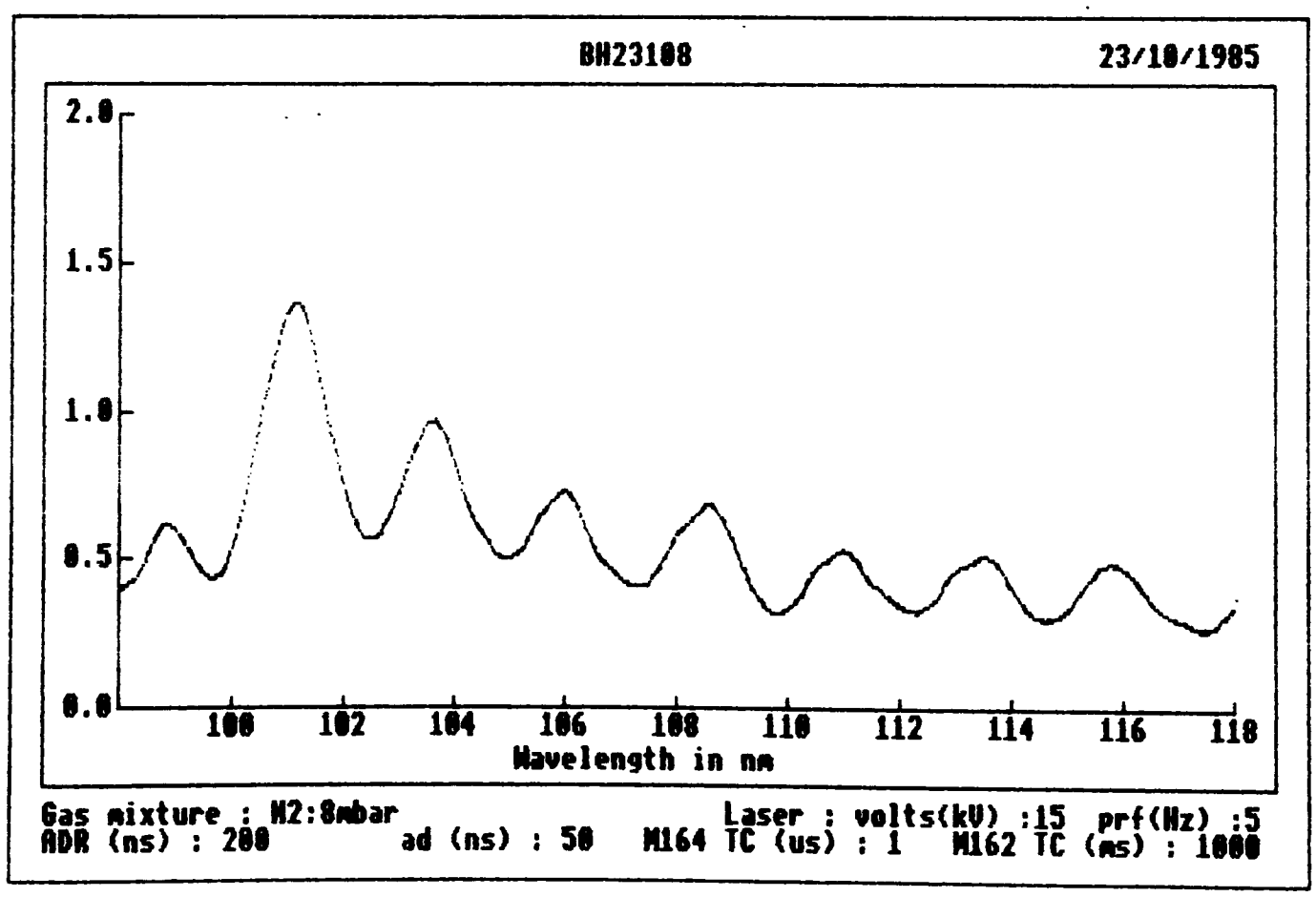
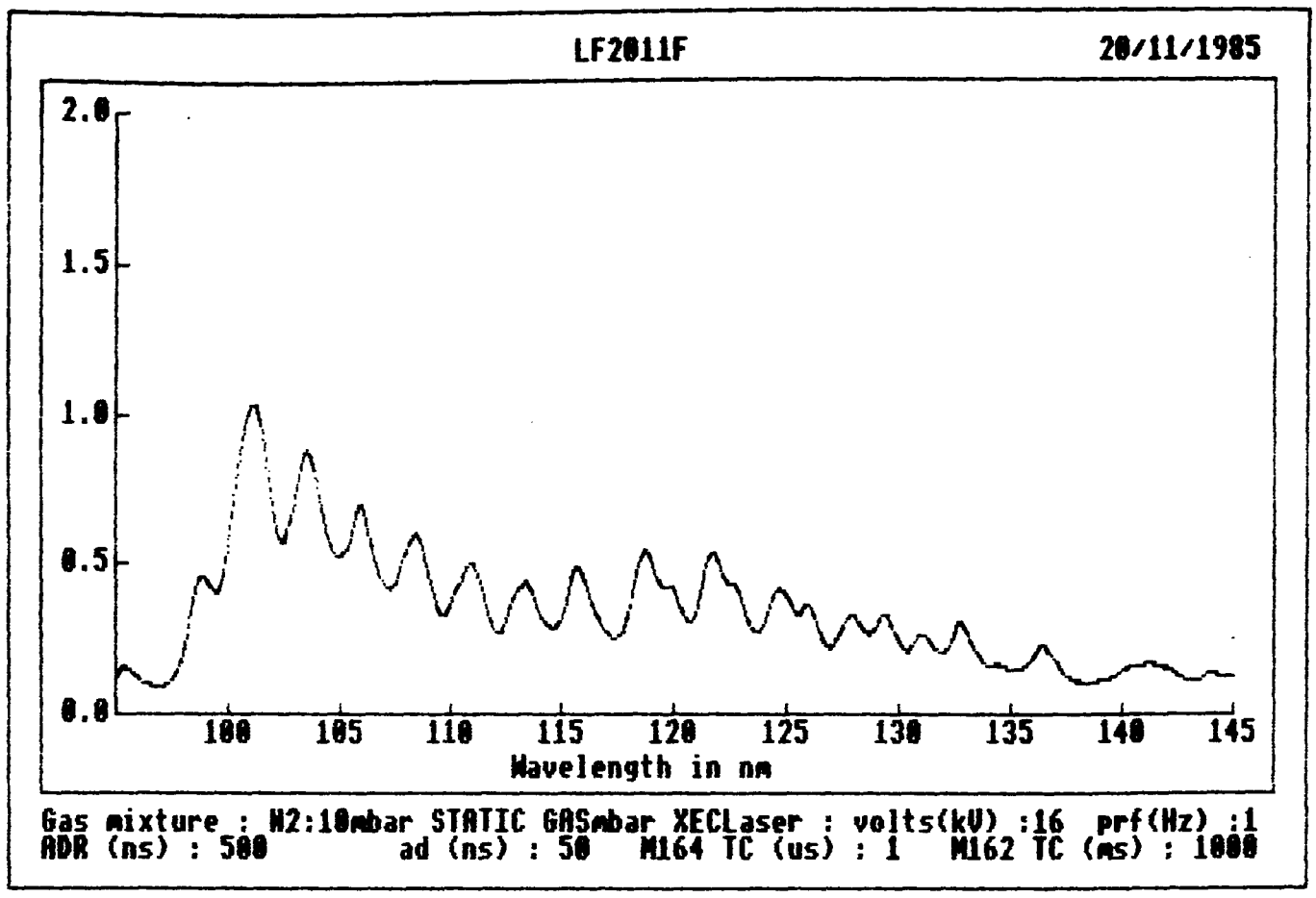


Figure 8.15a BH emission



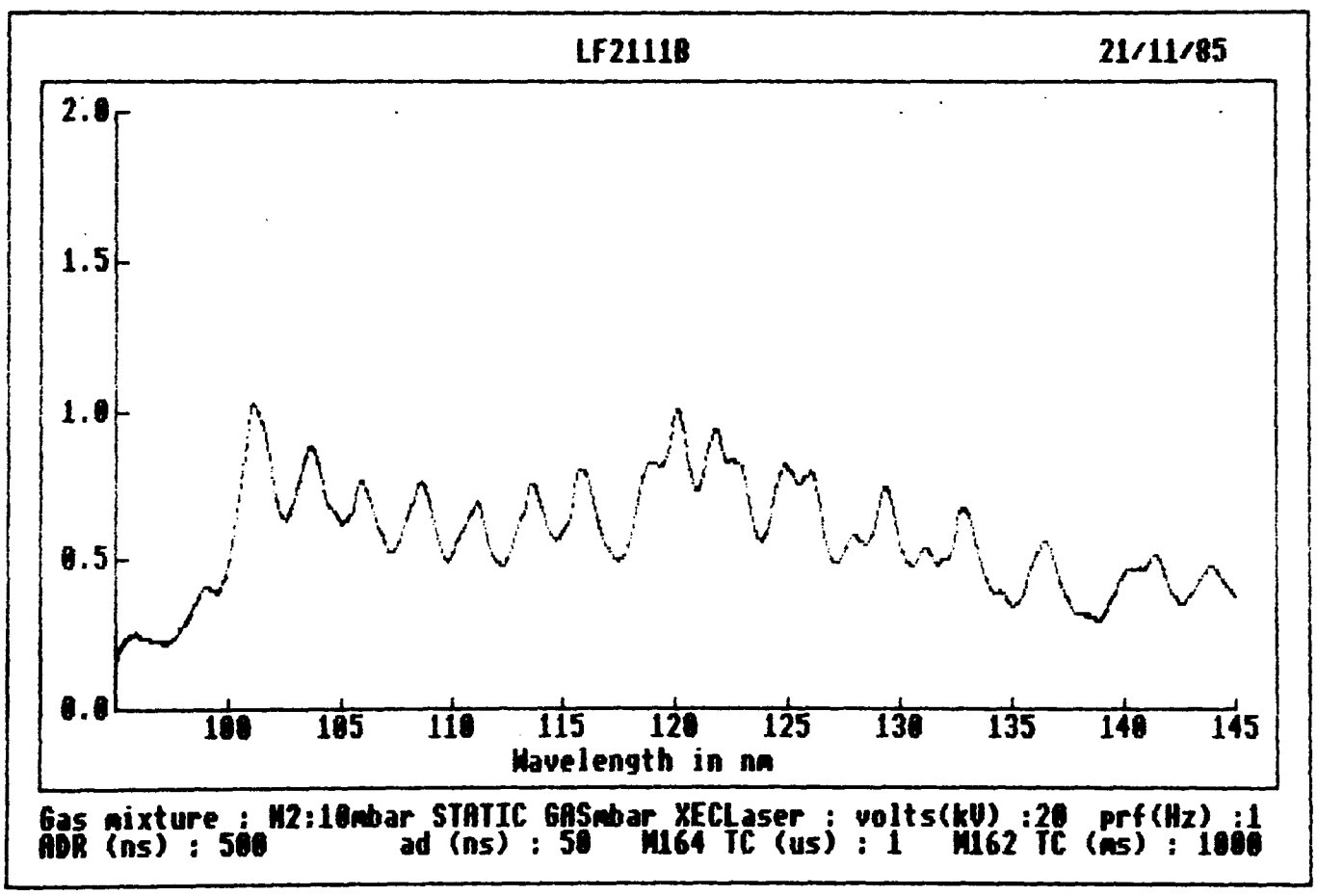


Figure 8.15b BH emission

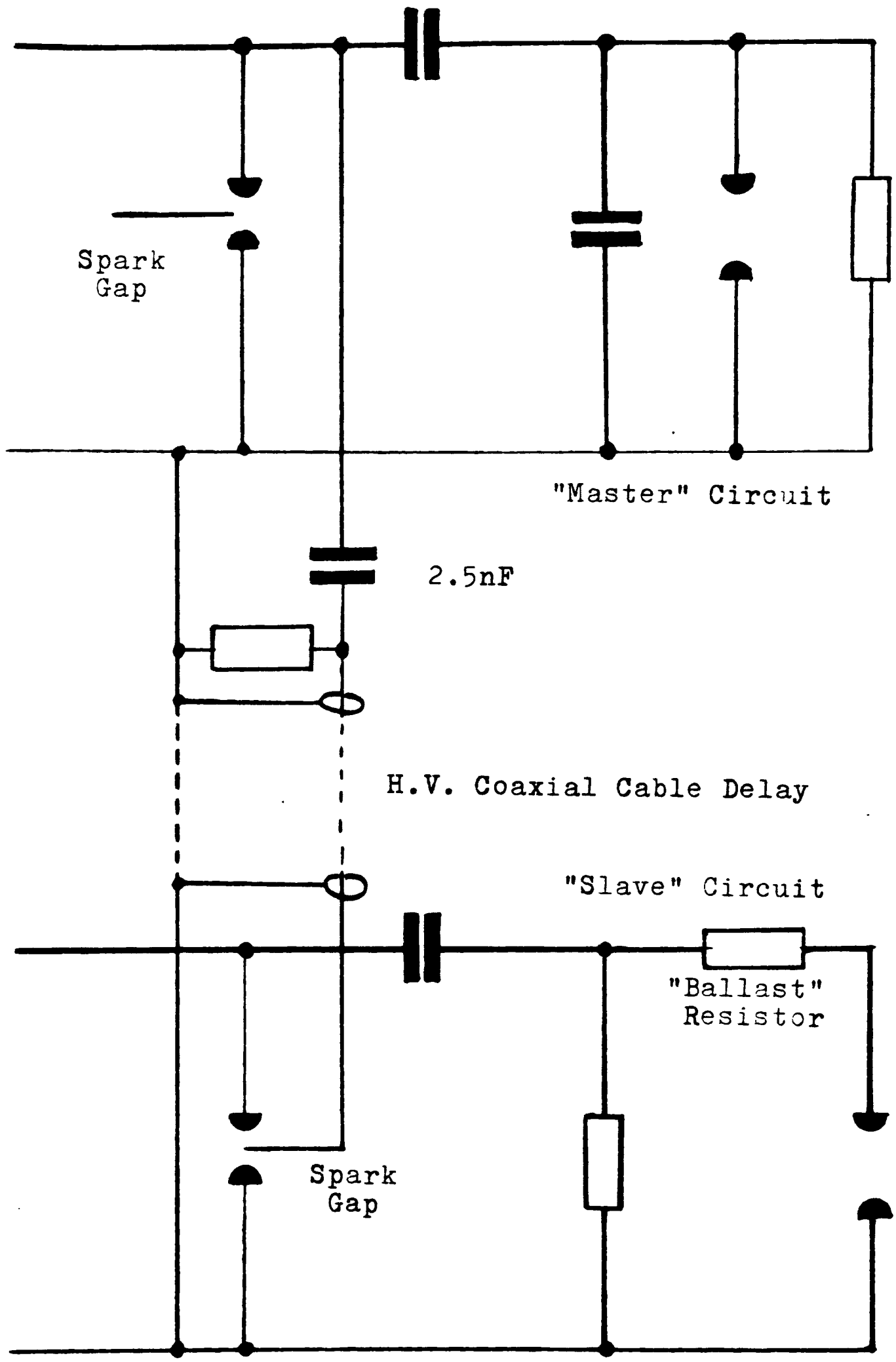


Figure 8.16 Master/Slave Discharge Circuits

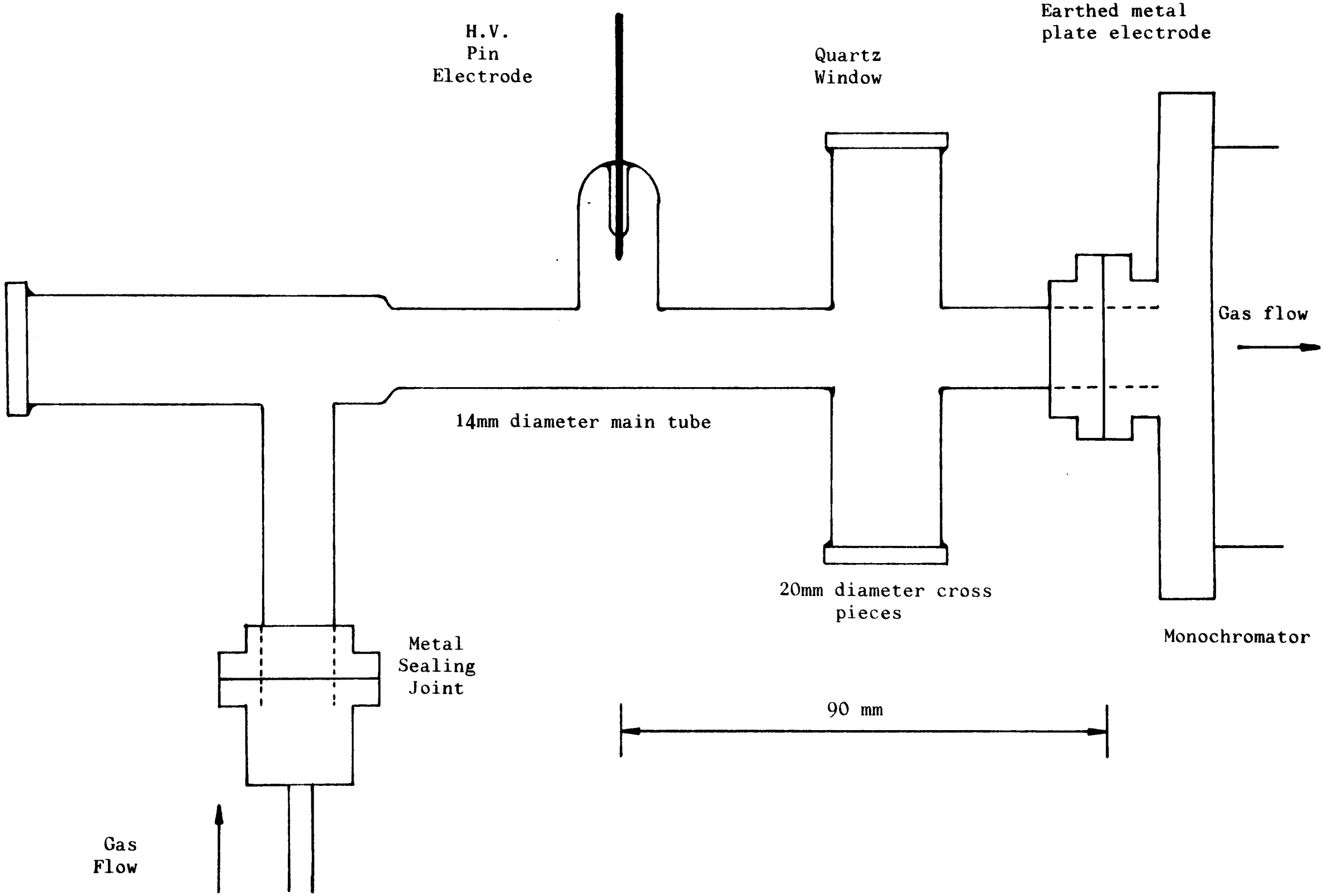


Figure 8.17 Pyrex cross piece discharge tube (DT IV)

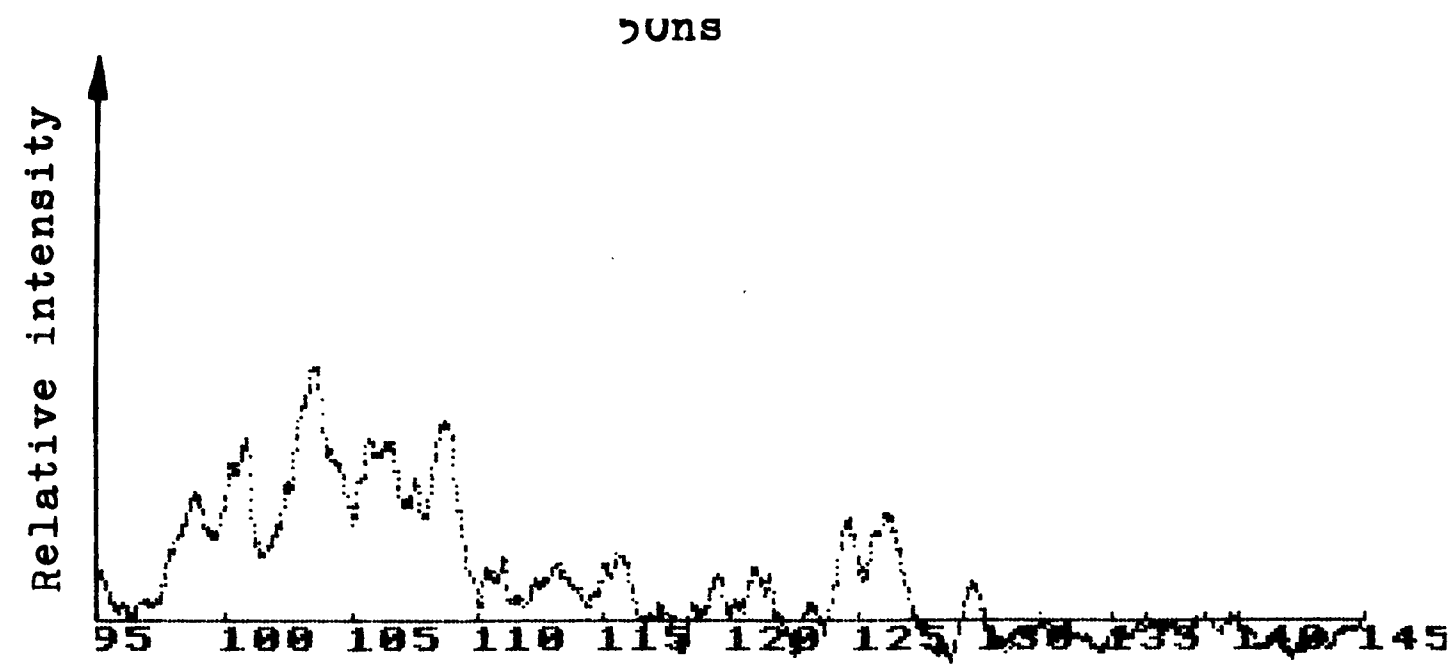


Figure 8.18 Nitrogen 'b'-'X' L.I.F.

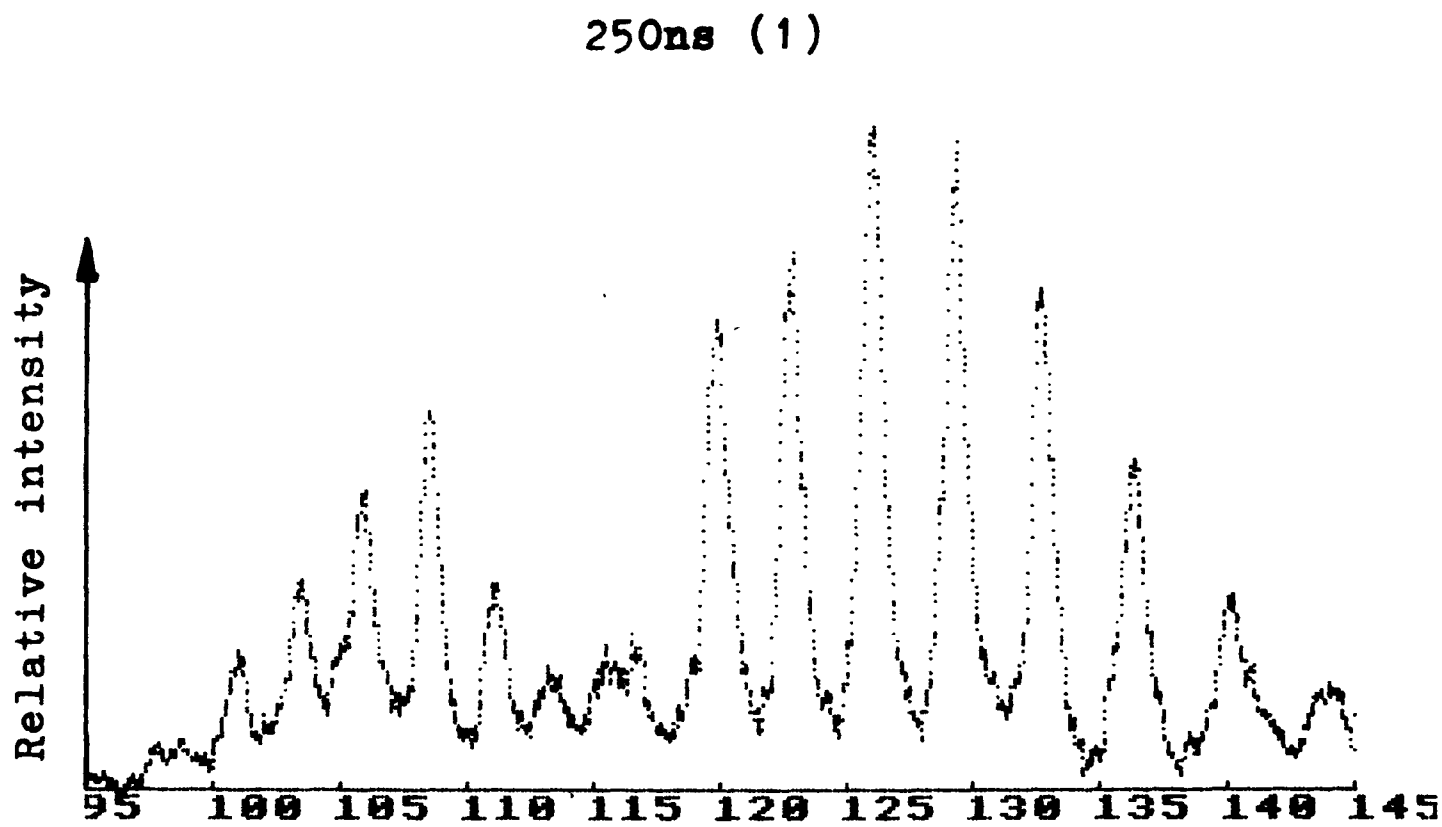


Figure 8.19 Nitrogen 'b'-'X' L.I.F.

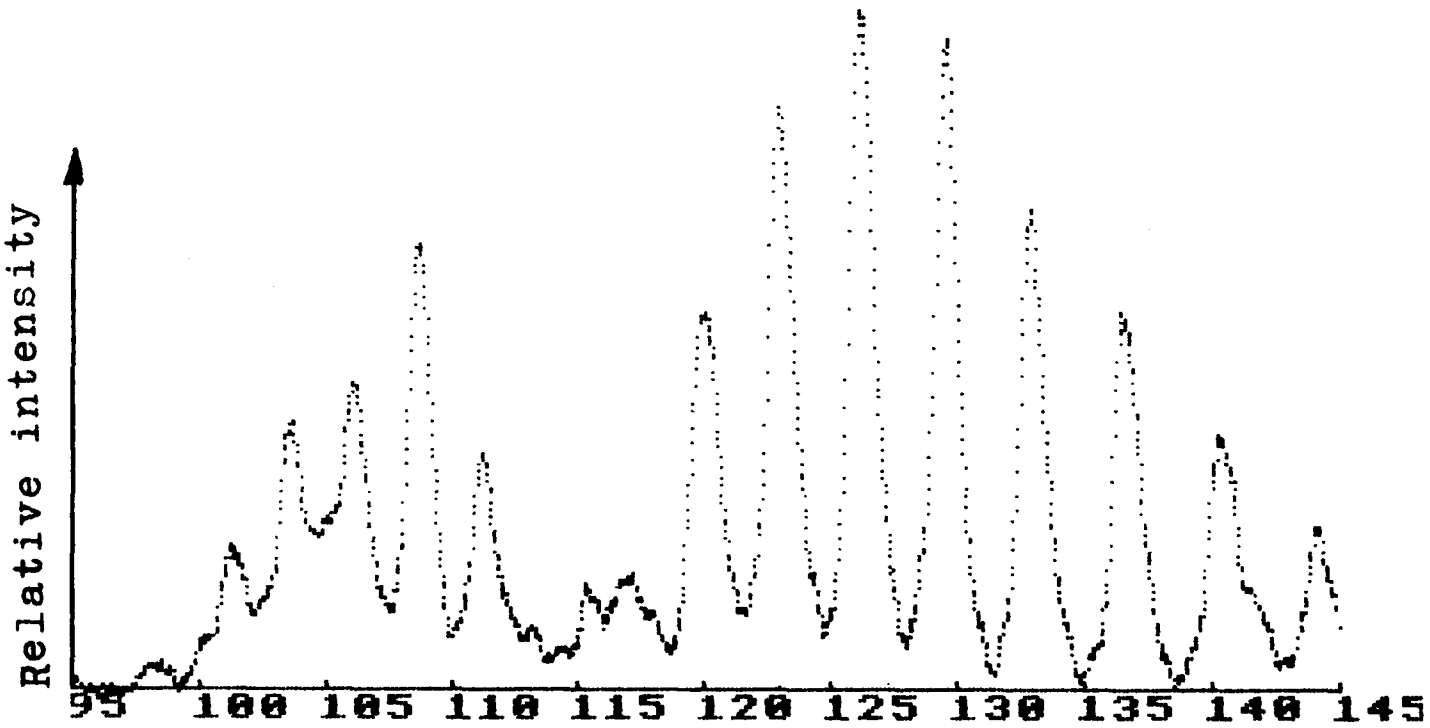
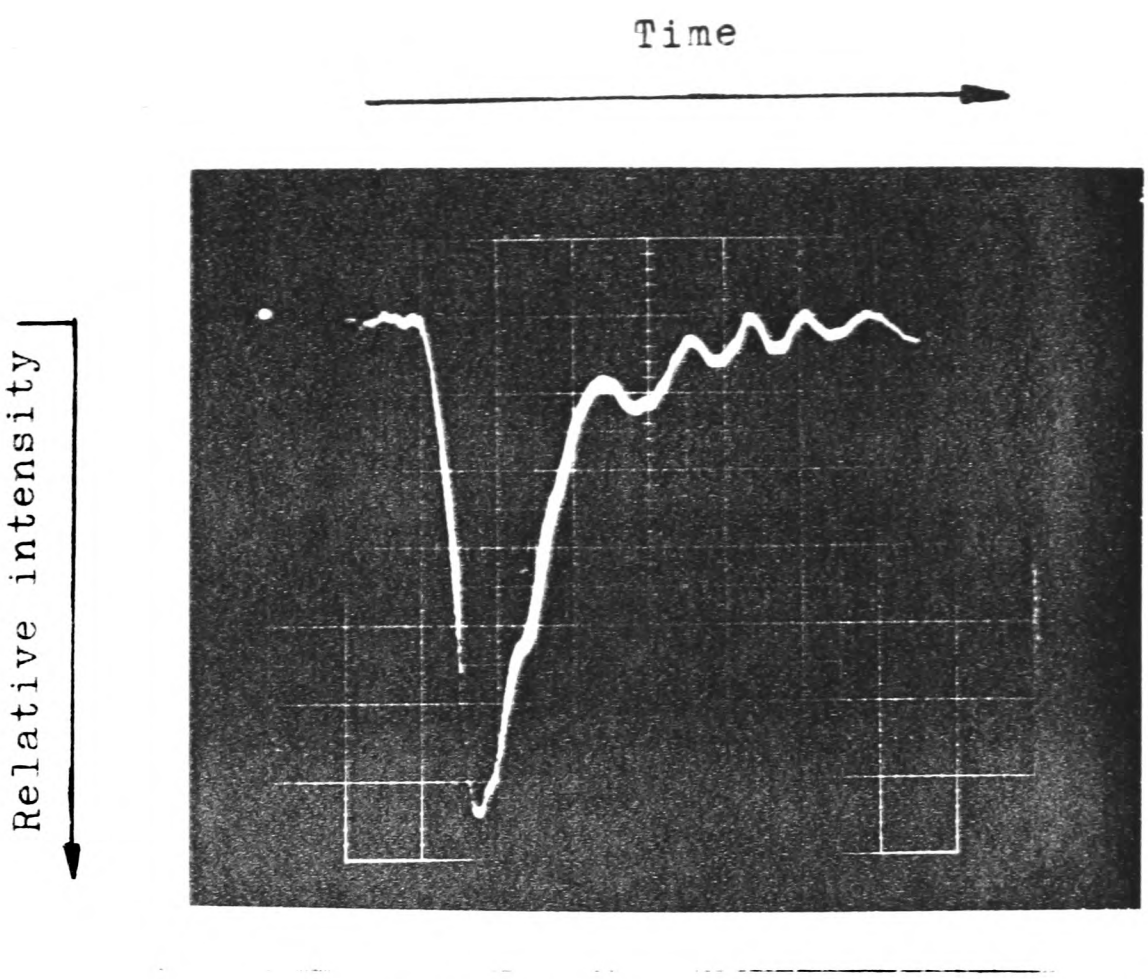


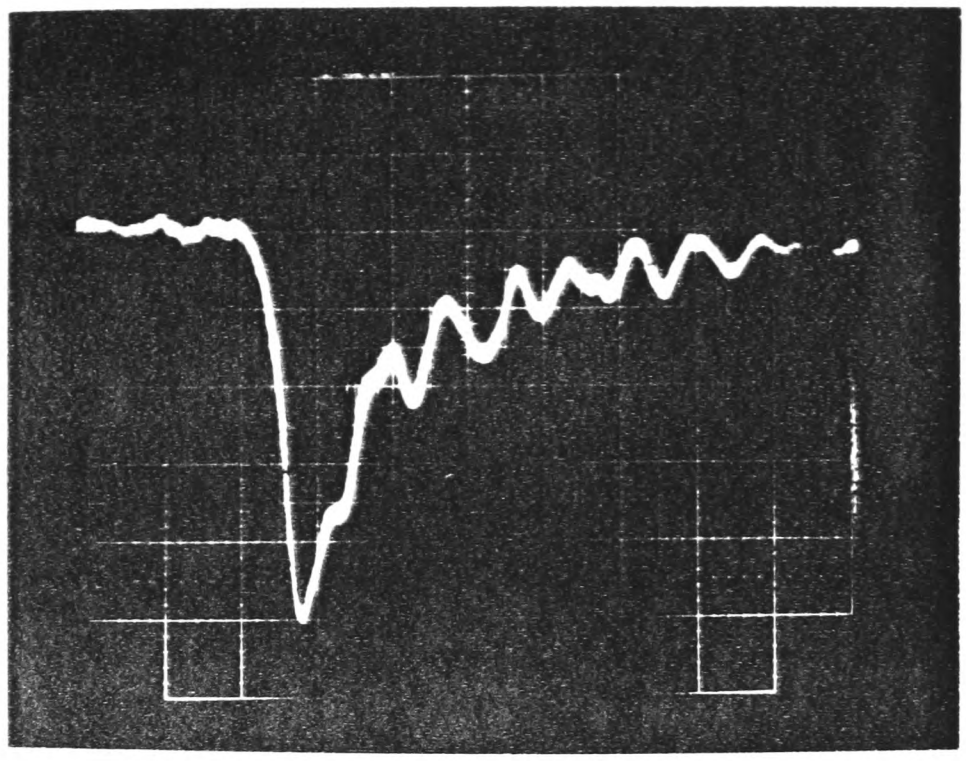
Figure 8.20 Nitrogen 'b'-'X' L.I.F.



Timebase: 50ns/division

Figure 8.21 Emission at 108.3nm showing LIF

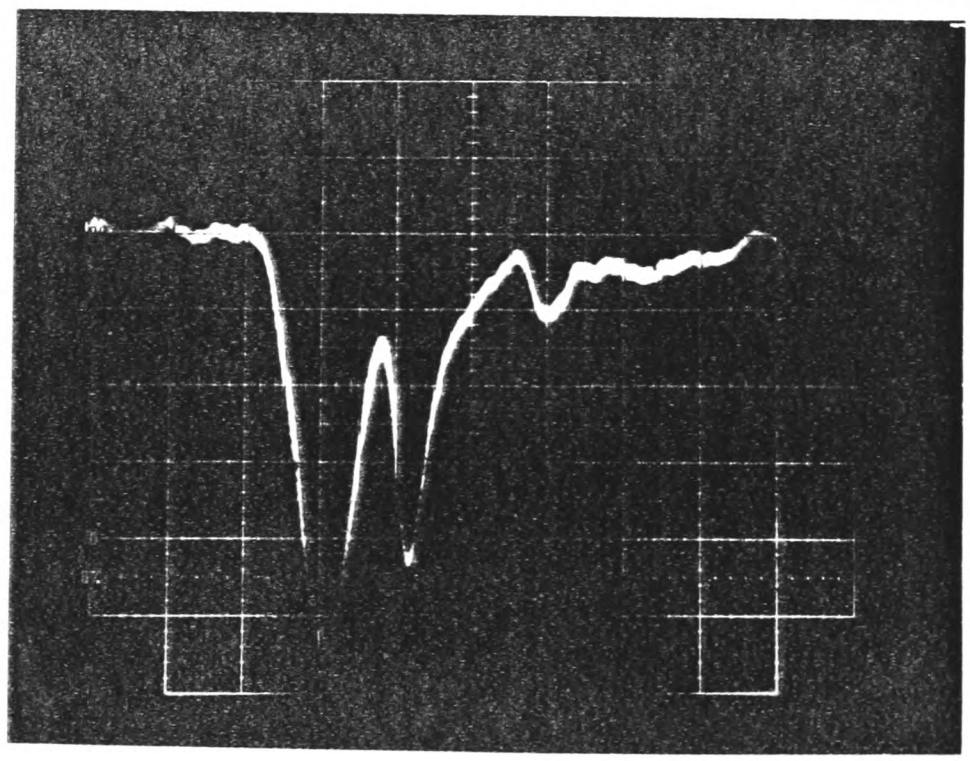
Time



Relative intensity

XeCl laser off (no LIF)

Time



Relative intensity

XeCl laser on (LIF evident)

Timebase: 50ns/division

Figure 8.22 Emission at 125.9nm showing LIF

CHAPTER 9 : POTENTIAL OF PROPOSED VUV LASER

9.1 INTRODUCTION

In the previous chapter the results of the experiments undertaken to investigate the practical realisation of the new VUV laser scheme were given. Those results showed that the basic principles of the scheme could be achieved in practice.

In this chapter those results are discussed in detail. From the intensity of the emissions observed, estimates of the populations in the states of molecular nitrogen of interest are made. From the results of the LIF measurements the population density transferred by the XeCl laser is found. The implications of this population density for the operation of a VUV laser on the proposed scheme are discussed. Further proposals are made for improvements to the experimental apparatus used for this work to facilitate production of such a VUV laser.

9.2 DISCUSSION OF RESULTS

9.2.1 Population of excited molecules due to discharge excitation alone

The method of calculating the density of molecules in emitting states from the intensity recorded by the detection system was discussed in section 8.2.2, and the program used to perform the numerical calculations is in appendix 3. This has been used to find the density of excited molecules in both the $a^1\pi_g$ and $b^1\pi_u$ states for a number of the different discharge configurations used. For the higher pressure discharges (in the cases where the earth return was laid as a foil sheet along the top of the discharge tube) it has been noted that the discharge tended to constrict and run in the part of the tube directly adjacent to the earth plane. This leads to the most luminous part of the discharge lying in the top 4mm only of the

tube. Therefore, in the tables of results two values for the density of excited molecules are given - one of which applies if it is assumed that there is a constant distribution throughout the cross-section of the discharge tube, and the other if the emitting molecules are concentrated into the top 4mm region. Since there is unlikely to be a uniform distribution of concentration throughout any region of the tube, the larger value given will represent an upper limiting value for the number density in the region where the discharge is most luminous. The calculated number density of molecules in each state varies according to the specific transition whose emission provided the data from which the density was calculated. The values are given for each transition. As postulated earlier, for the case of the dc discharge in nitrogen, discrepancies can arise, at least in part due to self-absorption from the vibrationally excited nitrogen electronic ground state. For the emission from the 'b' state the discrepancy could be due to the change in the efficiency of the grating with wavelength in this region. The aluminised grating used was overcoated with magnesium fluoride. The manufacturers only grating efficiency calibration in the region of interest was a single point at 121.6nm corresponding to an efficiency value of 6.6%. However this region is close to the MgF_2 cutoff wavelength of 120nm. Data on the reflection of these dual layer coatings as a function of wavelength in this region (Hunter,1962) show a rapid fall off below 120nm, from about 80% at 120nm to 10% at 100nm. This would explain the fall off in intensity for these short wavelength transitions below values predicted from the transition rates. As the intensity is less, then this would give a reduced value for the number density. If an accurate calibration for the grating was available this could be incorporated into the program calculating the density of states, however in the absence of such a calibration there are variations in the number densities shown. From this argument the value obtained from the $v'=1 - v''=9$ transition at 122.7nm will give the most valid data.

Densities of nitrogen molecules in the $a^1\pi_g$ (v'=0) state

The calculated density of nitrogen molecules in the $a^1\pi_g$ (v'=0) state for various discharge conditions are given in Tables 9.1 to 9.3 below. In these tables the values given for case A are calculated with the assumption that there is an even distribution of molecules throughout the discharge volume. Case B assumes that the excited molecules are confined to the top 4mm region of the discharge tube.

Table 9.1 DC discharge. 80mA 0.3mbar nitrogen

Transition (v'-v")		0-2	0-3	0-4
Population ($x10^7$ cm^{-3})		1.6	2.8	5.3

Table 9.2 Pulsed discharge. 9kV 9mbar nitrogen

Transition (v'-v")		0-2	0-3	0-4
Population ($x10^{12}$ cm^{-3})	A	5.3	5.5	6.0
	B	26	27	29

Table 9.3 Pulsed discharge. 16kV 12mbar nitrogen

Transition (v'-v")		0-2	0-3	0-4
Population ($x10^{11}$ cm^{-3})	A	7.6	6.8	7.1
	B	37	33	35

Densities of nitrogen molecules in the $b^1\pi_u$ (v'=1) state

The calculated density of nitrogen molecules in the $b^1\pi_u$ (v'=1) state for various discharge conditions are given in Tables 9.4 to 9.6 below. All these result were calculated from the emissions of pulsed discharges.

Table 9.4 9kV 5mbar nitrogen

Transition (v'-v")		1-2	1-3
Population ($x10^7$ cm^{-3})	A	6.9	7.9
	B	33	39

Table9.5 15kV 4mbar nitrogen

Transition (v'-v")		1-1	1-2	1-3	1-4	1-5
Population ($x10^8 cm^{-3}$)	A	2.8	2.0	2.4	4.9	14.0
	B	14	10	12	24	68

Table 9.6 15kV 8mbar nitrogen

Transition (v'-v")		1-1	1-2	1-3	1-4	1-5
Population	A	2.3	1.6	1.9	4.0	13.0
($x10^8$ cm^{-3})	B	11	8	9	20	63

9.2.2 Population density of excited molecules transferred by XeCl laser

The values of population of molecules in the excited states due to the action of the "transfer" laser have been calculated from the values of the laser induced fluorescence (LIF) signals by comparing the height of the signal traces recorded when the transfer laser was passing through the nitrogen discharge and when it was not. As with the data presented above there is an apparent variation in the number densities calculated from the different transitions. Again this could be due to the variation of efficiency of the grating which degrades towards shorter wavelength. It was originally thought that the variation might also be due to self absorption arising from unwanted population in the lower vibrational levels of the ground state due to discharge excitation. However attempts to fit the data to a single vibrational temperature did not yield any meaningful results. The calculated number densities are given for different values of t_d, the time delay between the start of the nitrogen discharge and the time of firing the XeCl "transfer" laser (see Tables 9.7 to 9.11). It will be seen that the greatest populations were produced using a time delay, t_d, of 250ns, although the range of variation of "transfer" laser induced populations is only a factor of three between the largest and smallest.

9.2.3 Calculation of gain coefficients for the VUV

With the knowledge of the number densities in the upper level of the proposed VUV laser system it is possible to make an estimate of the expected gain coefficient. This has been based on the assumption that the population in the lower level of the proposed laser transition would be negligible. This assumption is valid for the smallest values of t_d (time delay between start of

discharge excitation and application of "transfer" laser pulse). From the calculations of the population densities the optimum value of this time delay would be about 250ns. At this time the vibrational temperature of the discharge would be low, so that almost all the popualation of the ground state would be in the lowest vibrational levels. Thus the estimates for the gain will be valid for transitions with v" greater than 5. The transitions with v" less than 5 also have the extra inaccuracy of the uncertainty of the correct value of the population in the upper level, as discussed above.

For two states 1 and 2 of equal degeneracy, separated by an energy $h\nu$, the gain coefficient, k_0, at line centre is given by

$$k_0 = \frac{(N_2-N_1)\lambda^2 A_{21} \quad g(\nu_0)}{8\pi} \qquad 9.1$$

where A_{21} is the spontaneous transition rate for the transition, and $g(\nu_0)$ is the value of the lineshape function at line centre. For nitrogen at 10mbar the transition linewidth will be dominated by the Doppler broadening effect. The doppler linewidth for molecular nitrogen at 300K is given by equation 5.7 as

$$\Delta\nu_D = 2.34\text{x}10^{-6}\nu_0 \qquad 9.2$$

The lineshape function for the central frequency of the transition is given by

$$g(\nu_0) = \frac{2(\ln 2)^{1/2}}{\pi^{1/2}\Delta\nu_D} \qquad 9.3$$

Thus combining equations 9.1 to 9.3, the gain coefficient for the BH bands is given by

$$k = 5.34\text{x}10^{-7} \ (N_2-N_1)\lambda^3 A_{21} \qquad 9.4$$

with λ in cm, A_{21} in s^{-1} and the number densities in cm^{-3} to give the gain coefficient in cm^{-1}. Calculated values of the gain coefficient are shown in Tables 9.7 to 9.11. In these calculations the values given by Zipf and Gorman (1980) have been used for the transition probabilities of the (1,v") band of the Birge Hopfield system. The error on the calculated values for the

gain coefficients is estimated to be 25%.

Table 9.7 50ns delay

CASE A

v"	1	2	3	4	5	6	7	8	9	10	11	12	13	14
Density ($\times 10^{9}$ cm^{-3})	1.3	1.9	2.0	5.1	-	-	-	-	-	6.3	-	-	-	-
Gain ($\times 10^{-5}$ cm^{-1})	6.6	10.3	7.4	9.1	-	-	-	-	-	7.5	-	-	-	-

CASE B

v"	1	2	3	4	5	6	7	8	9	10	11	12	13	14
Density ($\times 10^{9}$ cm^{-3})	6.1	8.9	9.3	24.0	-	-	-	-	-	29.6	-	-	-	-
Gain ($\times 10^{-4}$ cm^{-1})	3.1	4.9	3.5	4.3	-	-	-	-	-	3.6	-	-	-	-

Table 9.8 75ns delay

CASE A

v"	1	2	3	4	5	6	7	8	9	10	11	12	13	14
Density ($\times 10^{9}$ cm^{-3})	-	0.4	0.7	1.3	2.5	-	-	3.0	2.7	3.2	3.6	4.2	6.2	4.1
Gain ($\times 10^{-5}$ cm^{-1})	-	2.0	2.6	2.4	1.1	-	-	1.9	2.8	3.9	4.1	3.7	3.8	1.5

CASE B

v"	1	2	3	4	5	6	7	8	9	10	11	12	13	14
Density ($\times 10^{10}$ cm^{-3})	-	0.2	0.3	0.6	1.2	-	-	1.4	1.3	1.5	1.7	2.0	2.9	2.0
Gain ($\times 10^{-4}$ cm^{-1})	-	0.9	1.2	1.1	0.5	-	-	0.9	1.3	1.8	1.9	1.7	1.8	0.7

Table 9.9 250ns delay (1)

CASE A

v"	1	2	3	4	5	6	7	8	9	10	11	12	13	14
Density ($\times 10^{9}$ cm^{-3})	0.2	0.3	0.7	1.9	4.0	-	-	8.8	6.7	8.0	8.9	9.7	9.9	10.5
Gain ($\times 10^{-5}$ cm^{-1})	0.9	1.6	2.6	3.4	1.9	-	-	5.7	7.0	9.6	9.9	8.6	6.1	3.9

CASE B

v"	1	2	3	4	5	6	7	8	9	10	11	12	13	14
Density ($\times 10^{10}$ cm^{-3})	0.1	0.1	0.3	0.9	1.9	-	-	4.2	3.1	3.8	4.2	4.6	4.7	5.0
Gain ($\times 10^{-4}$ cm^{-1})	0.4	0.8	1.2	1.6	0.9	-	-	2.7	3.3	4.6	4.7	4.1	2.9	1.9

Table 9.10 250ns delay (2)

CASE A

v"	1	2	3	4	5	6	7	8	9	10	11	12	13	14
Density ($x10^{9}cm^{-3}$)	0.2	0.3	1.0	1.8	4.0	-	-	2.7	7.2	9.7	8.7	9.5	12.6	13.3
Gain ($x10^{-5}cm^{-1}$)	0.8	1.9	3.6	3.3	1.9	-	-	1.7	7.5	11.7	9.8	8.4	7.7	5.0

CASE B

v"	1	2	3	4	5	6	7	8	9	10	11	12	13	14
Density ($x10^{10}cm^{-3}$)	0.1	0.2	0.5	0.9	1.9	-	-	1.3	3.4	4.6	4.1	4.5	5.9	6.3
Gain ($x10^{-4}cm^{-1}$)	0.4	0.9	1.7	1.6	0.9	-	-	0.8	3.6	5.6	4.6	4.0	3.6	2.3

Table 9.11 350ns delay

CASE A

v"	1	2	3	4	5	6	7	8	9	10	11	12	13	14
Density ($x10^{9}cm^{-3}$)	0.1	0.2	0.3	1.2	2.7	-	-	3.8	3.9	4.2	4.8	4.6	5.6	6.6
Gain ($x10^{-5}cm^{-1}$)	0.5	1.1	1.3	2.2	1.2	-	-	2.4	4.1	5.0	5.3	4.0	3.4	2.5

CASE B

v"	1	2	3	4	5	6	7	8	9	10	11	12	13	14
Density ($x10^{10}cm^{-3}$)	0.0	0.1	0.2	0.6	1.3	-	-	1.8	1.8	2.0	2.2	2.2	2.6	3.1
Gain ($x10^{-4}cm^{-1}$)	0.3	0.5	0.6	1.0	0.6	-	-	1.2	1.9	2.4	2.5	1.9	1.6	1.2

9.3 APPRAISAL OF PROPOSED NEW LASER SYSTEM

The values for the gain coefficients calculated above allow the performance of the proposed new laser system to be estimated. There are uncertainties in the values of gain given due to deviations in the calculated number density of the 'b' states arising from an incomplete knowledge of the emitting volume and the anomalous intensity distribution for the short wavelength components, possibly due to a change in grating efficiency. However an estimate can be made as to whether this system could be made to undergo laser oscillation.

The calculated values of the gain have maximum values of $4x10^{-4}$ cm^{-1}. This is assuming that the laser interaction with the nitrogen discharge is mainly concentrated in the top 4mm of the discharge tube where it is most luminous.

9.3.1 Steady state conditions for laser oscillation

For laser oscillation the threshold condition is that the round trip gain in the cavity must equal the round trip losses. Working in the low gain and unsaturated regime this condition can be expressed as

$$1 - R_1R_2 = 2kl \qquad 9.5$$

where R_1 and R_2 are the mirror reflectivities and l is the gain length of the laser.

Mirrors for use in the VUV region have been discussed in chapter 1. High reflectivities are difficult to obtain because of the lack of suitable materials. A good Al/MgF_2 mirror as the rear cavity mirror might have a reflectivity as high as 90%. A suitable output coupler, having a low absorption transmission and yet a high reflectivity, would not be easily obtainable. A multilayer dielectric coating on a lithium fluoride substrate would have to be used. For the purposes of the discussion it will be assumed that such an optic, with a reflectivity of 80%, can be used in the cavity.

Thus the threshold condition for oscillation becomes, in this case,

$$k\,l = 0.14. \qquad 9.6$$

If the cavity length is made 100cm, not an unreasonably long value, then a value for k of

$$k = 1.4\text{x}10^{-3}\ \text{cm}^{-1},$$

is needed. This value is about three times greater than the gain values calculated for the system used in this work. This simplistic calculation would seem to indicate that the possibility of laser action on this system should be achievable with a relatively small increase in the pumping efficiency of the transfer laser.

9.3.2 Dynamic conditions for laser oscillation

However, the above calculation assumes that there are steady state conditions prevailing, and that the laser oscillations have an infinite time

to build up. For the system under consideration in this case the maximum time for which there can be gain is only the time the "transfer" laser pulse is interacting with the discharge excited nitrogen. The limited time for which there is gain means that the laser pulse must build up from noise in a restricted time. This in turn implies that there must be a faster rate of growth of the laser radiation, and thus a larger gain. These effects are taken into consideration in the following calculation.

Consider the gain medium as a cylinder of area S and length l, in a cavity length L (see figure 9.1). The spontaneous radiation reaching one end mirror from the excited volume which will be the initiating radiation for the laser will be that fraction of the radiation which is emitted by the volume into the solid angle subtended by the other mirror at that mirror (i.e. S/L^2). If the number density of emitting species is N, and the spontaneous transition rate is A then the number of photons, n, reaching the mirror per second from the volume (V=lS), into the specified solid angle, is given by

$$n = NAS1S \;/\; 4\pi L^2. \qquad 9.7$$

The spontaneous intensity at the mirror is then given by

$$I_0 = \frac{NAS1h\nu}{4\pi L^2} \qquad 9.8$$

where h is Plancks constant and ν is the frequency of the emitted radiation. This radiation will then be reflected back through the gain medium and will experience an exponential growth, with a gain coefficient, k, as given by 9.4. The reflectivity of the cavity mirrors will introduce a loss of intensity in each pass. Let the two mirror reflectivities be R_1 and R_2, then after m round trips through the medium the stimulated intensity will be

$$I_m = I_0(R_1R_2)^m \exp(2mkl). \qquad 9.9$$

For a laser the circulating intensity will need to be of the order of the transition's saturation intensity, I_s given by

$$I_s = h\nu/\sigma\tau \qquad 9.10$$

where τ is the upper level lifetime and σ is the cross section for stimulated

emission given by

$$k = (N_2-N_1)\sigma \qquad 9.11$$

which implies from equation 9.4 that

$$\sigma = 5.34x10^{-7}\lambda^3 A_{21} \qquad 9.12$$

As the circulating intensity approaches saturation its growth is no longer exponential with distance: it experiences a linear growth rate. For the purposes of this calculation this change of growth rate will be ignored as it will only be significant for the last few passes through the gain medium.

Setting $I_m=I_s$ gives

$$I_s/I_0 = (R_1R_2)^m exp(2mkl) \qquad 9.13$$

which by taking logarithms of both sides becomes

$$ln(I_s/I_0)-m(R_1R_2) = 2mkl \qquad 9.14$$

The time taken for the circulating intensity to reach I_s is given by

$$t = 2mL/c \qquad 9.15$$

During all of this time there must be an inversion maintained by the excitation mechanism.

Using the values for transition rates for the BH bands given by Zipf and Gorman (1980) the stimulated cross section for the v'=1 to v"=10 transition is calcualted as $\sigma = 1.2x10^{-14} cm^2$, which gives the saturation intensity as $50kWcm^{-2}$, with the upper level lifetime of 2.4ns.

The upper level populations measured were approximately $4x10^{10} cm^{-3}$. From the steady state calculation above it was seen that the experimentally achieved populations would not give rise to any laser action. Indeed they would need to be increased by a factor of 3 just to reach the steady state threshold condition that the round trip gain equals the round trip loss. If it is assumed that it would be possible to increase the transfer efficiency such that most of the population produced in the 'a' state was transferred into the 'b' state by the interaction of the XeCl laser, this would produce an increase of the population in the 'b' state of more than twenty times that measured in this work.

Using the conditions applied above (i.e. l=L=100cm, R_1=90% and R_2=80%) and a mode volume diameter of 10mm, with $N=8x10^{11}cm^{-3}$, I_0 is calculated as

$$I_0 = 0.011\ Wcm^{-2}$$

and the gain coefficient k as

$$k = 9.6x10^{-3}\ cm^{-1}.$$

The product 2kl then has a value of

$$2kl = 1.92.$$

The number of round trips, m_s, for the circulating intensity to build up to saturation can be found by rearranging equation 9.13 to give

$$m = \frac{\ln(I_s/I_0),}{(2kl + \ln(R_1R_2)} \qquad 9.16$$

and then inserting the relevant values. A value for the number of round trips, m_s of

$$m_s = 9.7$$

is then obtained. These 10 round trips to reach saturation would take 67ns.

Due to the long lifetime of the lower laser level of the proposed system, a laser operating on this scheme would belong to the class of self-terminating lasers. As discussed in chapter 1 the maximum time for which it is possible to maintain a population inversion in these cases is of the order of $(A_{ki})^{-1}$. In the case of the v'=1 to v"= 10 transition this maximum time is 88ns, as the spontaneous transition rate for the v'=1 to v"=10 transition is $1.13x10^7s^{-1}$ (Zipf and Gorman 1980). Therefore it might be possible to maintain an inversion for sufficient time for the ten round trips required to let the VUV radiation build up to its saturation intensity. However there is then a requirement for the XeCl laser to have a pulse length of 70ns, whereas typically discharge-excited XeCl lasers have pulse lengths of 20ns.

9.3.3 Considerations of laser pulse energy

A further consideration is the energy contained in the VUV laser pulse

from the proposed laser system. If it is assumed that every molecule in the 'b' state contributes to the laser pulse then an estimate can be made of the pulse energy. With an active volume of length 100cm and diameter 1cm and a population in the 'b' state of $8x10^{11}cm^{-3}$ there will be $6.3x10^{13}$ molecules contributing one photon each to each pulse. For the v'=1 to v"=10 transition at 125.9nm the photon energy is $1.58x10^{-18}J$ (9.8eV). Thus the energy per pulse would be 0.1mJ. This is small, but would make the laser an interesting proposition. If however the area of the VUV gain region were increased from 1cm diameter to 5cm diameter then the laser pulse energy, E_p would be

$$E_p = 2.5mJ.$$

This is then a reasonable value for a VUV laser, and compares favourably with reported values for the molecular hydrogen laser operating on the Werner bands at comparable wavelengths. However the demands on the "transfer" laser are now rather large.

9.3.4 General considerations

Alterations to the design of the system which might enable the lasing condition to be reached are discussed in the next section.

From the gain values calculated, it would be expected that laser action would first be achieved on transitions from v'=1 to v"=10 and 11. However if the lowering of the expected intensity for the transitions to low vibrational levels is due to a wavelength dependence of the detection system, then it would be expected that transitions to v"=2,3,4 might also oscillate.

The experimental results presented in this chapter apply to values of t_d of the order of 100ns. The populations transferred to the 'b' state by the XeCl laser do not depend critically on this delay. A delay of 250ns produced the largest populations in the 'b' state in the experiments performed. This delay gave a LIF signal at a time when the background radiation due to the discharge excited 'b' states had decayed substantially, and yet the population

in the 'a' state was still at densities of about 10^{11} cm^{-3}.

9.4 PROPOSED IMPROVEMENTS TO PRODUCE LASER ACTION

9.4.1 Potential for scaling to larger volumes and gain lengths

From the results presented above it is seen that at present the expected gain coefficient for this laser would be very small. However the laser has excellent prospects for scaling to larger devices to increase the pulse energy.

The potential for volume scaling of the laser compares well to the case of the hydrogen Lyman band laser excited by a discharge from a Blumlein circuit. It was shown in chapter 2 that, because of the high excitation current densities needed to effectively pump the molecular hydrogen laser its optimum performance was obtained for a very narrow discharge channel. The discharge could not be made wide as a way to increase the discharge volume because of the need for a very fast rising edge to the current excitation pulse, necessitating low inductance discharge circuits.

In the present proposed system the fast excitation pulse has been decoupled from the discharge by use of the XeCl transfer laser. It has been seen that the population of the intermediate 'a' state can take place in a period of a few hundred nanoseconds. By controlling the delay between the onset of the nitrogen discharge and the XeCl laser pulse the population can be transferred to the upper level at the time when the maximum population difference on the proposed laser transitions will be obtained. The lifetime of the 'b' state is short, about 2.4ns, so the LIF occurs coincident with the XeCl laser emission.

As there is no necessity for the initial discharge in nitrogen to have a short rise time, then there is no restriction on the size of the tube which can be made as large as is practical. In particular a long discharge tube could be fabricated. This would give the long gain length needed for laser

action due to the low gain coefficient. Further with the long absorption path length a greater proportion of the radiation from the XeCl laser could usefully be absorbed.

It will be noticed from the results presented above that the populations produced in the 'b' state by the transfer laser are of the order of $10^{10}cm^{-3}$. This is over a volume of interaction with the XeCl laser pulse of about $2.7cm^3$. Thus $2.7x10^{10}$ of the XeCl laser photons will have been absorbed. Now in the laser pulse of 20mJ at 308nm there are $3x10^{16}$ photons. Therefore only 10^{-6} of the photons from the transfer laser are actually contributing to the population in the 'b' state.

To enhance the absorption of the "transfer" laser radiation in order to utilise a greater fraction of the photons the "transfer" laser pulse should be multipassed through the discharge cell by reflecting it back into the cell at the end of each pass. Multipassing the XeCl pulse through the nitrogen cell would increase the time for which there would transfer of population from the 'a' state to the 'b' state. Increasing the length of time for which population was pumped into the upper laser level in this manner would enable the population to be maintained in the upper laser level for the time required for the VUV laser pulse to build up, as discussed in the last section. As calculated the pumping time would need to be increased to about 70ns. This would mean passing a typical discharge excited XeCl laser pulse through the cell approximately four times. As high reflectivity mirrors, for use with 308nm radiation, are readily obtainable, the XeCl laser pulse could be multipassed through the nitrogen cell with low losses.

9.4.2 Considerations of gas pressure

In the later stages of this work LIF was produced with a high intensity from higher pressure discharges than at first. Pressures of up to 15mbar were used and it is not thought that the maximum values consistent with the production of the 'b' states were used. If further work were undertaken

using the higher pressure discharges, along with the short delays between the firing of the discharge and the transfer laser, then it seems virtually certain that larger densities could be produced in the nitrogen ^{a}'b' state.

Initially the evidence seemed to indicate that population in the intermediate states could only be produced in a flowing gas discharge. It was later found that these states could also be produced by discharges in static gas fills because strong LIF can be observed from static gas fills. The gas purification techniques developed earlier on in this work could be used to extend the lifetimes of these static fills.

9.5 CONCLUDING REMARKS

This work has investigated the current state-of-the-art in discharge excited VUV lasers from both theoretical and practical perspectives. Aspects and problems peculiar to the production and detection of VUV radiation from a new system in nitrogen have been discussed. The main conclusion to be drawn from these studies is the need to keep any impurities within the discharge to extremely low levels.

Development of the fluorine VUV discharge excited laser was undertaken. By use of a cryogenic trap the useful lifetime of a gas fill was extended beyond the one hour timescale, thus increasing the usefulness of the laser in practical situations. The laser produced a greater pulse energy (50mJ) than previously reported for any discharge pumped fluorine device. Ways of further increasing this energy have been discussed.

The major part of this work concered with the proposed new laser system in molecular nitrogen. This system has been discussed fully from a theoretical viewpoint and investigated experimentally.

In the course of the practical investigation a XeCl laser was used to transfer population from the discharge excited $a^1\Pi_g$ state of nitrogen to the $b^1\Pi_u$ state from which the laser induced fluorescence was observed. At the

time it was performed, this experiment represented the shortest wavelength at which LIF has been observed from excited species, and also the shortest wavelength LIF involving single photon excitation.

The practical work undertaken has shown the possibility of achieving conditions under which laser action would be obtained. This would involve increasing the population in the upper laser level, transferred by the XeCl laser, by a factor of more than 10 times that achieved in this work. However the principle for a new laser system has been demonstrated. The expected pulse energies from such a laser system would be quite small. However, it has been shown that they could compare favourably with existing VUV lasers and should be of the order of a few millijoules: large enough to be of interest.

It is hoped that the future of VUV lasers in photolithography, photochemical and other applications will perhaps be enhanced by this work.

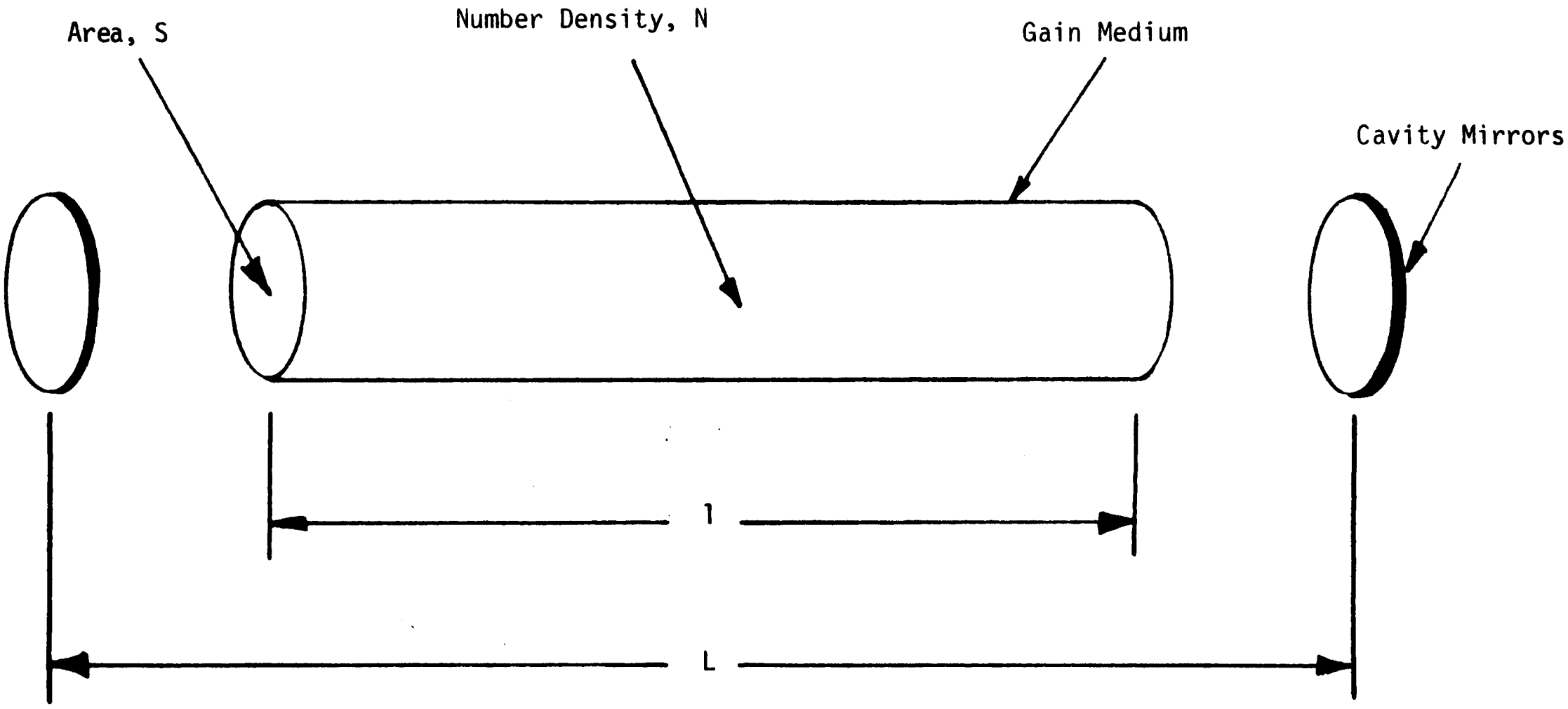


Figure 9.1 System used for gain calculation

APPENDIX 1 : HIGH VOLTAGE RAPID DISCHARGE CIRCUITS AND SWITCHES

A1.1 CAPACITOR TRANSFER CIRCUIT

A capacitor transfer circuit is shown in figure A1.1. A discharge circuit of this type was used to provide the fast excitation pulse for the molecular fluorine and xenon chloride lasers. Its mode of operation is as follows. The main energy storage capacitor, C_s, is charged to the applied voltage, V_h, via R_1 and R_2. R_2 is much less than R_1 so that point B is at a low voltage. R_2 determines the charging time. When C_s is fully charged the switch, S, is closed and point A is earthed. R_2 is large enough that no appreciable current flows through it from C_s, and the potential difference across C_s appears across the discharge gap, D, and the peaking capacitor, C_p. This is pulse charged with a characteristic time of $((L_1+L_s)C_sC_p/(C_s+C_p))$, and would achieve a peak voltage on it of $2V_hC_s/(C_s+C_p)$ if the main discharge gap did not break down. In normal usage the main gap is adjusted to break down before this peak voltage is reached, and the two capacitors discharge through it. In the case of low circuit resistances the curents through the two capacitors would oscillate with different periods given by,

$$T_1 = 2\pi(C_p(L_d+L_2))^{1/2} \qquad \text{A1.1}$$

and

$$T_2 = 2\pi(C_s(L_s+L_d+L_1+L_2))^{1/2}. \qquad \text{A1.2}$$

An important parameter for a laser discharge circuit is the current rise time. This is not easy to calculate analytically for this type of circuit, especially as the resistance of the discharge, R_d, changes with time. In the initial few nanoseconds after the gap breaksdown R_d falls rapidly to about 0.5Ω, when it remains appoximately constant. It can be shown (Sakurai, 1985) by numerical calculation, that the current rise time in this situation is from $T_1/3$ to $T_1/2$. The peak current depends on the value of the capacitors and

almost linearly on the applied voltage. The ratio of the capacitance of the storage to peaking capacitors governs the ratio between the peak magnitudes of the first and second oscillations of the current. A ratio of between two and six is found to be best in practice.

As is evident, the current rise time depends only on T_1, the period governing the discharge of the peaking capacitor. If this capacitor were not present the discharge would only come from the main storage capacitor and the rise time would be much longer due to the higher inductance of this discharge circuit, including that of the switch, the capacitor itself, the circuit connections and feedthroughs into the laser gas envelope. Using the peaking capacitors the inductance of the loop governing the ciurrent rise time can be very much reduced. The capacitors can be placed right alongside the discharge giving a very small discharge loop area, and inductance. The peaking capacitor can consist of a bank of small fast capacitors in parallel to further reduce the inductance.

A1.2 LC INVERTER

This circuit is shown in figure A1.2. The storage capacitors C_1 and C_2 are charged up from the high voltage supply via R_1, with R_2 enabling C_2 to be charged. When the switch, S, is closed the charge on C_1 flows through L_1, and eventually the polarity of C_1 is reversed, so that $2V_h$ appears across the discharge gap, D. In practice the discharge gap will break down before the full voltage appears across it, and then both capacitors will discharge through D and L_2. To give a fast discharge L_2 needs to be kept at a low value.

A1.3 BLUMLEIN CIRCUIT

This circuit is similar to the LC inverter, except that the lumped

storage capacitors are replaced by distributed capacitors as transmission lines (see figure A1.3). The lines are charged as in the LC inverter circuit. When the switch is closed a voltage pulse propagates down line 1 to the discontinuity, represented by the discharge channel, across which $2V_h$ appears. The gap then breaks down and the lines discharge through it. For the circuit to function as a transmission line the current rise time through the switch, given by L_s/Z_1, must be less than the two way transit time of the line. The impedance of the transmission lines is generally less than 1Ω to match the lines to the discharge impedance. This means that the inductance of the switch must be kept to a few nanohenries to give a sufficiently steep leading edge to the voltage pulse.

Shipman (1967) proposed a modification of the Blumlein circuit in which the voltage pulse is made to travel from one end of the discharge channel to the other at the velocity of light in the medium. This gives an almost unidirectional laser output for high gain systems which operate superradiantly. The excitation pulse starting from one end will cause some spontaneous emission. As excitation pulse travels down the channel, at the same speed as the light, the inverted population is immediately stimulated to emit by the light pulse, before it has been able to decay spontaneously. This travelling excitation pulse can be formed by using an angled transmission line, or by sequntially closing a number of switches placed along the edge of the line parallel to the discharge gap (see figure A1.4). Kirkland et al (1981) measured the velocity of propagation of the excitation pulse along the discharge channel of a low pressure hydrogen laser as 2.52×10^8 m/s.

A1.4 MARX BANK

A Marx bank is a multistage circuit capable of producing high voltage (up to 1MV) pulses from standard voltage sources of up to 100kV. The N capacitors are charged in parallel through the resistor chains (see figure

A1.5). The switches, S_n, are then closed simultaneously and the capacitors stacked in series to give N x V_h across the discharge gap, D. The speed of the final discharge can be increased by using the Marx bank to pulse charge another peaking capacitor stage through a self closing switch. A problem with this circuit is that of ensuring that all the stages switches are closed at the same time.

A1.5 TRIGGERED SPARK GAP

The construction of a standard spark gap is shown in figure A1.6. The spark gap is operated by applying a pulse to the trigger pin, of opposite polarity to that on the high voltage electrode. The gap between the high voltage electrode and the trigger pin then breaks-down and an arc is formed. The current path rapidly changes now to connect the H.V. electrode to earth. The operation is strongly dependant on the polarity applied to the trigger. If this is the same as that of the H.V. electrode, the gap between the pin and earth breaks-down and the main gap only closes due to being preionised by the spark. This leads to a less stable operation and reduced operating v oltage range. Low jitter operation can be achieved by adjusting the pressure in the spark gap so that for the applied voltage it is close to the self breakdown condition. The gap then very readily breaks down with the application of the trigger pulse. These switches can be used for operation at up to 100 pulses per second.

A1.6 SOLID DIELECTRIC SWITCH

Solid dielectric of switches can give extremely fast current rise times and low inductances. They consist of two foil electrodes separated by a thin insulating foil, just sufficient to give the required dc voltage hold-off. The switch is initiated by driving a pointed metal pin through the

top electrode and into the dielectric. As it approaches the other electode a very high electric field forms at its point. This causes the dielectric to breakdown and a plasma channel forms through which the current flows.

Although these switches give very low inductance they are limited in use due to their low repetition rate, determined by how quickly the ruptured dielectric can be replaced. This is at best about one shot every 20 seconds.

A1.7 RAIL GAPS

Rail gaps are similar to the spark gap in that they operate by the break down of a gas gap. The spark gap has a single discharge channel. However the rail gap will have multiple channels, if it can be arranged that before the voltage falls across the electrodes due to the formation of the first spark a number of other channels will form. The electrodes, which in this case consist of metal bars, must be held accurately parallel to ensure multichannel operation of the switch. As the inductance of each channel will appear in parallel the inductance of the switch as a whole can be reduced.

Rail gaps can be operated as self-closing switches by applying a high voltage pulse to one electrode, and are often used to speed up the final discharge loop of a fast discharge circuit. Another variation, with improved triggering jitter is to preionise the rail gap by passing UV radiation from a laser along the length of the channel.

Problems can be encountered in trying to ensure that the gap breaks down in multiple channels, which necessitates careful constructional techniques.

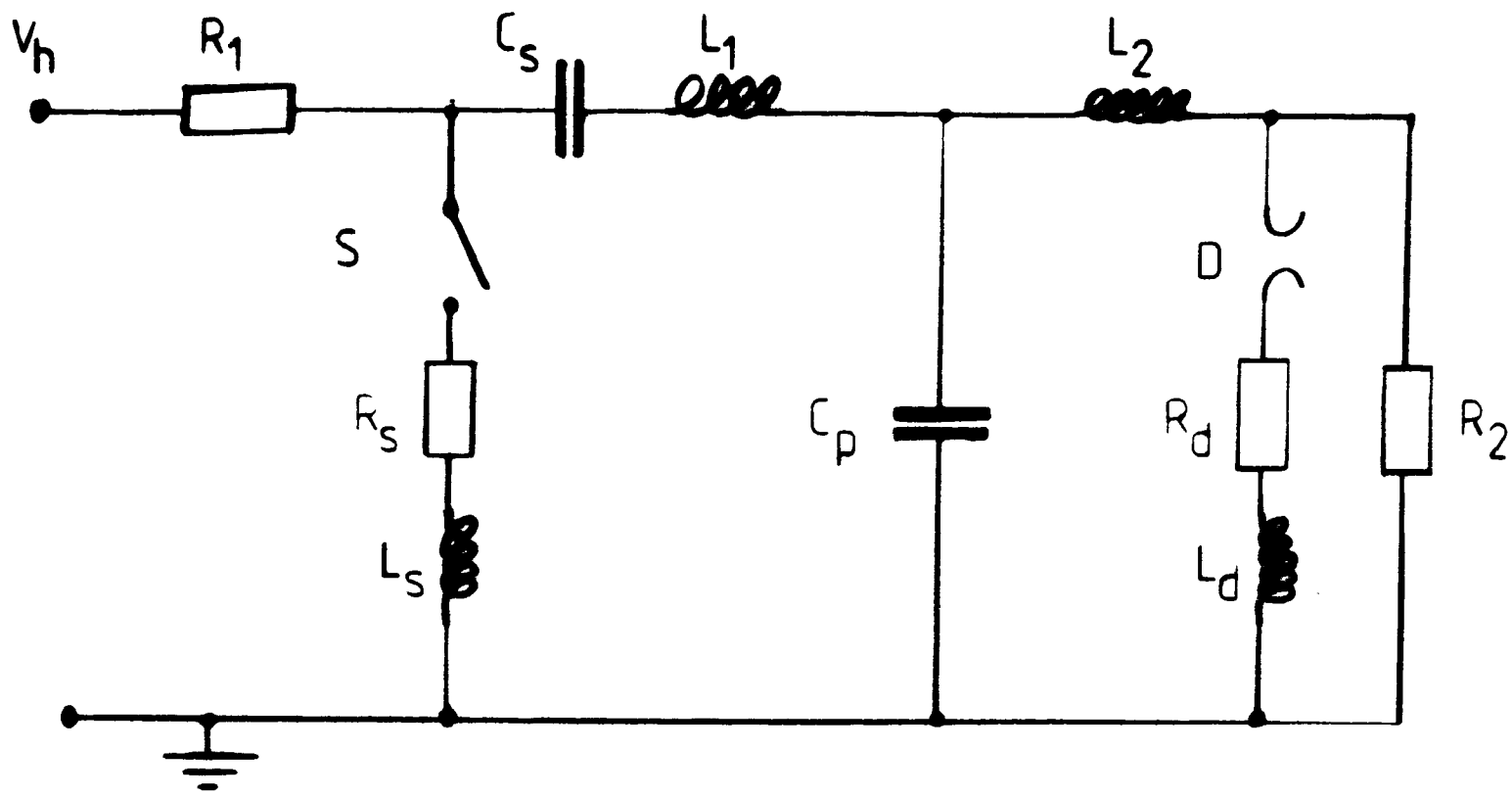


Figure A1.1 Capacitor transfer circuit

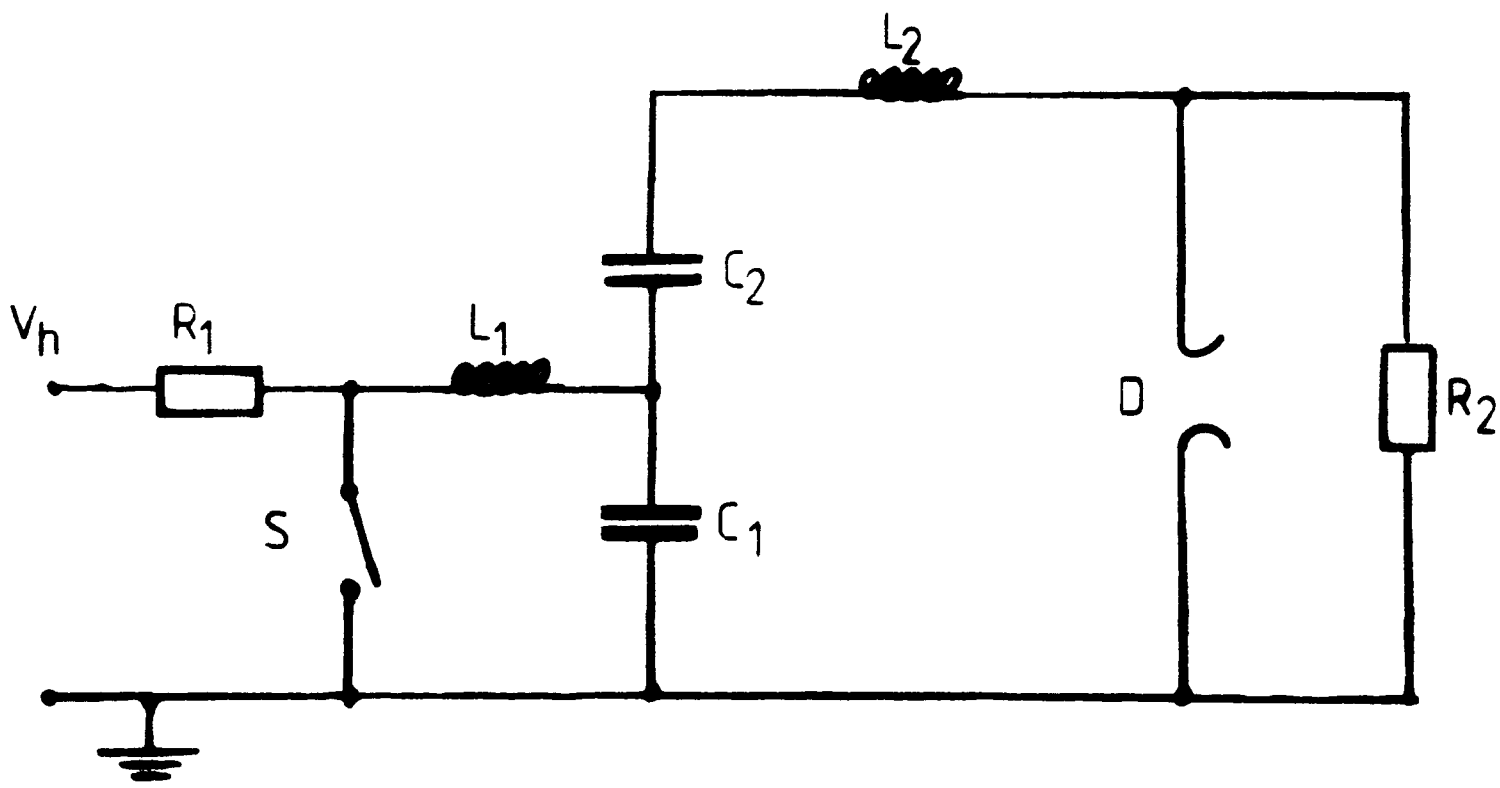


Figure A1.2 LC inverter circuit

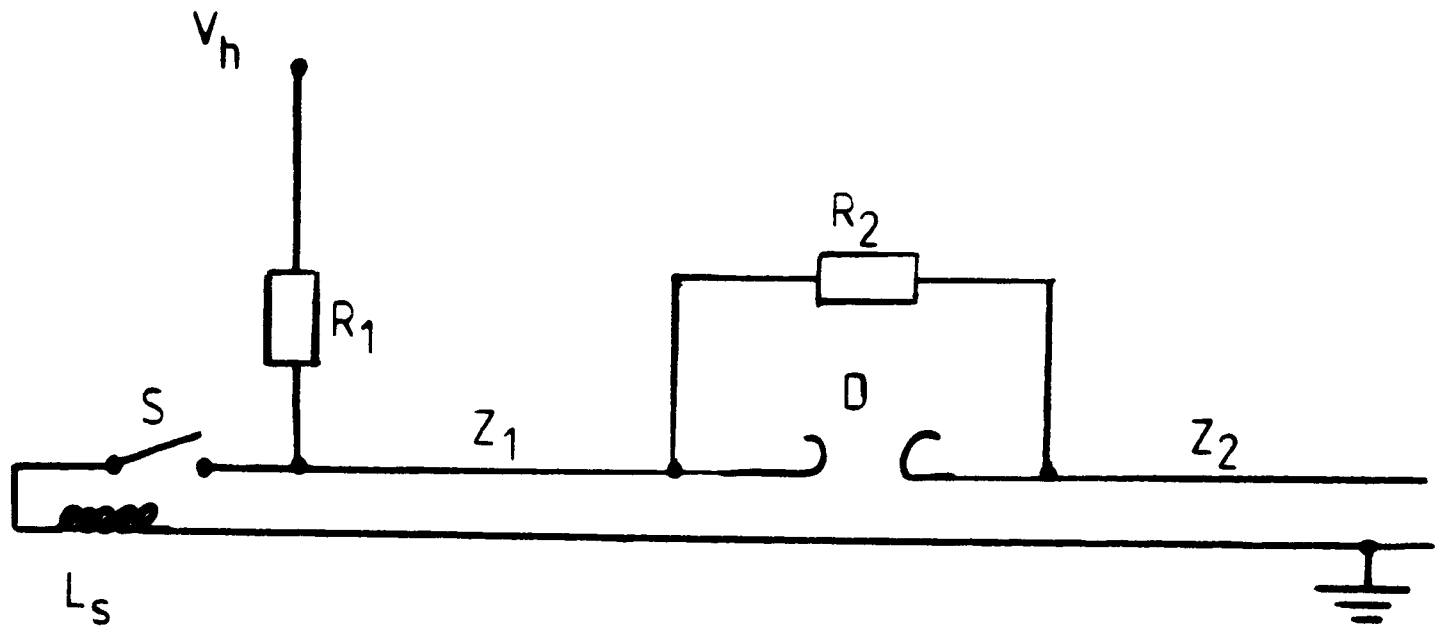


Figure A1.3 Blumlein circuit

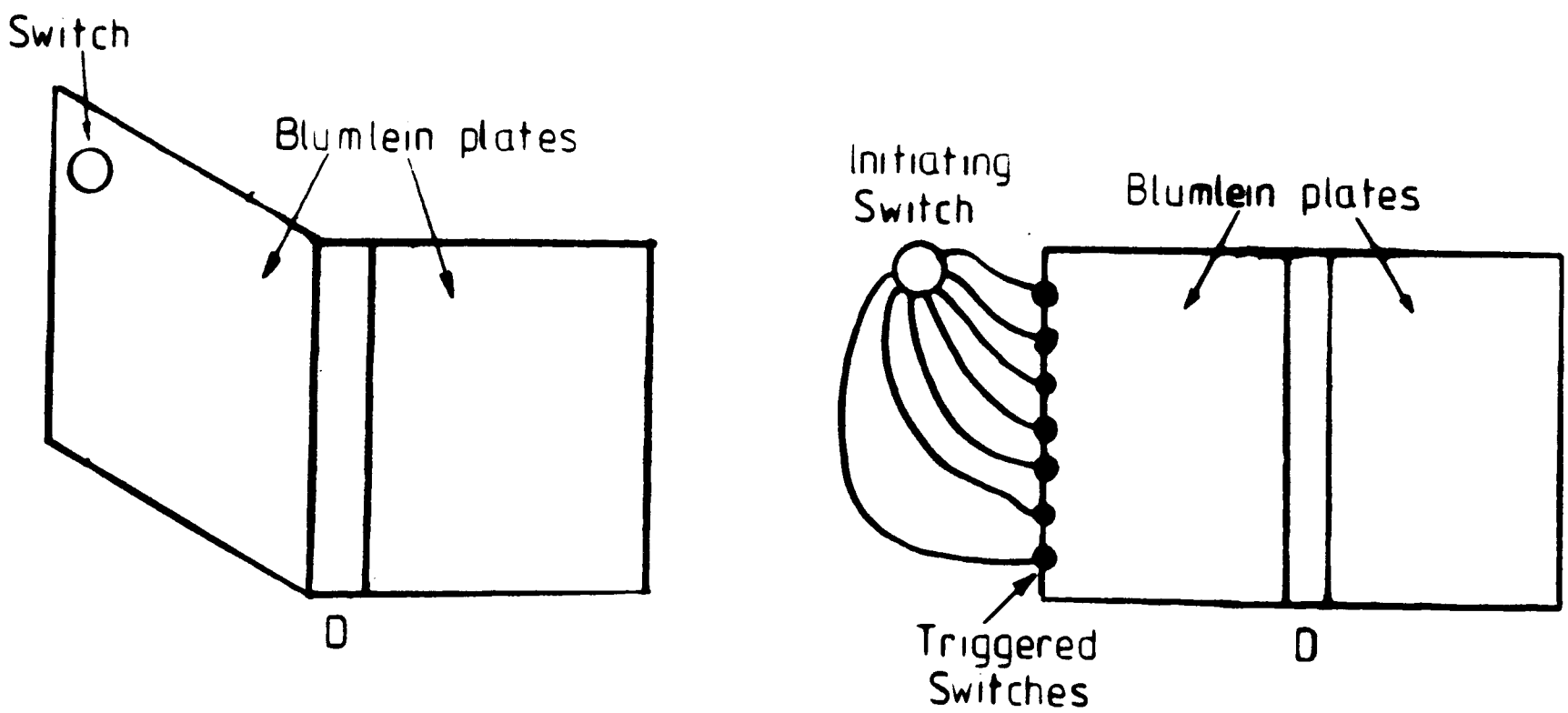


Figure A1.4 Travelling wave Blumlein circuits

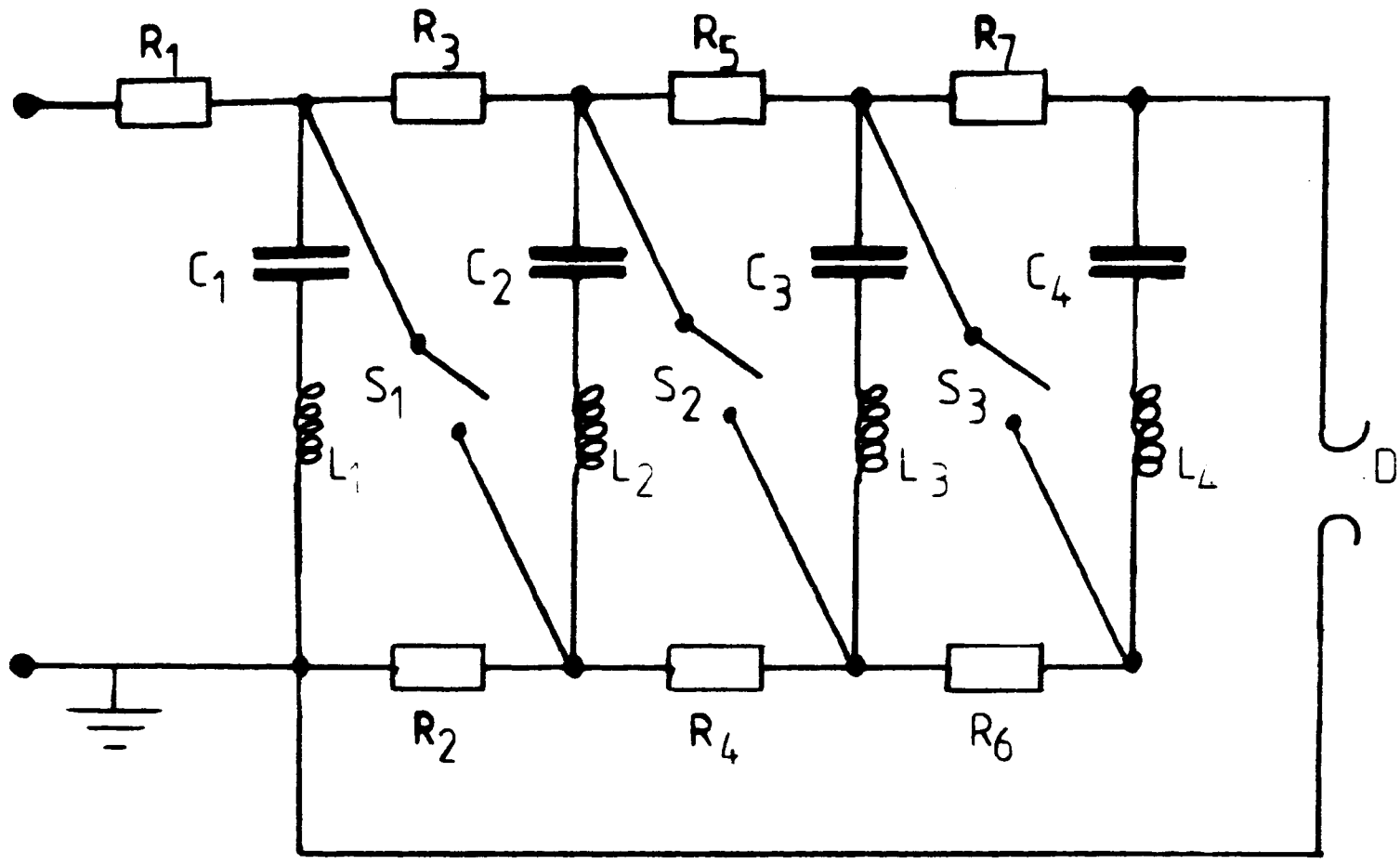


Figure A1.5 Marx bank

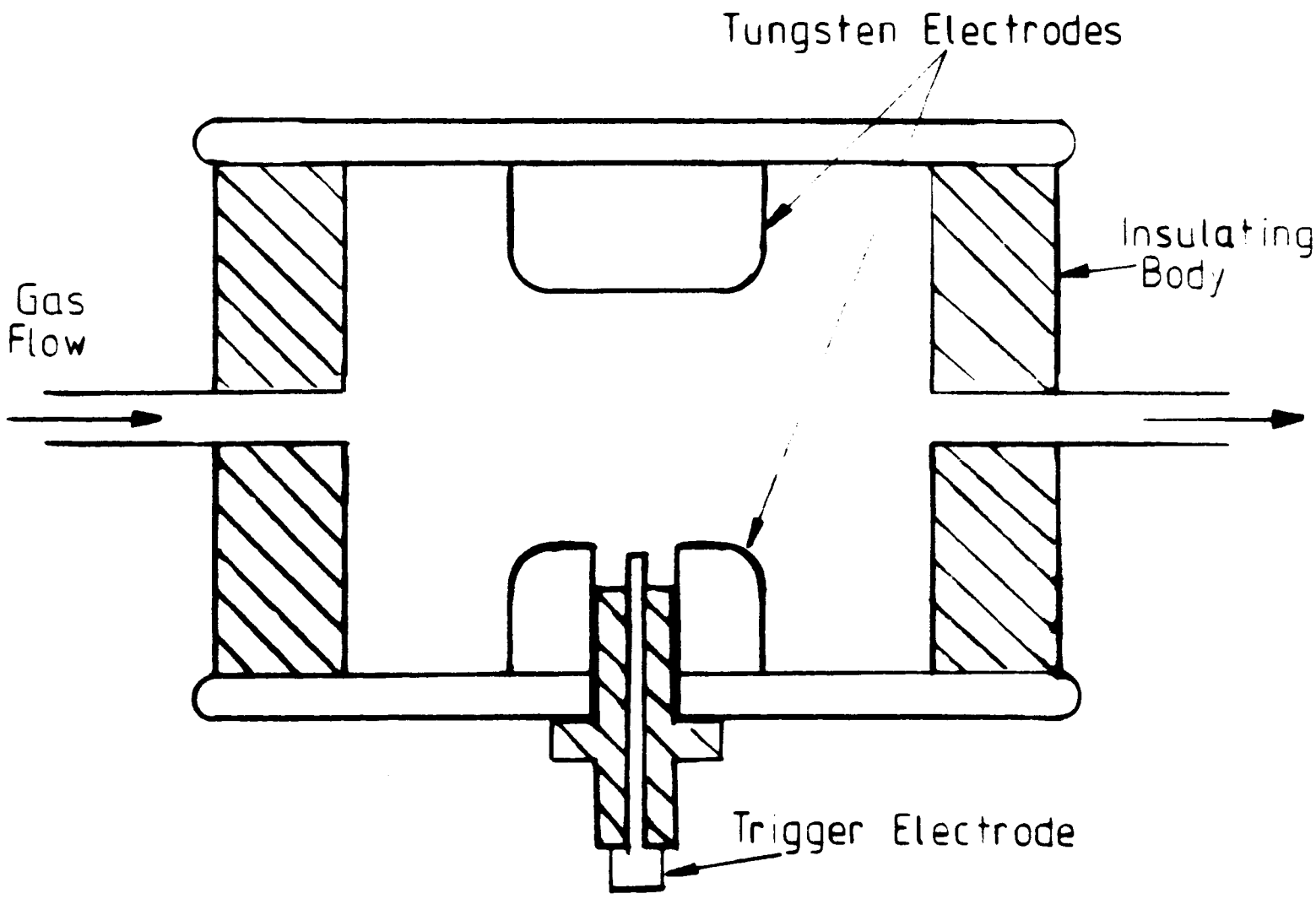


Figure A1.6 Triggered spark gap

APPENDIX 2 :APPLICATIONS OF VUV LASERS

A2.1 PHOTODISSOCIATION

Absorption of a high energy VUV photon by a molecule can leave the molecule in a repulsive state, or in a bound state but with vibrational energy greater then the dissociation energy. In either case the molecule will dissociate, often leaving the dissociation products in an electronically excited state and possibly vibrationally excited. The dissociation efficiency can be large - in certain cases values of dissociation efficiency approaching unity have been reported (Black et al, 1975a and b, Germany et al , 1983).

Interest is being shown in the photodissociation of molecules because of the possibility of making high energy lasers, perhaps for laser fusion experiments. For such a laser a suitable energy storage medium is required that will have a high excited state density, and yet be stable against both spontaneous decay and collisional deactivation. The energy will need to be efficiently extracted in a subnanosecond laser pulse.

Atoms of Group VI elements would fulfil the above requirements for such a laser. For instance, the $^1S_0$ level in atomic oxygen is resistant to collisional deactivation by a variety of other atoms and moleclules, and has a radiative lifetime of 0.9s. The transition of interest is the $^1S_0$ - $^1D_2$ quadrupole transition at 557.7nm (see figure A2.1). If the inversion density were as large as 10^{17} cm^{-3} the energy which could be extracted from an amplifier operating on this transition would be 30J/l and it would have a small signal gain of 1% cm^{-1}.

Photolytic reactions producing atoms in the $^1S_0$ and $^1D_2$ state from simple molecules are more specific than electron or molecular collisional reactions because there are fewer bodies leaving the reaction, thus reducing the number of allowed channels. The absorption of a photon by a molecule produces a defined energy change leading to predictable final states. The

high dissociation efficiencies mean that the energy storage states can be efficiently produced.

Germany et al (1983) studied the dissociation of molecular oxygen using a fluorine laser via the process

$$O_2(X^3\Sigma^-_g) + h\nu \rightarrow O_2(^3\Sigma^-_u) \qquad A2.1$$

$$O_2(^3\Sigma^-_u) \rightarrow O(^3P) + O(^1D) + \Delta E \qquad A2.2$$

where ΔE=0.8eV. The 157nm laser photon is not energetic enough to leave the oxygen atom in the $^1S_0$ state. These workers found that the dissociation efficiency can approach 100% at pressures of 20-40 millitorr when the 10mJ laser pulses were focused to a 1mm diameter waist. This efficiency was reduced at higher pressures as there is then absorption of the laser radiation as it traverses the cell filled with oxygen.

The fluorine laser has also been used by Ondrey et al (1983), to dissociate OCS:

$$OCS(^1\Sigma^+) + h\nu \rightarrow CO(^1\Sigma^+) + S(^1S_0) \qquad A2.3$$

Their laser produced 25mJ pulses, but only if the gas fill was changed every 15 minutes of operation. These workers studied the vibrational distribution of the CO and found that levels up to v"=7 were populated. Although the production of metastable sulphur was not measured in these experiments, Black et al (1975b) measured a value for the quantum efficiency of 0.82 using a low pressure hydrogen capillary discharge light source. The $S(^1S)$ state could be used as the upper laser level for high energy lasers operating on the $S(^1S)$ - $S(^1D)$ and $S(^1S)$ - $S(^3P)$ transitions at 772.5nm and 435.8nm respectively.

Metastable oxygen atoms can also be produced by the photolysis of carbon dioxide (Lawrence, 1972) or dinitrogen monoxide (Black et al, 1975a). Yields of $O(^1S_0)$ greater than 80% were found in the range 105 to 118nm from CO_2. N_2O gave a yield of $O(^1S_0)$ of 93% at 129nm. CO_2 has the advantage that the deactivation rates of CO and CO_2 on $O(^1S)$ are low, but the disadvantage that no efficient radiator in the range 110 to 115nm is available. In the

dissociation of N_2O, all of N_2O, N_2 and NO will deactivate the metastable oxygen readily. In this case however the fluorescence from the Ar^*_2 excimer continuum will act as an efficient photolytic source for the reaction. However the efficient use of these molecules as precursors for the production of $O(^1S_0)$ at a sufficient desity to be used as an energy storage laser will have to wait for the development of a laser operating in the VUV region of 100 - 130nm.

Other schemes for producing photodissociaton lasers have involved heated cells containing metal salt vapours. ArF lasers have been used as the source of the dissociating radiation. Ehrlich and Osgood (1979) dissociated alkali-iodides to produce a series of laser transitions in the visible to mid-infrared. Many of the states produced were strong spontaneous radiators and so the energy conversion efficiencies into the laser outputs were 1-3%, corresponding to quantum efficiencies of 5-10%. Burnham (1977) obtained super-radiant laser pulses at 451nm in Indium produced from the photodissociation of InI in a sealed cell above 200°C. The high temperature was necessary because only absorption from the v=2 or higher vibrational level of the ground electronic state of InI would leave the In in the $5p^2S_{1/2}$ upper laser level. The maximum laser energy of 0.5mJ was obtained at 330°C, when the InI pressure was 0.75 torr, and 30mJ of the 40mJ ArF laser output was absorbed. This gave a quantum yield of 40% per absorbed photon. Heating the cell further to increase the fraction of the vapour molecules in the v=2 level should increase the efficiency of the laser.

Photodissociation lasers could therefore prove to be efficient sources of visible coherent radiation.

A2.2 PHOTOEXCITATION

Although tuneable VUV lasers do not exist, the use of VUV laser as excitation sources allows the study of high lying molecular levels where

accidental resonances exist. The high photon fluxes cause the production of intense emission from the excited levels, which increases the ease with which the studies of the excited levels can be made, compared to the use of nonlinear techniques to produce these states. It may even be possible to produce inverted populations, and thus photoexciation lasers.

As an example the accidental resonance between the 157nm output of a molecular fluorine laser and the NO $X^2\Pi$ - $B'^2\Delta$ transition. This was studied by Taherian and Slanger (1984) who identified the transition as v"=0 - v'=3 on Q(7.5) line, which is 0.25cm^{-1} out of resonance with the 157.63nm laser line. They observed emission in the following regions; 175-155nm, 260-190nm and 520-670nm and studied the effect on the emission spectra of adding helium as a buffer to the NO cell. This was found to generate many more lines in the UV as the helium transfers the population to neighbouring states. These authors suggest that a possible use of this resonance is as a fluorine laser energy monitor. A 1cm long cell containing 1 torr of NO placed at the output of the laser would absorb 13% of the energy of the 157.63nm laser line only. It is thus specific to the stronger laser line.

As a footnote to this subsection, Burrows et al (1985) have observed lasing on the (0,1) and (0,2) $A^2\Sigma^+$ -> $X^2\Pi$ bands of NO at 237 and 248nm, obtained by longitudinal optical pumping NO at 0.5 torr on the v"=0 to v'=0 transition of that band at 227nm. Conversion efficiency of the pump radiation was about 15%, giving laser pulses of 13μJ

A2.3 PHOTOLITHOGRAPHY

A2.3.1 Mechanisms of image formation

Two types of photolithography have been studied using VUV lasers: conventional "wet etching" and "self-developing" photoablation. The main application area for these techniques would be in the manufacture of VLSI circuits. As the tendendancy is progressively to incorporate more components

onto the same silicon chip size it is necessary to reduce the size of individual components. Short wavelengths are needed to produce submicrometre features without undue problems from diffraction of light at the pattern mask. The short pulse lengths of the ArF and F_2 lasers, about 10ns long, but high peak powers of the order of a few megawatts, mean only a very short exposure time is necessary. This obviates the need to keep the stage, on which the wafer is mounted, stationary for the comparatively long times needed with conventional irradiation sources, which can typically provide only a fraction of a watt in the VUV. The short coherence length of the excimer laser radiation virtually eliminates any problems with speckle, and yet the linewidth of the laser radiation is narrow enough to prevent problems with chromatic aberration in the projection system. The reasonably good collimation of the laser beam also helps in making a simple exposure optical system.

A2.3.2 Laser systems suitable for photolithography

Argon fluoride lasers have been used to produce features of 500nm in conventional lithography, using masks of chromium on quartz substrates (Kawamura et al, 1982). The resist was 1μm thick polymethyl methacrylate (PMMA), again on a quartz substrate. The exposure was of 930mJ/cm^2, in a 20ns pulse, but the low absorption coefficient of the PMMA used meant that only 9.2% of the laser energy was absorbed by the resist.

However using the shorter wavelength light from the fluorine dimer laser at 157nm, resist lines as narrow as 150nm have been made (White el al, 1984). A contact lithography technique in a vacuum chamber was used, with electron beam fabricated masks on either calcium fluoride or sapphire substrates. Studies of suitable resists for use at this wavelength showed that a copolymer of methyl methacrylate (MMA) and methacrylic acid (MAA) was particularly sensitive. This could be developed in a solution of "cellosolve" in methanol in 4 seconds. A pattern mask thus made was succesfully used for

the reactive ion etching of silicon. An exposure dose of 0.2J cm^{-2} was found to be sufficient to adequetely develop the resist. Thus about 50 mJ would be necessary to expose the average 5mm square silicon chip.

"Self-developing" photoresists have been investigated for both the ArF and the F_2 lasers. Various simple models have been proposed for the mechanism by which photoablation of the resist occurs. Thes are discussed in the next section. The advantage of the self developing photoresist is that the mass transport of ablated material away from the exposed regions occurs during, or almost immediately after, the laser pulse. This does away with the need for a wet etch process, and so simplifies and quickens the photolithographic process.

Srinivasan and Mayne-Banton (1982) used an ArF laser with a 12ns pulse length and 250μm films of polyetylene terephathalate (PET) as the resist in their experiments. They found that the depth of etching was proportional to the energy flux in the range 50-400mJ/cm^2, being 120nm/pulse for pulses of 370mJ/cm^2. They produced 2μm wide lines on the resist using a lead film on the resist surface to define the irradiation pattern. Nitrocellulose was used as a photoresist by Deutsch and Geis (1983) for exposures made with an ArF laser. The self developing properties of nitrocellulose are believed not just to come from photolysis of the material into volatile monomers, as in most other cases, but instead the volatile products come from chemical reactions between oxidising, NO_3, and reducing, CH, groups. They found that the etch rate, expressed in terms of the thickness removed per unit fluence per pulse was not constant as a function of the fluence (energy per unit area). There was a threshold value of 20mJ/cm^2, below which the etch rate was immeasurable, and a maximum etch rate at 50mJ/cm^2. This variable etch rate leads to a variable contrast: a higher contrast is achieved using a number of lower energy pulses to remove the required resist thickness. To study the resolution of the system, the diffraction past the cleaved edge of a 100μm thick silicon wafer contacted to the 0.6μm thick nitrocellulose film on a

silicon substrate was used. Scanning electron microscope (SEM) studies of the etched pattern showed clear images of line pairs spaced as close as 0.25μm apart. This also showed the resist to have a high contrast as the intensity variation at the extremities of the diffraction pattern had a modulation of only 1% of the average intensity, and yet the lines in the resist were visible.

A molecular fluorine laser was used by Henderson et al (1985) as the exposure source for a self developing photolithographic process, again with nitrocellulose as the resist. The laser was used with pulse energies of about 3mJ in a 5ns pulse, but focussed with a calcium fluoride lens to give and energy density of 0.1J/cm^2. Again a threshold fluence of 25mJ/cm^2 was found, but above this the etch rate was approximately linear up to a fluence of 0.1J/cm^2, when approximately 100nm of resist was removed with each pulse. These results agree generally with those obtained using the ArF laser. To study the resoultion of this system mask were made in silicon films (200nm thick), by reactive ion etching, which were then supported on CaF_2 substrates. These were held in contact with the 180nm thick film of nitrocellulose, on a silicon substrate, and the laser radiation directed through the calcium fluoride. The exposure consisted of two laser shots at an energy density of 0.1J/cm^2. An SEM photograph of the resist showed little debris in the exposed area, and good reproduction of the 200nm wide line.

All these studies show that it is possible to produce submicron features in resists, on the surfaces of semiconductors, using VUV lasers and both wet and dry etch processes. The patterns in the masks could be transferred into the semiconductor, using the standard doping techniques, thus enabling very small components to be made part of the VLSI circuits.

A2.4 MEDICAL APPLICATIONS

The medical applications of the VUV radiation arise as a consequence of

the high energy of the VUV photons, which ensures efficient photolytic decomposition of organic materials. The absorption of the VUV radiation causes electronic excitation of the bonding electrons followed by bond breaking. This process is known as ablative photodecomposition (APD). It differs markedly from the interaction of visible and infrared radition with these organic materials which causes destruction of the tissues by pyrolysis due to the high intensity of radiation. The APD mechanism is characterised by a threshold energy of about 30mJ/cm^2/pulse. Another applcation of APD was disscussed in the previous section in the case of the self developing photoresists, which involve a similar mechanism.

The model for APD is that a high energy VUV photon is absorbed by the organic molecules. This causes to an electronic transition to a higher lying state. If this state is above the dissociation limit the molecule can dissociate almost immediately, or else it could enter a repulsive state through curve crossing. An organic polymer is made up of a number of monomer units. It is the bonds holding these units together which are broken by the photochemical reaction. The reaction leads to an increase in volume of these monomer units and they are ejected from the material surface at high velocity. Garrison and Srinivasan (1985) have calculated theortically that the average perpendicular velocity of the material is between 1000 and 2000m/s, and leaves within a cone of 30 degrees around the normal to the surface.

Generally the shorter wavelength radiation has a larger absorption coefficient. This gives rise to a lower threshold energy fluence if it is assumed that ablation will start when there is one photon incident on each bond molecule in the polymer. As the absorption depth decreases so the incident flux on the material surface is reduced to give the same energy density deposited in the material. The material then ablates layer by layer, with each pulse.

When the irradiating pulse is above the threshold fluence, the excess

energy is carried away as the kinetic energy of the ablated products. Some heating of the material will occur due to the energy deposited to break the molecular bonds, but this will also be minimised for the case of low threshold fluences. The advantage of low material heating is that it gives a clean etch, with material only removed where the laser pulse has struck the surface, and very little damage to the surrounding area. This would indicate that the fluorine laser may be the best choice for direct ablation of organic materials. The fluorine laser would only be useful for the treatment of surface material as there is no way of transporting the radiation to internal sites through low loss fibres of suitable dimensions. In cases where this is necessary a xenon chloride laser emitting at 308nm would probably be the best choice.

Studies of the micromachining of different organic polymer films have been made (Dyer and Sidhu, 1985) using the fluorine laser (actually a commercial version of the one developed in this work, with the samples in helium at atmospheric pressure). However the need to operate in a special environment has meant that work has not been carried out on animal tissue at 157nm. ArF laser radiation has been used to irradiate a variety of human and animal tissue. Puliafito (1985) has compared the effect of 248nm radiation (from a KrF excimer laser) and 193nm laser pulses on the cornea. More precise cuts were found with the shorter wavelength radiation. Using appropriate masks , cuts as narrow as 20μm were formed, with a damage zone adjacent to this of only 0.1-0.3μm. These corneal incisions could be used to change the refractive power of the eye to reduce myopia. Ablation with the 248nm radiation of comparable fluences produced incisions with ragged edges and wider and more severe damage zones. Comparative studies of bovine lens ablation with a short pulse IR CO_2 laser source showed marked adjacent thermal injury. A comparison, by Linsker et al (1984), of the pit characteristics of etching of an aortic wall due to irradiation at 193nm and 532nm (the frequency doubled output of a Nd:YAG laser), showed a similar increase in the damage to

adjacent tissue and distortion of the pit wall at the longer wavelength.

These results would imply that 157nm radiation might give very clean incisions. However it must be emphasised that the very short absorption depth of radiation at the VUV wavelengths means that the depth of material removed in each pulse is very short. So, although all the material in one absorption depth is removed very cleanly, a much greater number of pulses being needed to remove the same depth of material than if, for instance, a krypton fluoride laser were used .

For work on living tissue an atmosphere of helium or nitrogen could be created around the area to be irradiated through which the laser pulse would pass. The incident fluence could then easily be attenuated, if necessary, by bleeding some air into this atmosphere.

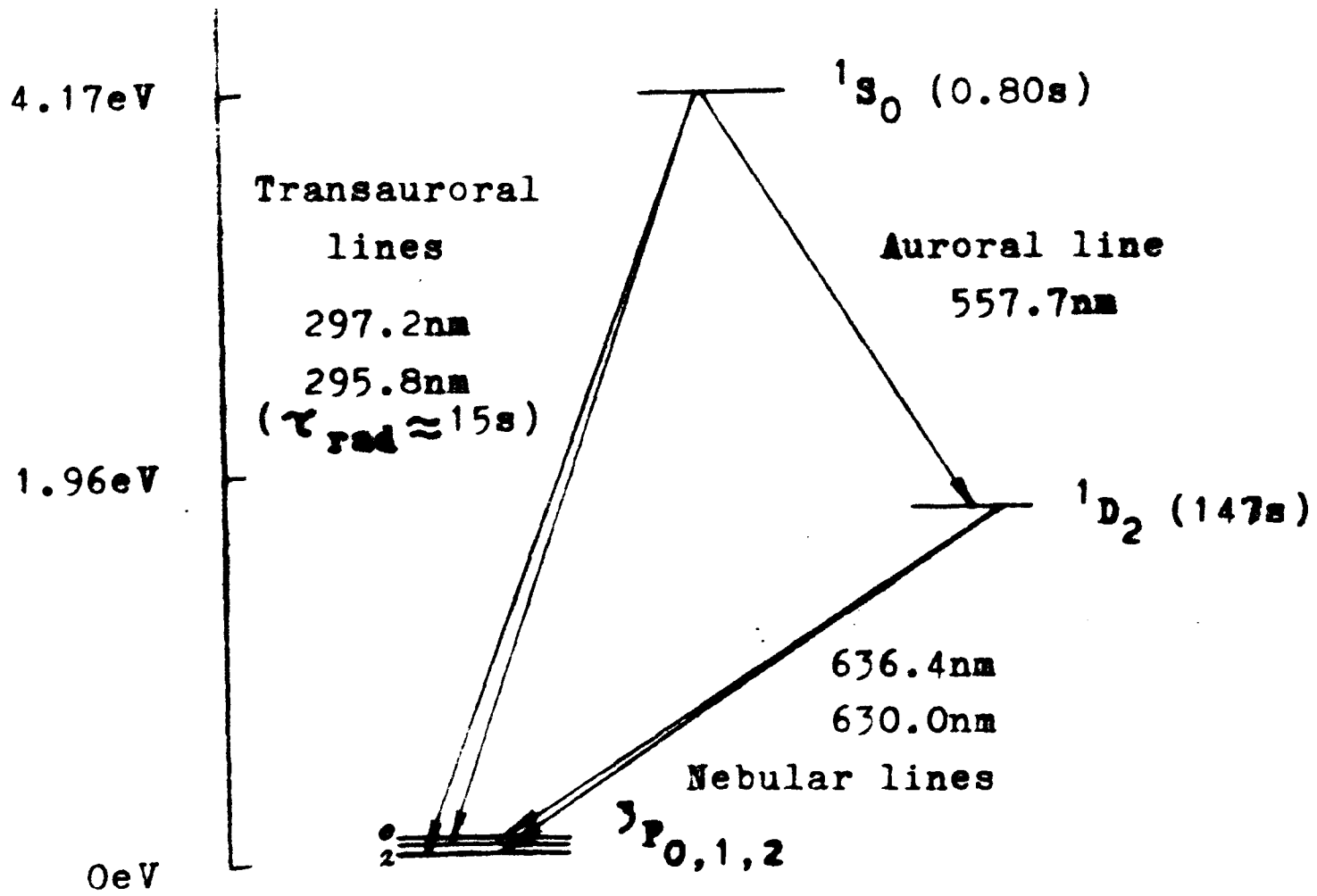


Figure A2.1 Energy levels of atomic oxygen

APPENDIX 3 : COMPUTER PROGRAMMES

A3.1 INTRODUCTION

This appendix contains some of the computer programmes used to assist in this work. The programmes can be divided into three categories: control programmes, analysis programmes and data generation programmes. The following sections have a brief explanation of each of the categories and example programmes.

All the programmes are written in BBC BASIC apart from the one called 'STATES' which is written in Acornsoft ISO Pascal.

A3.2 CONTROL PROGRAMMES

The control programmes formed a suite of software written to allow the microcomputer to control the experimental apparatus and gather the data generated. The examples listed here were used to gather data from the VUV monochromator in conjunction with the boxcar interator. Other programmes were used, for example, to ascertain the tuning curve of the XeCl laser.

The first programme was used when the monochromator was scanned to obtain the spectrally resolved emission, and the second if the relative timing of the boxcar gate was scanned to obtain a temporally resolved profile of the emission.

EXPSCAN

```
  0 REM **Control programme for wavelength scans**
 10 MODE7
 20 DIM P% 10000
 30 ?&FE62=255:?&FE60=0              Set up user port
 40 PROCinit
 50 REPEAT
 60  MODE7:VDU23,1,0;0;0;0;
 70  PROCconds
 80  PROCstart:PROCchoice
 90  MODE4:VDU23,1,0;0;0;0;
100  PROCdisp
```

```
110  PROCexpt
120  PROCoption
130  UNTILZ%>1
140 VDU29,0;0;4,30,12,23,1,1;0;0;0;
150 ?&FE60=0:MODE7
160 END
170 DEF PROCinit                          Initialise constants
180 *FX16,2
190 w1%=98:w2%=108
200 prf=5:spd%=0
210 res=0.2:adr%=1000
220 ad%=100:tc4%=1
230 tc2%=1000:int%=10
240 v%=15:ip%=5
250 sgp=1.0:g1$="N2:10mbar"
260 g2$="        ":g3$="      "
270 C$="           ":D$="23/10/1985"
280 orb%=&FE60
290 ENDPROC
300 DEF PROCconds                         Main menu for conditions
310 LOCAL F%:F%=FALSE
320 REPEAT
330  RESTORE420
340  CLS
350  PRINT'CHR$(141);CHR$130;TAB(10);"Set Conditions"
360  PRINTCHR$(141);CHR$130;TAB(10);"Set Conditions"'
370  C%=17
380  FOR I% = 1 TO C%
390   READ T$,V$
400   PRINTCHR$(I%+48);". ";T$;EVAL(V$)
410   NEXT
420  DATA"Initial wavelength(nm) = ",w1%
430  DATA"Final wavelength(nm) = ",w2%,"Laser prf(Hz) = ",prf
440  DATA"Resolution (A per point) = ",res
450  DATA"ADR(ns) = ",adr%,"AD(ns) = ",ad%
460  DATA"M164 TC(us) = ",tc4%,"M162 TC(ms) = ",tc2%
470  DATA"% initial for scan = ",int%,"Volts on laser(kV) = ",v%
480  DATA"Spark gap pressure(bar a) = ",sgp
490  DATA"Input dividing factor =  ",ip%
500  DATA"Gas 1(symbol/pressure) = ",g1$
510  DATA"Gas 2 = ",g2$,"Gas 3 = ",g3$
520  DATA"Comments(1 string) : ",C$,"Date = ",D$
530  *FX15,1
540  PRINTTAB(0,22);"Enter choice to update (0 to exit)"
550  Q=GET-48
560  IF Q=0 THEN F%=TRUE:GOTO600
570  IF Q>18 OR Q<1 THEN 540
580  IF Q>12 THEN INPUT"New string";a$ ELSE  INPUT"New value";a
590  ON Q GOSUB 620, 630, 640, 650, 660, 670, 680, 690, 700, 710, 720, 730,
740, 750, 760, 770, 780
600  UNTIL F%
610 ENDPROC
620 w1%=a:RETURN
630 w2%=a:RETURN
640 prf=a:RETURN
650 res=a:RETURN
660 adr%=a:RETURN
670 ad%=a:RETURN
680 tc4%=a:RETURN
690 tc2%=a:RETURN
```

```
700 int%=a:RETURN
710 v%=a:RETURN
720 sgp=a:RETURN
730 ip%=a:RETURN
740 g1$=a$+"mbar":RETURN
750 g2$=a$+"mbar":RETURN
760 g3$=a$+"mbar":RETURN
770 C$=a$:RETURN
780 D$=a$:RETURN
790 ENDPROC
800 DEF PROCstart                          Set up experimental values
810 M%=P%
820 ws%=w2%-w1%
830 IFws%<0 THEN rs=-1:fb%=6 ELSE rs=1:fb%=2
840 np=ABS(ws%)*200:D=ws%/120
850 sf=1200/np
860 npp=20*res
870 t%=100/prf
880 PRINTTAB(0,22);CHR$130;CHR$136;"  Set all conditions as above    "
890 PRINTTAB(5,24);"Press any key to continue";
900 a=GET
910 ENDPROC
920 DEF PROCchoice                         Information on options
930 CLS
940 PRINT'''CHR$141;CHR$134;" Options during run"
950 PRINTCHR$141;CHR$134;" Options during run"
960 PRINT''"H = Hold scan"
970 PRINT'"G = Release hold (Go)"
980 PRINT'"A = Abort run - then completion options     available"
990 PROCwait
1000 CLS
1010 PRINT'''CHR$141;CHR$131;" Options on completion of run"
1020 PRINTCHR$141;CHR$131;" Options on completion of run"
1030 PRINT''"D = Screen dump to printer"
1040 PRINT'"C = Cursor with wavelengths"
1050 PRINT" (Use < & > , or L & ; for fast moves.)"
1060 PRINT"S = Save data to disc file"
1070 PRINT'"R = Repeat programme"
1080 PRINT'"E = Exit Programme"
1090 PRINT''"Enter choice when plotting is completed."
1100 PRINT"  Screen dump must be selected first if  required as other options
will destroy  display"
1110 PROCwait
1120 ENDPROC
1130 DEF PROCexpt                          Run experiment
1140 ST=3*SQR((1E5*tc4%/ad%/prf)^2+(0.1*tc2%)^2)
1150 IFST>1000 THEN ST=1000
1160 TIME=0
1170 REPEAT                                Initial delay before recording
1180  ?orb%=97:?orb%=96
1190  A=INKEY(t%)
1200  UNTIL TIME >ST
1210 N%=0:0%=0: PROCfire
1220 FOR N%=0 TO np STEP npp               Loop to pulse discharge
1230  FOR L%=1 TO npp
1240   ?orb%=96+fb%:?orb%=96
1250   NEXT
1260  REPEAT
1270   IFINKEY(-85)THEN REPEAT:UNTIL GET$="G"
1280   IF INKEY(-66)THEN TIME=2*t%:0%=N%+npp:N%=np
```

```
1290   UNTIL TIME>=t%:PROCfire
1300  NEXT N%
1310 ?orb%=0
1320 ENDPROC
1330 DEF PROCfire                          Pulse discharge and record data
1340 ?orb%=97
1350 ?orb%=96
1360 TIME=0
1370 *FX17,2
1380 A=INKEY(1)
1390 R%=ADVAL(2)                           Read reference value
1400 *FX17,1
1410 A=INKEY(1)
1420 S%=ADVAL(1)                           Read data point
1430 A%=4000*(S%/R%)
1440 ?M%=A% DIV &100
1450 M%?1=A% AND &FF
1460 M%=M%+2
1470 PLOT 69,N%*sf,A% DIV 4
1480 ENDPROC
1490 DEF PROCdisp                          Plot and label wavelength axis
1500 VDU5,29,0;40;
1510 MOVE0,0:DRAW 1200,0
1520 FOR I%=0 TO 1200 STEP 120
1530  MOVE I%,0:DRAW I%,10:MOVEI%-5,-8:PRINTSTR$(INT(w1%+ws%*I%/1200))
1540  NEXT
1550 ENDPROC
1560 DEF PROCoption                        Options available when run over
1570 Z%=0:VDU4,29,0;0;
1580 REPEAT
1590  *FX15,1
1600  A$=GET$
1610  IF A$="C" THEN PROCcur
1620  IF A$="D" THEN CALL&900              Copy screen to printer
1630  IF A$="S" THEN PROCfsave
1640  IF A$="R" THEN PROCrewind:Z%=1
1650  IF A$="E" THEN Z%=2
1660  UNTIL Z%>0
1670 ENDPROC
1680 DEF PROCfsave                         Save data to file
1690 CLS: *DIR E
1700 INPUT'"Enter filename ";f$
1710 *DR.2
1720 Z=OPENOUT f$
1730 PRINT#Z,w1%,w2%,prf,spd%,res,adr%
1740 PRINT#Z,ad%,tc4%,tc2%,int%,v%,sgp
1750 PRINT#Z,ip%,g1$,g2$,g3$,C$,D$
1760 FOR I%=P% TO M%-2
1770  B%=?I%
1780  BPUT#Z,B%
1790  NEXT
1800 CLOSE#Z:PRINT'"File saved"
1810 *DIR $
1820 *DR.0
1830 ENDPROC
1840 DEF PROCrewind                        Reposition spectrometer
1850 IF 0%=0 THEN 0%=np
1860 cw=w1%+rs*0%/200
1870 CLS:PRINT'''"Reposition Spectrometer (Y/N) ?"
1880 REPEAT
```

```
1890  *FX15,1
1900  B$=GET$
1910  IF B$="N" THEN w1%=cw:B$="EX"
1920  IF B$="Y" THEN PROCrwd:B$="EX"
1930  UNTIL B$="EX"
1940 ENDPROC
1950 DEF PROCrwd
1960 PRINT''"Input new wavelength in nm."
1970 PRINT"<RETURN> for ";w1%;"nm ";:INPUT tw%
1980 IF tw%=0 THEN tw%=w1%
1990 N%=200*(tw%-cw)
2000 IF N%<0 THEN N%=ABS(N%):fb%=6 ELSE fb%=2
2010 FOR N= 0 TO N%
2020  ?orb%=fb%:?orb%=0
2030  NEXT
2040 w1%=tw%
2050 PRINT''"Spectrometer reset to ";tw%;"nm"
2060 PROCwait
2070 ENDPROC
2080 DEF PROCwait:LOCAL A
2090 PRINT''"Press a key to continue":A=GET
2100 ENDPROC
2110 DEF PROCcur                          Cursor for wavelength readout
2120 LOCALX,A,F
2130 X=0:A=0:F=FALSE
2140 GCOL3,1
2150 MOVE0,45:DRAW0,750
2160 REPEAT
2170  IF INKEY(-103) THEN X=X-1:PROCline
2180  IF INKEY(-104) THEN X=X+1:PROCline
2190  IF INKEY(-88) THEN X=X+10:PROCline
2200  IF INKEY(-87) THEN X=X-10:PROCline
2210  IF INKEY(-35) THEN F=TRUE
2220  UNTIL F
2230 MOVEX,45:DRAWX,750:PRINTTAB(35,1);"     "
2240 GCOL0,1:*FX15,1
2250 ENDPROC
2260 DEF PROCline                         Draw cursor line
2270 MOVEA,45:DRAWA,750
2280 MOVEX,45:DRAWX,750
2290 W%=10*w1%+D*X:A=X
2300 PRINTTAB(35,1);W%
2310 ENDPROC
```

TIMSCAN

```
   0 REM **Control programme for time scans**
  10 MODE7: DIM P% 10000
  20 ?&FE62=255:?&FE60=0
  30 PROCinit
  40 REPEAT
  50  MODE7:VDU23,1,0;0;0;0;
  60  PROCconds
  70  PROCstart:PROCchoice
  80  MODE4:VDU23,1,0;0;0;0;
  90  PROCdisp
 100  PROCexpt
 110  PROCoption
 120  UNTIL Z%=2
```

```
130 VDU4,30,12,23,1,1;0;0;0;
140 ?&FE60=0
150 END
160 DEF PROCinit
170 *FX16,3
180 w1%=1033:dum%=0
190 prf=5:st%=100
200 dum=0:adr%=1000
210 ad%=10:tc4%=1
220 tc2%=1000:int%=5
230 v%=12:ip%=5
240 sgp=1.0:g1$="N2:10mbar"
250 g2$="      ":g3$="      "
260 C$="              ":D$="18/10/1985"
270 orb%=&FE60:max%=60600
280 ENDPROC
290 DEF PROCconds
300 LOCAL F%:F%=FALSE
310 REPEAT
320  RESTORE410
330  CLS
340  PRINT'CHR$(141);CHR$130;TAB(10);"Set Conditions"
350  PRINTCHR$(141);CHR$130;TAB(10);"Set Conditions"'
360  C%=16
370  FOR I% = 1 TO C%
380   READ T$,V$
390   PRINTCHR$(I%+48);". ";T$;EVAL(V$)
400   NEXT
410  DATA"Wavelength(A) = ",w1%
420  DATA"Laser prf(Hz) = ",prf
430  DATA"Total scan time(s) = ",st%
440  DATA"ADR(ns) = ",adr%,"AD(ns) = ",ad%
450  DATA"M164 TC(us) = ",tc4%,"M162 TC(ms) = ",tc2%
460  DATA"% initial for scan = ",int%,"Volts on laser(kV) = ",v%
470  DATA"Spark gap pressure(bar a) = ",sgp
480  DATA"Input dividing factor =  ",ip%
490  DATA"Gas 1(symbol/pressure) = ",g1$
500  DATA"Gas 2 = ",g2$,"Gas 3 = ",g3$
510  DATA"Comments(1 string) : ",C$,"Date = ",D$
520  *FX15,1
530  PRINTTAB(0,22);"Enter choice to update (0 to exit)"
540  Q=GET-48
550  IF Q=0 THEN F%=TRUE:GOTO590
560  IF Q>16 OR Q<1 THEN 530
570  IF Q>11 THEN INPUT"New string";a$ ELSE INPUT"New value";a
580  ON Q GOSUB 610, 620, 630, 640, 650, 660, 670, 680, 690, 700, 710, 720,
730, 740, 750, 760
590  UNTIL F%
600 ENDPROC
610 w1%=a:RETURN
620 prf=a:RETURN
630 st%=a:RETURN
640 adr%=a:RETURN
650 ad%=a:RETURN
660 tc4%=a:RETURN
670 tc2%=a:RETURN
680 int%=a:RETURN
690 v%=a:RETURN
700 sgp=a:RETURN
710 ip%=a:RETURN
```

```
 720 g1$=a$+"mbar":RETURN
 730 g2$=a$+"mbar":RETURN
 740 g3$=a$+"mbar":RETURN
 750 C$=a$:RETURN
 760 D$=a$:RETURN
 770 ENDPROC
 780 DEF PROCstart
 790 G%=600:N%=0
 800 M%=P%:TO%=int%*max%/100
 810 sf=12/40:T1%=TO%
 820 np%=st%*prf
 830 IFnp%>G% THEN npp% = np% DIV G% ELSEnpp%=1
 840 t%=100/prf
 850 PRINTTAB(0,22);CHR$130;CHR$136;"  Set all conditions as above    "
 860 PRINTTAB(5,24);"Press any key to continue";
 870 a=GET
 880 ENDPROC
 890 DEF PROCchoice
 900 CLS
 910 PRINT'''CHR$141;CHR$134;" Options during run"
 920 PRINTCHR$141;CHR$134;" Options during run"
 930 PRINT''"H = Hold scan"
 940 PRINT'"G = Release hold (Go)"
 950 PRINT'"A = Abort run - then completion options     available"
 960 PRINT''"Press any key to continue"
 970 A=GET
 980 CLS
 990 PRINT'''CHR$141;CHR$131;" Options on completion of run"
1000 PRINTCHR$141;CHR$131;" Options on completion of run"
1010 PRINT''"D = Screen dump to printer"
1020 PRINT'"S = Save data to disc file"
1030 PRINT'"R = Repeat programme"
1040 PRINT'"L = Log plot of data"
1050 PRINT'"E = Exit Programme"
1060 PRINT''"Enter choice when plotting is completed."
1070 PRINT"  Screen dump must be selected first if  required as other options
will destroy  display"
1080 PRINT'"Press any key to continue"
1090 A=GET
1100 ENDPROC
1110 DEF PROCexpt
1120 TIME=0
1130 REPEAT
1140  ?orb%=97:?orb%=96:A=INKEY(t%)
1150  UNTIL TIME>1000
1160 PROCfire
1170 REPEAT
1180  REPEAT  UNTIL TIME>=t%
1190  ?orb%=225                          Scan reset
1200  ?orb%=224                          Scan hold
1210  IF N%=0 THEN PROCfire
1220  N%=(N%+1) MOD npp%
1230  A$=INKEY$(1)
1240  IFA$="H" THEN ?orb%=96:REPEAT:UNTIL GET$="G":?orb%=224
1250  IFA$="A"THEN T%=70E3
1260  UNTIL T%>max%
1270 ?orb%=0
1280 ENDPROC
1290 DEF PROCfire
1300 TIME=0
```

```
1310 *FX17,3
1320 A=INKEY(1)
1330 T%=ADVAL(3)                                Read time value
1340 IF ABS(T%-T1%-(max% DIV G%))>200 ANDT%>TO%+200 THEN T%=T1%+(max% DIV G%)
1350 *FX17,2
1360 A=INKEY(1)
1370 R%=ADVAL(2)                                Read reference value
1380 *FX17,1
1390 A=INKEY(1)
1400 S%=ADVAL(1)                                Read data point
1410 A%=4000*(S%/R%)
1420 B%=4000*(T%/max%)
1430 ?M%=B% DIV &100
1440 M%?1=B% AND &FF
1450 M%?2=A% DIV &100
1460 M%?3=A% AND &FF
1470 M%=M%+4
1480 PLOT 69,B%*sf,A% DIV 4
1490 T1%=T%
1500 ENDPROC
1510 DEF PROCdisp
1520 VDU5,29,0;40;
1530 MOVE0,0:DRAW 1200,0
1540 FOR I%=0 TO 1200 STEP 120
1550  MOVE I%,0:DRAW I%,10:MOVEI%-5,-8:PRINTSTR$(INT(adr%*I%/1200))
1560  NEXT
1570 ENDPROC
1580 DEF PROCoption
1590 Z%=0:VDU4,30,29,0;0;
1600 REPEAT
1610  *FX15,1
1620  A$=GET$
1630  IF A$="D" THEN CALL&900
1640  IF A$="S" THEN PROCfsave
1650  IF A$="R" THEN Z%=1
1660  IF A$="L" THEN PROClog
1670  IF A$="E" THEN Z%=2
1680  UNTIL Z%>0
1690 ENDPROC
1700 DEF PROCfsave
1710 CLS: *DIR T
1720 INPUT''"Enter filename ";f$
1730 Z=OPENOUT f$
1740 PRINT#Z,w1%,dum%,prf,st%,dum,adr%
1750 PRINT#Z,ad%,tc4%,tc2%,int%,v%,sgp
1760 PRINT#Z,ip%,g1$,g2$,g3$,C$,D$
1770 FOR I%=P% TO M%-4
1780  B%=?I%
1790  BPUT#Z,B%
1800  NEXT
1810 CLOSE#Z:PRINT''"File saved"
1820 *DIR $
1830 ENDPROC
1840 DEF PROClog
1850 VDU4,30:INPUT''"Enter times for lifetime ",t1,t2
1860 XS=0:YS=0:XXS=0:YYS=0:SXY=0:N%=0
1870 F=adr%/4000:S=1200/adr%:%%=&20108
1880 CLS: PROCdisp:VDU4,30
1890 FOR I%=P% TO M%-4  STEP 4          Use straight line fit on log
1900  T=F*(&100*?I%+I%?1)               of data values to find time
```

```
1910  IF T<t1 THEN 1980                    constant of signal decay
1920  XS=XS+T:XXS=XXS+T*T
1930  V=100*LN(&100*I%?2+I%?3)
1940  YS=YS+V:YYS=YYS+V*V
1950  SXY=SXY+T*V
1960  N%=N%+1:PLOT69,T*S,V
1970  IF T>t2 THEN I%=M%
1980  NEXTI%
1990 xb=XS/N%:yb=YS/N%
2000 sxy=SXY-N%*xb*yb:sxx=XXS-N%*xb*xb:syy=YYS-N%*yb*yb
2010 slope=sxy/sxx:sdslope=SQR((syy/sxx-(sxy/sxx)^2)/(N%-2))
2020 PRINTTAB(0,1)"Lifetime = ";-100/slope;" +/- ";100*sdslope/(slope)^2;"ns"
2030 k=yb-slope*xb
2040 MOVEt1*S,(slope*t1+k)
2050 DRAWt2*S,(slope*t2+k)
2060 %%=&90A:VDU29,0;0;
2070 ENDPROC
```

A3.3 ANALYSIS PROGRAMMES

The programmes listed in this section are examples of those written to analyse the data generated by the experiments to obtain the information required.

The first programme was used to calculate the number density of molecules in a particular state from the intensity of radiation emitted on transitions from that state. The calculation for this is explained in section 8.2.

The second programme performed a point by point subtraction of two data files. This was used to obtain the LIF signal alone by removing the component due to the background discharge excited emission.

STATES

```
programme states(input,output);

const xg=18000 {corners of grating};
      yg=20000;
      zg=0;
      zs=200000 {corners of slits};
      xs=5000;
      step=1000;
      fourpi=12.5664;
      electron=1.6e-19;
      NaSaleff=0.2;
      PMTQE=0.25;
```

```
type  posint=0..maxint;

var   ys,xd,yd,zd,zds,w : posint {discharge dimensions};
      x,y,z : posint;
      yforx,xstart : posint;
      sum,domega : real;
       dtheta1,dtheta11,dtheta2,dtheta22,dtheta : real {parallel to slit
width};
      dphi1,dphi11,dphi2,dphi22,dphi :real {angles parallel to slit height};
      R,alpha,V,gain:integer;
      n,Grateff,volume,A:real;
      s:char;

function ratio(a,b,c,d :integer):real;
      begin ratio:=(a-b)/(c-d) end;

begin
      page;
      writeln;
      writeln('All dimensions in micrometers (um).');
      writeln;
      write(' Enter slit width --> ');
      readln(w);ys:=w div 2;
      writeln;
      write(' Enter distance of emitting volume from slits --> ');
      readln(w);zds:=w+zs;
      writeln;
      writeln(' Enter dimensions of emitting volume');
      write(' along axis --> ');readln(zd);
      write(' parallel to slit height --> ');
      readln(w);xd:=w div 2;
      write(' parallel to slit width --> ');
      readln(w);yd:=w div 2;
      write('Bottom of discharge --> ');
      readln(w);xstart:=w;
      writeln;
      write('Boxcar input resistance --> ');
      repeat
           readln(R)
           until (R=50) or(R=1000000);
      write('PMT voltage --> ');
      repeat
           readln(V);V:=V div 100
           until V in [17,18,19,20];
      case V of
           17:gain:=2700000 {PMT gain};
           18:gain:=5800000;
           19:gain:=10000000;
           20:gain:=20000000;
           end;
      write('a-X (a) or b-X (b) transition --> ');
      readln(s);
      if s='a' then Grateff:=0.034 else Grateff:=0.066;
      write('Dividing factor into computer -->');
      readln(V);
      if V=2 then alpha:=2500 else alpha:=978 {Chart height conversion
factor};
      write('Absolute transition probability --> ');
      readln(A);
      write('Enter height of signal on printout in mm --> ');
```

```
      readln(V);
      writeln;

volume:=step*step*step*1e-12;z:=zds;sum:=0;

while z<=zd+zds do
begin writeln(' z = ',z:7);
      x:=xstart+500;
      while x<= xd do
      begin y:=500;
            yforx:=trunc(sqrt(sqr(yd)-sqr(x))+0.45) {Circular discharge area};
            dphi1:=ratio(x,xs,z,zs);
            dphi11:=ratio(x,xg,z,zg);
            dphi2:=ratio(x,-xs,z,zs);
            dphi22:=ratio(x,-xg,z,zg);
            if dphi1<dphi11 then dphi1:=dphi11 {larger of dphi1 and dphi11};
            if dphi2>dphi22 then dphi2:=dphi22 {smaller of dphi2 and dphi22};
            dphi:=arctan(dphi2)-arctan(dphi1);
            if dphi<0 then dphi:=0;
            while y<=yforx do
            begin dtheta1:=ratio(y,ys,z,zs);
                  dtheta11:=ratio(y,yg,z,zg);
                  dtheta2:=ratio(y,-ys,z,zs);
                  dtheta22:=ratio(y,-yg,z,zg);
                  if dtheta1<dtheta11 then dtheta1:=dtheta11
                                          {larger of dtheta1 and dtheta11};
                  if dtheta2>dtheta22 then dtheta2:=dtheta22
                                          {smaller of dtheta2 and dtheta22};
                  dtheta:=arctan(dtheta2)-arctan(dtheta1);
                  if dtheta<0 then dtheta:=0;
                  domega:=dtheta*dphi {solid angle subtended at grating};
                  sum:=sum+domega;
                  write(domega*10000:4:1);
                  y:=y+step;
                  end;
            x:=x+step;
            writeln;
            end;
      z:=z+step;
      writeln;
      end;

sum:=sum*4 {only one quadrant summed over};

{Number density in state required}
n:=V*fourpi/(volume*alpha*R*gain*electron*A*sum*PMTQE*Grateff*NaSaleff);

writeln;
writeln('Density of molecules in ',s,' state is',n:9,' cm-3');
writeln;
end.
```

DIFFEXP

```
  0 REM. **Programme to find difference between two spectra**
 10 IF ?&900<>&A9 THEN *LOAD APRINT  Screen hard copy routine
 20 MODE7:PROCtitle
 30 DIM M% 12000                     Reserve space for data
 40 REPEAT
```

```
 50  MODE7:I%=0:Z%=0
 60  PRINT''"First file":PROCload:J%=I%:f1$=f$
 70  PRINT''"File to be subtracted":PROCload
 80  ws%=w2%-w1%:npp=20*res            Set constants from data
 90  np=ws%*200:sf=npp*600/np          read in from file
100  MODE4: PROCdisp
110  FOR K%=M% TO M%+J%-1 STEP 2       Subtract two spectra and plot
120   A%=&100*?K%+K%?1
130   B%=&100*K%?J%+K%?(J%+1)
140   C%=A%-B%
150   ?K%=C% DIV &100:K%?1= C% AND &FF
160   PLOT 69,sf*(K%-M%),C% DIV 8
170   NEXT
180  VDU4,29,0;0;
190  REPEAT:*FX15,1
200   A$=GET$
210   IF A$="D" THEN CALL&900
220   IF A$="E" THEN Z%=2
230   IF A$="R" THEN Z%=1
240   IF A$="S" THEN PROCsave
250   UNTIL Z%>0
260  UNTIL Z%>1
270 END
280 DEF PROCdisp                        Plot and label axis
290 PRINTTAB(10,1);f1$;" - ";f$
300 VDU5,29,0;540;
310 MOVE0,0:DRAW 1200,0
320 FOR I%=0 TO 1200 STEP 120
330  MOVE I%,0:DRAW I%,10:MOVEI%-5,-8:PRINTSTR$(INT(w1%+ws%*I%/1200))
340  NEXT
350 ENDPROC
360 DEF PROCload                        Load data in from file
370 INPUT'"Enter filename ";f$
380 PRINT'"Enter Directory ":C$=GET$
390 PRINT'"Enter Drive ":D$=GET$
400 OSCLI("DRIVE "+D$)
410 F$=C$+"."+f$
420 Z=OPENIN F$
430 INPUT#Z,w1%,w2%,prf,spd%,res,adr%
440 INPUT#Z,ad%,tc4%,tc2%,int%,v%,sgp
450 INPUT#Z,ip%,g1$,g2$,g3$,C$,D$
460 REPEAT
470  B%=BGET#Z
480  M%?I%=B%:I%=I%+1
490  UNTIL EOF£Z
500 CLOSE#Z
510 *DIR $
520 *DR.0
530 ENDPROC
540 DEF PROCsave                        Save subtracted file
550 CLS:INPUT"ENTER FILENAME",F$
560 *DIR D
570 OSCLI("DRIVE "+D$)
580 Z=OPENOUT F$
590 PRINT#Z,w1%,w2%,prf,spd%,res,adr%
600 PRINT#Z,ad%,tc4%,tc2%,int%,v%,sgp
610 PRINT#Z,ip%,g1$,g2$,g3$,C$,D$
620 FOR K%=M% TO M%+J%-1
630  L%=?K%:BPUT#Z,L%
640  NEXT
```

```
 650 PRINT"FILE SAVED"
 660 CLOSE#Z:*DIR$
 670 *DR.0
 680 ENDPROC
 690 DEF PROCtitle
 700 PRINT'"   This programme enables the difference  between two spectra to
be obtained."
 710 PRINT'"   After entering the filenames their   difference is displayed."
 720 PRINT'"At this stage a number of options can beselected."
 730 PRINT'"D Screen dump to printer."
 740 PRINT"S Save display to disc"
 750 PRINT"R Rerun programme"
 760 PRINT"E Exit programme"
 770 PRINT'"   Do screen dump first, if required, as others will destroy
display."
 780 PRINT'"Press a key to continue."
 790 a=GET:ENDPROC
```

A3.4 DATA GENERATION PROGRAMMES

This section contains programmes that were used to calculate various quantities and present the information in a manner useful as a guide for the experimental conditions, or as an immediate check on the experimental results.

The first programme (SPECTRA) was used to synthesise the spectra expected from the VUV monochromator, allowing for the instrumental linewidth, for given experimental conditions. This was achieved by taking in data, either from file or directly from the keyboard, of the wavelengths and relative intensities of the lines of interest and calculating the profile of each line out to three halfwidths, and summing over the contributions for each line. A background contribution could also be added in to the spectra to make allowance for a continuum emission, for example. The resulting spectra was then displayed on the screen.

The next programme (PRISPLT) calculated the beam expansion factors and polarisation dependant reflection energy losses as a function of the angles of incidence of the beam on the two beam expansion prisms. The results were dispayed as a table and a '3-D' graph. The use of this programme was explained in section 6.2.

The last programme (ROTABN) calculates the relative absorption strengths

of the rotational lines of the 'a'(v"=0) to 'b'(v'=1) transition of molecular nitrogen. The results are displayed as a stick spectra for the P, Q and R branches, with the output of an untuned XeCl laser overlaid.

SPECTRA

```
  0 REM **Programme to synthesise VUV spectra**
 10 MODE7:PROCinit
 20 DIMW%(100),I%(100),P%(1200)
 30 REPEAT
 40  N%=0:H%=0:F$="        "
 50  INPUT''"Is data on file (Y/N) ";Q$
 60  IF Q$="Y" THEN PROCfile ELSE PROCenter
 70  INPUT''"Check data has been correctly entered   (Y/N)";Q$
 80  IF Q$="Y" THEN PROCcheck:PROCsave
 90  REPEAT
100   INPUT''"Slit width (um) ",S
110   INPUT"Wavelength range (nm)",L1,L2
120   INPUT"Background (f(X)=f(wavelength(A))) ";B$
130   A=10000*LN2/16/S/S:D=(L2-L1)/120:HW=0.04*S
140   MODE4:PROCAXES
150   IF B$<>"" THEN PROCback
160   FOR M%=0 TO N%                    For each line
170    W1=W%(M%)-3*HW:W2=W%(M%)+3*HW
180    FOR C=W1 TO W2 STEP D            Line shape out to three halfwidths
190     X%=(C-10*L1)/D
200     IF X%<0 OR X%>1200 THEN 230
210     P%(X%)=P%(X%)+10000*I%(M%)*EXP(-A*(C-W%(M%))*(C-W%(M%)))
220     IFP%(X%)>H% THEN H%=P%(X%)
230     NEXTC
240   NEXTM%
250  MOVE0,950*P%(0)/H%                Plot synthesised spectra
260   FOR C% = 1 TO 1200
270   P%(C%)=950*P%(C%)/H%
280   DRAWC%,P%(C%)
290   NEXTC%
300  Z%=0:VDU29,0;0;
310  REPEAT:*FX15,1                    Options - see PROCinit
320   A$=GET$
330   IF A$="D" THEN G=USR(&0A00)
340   IF A$="E" THEN Z%=3
350   IF A$="R" THEN Z%=1
360   IF A$="N" THEN Z%=2
370   UNTIL Z%>0
380  UNTIL Z%>1
390  MODE7:PROCsave
400  UNTIL Z%>2
410 *DIR $
420 END
430 DEFPROCAXES                       Draw and label wavelength axis
440 PRINTTAB(16,0);F$;TAB(28,0);S;"um slits"
450 VDU5,29,0;40;
460 MOVE0,0:DRAW1200,0
470 FOR X=0 TO 1200 STEP 120
480  MOVEX,0:DRAWX,15
490  MOVEX-16,-6:PRINTSTR$(INT(L1+D*X/10))
500  NEXTX
```

```
510 VDU4:ENDPROC
520 DEF PROCenter                       Read in data from keyboard
530 LOCAL F:F=FALSE
540 PRINT''"Enter wavelength(A) & rel. intensity.    (Use -1,-1 to end)"
550 REPEAT
560  INPUT W%(N%),I%(N%)
570  IF W%(N%)=-1 THEN F=TRUE:N%=N%-2
580  N%=N%+1
590  UNTIL F
600 ENDPROC
610 DEF PROCfile                        Read in data from specified file
620 INPUT''"Filename ";F$
630 Z=OPENIN F$
640 REPEAT
650  INPUT#Z,W%(N%),I%(N%)
660  N%=N%+1
670  UNTIL EOF £Z
680 CLOSE#Z:N%=N%-1
690 ENDPROC
700 DEF PROCsave                        Save data to file
710 INPUT''"Save spectrum (Y/N) ";Q$
720 IF Q$="N" THEN ENDPROC
730 INPUT"Filename ";F$
740 Z=OPENOUT F$
750 FOR C% = 0 TO N%
760  PRINT#Z,W%(C%),I%(C%)
770  NEXT C%
780 CLOSE #Z
790 ENDPROC
 800 DEF PROCback                       Evaluate background emission
 810 FOR C% = 0 TO 1200
 820  X=10*L1+C%*D
 830  P%(C%)=10000*EVAL B$
 840  NEXTC%
 850 ENDPROC
 860 DEF PROCinit                       Initial instructions
 870 PRINT''"This programme simulates expected spectra from the VUV
monochrometer."
 880 PRINT''"The 'stick' spectrum is input, and from this the expected spectrum
is calculatedusing the effective instrument linewidth"
 890 a=INKEY(500)
 900 CLS
 910 PRINTTAB(2,3)"Options when spectrum completed"''
 920 PRINT"  D  Screen dump to printer"
 930 PRINT"  R  Rerun with same spectrum"
 940 PRINT"  N  Rerun with new spectrum"
 950 PRINT"  E  Exit programme"
 960 PRINT''"Press a key to continue"
 970 A=GET:CLS
 980 *LOAD PRINT
 990 *DIR S
1000 ENDPROC
1010 DEF PROCcheck                      Check data is correct
1020 FOR I%=0 TO N% STEP 10
1030  PRINTTAB(8);"No.";TAB(14);"wavelength";TAB(26);"intensity"
1040  FOR J%=0 TO 9
1050   K%=I%+J%
1060   PRINTK%,W%(K%),I%(K%)
1070   NEXT
1080  PROCalt                          Alter existing data if required
```

```
1090  NEXT
1100 INPUT'"Add more lines (Y/N) ";Q$
1110 IF Q$="Y" THEN PROCenter
1120 ENDPROC
1130 DEF PROCalt
1140 LOCAL F:F=FALSE
1150 PRINT'"   Enter number of data to be corrected then <RET>, followed by
new wavelength and intensity (Use -1 as number to end)"
1160 REPEAT
1170  INPUTL%
1180  IF L%=-1 THEN F=TRUE:GOTO 1200
1190  INPUTW%(L%),I%(L%)
1200  UNTIL F:CLS
1210 ENDPROC
```

PRISPLT

```
   0 REM **Programme to calculate prism expansion factors and reflection
losses**
  10 DIM I(3),R(3),W(4),N(3),P(3),E(1)
  20 DIM E% 255:DIM Q% 255:DIM P% 31
  30 MODE3:PROCinit
  40 *FX201,1                              Disable keyboard speed up calculation
  50 PRINTTAB(25,1)"C A L C U L A T I N G"
  60 FOR A%=0 TO AE%                       For all angles Prism  0
  70  C%=A%*(BE%+1)
  80  PRINTA%+AL%,;
  90  IP=1/2:IN=1/2
 100  PROCangles(A%+AL%,0)
 110  IN1=IN:IP1=IP
 120  P%?(2*A%)=INT(100*(N(0)+N(1)+P(0)+P(1))+0.5)
 130  P%?(2*A%+1)=INT(E(0)+0.5)
 140  FOR B%=0 TO BE%                     For all angles on Prism  1
 150   D%=B%+BL%:IN=IN1:IP=IP1
 160   PRINTD%,;
 170   PROCangles(D%,1)
 180   Q%?(C%+B%)=P%?(2*A%)+INT(100*(N(2)+N(3)+P(2)+P(3))+0.5)
 190   E%?(C%+B%)=E(0)*E(1)
 200  NEXT:PRINT:NEXT
 210 *FX201,0
 220 PROCPrint
 230 MODE1:PROCPlot
 240 VDU4,26,29,0;0;23;11,255;0;0;0
 250 END
 260 DEFPROCangles(0%,F%)
 270 I(2*F%)=RAD(0%)                      Calculate incident and refracted
 280 R(2*F%)=ASN(SIN(I(2*F%))/n)          angles at both faces of
 290 I(2*F%+1)=PI/4-R(2*F%)               the prism
 300 R(2*F%+1)=ASN(n*SIN(I(2*F%+1)))
 310 FOR Z%=2*F% TO 2*F%+1                Calculate reflection losses
 320  N=FNrn(I(Z%),R(Z%))                 at both faces of prism
 330  P=FNrp(I(Z%),R(Z%))
 340  N(Z%)=IN*N
 350  IN=IN*(1-N)
 360  P(Z%)=IP*P
 370  IP=IP*(1-P)
 380  NEXT Z%
                                          Beam expansion factor for prism
 390 E(F%)=COS(R(2*F%+1))*COS(R(2*F%))/COS(I(2*F%))/COS(I(2*F%+1))
```

```
 400 ENDPROC
                                        Fresnel reflection coefficients
 410 DEF FNrn(A,B)=(SIN(A-B)*SIN(A-B))/(SIN(A+B)*SIN(A+B))
 420 DEF FNrp(A,B)=(TAN(A-B)*TAN(A-B))/(TAN(A+B)*TAN(A+B))
 430 DEFPROCAXES                        Plot x, y and z axes for graph
 440 VDU5,29,80-offset%;60;
 450 PROCline(0,0,0,AE%,0,0)
 460 PROCline(0,0,0,0,BE%,0)
 470 PROCline(0,0,0,0,0,ZE%)
 480 FOR Y%=0 TO AE%
 490  PROCline(Y%,BE%,0,Y%,0,0)
 500  PLOT1,0,-10
 510  IF Y%/2=INT(Y%/2) THEN MOVE(Y%*R%*CA) DIV 10,(Y%*R%*SA) DIV 10
-14:PRINTSTR$(Y%+AL%)
 520  NEXT
 530 FOR Y%=0 TO BE%
 540  PROCline(0,Y%,0,AE%,Y%,0)
 550  NEXT
 560 FOR Y%=0 TO ZE% STEP 10
 570  MOVE0,(Y%*T%) DIV 10:PLOT1,-10,0
 580  MOVE-80,(Y%*T%) DIV 10:PRINTSTR$(Y%+ZL%)
 590  NEXT
 600 VDU19,1,2;0;
 610 VDU19,2,6;0;
 620 ENDPROC
 630 DEFPROCPlot                        Plot all calculated data in '3-D'
 640 GCOLO,3:PROCAXES
 650 GCOLO,1:PROCGRAPH(E%)
 660 IF GET$="P" AND PO% THEN PROCgdump
 670 GCOLO,3:CLS:PROCAXES
 680 GCOLO,2:PROCGRAPH(Q%)
 690 IF GET$="P" AND PO% THEN PROCgdump
 700 ENDPROC
 710 DEFPROCGRAPH(Y%)                   Plot data points linked by grid
 720 FOR A%=0 TO AE%
 730  C%=A%*(BE%+1)
 740  PROCplot(4,A%,0,Y%?C%)
 750  FOR B%=0 TO BE%
 760   PROCplot(5,A%,B%,Y%?(C%+B%))
 770   NEXT:NEXT
 780 FOR B%=0 TO BE%
 790  PROCplot(4,0,B%,Y%?B%)
 800  FOR A%=0 TO AE%
 810   PROCplot(5,A%,B%,Y%?(B%+A%*(BE%+1)))
 820   NEXT:NEXT
 830 ENDPROC
 840 DEF PROCPrint                      Print table of results...
 850 CLS:IF PO%=TRUE THEN VDU2          to printer if required
 860 PRINTTAB(7)"One",TAB(10,0);
 870 FOR B%=BL% TO BH%:PRINTB%,;:NEXT:PRINT
 880 PRINTTAB(6)"Prism"
 890 VDU28,0,24,79,2
 900 FOR A%=0 TO AE%
 910  PRINTA%+AL%,P%?(2*A%),;
 920  FOR B%=0 TO BE%
 930   PRINTQ%?(A%*(BE%+1)+B%),;
 940   NEXT:PRINT'" ",P%?(2*A%+1),;
 950  FOR B%=0 TO BE%
 960   PRINTE%?(A%*(BE%+1)+B%),;
 970   NEXT:PRINT
```

```
 980  NEXT
 990 A=GET:VDU3
1000 ENDPROC
1010 DEF PROCinit                          Set up initial conditions
1020 PO%=FALSE
1030 PRINT'"Printer Copy ? (Y/N)"
1040 IF GET$="Y" THEN PROCprinter
1050 CLS
1060 %%=&5:VDU23;11,0;0;0;0,19,0,4;0;
1070 AL%=74:AH%=86:AE%=AH%-AL%             Range of angles Prism £0
1080 BL%=74:BH%=86:BE%=BH%-BL%             Range of angles Prism £1
1090 ZL%=0:ZH%=100:ZE%=ZH%-ZL%
1100 T=RAD(20):CA=COS(T):SA=SIN(T)         Plotting parameters
1110 T=RAD(160):CB=COS(T):SB=SIN(T)
1120 X%=10000/(1+SA+SB)
1130 R%=X%/AE%
1140 S%=X%/BE%
1150 T%=X%/ZE%
1160 n=1.485:W(0)=1.2
1170 F=39:H=56
1180 IF CB<0 THEN offset%=X%*CB DIV 10 ELSE offset%=0
1190 ENDPROC
1200 DEF PROCplot(P%,U%,V%,W%)             Convert point in '3-D' coordinates
1210 G%=(U%*CA*R%+V%*CB*S%) DIV 10         to 'screen' coordinates
1220 H%=(U%*SA*R%+V%*SB*S%+W%*T%) DIV 10
1230 PLOTP%,G%,H%
1240 ENDPROC
1250 DEF PROCline(I%,J%,K%,L%,M%,N%)       Plot line in '3-D'
1260 PROCplot(4,I%,J%,K%)
1270 PROCplot(5,L%,M%,N%)
1280 ENDPROC
1290 DEF PROCprinter                       Set up printer parameters
1300 *LOAD GDUMP
1310 ?&2B0=130
1320 PO%=TRUE
1330 VDU2
1340 VDU1,27,1,33,1,17:REM ELITE D.S.
1350 VDU1,27,1,108,1,12:REM MARGIN
1360 VDU3
1370 ENDPROC
1380 DEF PROCgdump                         Copy screen to printer
1390 VDU29,0;0;2
1400 *GDUMP0 1 0 0 0
1410 VDU3
1420 ENDPROC
```

ROTABN

```
   0 REM **Programme to calculate relative absorptions of rotational
transitions**
  10 IF ?&900<>&A9 THEN *LOAD APRINT  Routine to copy screen to printer
  20 DIM E(100),I(2,3,30),X(2,30)
  30 PROCenergy_levels
  40 PROCxcdat
  50 MODE0
  60 REPEAT:CLS
  70  INPUT "Temperature = ",T
  80  KT=0.69503*T
  90  J%=1:T1=FNterm_lower
```

```
100  Q=FNPAR                              Partition function
110  FOR J%=1 TO 30
120   TL=FNterm_lower                     Energy of lower level
130   B=EXP(-(TL-T1)/(KT))/Q/10           Boltzmann factor term
140   FOR A%=1 TO 3
150    K%=J%+2-A%
160    TU=FNterm_upper                    Energy of upper level
170    IF A%=1 THEN S=FNSJR
180    IF A%=2 THEN S=FNSJQ
190    IF A%=3 THEN S=FNSJP
200    I(2,A%,J%)=TU-E(J%)+32500.33       Transition energy
210    I(1,A%,J%)=I(2,A%,J%)*S*B          Transition intensity
220    NEXT A%
230   NEXT J%
240  CLS
250  PROCDISPLAY
260  INPUT"Another temperature (Y/N) ";Q$
270  UNTIL Q$="N":CLS
280 END
290 DEF FNSJR=J%*(J%+2)/(J%+1)           Honl-London factors
300 DEF FNSJQ=(2*J%+1)/(J%*(J%+1))       for R, P and Q branches
310 DEF FNSJP=(J%*J%-1)/J%
320 DEF PROCTABLE                        Produces table of results
330 VDU14                                if required
340 PRINT TAB(20);"ROTATIONAL ABSORPTION INTENSITIES (T=";T;"K)"
350 PRINT
360 PRINT "J";TAB(15);"R(J)";TAB(30);"Q(J)";TAB(45);"P(J)"
370 FOR J%=1 TO 30
380  PRINT J%;TAB(15);I(1,1,J%);TAB(30);I(1,2,J%);TAB(45);I(1,3,J%)
390  PRINT TAB(15);I(2,1,J%);TAB(30);I(2,2,J%);TAB(45);I(2,3,J%)
400  PRINT
410  NEXT J%
420 VDU 3
430 ENDPROC
440 DEF FNPAR                            Calculate partition function
450 LOCAL Q,J%
460 J%=1
470 REPEAT
480  DQ=(2*J%+1)*EXP(-E(J%)/(KT))
490  Q=Q+DQ
500  J%=J%+1
510  UNTIL (DQ/Q)<0.001
520 =Q
530 DEF FNterm_upper                     Energy of levels in 'b' v'=1 state
540 =1.4085*K%*(K%+1)-18.5E-6*K%*K%*(K%+1)*(K%+1)
                                         Energy of levels in 'a' v"=0 state
550 DEF FNterm_lower=1.607928*J%*(J%+1)-5.89E-6*J%*J%*(J%+1)*(J%+1)
560 DEF PROCenergy_levels
570 FOR J%=0 TO 100
580  E(J%)=FNterm_lower
590  NEXT
600 ENDPROC
610 DEF PROCDISPLAY                      Plot relative intensity of lines
620 FOR A%=1 TO 3                        against wavenumber for
630  VDU29,32;100+(A%-1)*300;5           the three branches
640  MOVE0,0:DRAW1200,0
650  IF A%=1 THEN MOVE -32,-20: PRINT"32"
660  MOVE1200,150:PRINTCHR$(ASC"S"-A%)
670  FOR X%=0 TO 10
680   I%=X%*120
```

```
690   MOVEI%,0:DRAW I%,-15
700   IF A%=1 THEN MOVEI%,-20:PRINTSTR$(550-20*X%)
710   NEXT X%
720  IF A%=2 THEN PROCpltxc
730  FOR J%=1 TO 30
740   MOVE (32550-I(2,A%,J%))*6,0
750   DRAW (32550-I(2,A%,J%))*6,I(1,A%,J%)*2
760   NEXT J%
770  NEXT A%
780 MOVE-32,323:PRINTSTR$(T);"K rotational temperature"
790 MOVE 1000,323:PRINT"ABSORPTION"
800 VDU4,29,0;0;
810 A=GET:IF A=ASC"D" THEN CALL &900
820 ENDPROC
830 DEF PROCxcdat                        Set up data for XeCl laser output
840 LOCALn:n=1.00029
850 FOR I%=0 TO 30
860  READX,Y
870  X(1,I%)=(32550-1E8/n/(3088-2*X/9))*6
880  X(2,I%)=10*(Y-1)
890  NEXT I%
900 DATA2.5,1,12,5.5,14,15.5,14.5,16,15.5,15.5,18,13,20.5,12,22,11.5
910 DATA23,12,24,13,26,30.5,26.5,31,28,25.5,29,21.5,32.5,15,34,13
920 DATA34.5,12.5,37.5,30.5,38.5,31,39,30,41.5,15,43,11.5,45,11
930 DATA46,11.5,48,12,49.5,14,50.5,14.5,51,13,52,10,53,7.5,56,4,61,2
940 ENDPROC
950 DEF PROCpltxc                        Plot overlay of XeCl laser output
960 MOVE0,250:PRINT"XeCl gain"
970 MOVEX(1,0),X(2,0)
 980 FOR I%=1 TO 30
 990  DRAWX(1,I%),X(2,I%)
1000  NEXT I%
1010 ENDPROC
```

REFERENCES

Ajello J M 1970 J. Chem. Phys. 53 1156

Allan M 1985 J. Phys. B: At. Mol. Phys. 18 4511

Andrew J E, Dyer P E and Roebuck P J 1984 Opt. Comm. 49 189

Babis J S, Thomas C H and Denton M B 1985 Rev. Sci. Instrum. 56 1969

Bayes K D and Kistiakowsky G B 1960 J. Chem. Phys. 32 992

Bazhulin P A, Knyazev I N and Petrash G G 1965 Sov. Phys. JETP 23 649

Berkowitz J, Chupka W A and Kistiakowsky G B 1956 J. Chem. Phys. 25 457

Berning P H, Hass G and Madden R P 1960 J. Opt. Soc. Am. 50 587

Black G, Sharpless R, Slanger T and Lorents D 1975a J. Chem. Phys. 62 4266

Black G, Sharpless R, Slanger T and Lorents D 1975b J. Chem Phys. 62 4274

Borst W L 1972 Phys. Rev. A 5 648

Brinkman R T and Trajmar S 1970 Ann. Geophys. 26 201

Burrows M D, Baughcum S L and Oldenberg R C 1985 Appl. Phys. Lett. 46 22

Burnham R and Djeu N 1976 Appl. Phys. Lett. 29 707

Burnham R 1977 Appl. Phys. Lett. 30 132

Capitelli M, Dilonardo M and Gorse C 1981 Chem. Phys. 56 29

Carroll P K 1962 J. Chem. Phys. 37 805

Carroll P K and Mulliken R S 1965 J. Chem. Phys. 43 2170

Carroll P K and Collins C P 1969 Can. J. Phys. 47 563

Cartwright D C, Trajmar S, Chutjian A and Williams W 1977 Phys. Rev. A 16 1041

Cartwright D C and Hay P J 1979 J. Chem. Phys. 70 3191

Caro R G, Costella A, Smith N P and Webb C E 1985 J. Phys D: Appl. Phys. 18 1291

Cefalas A C, Skordoulis C Komptis M and Nicolaides C A 1985 Opt. Comm. 55 423

Chandra N and Temkin A 1976 Phys. Rev. A 14 507

Chen J C 1964 J. Chem. Phys. 40 3513

Corkum P B and Taylor R S 1982 IEEE J. Quant. Electron. 18 1962

Corney A 1977 Atomic and laser spectroscopy (Oxford University Press) Chapt 8

Coutts J and Webb C E 1986 J. Appl. Phys. 59 704

Cox J T, Hass G, Ramsey J B and Hunter W R 1973 J. Opt. Soc. Am. 63 435

Deutsch T F and Geis M W 1983 J. Appl. Phys. 54 7201

Dewey H J 1976 IEEE J. Quant. Electron. 12 303

Diegelmann M, Hohla K, Rebentrost F and Kompa K L 1982 J. Chem. Phys. 76 1233

Dressler K 1969 Can. J. Phys. 47 547

Dreyfus R W and Hodgson R T 1974 Phys. Rev. A 9 2635

Dube L and Herzenberg A 1978 Phys. Rev. A 20 194

Dunning F B, Tittel F K and Stebbings R F 1973 Opt. Comm. 7 181

Dyer P E and Sidhu J 1985 Conf. Lasers Elect. Opt.(21-24 May 1985, Baltimore) paper FQ5

Ehrlich D J and Osgood R M 1979 Appl. Phys. Lett. 34 655

Filseth S V, Wallenstein R and Zacharias H 1977 Opt. Comm. 23 231

Finn T G and Doering J P 1975 J. Chem. Phys. 64 4490

Freund R S 1972 J. Chem. Phys. 56 4344

Ganeev R A, Gorbushin V V, Kulagin I A and Usmanov T 1986 Sov. J. Quant. Electron. 16 115

Garrison B J and Srinivasan R 1985 J. Appl. Phys. 57 2909

Gaydon A G 1944 Proc. R. Soc. Lond. 182 286

Germany G A, Salamo G J and Anderson R J 1983 J. Appl. Phys. 54 4573

Golde M F and Thrush B A 1972 Proc. R. Soc. Lond. 330 79

Goldsmith J E and Knyazev I N 1977 J. Appl. Phys. 48 4912

Govindanunny T and Maitland A 1983 J. Phys. D: Appl. Phys. 16 2425

Gower M C, Kearsley A J and Webb C E 1980 IEEE J. Quant. Electron. QE-16 231

Herzberg G H 1963 Spectra of Diatomic Molecules (Princeton N J: Van Nostrand)

Hodgson R T 1970 Phys. Rev. Lett. 25 494

Hodgson R T 1971 J. Chem. Phys. 55 5378

Hodgson R T and Dreyfus R W 1972 Phys. Rev. Lett. 28 536

Hoffman J M, Hays A K and Tisone G C 1976 Appl. Phys. Lett. 28 539

Hunter W R 1962 Opt. Acta 9 255

Hutchinson H R 1980 Appl. Opt. 19 3883

Hutchinson M H R and Manning R J 1985 Opt. Comm. 55 55

Jacquinot P 1960 Rep. Prog. Phys. 33 267

Jung K, Antoni T, Muller R, Kochem K-H and Ehrhardt H 1982 J. Phys. B: At. Mol. Phys. 15 3535

Kawamura Y, Toyoda K and Namba S 1982 J. Appl. Phys. 53 6489

Kearsley A J, Gower M C, and Webb C E 1979a Proc. Fourth Nat. Quant. Electron. Conf. (Ed. Wherret B S :Wiley)

Kearsley A J, Andrews A J and Webb C E 1979b Opt. Comm. 31 181

Kearsley A J, Andrews A J, Webb C E, Errey K and Coutts J 1983 Excimer Lasers - 1983 (New York: American Institute of Physics) pp107-111

Kirkland J, Doggett W O and Kim J J 1981 Rev. Sci. Instrum. 52 1338

Knyazev I N, Letokhov V S and Movshev V G 1975 IEEE J. Quant. Electron. 11 805

Lawrence G M 1972 J. Chem. Phys. 57 5616

Liegel J, Spiegel H, Sauerbrey R and Langhoff H 1983 J. Chem. Phys. 79 247

Liegel J, Emmert F, Sauerbrey R and Langhoff H 1984 Opt. Comm. 50 95

Linsker R, Srinivasan R, Wynne J and Alonso 1984 Lasers in Surgery and Medicine 4 201

MacFarlane R A 1966a Phys. Rev. 146 37

References

MacFarlane R A 1966b IEEE J. Quant. Electron. 2 229

McKee T J 1984 Can. J. Phys. 63 214

Murray J R and Rhodes C K 1976 J. Appl. Phys. 47 5041

Nee J B and Lee L C 1984 J. Chem. Phys. 81 31

Nighan W L 1970 Phys. Rev. A 2 1989

Nishimura H, Cartwright D C and Trajmar S 1979 J. Chem. Phys. 71 5039

Patterson D A and Vaughan W H 1963 J. Opt. Soc. Am. 53 851

Puliafito C A 1985 Conf. Lasers Elect. Opt. (21-24 May 1985, Baltimore) paper WL1

Pummer H, Hohla M, Diegelmann M and Reilly J P 1979 Opt. Comm. 28 104

Rajan K J 1974 Proc. Roy. Irish Ac. 74 17

Reintjes J 1980 Appl. Opt. 19 3889

Rice J K, Hays A K and Woodworth J R 1977 Appl. Phys. Lett. 31 31

Sakurai T 1985 To be published

Sakurai T and Watanabe T 1986 J. Appl.Phys. 59 4007

Samson J 1967 Techniques of Vacuum UV Spectroscopy (New York: Wiley)

Schulz G J 1964 Phys. Rev. 135 A988

Schulz G J 1976 Principles of laser plasmas Ed. Bekefi G (New York: Wiley) p33

Shemansky D E 1969 J. Chem. Phys. 51 5487

Shipman J D 1967 Appl. Phys. Lett. 10 3

Shishatskaya L P and Ryzhova L S 1973 Sov. J. Opt. Tech. 40 130

Srinivasan R and Mayne-Banton V 1982 Appl. Phys. Lett. 41 576

Sumida S, Obara M and Fujioka T 1979 J. Appl. Phys. 50 3884

Sze R C and Scott P B 1978 Appl. Phys. Lett. 33 419

Taherian M R and Slanger T G 1984 J. Chem. Phys. 81 3814

Takahashi A, Sumi M and Maeda M 1985 Opt. Comm. 55 193

Telle H, Huffer W and Basting D 1981 Opt. Comm. 38 402

Tellinghuisen J, Hoffman J M, Tisone G C and Hays A K 1976 J. Chem. Phys. 64 2484

Tellinghuisen J B 1977 Chem. Phys Lett 49 485

Tilford S G and Wilkinson P G 1964 J. Mol. Spectrosc. 12 231

Treanor C E, Rich J W and Rehm R G 1967 J. Chem. Phys. 48 1798

Uehara Y et al 1985 Opt. Lett. 10 487

van Veen N, Brewer P, Das P and Bersohk R 1982 J. Chem. Phys. 77 4326

Vanderslice J T, Wilkinson P G and Tilford S G 1965 J. Chem. Phys. 42 2681

Wang R-G, Wang Z-W, Dillon M A and Spence D 1979 J. Chem. Phys. 80 3574

Warneck P 1965 J. Opt. Soc. Am. 55 921

Watanabe K, Inn E C and Zelikoff M 1953 J. Chem. Phys. 21 1026

Waynant R W, Shipman J D, Elton R C and Ali A W 1970 Appl. Phys. Lett. 17 383

Waynant R W 1972 Phys. Rev. Lett. 28 533

Waynant R W 1977 Appl. Phys. Lett. 30 234

White J, Craighead H, Howard R, Jackel L, Behringer R, Epworth R, Henderson D and Sweeney J 1984 Appl. Phys. Lett. 44 22

Wilkinson P G and Mulliken R S 1957 Astrophys. J. 126 10

Woodworth J R and Rice J K 1978 J. Chem. Phys. 69 2500

Young R A 1960 J. Chem. Phys. 33 1112

Zipf E C and Gorman M R 1980 J. Chem. Phys. 73 813